University of Oxford

Department of Engineering Science

Extrusion Processing of Chocolate Crumb Paste

by

Alasdair Michael Walker

St. Catherine's College, Oxford

A thesis submitted for the degree of Doctor of Philosophy at the University of Oxford

Trinity Term 2011

“The history of mankind is carried on the back of the horse”

Anonymous

Acknowledgements

A number of people have helped me with this project over the last few years and I would like to take this opportunity to thank them.

I thank my supervisors Dr Peter Martin & Dr Chris Martin for their support and guidance over the course of my work. I am also grateful for the help from my various industrial supervisors at the company Mars - namely Isabella Van Damme, Will Taylor, Dale Cunningham and Ben Hook.

I note my debt to the following people for their time and support in making equipment available to me that contributed so greatly to the project:

- Patrick Hill, Tom Rutherford, Professor Zhanfeng Cui, Pierre Alexis-Mouthuy, Dr Alison Crossley and Richard Turner

Notable thanks is given to Richard Tweedie for his attendance at the extruder trials and perserverance with equipment. Financial support from the Engineering and Physical Sciences Research Council and Mars is gratefully acknowledged.

Extrusion Processing of Chocolate Crumb Paste

Alasdair Michael Walker, St. Catherine's College, Oxford

Doctor of Philosophy, Trinity Term 2011

Abstract

This project considers the co-rotating twin screw extrusion of a confectionery paste comprising powdered proteins, sugars, water and fats. As is the case with many food industry products, this process has been developed experimentally with little quantitative understanding of how variations in processing conditions influence the formation of the extrudate. A variety of techniques have therefore been developed to characterise and quantify the dispersive mixing, distributive mixing and rheological flow properties of this complex, multiphase, viscoelastic, unstable material. These techniques have then been utilised in a pilot plant extruder study of the mechanics of mixing and paste formation during extrusion, considering the influence of both processing conditions and screw profile. The internal evolution of paste microstructure has been successfully tracked along the length of screw profile using dead-stop extractions of the screws.

A rigorous off-line assessment of shear yield strength behaviour using cone penetrometry has shown the use of conventional off-line rheometers to be unviable due to rapid post extrusion hardening. This highlighted the need for an in-line rheological measurement technique for continuous extrusion analysis where the extruded material is severely time dependent and not extractable. In pursuit of this, a novel arrangement of bender elements is proposed and trialled, to rapidly characterise material parameters of viscoelastic pastes. A second technique looking to extend the application of shear wave interface reflection to multiphase pastes is also trialled.

A novel analysis of thermogravimetric data (TGA) has generated a viable index of distributive mixing, suitable for use on complex multi-component materials where thermal decomposition temperatures of the components are not well defined. Quantitative image analysis of pastes using scanning electron microscopy (SEM), optical microscopy protein staining and a novel application of multiphoton microscopy (MPM) have been used to visualise paste microstructure and quantify dispersive mixing.

From the pilot plant extruder study, the application of these techniques was successful in mapping the evolution of paste mixing and the resulting microstructure, as well as identifying key differences between pastes mixed by twin screw extrusion and batch mixing.

Contents

Contents ..... **i**
Notation ..... **iii**
Figures ..... **v**
Tables ..... **ix**
Chapter 1 Introduction **1**
1.1 Crumb paste extrusion 1
1.2 Recipe & ingredients 6
1.3 Project aim 10
1.4 Thesis outline 12
Chapter 2 Extrusion processing of food pastes **14**
2.1 Food quality control 14
2.2 Pastes 17
2.3 Twin screw extruders 24
Chapter 3 Off-line characterisation of crumb paste **30**
3.1 Cone penetrometry 31
3.2 Preliminary results 38
3.3 Determining paste shear yield strength from penetrometry data 44
3.4 Crumb paste observations 63
3.5 Conclusion 69
Chapter 4 In-line characterisation of crumb paste **72**
4.1 In-line extrusion monitoring techniques 73
4.2 Shear wave propagation 73
4.3 Shear wave propagation using play dough 85
4.4 Shear wave interface reflection 95

Chapter 5 Distributive mixing of crumb paste 98

5.1 Distributive mixing 99

5.2 Thermogravimetric analysis (TGA) of LM crumb paste 104

5.3 Alternative TGA analysis 113

5.4 Results 115

5.5 Conclusion 120

Chapter 6 Dispersive mixing of crumb paste 122

6.1 Dispersive mixing and paste visualisation 123

6.2 Scanning electron microscopy (SEM) of LM crumb paste 128

6.3 Optical microscopy of LM crumb paste 137

6.4 Multiphoton microscopy (MPM) of LM crumb paste 162

6.5 Conclusions 179

Chapter 7 Extruder study of crumb paste 182

7.1 Pilot plant extruder 183

7.2 Dead-stop experiment images 189

7.3 Density of extruded crumb pastes 192

7.4 Cone penetrometry of extruded crumb paste 195

7.5 Shear wave reflection 201

7.6 Thermogravimetric analysis (TGA) of extruded crumb paste 206

7.7 MPM 208

7.8 Evolution of paste microstructure 218

7.9 Energy cost of extrusion 226

7.10 Conclusions 227

Chapter 8 Conclusions and future work 230

8.1 Restatement of aims 230

8.2 Project overview & contributions 231

8.3 Discussion 237

References 241

Notation

Roman

c	component concentration
$\bar{c}$	mean concentration
C	cone geometry constant
D	Deborah number
D_0	barrel diameter (m)
f	cyclic frequency (Hz)
F	ANOVA F-test value
g	acceleration due to gravity (m/s^2)
G	shear modulus (Pa)
G^*	complex shear modulus (Pa)
G'	elastic storage modulus (Pa)
G''	viscous loss modulus (Pa)
H	hardness or yield (N/m^2)
k	angular wave number
K	(i) consistency coefficient (ii) cone penetration constant
L	(i) length scale (m) (ii) distance between sampling points (m) (iii) wave propagation distance (m)
M	mass of penetrating assembly (kg)
MI	integral mixing index
m	(i) Benbow-Bridgwater parameter (ii) cone penetration constant (iii) mass (kg)
n	(i) flow index (ii) cone penetration exponent
N	number of samples
p	statistical p-value
p	penetration depth (m)
P	pressure (Pa)
r	(i) magnitude ratio (ii) radius of cone at surface level (m)
R	(i) receiver (ii) reflection coefficient
R^2	coefficient of determination
S	cone sensitivity
tanδ	loss factor
T	(i) transducer (ii) temperature (°C) (iii) time period (s)
v	shear wave phase velocity (m/s)
V	(i) volume (m^3) (ii) displaced volume (m^3) (iii) paste velocity (m/s)
w	(i) water content (ii) weight (N)
W	mass of cone assembly (kg)
x	distance from transmitter (m)
Δx	virtual gap (m)
x_0	exponential attenuation distance (m)
X	RSM independent primary variable

Y (i) RSM experimental response (ii) shear yield strength (Pa)
Z shear impedance (N.s/m^3)

Greek

α (i) statistical confidence (ii) Benbow-Bridgwater parameter (iii) cone angle (°) (iv) dimensionless groups constant
β (i) Benbow-Bridgwater parameter (ii) dimensionless groups constant
γ shear strain
$\dot{\gamma}$ shear rate (s^{-1})
Γ complex wave propagation constant
δ phase angle between stress and strain (°)
η Benbow-Bridgwater parameter
θ cone angle (°)
λ (i) laser wavelength (m) (ii) structural parameter (iii) shear wavelength (m)
μ viscosity (Pa.s)
ρ density (kg/m^3)
σ standard deviation
σ_o (i) maximum standard deviation of segregated system (ii) Benbow-Bridgwater parameter
σ^2 variance
σ_0^2 maximum variance for segregated system
τ (i) characteristic relaxation time (s) (ii) shear stress (N/m^2)
ϕ (i) TGA cylinder sampler diameter (m) (ii) phase difference (rad)
ω angular frequency (rad/s)

Subscripts

1 (i) at receiver 1 (ii) 1mm length dimension (iii) pressure loss at die entry
2 (i) at receiver 2 (ii) 2mm length dimension (iii) pressure loss due to capillary shear
air associated with air
c (i) calibration material (ii) associated with critical value
DL associated with delay line
i associated with component i
j associated with sample j
I imaginary component
ref associated with reference fluid
R real component
max associated with a maximum
min associated with a minimum
s (i) associated with sample (ii) associated with submerged cone
x associated with the *x*-direction
y (i) associated with the *y*-direction (ii) at yield point
z associated with the *z*-direction

Figures

Figure 1.1 Schematic representation of chocolate crumb production 3
Figure 1.2 Forward conveying screw elements used in extruder showing key screw features 4
Figure 1.3 Kneading block with 90° stagger 5
Figure 1.4 Factory configuration of Werner & Pfleider co-rotating extruder (dimensions in mm) 6
Figure 1.5 Constituent components of milk 9
Figure 2.1 Schematic showing the rheological spectrum of shear deformation behaviours for two phase materials 18
Figure 2.2 Characteristic flow curves for a range of model behaviours 19
Figure 2.3 Illustration of the complex shear modulus (G^*) and the phase angle between stress and strain at small strain magnitudes for dynamic oscillatory shear rheometry 22
Figure 3.1 Cone penetrometer geometry showing depth of penetration, p and cone angle, α 32
Figure 3.2 Mixing procedure for LM paste 35
Figure 3.3 Crypto Peerless planetary mixer 35
Figure 3.4 Central Ignition Company cone penetrometer 36
Figure 3.5 Penetration depth versus water content during cone penetration tests on LM crumb pastes at 690 s after mixing using 70° cone (251 g) 39
Figure 3.6 Penetration depth versus water content during cone penetration tests on LM crumb pastes at 690 s after mixing using 70° cone (251 g) 40
Figure 3.7 Cone penetration depths on factory extruded paste during working day using 70° cone (290 g), at 180 s, 390 s and 510 s after extraction 42
Figure 3.8 Cone penetration depths on factory extruded paste during period of stable extrusion diagnostics using 70° cone (290 g), at 180 s, 390 s and 510 s after extraction 43
Figure 3.9 Double logarithmic plot of penetration depth versus shear yield strength for cone penetration tests on butters (Haighton, 1959) 45
Figure 3.10 TORVANE Handheld shear vane with three different vane sizes 49
Figure 3.11 Double logarithmic plot of penetration depth versus shear yield strength for cone penetration tests on LM crumb pastes showing the large discrepancy between penetration depths predicted by the Haighton formula for each cone assembly and those found experimentally 50
Figure 3.12 Cone geometry and positioning at time zero (t = 0) and time of equilibrium ($t = t_e$) 52
Figure 3.13 Force balance on sample in air and a reference fluid of known density used to determine paste densities using the double cup density measurement ....
Figure 3.14 Double cup density measurement apparatus 56
Figure 3.15 LM paste density variation with added water content as measured using double cup technique 57
Figure 3.16 Plot of dimensionless groups used in analysis of shear yield-penetration correlation 58
Figure 3.17 Experimental and modeled shear yield-penetration plots for 10° cone penetration tests on LM crumb paste 59
Figure 3.18 Experimental and modeled shear yield-penetration plots for 30° cone penetration tests on LM crumb pastes 60
Figure 3.19 Experimental and modeled shear yield-penetration plots for 50° cone penetration tests on LM crumb pastes 60
Figure 3.20 Experimental and modeled shear yield-penetration plots for 70° cone penetration tests on LM crumb pastes 61
Figure 3.21 Shear yield strength determined by cone penetrations versus added water content for LM pastes at 390s after mixing 63
Figure 3.22 Shear yield strength determined by cone penetrations versus time after mixing for LM pastes of differing water content 64
Figure 3.23 Shear yield strength determined by cone penetrations versus time after mixing for LM paste kept at room temperature (23.9°C) after mixing and in an 80 °C water bath after mixing 66

Figure 3.24 8% water LM paste appearance showing soft internal bulk and hardened surface exposed to air (width of image 100 mm) 66
Figure 3.25 Shear yield strength as determined by cone penetrations versus time after mixing for 6% water factory extruded paste and 8% water LM paste 68
Figure 4.1 The virtual gap geometry 78
Figure 4.2 Virtual gap rheometer signal response (Williams & Williams, 1992) 79
Figure 4.3 Layout and instrumentation of side mounted bender elements (Clayton et al., 2004) 83
Figure 4.4 Potted bender element dimensions (mm) and plane of shear wave generation (transmitter) 87
Figure 4.5 Schematic of virtual gap bender element arrangement 87
Figure 4.6 Received signal from side mounted bender elements 89
Figure 4.7 Perspex test cell showing virtual gap arrangement of side mounted bender elements 90
Figure 4.8 Noise vibration received at receiver elements when applying an $11V_{pp}$ 10kHz signal to transducer T in empty test cell. 92
Figure 5.1 Changing 8% water LM paste appearance with increased batch mixing time (scale bar 70mm) 100
Figure 5.2 Well defined TGA thermogram for a three component mixture (Kalyon et al., 2006) 105
Figure 5.3 Mixing routine for LM crumb paste showing point of reference for time of mixing 106
Figure 5.4 TGA sample dimensions for length scales L1 and L2 107
Figure 5.5 Particle size distributions of dry ingredients (provided by Mars UK Ltd) 107
Figure 5.6 One of two sets of custom sample cutters and sampling template showing relative dimensions in terms of the length scale, L 108
Figure 5.7 Example of nine L2 8% water LM crumb paste samples for use in TGA 109
Figure 5.8 Mass remaining at 190°C during TGA versus age of L2 sample (8% LM paste) for samples stored both in air and sealed containers with desicant 110
Figure 5.9 A typical TGA thermogram for L2 samples of LM crumb paste obtained during preliminary TGA tests at 30°C/min 111
Figure 5.10 Thermograms of 7 L2 crumb samples (heated at 30°C/min) which have undergone 15 seconds of mixing 112
Figure 5.11 Thermograms of 7 L2 crumb samples (heated at 30°C/min) which have undergone 60 seconds of mixing 113
Figure 5.12 Thermogram gradients for alternative TGA analysis 114
Figure 5.13 Integral mixing index versus mixing time for 1 mm (L1) and 2 mm (L2) length scale samples 116
Figure 5.14 Waterfall plot to show the changing temperature distribution of thermal decomposition rate inhomogeneities obtained using TGA for sample sets which have undergone increased mixing time 117
Figure 5.15 Inhomogeneity peak (bottom) matched to cocoa mass decomposition peaks (top) using TGA 118
Figure 5.16 Individual ingredient mixing versus mixing time for LM crumb paste using TGA analysis 120
Figure 6.1 ESEM images of powdered blend pre-processing (x800 left, x1600 right) 130
Figure 6.2 EDS Spectra of angular volume in blend (believed to be sucrose) 130
Figure 6.3 EDS spectra of "whispy" volume in blend (believed to by lactose) 131
Figure 6.4 EDS Spectra of spherical particles in blend (believed to be SMP) 131
Figure 6.5 ESEM image of cocoa mass (x1000) 131
Figure 6.6 EDS spectra of solid cocoa mass 132
Figure 6.7 ESEM image of solid cocoa butter (x1000) 132
Figure 6.8 EDS spectra of cocoa butter 132
Figure 6.9 ESEM image of 8% water LM crumb paste fractured 15 minutes after mixing (x1000) 133
Figure 6.10 ESEM images of 8% water LM crumb paste fractured 15 minutes after mixing (x500 left, x2000 right) 134
Figure 6.11 ESEM images of 8% water LM crumb paste fractured 90 minutes after mixing (x500 left, x1000 right) 135

Figure 6.12 ESEM image of 8% water LM crumb paste fractured 90 minutes after mixing (x600)..135
Figure 6.13 ESEM image of 8% water LM crumb paste surface (unfractured) 75 minutes after mixing (x600 left, x1000 right).....136
Figure 6.14 LM paste micing routine with marked sample points for degree of mixing study 138
Figure 6.15 Key features of stained microtome sections of 8% water LM paste subjected to 20s mixing as viewed under an optical microscope – x10 brightfield (top) x10 polarised (bottom) 141
Figure 6.16 Optical micrographs of 8% LM crumb pastes after varying degrees of mixing. S.....144
Figure 6.17 Optical micrographs of LM crumb pastes of varying water contents subjected to sixty seconds of mixing.....146
Figure 6.18 Undispersed protein image analysis segmentation algorithm.....
Figure 6.19 Schematic illustration of binary image multiplication with black pixels representing 1 and white pixels 0.....149
Figure 6.20 Binary image multiplication to determine actual protein covered crystalline material ...151
Figure 6.21 Discrete protein fraction versus degree of mixing (8% water LM paste).....153
Figure 6.22 Protein covered crystal fraction versus degree of mixing (8% water LM paste).....153
Figure 6.23 Discrete protein fraction versus added water content (60 s of mixing) 155
Figure 6.24 Protein covered crystal fraction versus added water content (60 s of mixing).....155
Figure 6.25 Inconsistent protein staining of 8% water LM crumb paste sections using Eosin Yellow after 50 seconds of mixing.....157
Figure 6.26 Indiscriminate nature of protein staining making it difficult to distinguish between dispersed and undispersed protein 158
Figure 6.27 Discrete protein fraction (dispersed and undispersed) versus mixing time for 8% water LM crumb paste, using 15 microtomed samples for image analysis at each point.....159
Figure 6.28 Protein covered crystal fraction versus mixing time for 8% water LM crumb paste, using 15 microtomed samples for image analysis at each point.....161
Figure 6.29 MPM section image of unstained 8% water LM crumb paste.....165
Figure 6.30 MPM channel images of section through sucrose (scale bar 100 μm) 167
Figure 6.31 MPM channel images of section through powdered lactose (scale bar 100 μm) 167
Figure 6.32 MPM channel images of section through skimmed milk powder (scale bar 100 μm) 168
Figure 6.33 MPM channel images of section through whey powder (scale bar 100 μm).....168
Figure 6.34 MPM channel images of section through solid cocoa mass (scale bar 100 μm) 169
Figure 6.35 3D MPM of 8% water LM crumb paste showing blue channel only 170
Figure 6.36 MPM section image of 8% water LM crumb paste showing depth profiles in z-direction 170
Figure 6.37 x-z projections of point spread functions with different degrees of aberration 172
Figure 6.38 MPM images of various LM crumb pastes showing red (cocoa mass) and blue (sugars) channels only 176
Figure 6.39 MPM images of various LM crumb pastes showing green (cocoa mass & dairy proteins) and blue (sugars) channels only.....177
Figure 7.1 Buhler BCTL-42 Co-rotating twin-screw extrusion system.....184
Figure 7.2 Extruder barrel showing integrated water cooling connections and liquid feed inputs ...184
Figure 7.3 Extruder endplate with circular die.....185
Figure 7.4 Modular elements that slide over common twin screw shafts 186
Figure 7.5 Standard pilot plant screw profile (dimensions in mm).....186
Figure 7.6 Sampling points along screw length for dead-stop experiments once screws are removed from the extruder 189
Figure 7.7 Dead-stop screw photo of paste S1 - 100 kg/hr - 300rpm - 5% water - with Mixing Element.....191
Figure 7.8 Dead-stop screw photo of paste S2 - 100 kg/hr - 300rpm - 8% water - with Mixing Element.....191
Figure 7.9 Dead-stop screw photo of paste S3 - 100 kg/hr - 300rpm - 2% water - with Mixing Element.....191
Figure 7.10 Dead-stop screw photo of paste S5 - 100 kg/hr - 300rpm - 5% water – no Mixing Element 191

Figure 7.11 Extruded paste densities versus time after extrusion measured using double cup method 193
Figure 7.12 Density versus time after extrusion for paste S5 using double cup method with control sample immersed after 12 minutes 193
Figure 7.13 Densities for extruded crumb paste and LM crumb paste measured using double cup method 180 seconds after extrusion or mixing.....195
Figure 7.14 Shear yield strengths of extruded crumb pastes versus time after extrusion 198
Figure 7.15 Off-line comparison of extruded and LM crumb paste shear yield strengths versus time after mixing using cone penetrometry 200
Figure 7.16 Shear wave reflection transducer arrangement.....202
Figure 7.17 Calibrated reflection coefficient (real) of extruded crumb pastes versus frequency 100 s post extrusion.....203
Figure 7.18 Calibrated reflection coefficient (imaginary) of extruded crumb pastes versus frequency 100 s post extrusion 204
Figure 7.19 Calibrated reflection coefficient (real) of extruded crumb pastes versus time post extrusion 204
Figure 7.20 Calibrated reflection coefficient (imaginary) of extruded crumb pastes versus time post extrusion 205
Figure 7.21 TGA Integral mixing index of extruded pastes versus water content using L1 length scale 207
Figure 7.22 TGA Integral mixing index of extruded paste versus screw position using L1 length scale 207
Figure 7.23 Dead-stop screw photo of paste S6 - 100 kg/hr - 300 rpm - 5% water (no CM) - with Mixing Element 210
Figure 7.24 Dead-stop screw photo of paste S7 - 100 kg/hr - 300 rpm - 8% water (no CM) - with Mixing Element 210
Figure 7.25 Dead-stop screw photo of paste S8 - 100 kg/hr - 300 rpm - 2% water (no CM) - with Mixing Element 210
Figure 7.26 Dead-stop screw photo of paste S9 - 100 kg/hr - 300 rpm - 5% water (no CM) - no Mixing Element 210
Figure 7.27 MPM images - Green & blue channel S6 - 5% water - with mixing element (scale bar = 50 μm).....212
Figure 7.28 MPM images - Green & blue channel S7 - 8% water - with mixing element (scale bar = 50 μm).....212
Figure 7.29 MPM images - Green & blue channel S8 - 2% water - with mixing element (scale bar = 50 μm).....212
Figure 7.30 MPM images - Green & blue channel S9 - 5% water - without mixing element (scale bar = 50 μm) 213
Figure 7.31 Fraction of MPM sugar signal colocalised with protein signal versus water content.....215
Figure 7.32 Fraction of MPM protein signal colocalised with sugar signal versus water content.....215
Figure 7.33 Colocalisation of MPM sugar channel as a function of position along screw profile 217
Figure 7.34 Microstructural evolution along screw profile with mixing element.....223
Figure 7.35 Microstructural evolution along screw profile without mixing element 224
Figure 7.36 Microstructural evolution of LM crumb paste during batch mixing 225
Figure 7.37 Specific Mechanical Energy (SME) input required to extrude pastes at 100 kg/hr.....226

Tables

Table 1.1 Extruded crumb paste recipe by mass fraction 7
Table 3.1 LM recipe by mass.....33
Table 3.2 Cone angles & corresponding cone assembly mass used for cone penetration tests.....37
Table 3.3 Shear yield strength calculations of similar pastes using cone penetrations depths obtained using three cone angels and the Haighton formula.....47
Table 3.4 Variables in dimensional analysis of shear yield-penetration correlation 51
Table 4.1 Standard 42% liquid play dough recipe by mass.....86
Table 6.1 Sample properties of six LM pastes imaged.....138
Table 6.2 Fraction of crystalline material covered by protein in response to mixing time for 8% water LM crumb paste, using 15 microtomed samples for image analysis at each point. 161
Table 6.3 LM crumb paste samples imaged using MPM 163
Table 7.1 Experimental design for pilot plant extruder trials 188
Table 7.2 Cone assemblies used for penetrometry on pilot plant extrudates.....196
Table 7.3 Extruded crumb paste shear yield strengths as determined by cone penetrometry. 199
Table 7.4 Sugar fraction colocalised with protein as determined by MPM colocalisation image analysis 216

Chapter 1 Introduction

This thesis presents the results of a research project into the extrusion processing of chocolate crumb paste in co-rotating twin screw extruders. The project was initiated and sponsored by Mars, a global food manufacturer, who use these extruders as an integral stage in their chocolate making process. The process of crumb paste extrusion was selected by the company as the general remit for the project, however the direction of the work and the approach adopted was that of the author.

The remit of the project is presented in this introduction, with Section 1.1 introducing the company and crumb paste extrusion in the context of the entire chocolate making process. Section 1.2 then introduces the components of the chocolate crumb recipe. Section 1.3 outlines the aims of the project with Section 1.4 outlining the structure of this thesis.

1.1 Crumb paste extrusion

1.1.1 Mars chocolate production

Mars (a division of Mars UK Limited) was formed in January 2002 by the merger of Mars Confectionery and Pedigree Mars. It forms part of the global Mars company for whom Chocolate is one of six business segments, along with Food, Petcare, Drinks, Gums and Symbioscience. Confectionery and snack food production within the UK, along with research and development, is located in Slough where some 200,000 tons of confectionery

are manufactured each year, including 3 million Mars bars a day. Mars have a need to ensure product quality whilst simultaneously improving efficiency and process design to further their success. In addition to this, a key issue for the company is maintaining consistent product quality when introducing new technologies into the building of new factories around the world.

When considering the process of chocolate production, rather than combining raw ingredients and processing entirely to the end product, the company include an additional stage by first mixing the raw ingredients into an intermediate material known as *chocolate crumb*. This process of chocolate crumb extrusion, shown schematically in Figure 1.1, takes powdered raw ingredients including milk powder, whey and sucrose and feeds them into an intermeshing co-rotating twin screw extruder where they are initially dry mixed. In turn cocoa mass, cocoa butter and water are added and the paste is then homogenised along the extruder by the shearing action of the rotating extruder blades, before being pumped under extrusion pressure to ovens where the paste is dried hard as crumb blocks.

In this state, crumb can be distributed to other factories, stored, or ground down for immediate use in the downstream stages of complete chocolate production. These include *conching* – where the crumb is mixed with further cocoa butter for rolling and kneading to create a fine silky texture and finally *tempering* – where the conched mixture is subjected to controlled cooling and ensures a specific microstructure of crystals. This method of production, which generates crumb paste as an intermediate material, allows for a great deal of flexibility and facilitates the central processing of all chocolate raw materials, ready for distribution throughout the company as required.

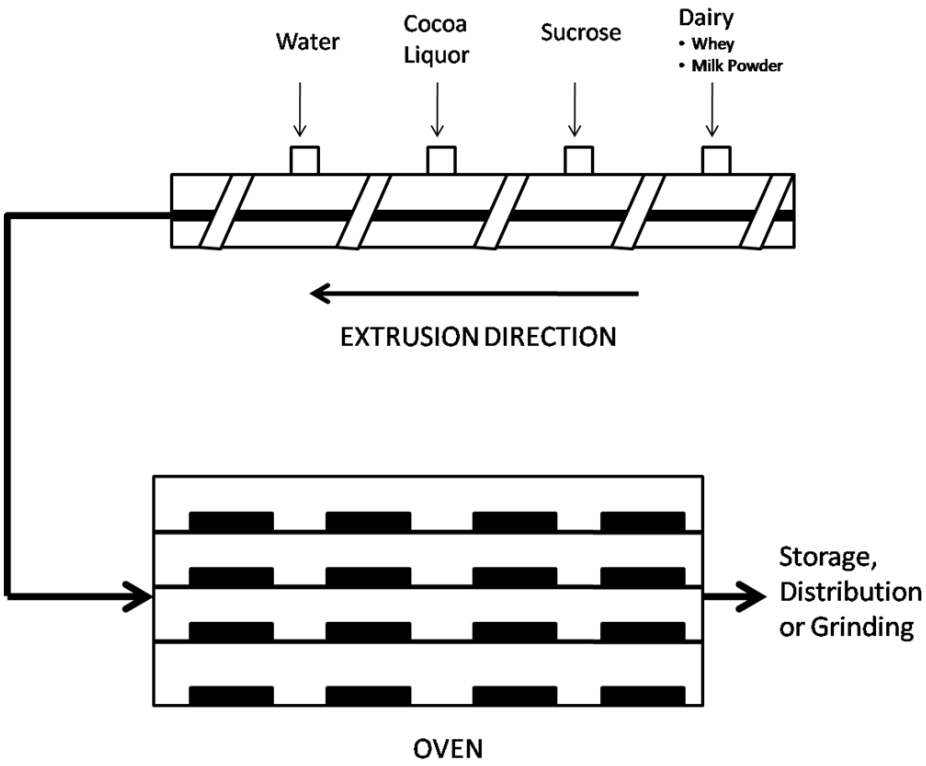

Figure 1.1 Schematic representation of chocolate crumb production

1.1.2 Extrusion processing

Extrusion can be defined simply as "the pushing of an extrudate through an opening to produce a predefined shape" (Huber, 2000) and in its simplest form consists of a piston ram within a cylinder which moves forward to create pressure and push material through a shaping orifice known as a *die*. This simple process can then be made continuous by replacing the piston ram with a rotating helical screw which transports material from an inlet to the die, where similarly the pressure builds until material is propelled through. If instead, the single helical screw is replaced with two helical screws side by side within a tight fitting barrel, it is then possible to mix, process and extrude discrete components or ingredients in a single operation, as is the case with crumb paste extrusion.

Twin screw extrusion has become a widely adopted method of processing in both the polymer melt and food industries and the intermeshing co-rotating design is

particularly popular due to its positive conveying and self-cleaning attributes. The modular design of most co-rotating twin screw extruders, with a variety of individual elements which slide over two adjacent common shafts housed inside a barrel, also offers an attractive degree of design flexibility. As with the extrusion processing of chocolate crumb paste, the majority of systems consist of *conveying elements* and *kneading elements*. The self-wiping conveying elements (as shown in Figure 1.2) form shaped wedges, or channels, that enable material to be transferred from one screw to the other and convey the material in the direction of extrusion. Material is prevented from adhering to the screw root as one crest edge wipes the flanks of the other screw with a tangential motion.

Kneading sections, containing elements such as those shown in Figure 1.3, can vary in disc width and stagger angle, but are generally designed to create high shear regions. The number of kneading sections and the intervals between them is then dependent on the material and process being performed. A broader description of extruders and their use is included in Chapter 2.

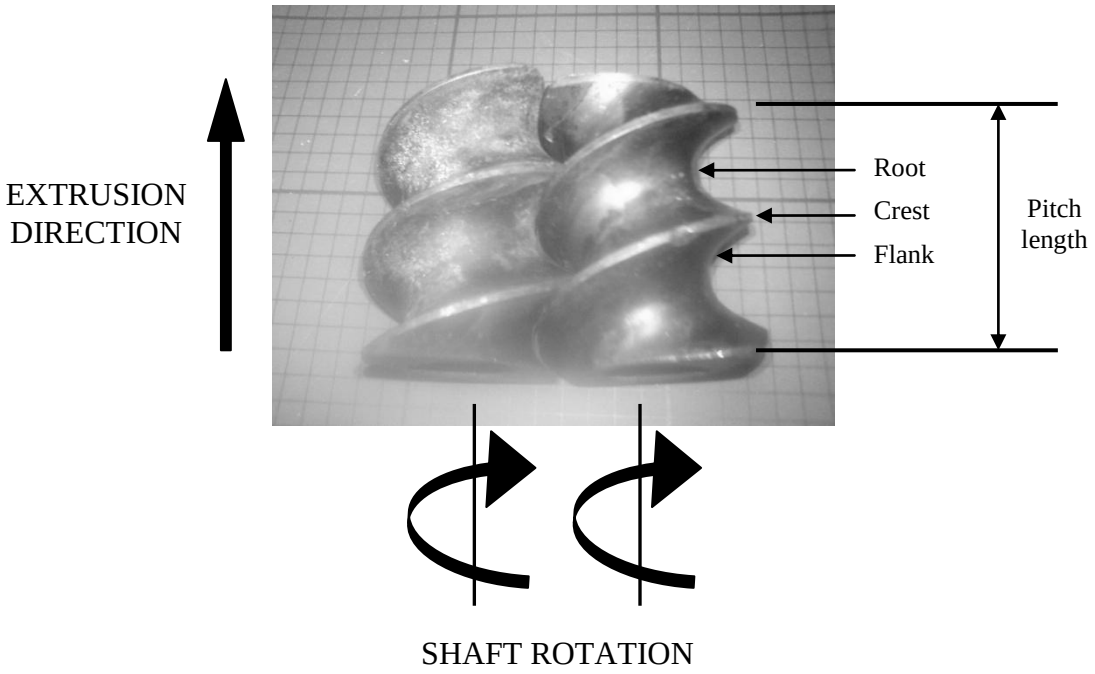

Figure 1.2 Forward conveying screw elements used in extruder showing key screw features

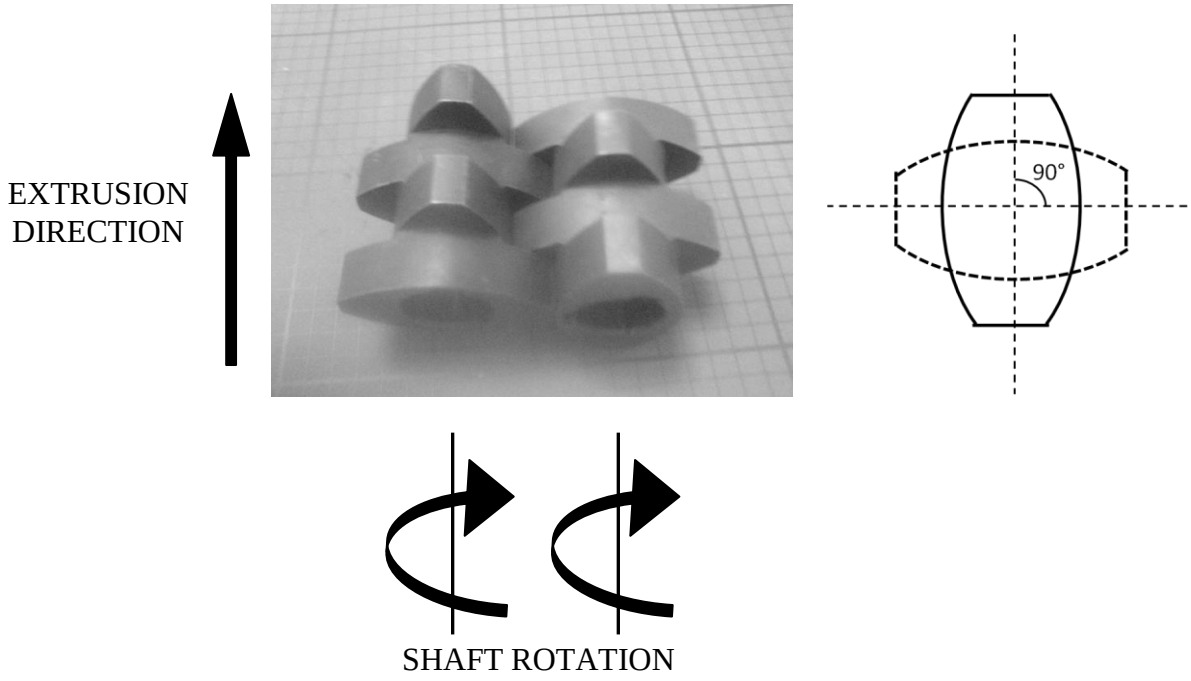

Figure 1.3 Kneading block with 90° stagger

1.1.3 Extruder configuration

The current configuration of extruder used by the company is shown in Figure 1.4. Raw ingredients are injected into a constant pitch, constant diameter forward conveying screw region, before passing through a kneading zone designed to exert high degrees of mixing. Finally, the paste passes through a further forward conveying region before being extruded through the die.

Whilst the configuration shown in Figure 1.4 is the one used at the time of writing, an alternative arrangement which included two separate kneading sections was in place at the commencement of the project. The removal of the second kneading section was driven by the company's aim to reduce the final temperature of the crumb paste during extrusion. Whilst this recent modification appears to have achieved the desired effect of reducing paste temperature within the extruder, it is believed that no scientific enquiry has been made into how this change may or may not have altered any crumb paste properties.

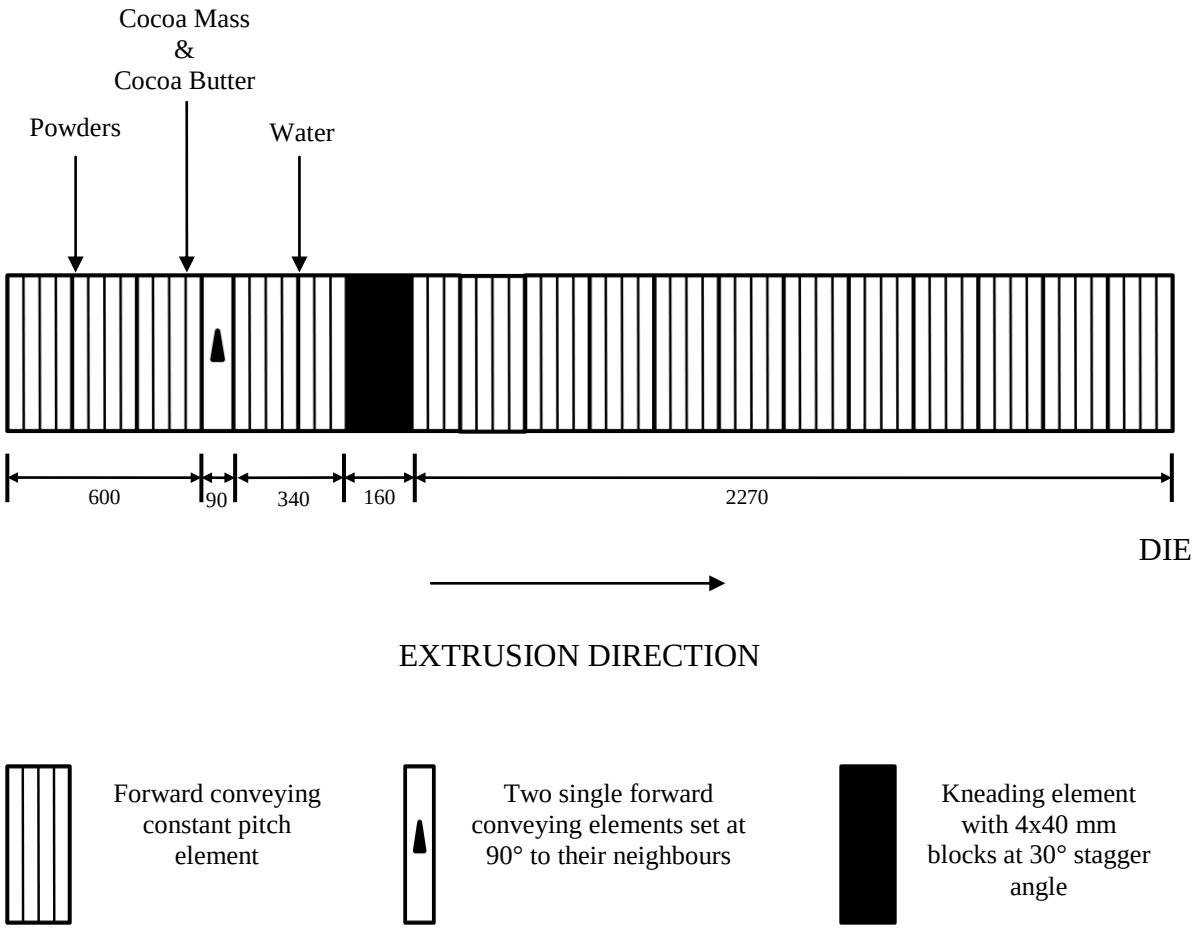

Figure 1.4 Factory configuration of Werner & Pfleider co-rotating extruder (dimensions in mm)

1.2 Recipe & ingredients

The recipe used for extruded crumb paste is shown in Table 1.1, comprising mainly sugar, cocoa components, dairy products and water. Each of the ingredients is then discussed in more detail in the following sub-sections.

Table 1.1 Extruded crumb paste recipe by mass fraction

Ingredient	Mass Fraction (%)
Sugar	52.4
Cocoa Mass (CM)	10.2
Cocoa Butter (CB)	2.2
Skimmed Milk Powder (SMP)	18.3
Lactose	5.7
Whey	5.2
Water	6.0

1.2.1 Cocoa mass (CM)

In order to produce cocoa mass, also known as cocoa liquor, cocoa beans are cleaned using blowers and sieves to remove extraneous matter and the husks (or shells) are removed. The nibs (the inside of the bean) are then roasted at 120 °C for 15 minutes to develop flavour. Once roasted, the nibs are then milled into a paste where the heat generated by the process causes the cocoa butter in the nib to melt and molten cocoa mass is the result.

If stored in suitable sealed containers, cocoa mass can be allowed to set and stored for melting as required. If being kept in its molten state, it must remain well mixed as the cocoa butter tends to separate out from the cocoa solids if left to settle for long periods.

1.2.2 Cocoa butter (CB)

Cocoa butter is the fat contained within the nibs of cocoa beans and is extracted by pressing cocoa mass through filters to separate the butter from the solid cocoa powder. Like cocoa mass, it can be stored in solid form for use as required.

Both cocoa mass and cocoa butter will melt at around 35 °C given enough time, but will melt much more rapidly at higher temperatures. In the plant extruder, both are stored in continuously stirred silos and injected together at 45 °C.

1.2.3 Skimmed milk powder (SMP)

The skimmed milk powder used here has been processed into powder form by spray drying liquid skimmed milk in hot air, where it is dried from approximately 87% water content to approximately 3-4% in around a second. Although exposed to high temperatures, the short time scale of the drying process means that there is negligible protein denaturing as droplets only momentarily reach their maximum temperature, not usually above 70 °C, before the drying is complete. Consequently, spray drying does not significantly affect protein solubility in water and most enzymes remain active.

A breakdown of the constituent components in milk is shown in Figure 1.5 and helps to define the three main dairy ingredients used in the crumb paste recipe. Milk can be split into plasma and fat globules. Milk minus these fat globules leaves what is known as *skimmed milk* and can be closely approximated to plasma, although separation will never be entirely complete. Observation at the next microscopic level reveals that plasma itself is comprised of serum plus casein micelles (large agglomerates of casein protein). Casein micelles can be removed from milk plasma by clotting with rennet and leaves the liquid known as *whey*. This can be closely approximated to milk serum, but is again not entirely equivalent, due to the presence of residual casein polypeptides that are generated by the rennet clotting process. Whey then contains water, lactose, whey proteins and many other minor components. Lactose is the only carbohydrate present in milk in more than a trace and is the distinctive sugar in milk which is responsible for its slightly sweet taste.

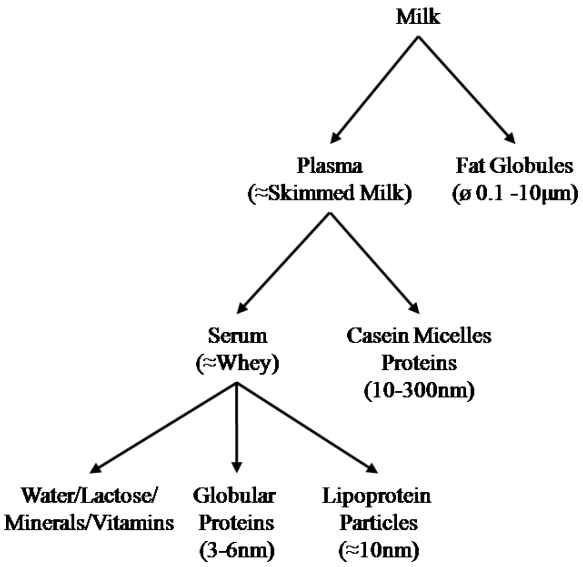

Figure 1.5 Constituent components of milk

1.2.4 Whey, lactose, sugar & water

As described in Section 1.2.3, whey is the liquid that is left after casein micelles are removed from skimmed milk by clotting with rennet. Lactose is a carbohydrate present in whey. Although whey and lactose are substances already present in SMP, both are added into the crumb recipe in additional quantities as a cost saving measure to reduce the amount of milk required.

The sugar used in crumb recipes is sucrose and is injected in the form of icing sugar. Tap water sourced from the hard water area of Slough is currently injected into the extruder at approximately 25 °C. As yet, there is no information on whether water temperature or quality affects the quality of crumb.

1.2.5 Lab made (LM) crumb paste

For research purposes, a laboratory made recipe designed to try to replicate extruder paste is currently used by the company in conjunction with a planetary mixing process, such that small batches of approximately 2 kg can be produced. With the

exception of water content, all of the ingredients appear in the same relative proportions as the extruded paste. The water content added is increased from 6% to 8% in order to try to compensate for the lower shear and temperatures experienced in an open planetary mixer. It is not currently known whether Lab Made (LM) crumb paste is a representative replication of extruded crumb paste. The method used for mixing LM crumb paste in these quantities is described in Section 3.1.1.

1.2.6 Crumb paste hardening

Once extruded, crumb paste samples extracted from immediately after the die will undergo a noticeable hardening that can be appreciated in hand after only a few minutes. At the commencement of this project, the author was aware of no consensus within the company as to the exact cause of this hardening.

1.3 Project aim

As with a great many industrial and food processes, the crumb extrusion mixing process has been developed over the last thirty years in house on a trial and error basis. Recent times have seen an ever increasing degree of scientific enquiry into the chocolate making process as a whole, but the extrusion mixing stage has itself received very little attention – being perceived simply as a crude, yet effective form of continuous mixing which combines the ingredients into a suitable paste for the next stage of production.

However, there are significant cost considerations to be made when considering the extrusion mixing of crumb paste. From a capital cost perspective, twin screw extruders are expensive to install. Operating costs are then considerable with the continuous running of

the motors and parts that wear quickly and are expensive to replace - this is particularly true of the screws which are complex to machine.

Additionally, water is currently added at the extrusion mixing stage, only to be removed at considerable energy cost in the drying stage immediately after. As such, this area of extrusion mixing has been targeted as an area of potential inefficiency. A recent set of trials performed by the company compared final product chocolates produced with both extruded and LM crumb pastes of varying water contents. These included pastes mixed with no added water at all. When considering the chocolates produced from extruded crumb, taste testers reported no noticeable deviations in taste and texture from regular chocolate for any of the water contents. However for LM crumb pastes mixed with reduced water, noticeable taste and texture deviations were observed suggesting that the extrusion processing performs a role other than simple large scale mixing. These results have prompted newfound interest in the extruder stage and as a consequence pose the questions:

1. What contribution does extrusion mixing of the ingredients make to the process and how?
2. How might the process be optimised given a greater understanding of how crumb properties evolve during extrusion?
3. How do proteins interact with sugars?
4. Is batch mixed LM paste representative of extruded crumb paste?

Whilst the desire now exists to investigate how crumb properties and the processes used to produce it affect the end product, there are currently no scientific criteria on which to evaluate the quality of crumb paste produced at any given moment. Instead, current

operations see no characterisation measurements on crumb paste beyond operator judgement, before progressing to the drying stage. Currently, the only way of testing crumb quality is to turn it into chocolate and present it to taste testers, which is inefficient and time consuming.

With little previous quantitative investigation of how processing conditions affect microstructure and material properties, a deeper understanding of those processing conditions required to produce a high quality crumb paste is the desired outcome of research, such that existing energy inputs can be optimised and alternative, cheaper methods of crumb preparation may be explored. However, this is an impossible task without suitable tools and analysis to characterise relevant material properties and compare pastes produced.

It is therefore the objective of this study to design and implement a variety of characterisation techniques which may identify the trends of ingredient dispersion that are required for a well mixed paste. It is also the goal of this study to track changes in paste microstructure along the length of the screw profile, thereby facilitating the quantitative comparison of differing screw profile designs.

1.4 Thesis outline

As stated in Section 1.3, the aims of this project are a greater understanding of how processing conditions and equipment affect the microstructure and material properties of crumb paste, since there are currently no characterisation techniques in place for this complex, multiphase, multicomponent, naturally sourced material paste which is reported to display time dependent hardening once formed.

1.4.1 Project methodology

The methodology for this study has been to investigate and develop a range of characterisation techniques suitable for quantifying *dispersive mixing* (changes in the physical characteristics of the ingredients), *distributive mixing* (the homogeneity of components) and rheological properties of the paste.

Preliminary investigations of crumb paste behaviour using LM paste and off-line tests for yield strength and density are described in Chapter 3, including a discussion of the difficulties involved with using off-line rheological characterisation tests on this material. Chapter 4 then presents the results of a review into the potential for in-line rheological characterisation of pastes using wave based techniques. The development of novel techniques and analysis for quantifying distributive and dispersive mixing within crumb paste are then presented in Chapters 5 and 6 respectively.

Characterisation techniques developed in Chapters 3 to 6 have then been utilised in a large pilot scale extruder trial as presented in Chapter 7. Here, rheological tests have been performed on varying extrudates, whilst dispersive and distributive mixing have been analysed at various points within the extruder using dead-stop experiments (where the extruder is run under steady state conditions and stopped dead to remove the screws). A range of water contents and screw profiles have been tested. Finally, conclusions from the project are discussed in Chapter 8.

It is hoped that the results of this work will further contribute to the mixing analysis of and the development of in-line rheological measurements for complex food pastes generally. In the context of this industrial application, it is hoped that implementation of these characterisation techniques will create the necessary platform for variations in the final product (chocolate) properties to be referenced against properties of the intermediate crumb paste.

Chapter 2 Extrusion processing of food pastes

This chapter presents and reviews the current state of knowledge and research surrounding the extrusion processing of food pastes. The aim of this chapter is to discuss the key issues and considerations for this project and present a coherent research methodology suitable for delivering an advancement of scientific knowledge to the specific process considered as well as the research field as a whole.

Section 2.1 begins with a broad discussion on how best to approach the quality control of foods and is followed by a more detailed review of pastes and how they may be characterised in Section 2.2. Finally Section 2.3 reviews the field of research for the twin screw extrusion of pastes.

2.1 Food quality control

Bourne (2002) categorises the three main acceptability factors of food as appearance, flavour and texture. It is the last of these that is most attractive as a guide for determining product quality, since appearance is almost entirely subjective and the mechanical evaluation of taste and flavour is not yet sufficiently understood or developed. Bourne offers the following definition of texture, which highlights the suitability of textural properties as mechanical instrument testing parameters:

"The textural properties of a food are that group of physical characteristics that arise from the structural elements of the food, are sensed primarily by the feeling of touch, are related to the deformation, disintegration and flow of the food under a force and are measured objectively by functions of mass, time and distance."

However, Muller (1969) claims that those broader definitions of food texture, such as Bourne's, are not sufficient since the term texture simultaneously refers to both physical and perceived properties and that a distinction between the two is required. He proposed that the term *texture* be sub-divided into (i) *rheology* - a branch of physics describing physical properties of the food and (ii) *haptaesthesis* - a branch of psychology that deals with the perception of the mechanical behaviour of materials. To illustrate the point, he considers the study of light which can be split into *optics* - the physical properties of light and *vision* - the human response to light, such as the perception of objects and colour. It follows then, that in this food based mechanical research study, a rheological assessment of paste quality is the only way to deliver a quality control test which also acts as a useful output in a study aimed at understanding the mixing behaviour involved with paste formation. Correlation of these tests to the sensory perception of mechanical behaviours (i.e. their effect on taste) therefore lies outside the scope of this particular study, but is a long term objective of research in this area.

Rheology is now well established as *the science of the deformation and flow of materials* (Steffe, 1996) and is the study of the manner in which materials respond to applied stress or strain. This can then be extended to a definition of food rheology as *the study of the deformation and flow of the raw materials, the intermediate products and the final products of the food industry* (White, 1970). The relevance of crumb paste quality control as a rheological problem is further confirmed by Bourne (2002) who cites the

rheology of bread dough, milk curd and meat emulsions as important aspects in the manufacture of high quality bread, cheese and sausage products - namely food processing operations that rely heavily on the rheological properties of intermediate products because of the significant effect they have on the quality of the finished product.

A wide range of food texture measurement techniques exists, but it is important to bear in mind that objective texture measurement can be classified into *fundamental* and *empirical tests*. Fundamental tests measure well defined intrinsic rheological properties and results are independent of the instruments used to measure them. This however, is an ideal concept and different instruments, which are often expensive, rarely yield identical results (Steffe, 1996). Nonetheless, they provide useful information when studying theoretical behaviour. Empirical tests on the other hand, measure parameters that are poorly defined, but from practical experience are found to be well related to textural quality (Bourne, 2002). These tests are more likely to be simple and inexpensive, but are by their very nature arbitrary and frequently are only useful with a limited number of commodities. In the context of this project, purely empirical data is of little use for furthering mechanical understanding outside of this particular application and consequently any data obtained must be correlated in some way to fundamental parameters.

The examples above serve to illustrate the widespread use of instrumental rheological texture measurements as gauges of product quality in the food industry. However, the individual properties used vary greatly due to the large range of materials considered and the lack of distinction that often exists between solid, liquid and semi-liquid foods. Indeed, many food products can be considered to behave as both a solid and a liquid depending on the stress environment applied. For example, a material may appear to deform elastically when a test is performed quickly, but appear more viscous when the

same test is applied over a longer time scale. This concept was appropriately captured by Reiner (1964) with the introduction of the Deborah number, describing the effect that given enough time, everything will flow:

$$D = \frac{\tau}{T} \tag{1}$$

where D is the Deborah number, τ is the characteristic relaxation time (s) of the material (infinite for Hookean elastic solids and zero for perfectly Newtonian liquids) and T is the time over which the deformation is observed (s). As such, a high Deborah number corresponding to solid like behaviour, can be the result of either a high characteristic relaxation time or a small deformation time. The Deborah number introduces the concept that in certain situations, simultaneous consideration of solid material parameters and liquid fluid parameters may be required.

2.2 Pastes

The simultaneous existence of solid and liquid deformation behaviours is a phenomenon often seen in multiphase pastes such as the subject of this work. A *paste* or *concentrated suspension* is considered to be a two phase material in which solid particles are bound together by a continuous viscous liquid binder phase. Naturally, there can exist a broad spectrum of rheological behaviours as shown in Figure 2.1, each dependent on the ratio of solid and liquid phase present.

The high solid fraction and particle interaction of these pastes has the effect of increasing the apparent viscosity of the mixture beyond that of the interstitial medium. Consequently, this particle interaction can cause the material to demonstrate *viscoplastic behaviour* - possessing an apparent yield stress whilst also being readily deformable.

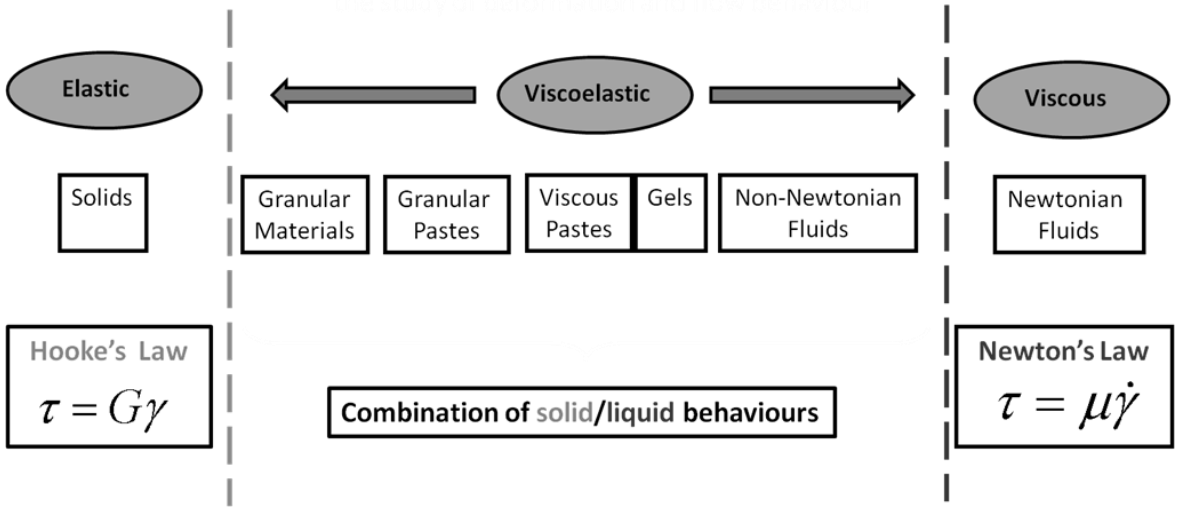

Figure 2.1 Schematic showing the rheological spectrum of shear deformation behaviours for two phase materials

2.2.1 Paste characterisation

The basic flow behaviour of a paste can often be found to be a superposition of the individual behaviours associated with the two phases present. Figure 2.2 shows some of these characteristic behaviours when considering the shear stress developed in the material τ (Pa), as a function of shear rate, $\dot{\gamma}$ (s^{-1}), also known as the *flow curve*. For a *perfect plastic* solid phase, the shear stress during shearing is independent of the shear rate at the yield stress, τ_y. By comparison, a *Newtonian* fluid displays a linear relationship between shear stress and shear rate, given by:

$$\tau = \mu\dot{\gamma} \tag{2}$$

where μ is the viscosity of the fluid (Pa.s). A material that demonstrates a superposition of these two ideals (i.e. an apparent yield stress with a linear shear rate dependence), is known as a *Bingham plastic*. However when considering a two phase paste, dilation effects can lead to varying voidage between slip planes. *Shear thickening* relates to increased relative shear stresses with increased shear rate whilst the reverse effect is known as *shear thinning*. For example, many cosmetic products such as creams or gels

exploit the effect of shear thinning to remain conveniently viscous for packaging and storage whilst thinning upon application to the skin at a suitable shear rate. This effect can usually be accounted for by a power law rate dependence and a material which combines all of the above properties can conveniently be described in full by the Herschel-Bulkley model (Herschel & Bulkley, 1926):

$$\tau = \tau_y + K\dot{\gamma}^n \tag{3}$$

where τ = shear yield stress, K = consistency coefficient (semi-analogous to viscosity) and n = flow behaviour index. Using this model, shear thinning is described by $n < 1$, shear thickening by $n > 1$ and Newtonian fluid flow by $n = 1$ (with $\tau_y = 0$). So long as any dilation effects can adequately be captured by the power law variation, the Herschel-Bulkley model is a convenient way of describing a wide range of flow curve behaviours.

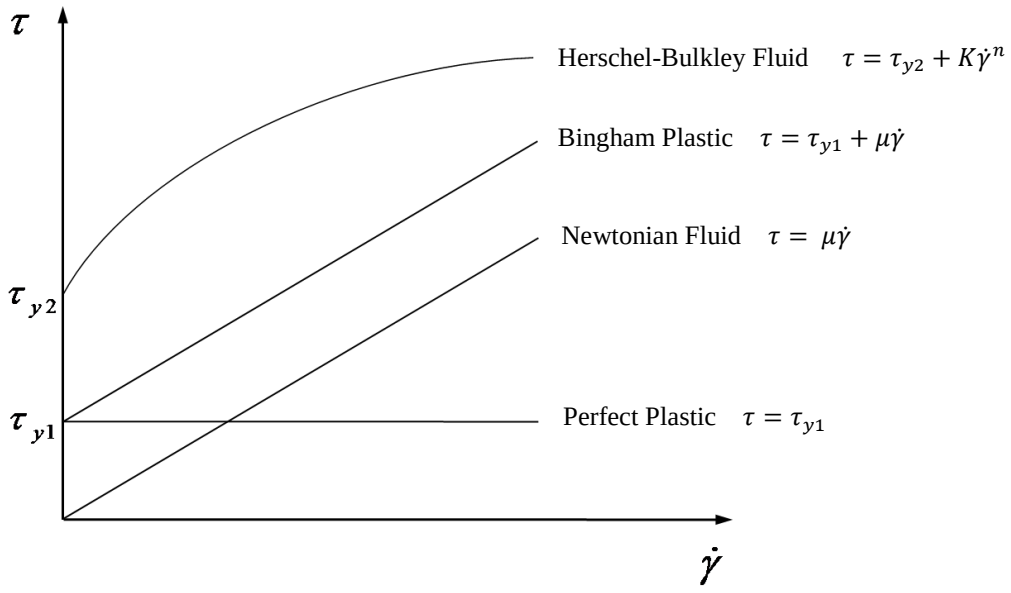

Figure 2.2 Characteristic flow curves for a range of model behaviours

When considering the characteristics of dense solid-liquid pastes, Wilson & Rough (2006) support the consensus that even time stable pastes are notoriously difficult to

control or characterise in standard rheometers. Instruments such as rotating parallel plate and cone or concentric cylinder viscometers are designed to handle much less viscous materials than pastes, where uniform shearing throughout the thickness of the sample can be ensured. Conversely, for dense pastes where particle interactions can be significant, Coussot (2007) describes the effect of *shear banding* that can occur in steady state cone and plate geometries due the existence of both a critical shear stress, τ_c and a critical shear rate, $\dot{\gamma}_c$ that must both be exceeded in order for steady homogenous flow to occur. At low velocities, the sample is instead composed of several layers in which the shear rate is equal to either 0 or $\dot{\gamma}_c$, thereby corrupting the interpretation of rheological data. Gujral & Sodhi (2002) support this limitation that rotational viscometers cannot be used to study such lumpy fluids as pastes for the additional reason that pulsating torque readings are exhibited.

When dealing with pastes or slurries of this nature, an alternative approach of *ram extrusion* or *capillary rheometry* can often be adopted instead, where the material is driven by a piston from a large barrel and extruded through a narrow die and capillary inducing shear within the length of the capillary. By varying the piston speed, the shear rate through the capillary can be controlled. The stress required to extrude the material through the capillary at the set shear rate is then measured via the pressure on the piston. For fluids where viscous effects dominate deformation and flow, provided corrections are made for entrance and exit effects, flow curves such as those described in Figure 2.2 can be constructed by controlling the shear rate (piston speed) in a stepwise fashion until stable stresses (pressures) are recorded for each shear rate.

For denser pastes where particle interactions are significant, Benbow & Bridgwater (1993) proposed that pastes could be characterised by incorporating a plasticity approach into the interpretation of capillary rheometer tests. Using their approach, the force required

to extrude a paste from a barrel of diameter, D_0 (m), through a concentric capillary of length, *L* (m), and diameter, *D* (m), is expressed as:

$$P = P_1 + P_2$$

$$= 2(\sigma_0 + \alpha V^m) ln\left(\frac{D_0}{D}\right) + 4(\tau_0 + \beta V^n)\frac{L}{D} \quad (4)$$

where *P* is the average extrusion pressure exerted by the piston (Pa) and *V* is the velocity of paste in the die land (m/s). The first term on the right hand side describes entry through the die using a simple plastic deformation result and the second term describes shear flow through the capillary, considered to be dominated by wall slip. From this equation it can be seen that six parameters ($\sigma_0, \alpha, m, \tau_0, \beta, n$) are required to describe the flow of a paste through ram extrusion.

Whilst both of the above approaches to paste characterisation have received widespread application for time stable materials, capillary rheometry tests of this nature are likely to prove unviable for crumb paste if the reported hardening post extrusion is found to be significant. Under these circumstances, this will be true of any test procedures that rely on taking a number of readings over a period of time in order to exert a range of stress environments and achieve characterisation.

It is clear from the literature that a universal approach to characterising pastes is elusive. A further form of characterisation that is widely used for pastes is the adoption of a complex shear modulus to describe the relationship between stress and strain. This concept, utilised commonly by dynamic oscillatory rheometry, considers an applied oscillatory stress or strain and both the magnitude and phase of the response, as shown in Figure 2.3.

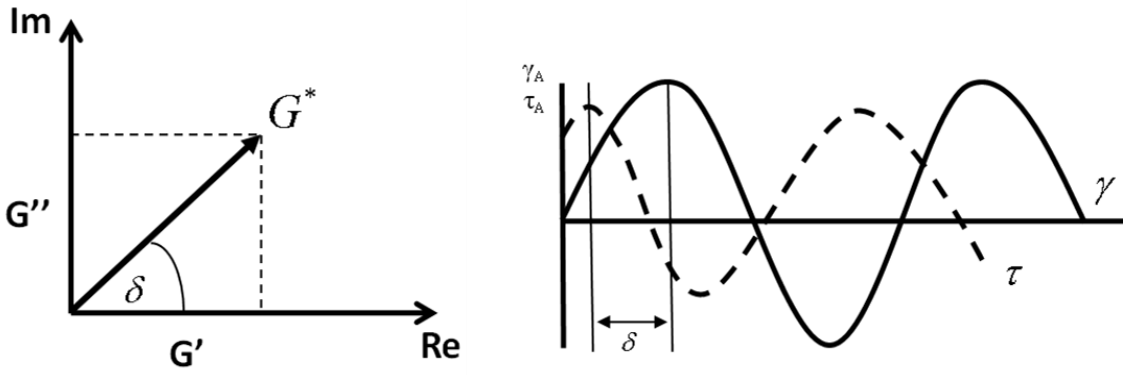

Figure 2.3 Illustration of the complex shear modulus (G^*) and the phase angle between stress and strain at small strain magnitudes for dynamic oscillatory shear rheometry

The complex shear modulus is then given by:

$$G^* = \frac{\tau}{\gamma} = G' + iG''$$

$$= \frac{\tau_A}{\gamma_A} cos\delta + i \frac{\tau_A}{\gamma_A} sin\delta \qquad (5)$$

$$tan\delta = \frac{G''}{G'} \qquad (6)$$

where *G'* is the elastic storage modulus (Pa), *G''* is the viscous loss modulus (Pa) and δ is the phase angle between shear stress and shear strain (degrees). The loss factor, tanδ, therefore provides information on the relative proportion of viscous and elastic behaviour apparent in a material when subjected to dynamic deformation. In the extremes, $\delta = 0°$ for a perfect elastic and $\delta = 90°$ for a Newtonian fluid. A spectrum of viscoelastic behaviour is then described in the range $0 \leq \delta \leq 90$. Since the parameters described are only valid in the linear viscoelastic range (LVR), dynamic oscillatory rheometry can be applied non-destructively.

2.2.2 Paste microstructure

It is shown in Figure 1.4 that crumb paste is prepared by adding water and liquid fats to a mixture of dry powders. It is therefore hypothesised that the formation of crumb paste microstructure may at least in part follow the formation of paste microstructure with increasing added water described by Newitt & Conway-Jones (1958).

With no liquid present, the dry powders behave as a frictional material with the shear stresses and normal stresses being interrelated. The first liquid added will then be adsorbed onto the surface of the particles to form a thin coating around them and the soluble powders will begin to enter the aqueous phase. Further liquid will then start bridging between the films at points of contact between the solid particles (known as the pendular state). This liquid bridging will provide the first cohesive forces which allow the mixture to retain its shape under a shearing stress. The next stage is the filling of the voids between the particles with liquid (funicular state). Once these voids are full (capillary state), additional liquid causes progressive separation of the particles. With only a slight excess liquid, the mixture is still able to retain its shape under low shearing stresses. Larger amounts of excess water produce a thick cream which readily flows under low stresses. With increasing water addition, the suspension properties tend towards those of the pure liquid-phase. In practice the liquid-phase rarely fills the voids completely due to the presence of entrapped air, making most pastes three-phase mixtures.

If Newitt & Conway-Jones' description of multiphase paste formation is considered to be relevant to the formation of crumb paste, it can be seen that a great variety of microstructures and rheological behaviours may be present, not only in extruded pastes of differing water contents, but also within the length of the extruder itself. Consequently, a greater understanding of how crumb paste microstructure is affected by

the process used to produce it and also how it evolves along the extruder is a pre-requisite for optimising the current method of mixing or designing alternatives.

2.2.3 Mixing mechanisms

When attempting to study mixing mechanisms of pastes or fluids within extruders, or other mixing devices, the mixing mechanisms occurring within the system can be broadly distinguished into two forms. In order to understand the mixing conditions necessary for a well mixed crumb paste, both forms of mixing must be considered.

The first is known as *dispersive mixing* and refers to changes in the physical properties of the material constituents on a micro scale and the breakup of agglomerates and particles within the material. The operative mechanism for this form of mixing is the existence of elongational forces and/or shear stresses (Van Zuilichem *et al.*, 1999).

Secondly, the *distributive mixing* is a reflection of the homogeneity of the material and refers to how evenly distributed the concentration of all components are within the material volume. The operative mechanism for distributive mixing is frequent stretching and reorientation of the flow (Alsteens *et al.*, 2004).

2.3 Twin screw extruders

2.3.1 Screw extrusion modelling

Owing to the growth of screw extrusion processing over the last sixty years, numerous studies have attempted to model the internal environment of both single and twin screw extruders. Some analytical solutions have been presented for the screw elements of a twin screw extruder, however the complex geometry of the kneading elements necessitates finite element modeling over analytical solutions. This in itself is

still a challenging problem with the complex moving geometry and changing boundary conditions. Where a successful model has been created, the degree of mixing taking place within systems is often assessed by tracking the experience of *virtual particles* released into the extruder and relating residence time distributions (RTD), shear stress histories and area stretch to draw insight into the mixing flows within extruders.

Of the modeling work available, most relates to inelastic, purely viscous fluids with little on the modeling of viscoplastic materials. Those examples of literature found include an analytical solution for a Herschel-Bulkley material in the screw elements only (which assumes unwound channels and generalized Couette flow) (Lawal & Kalyon, 1999) and a finite element model of a dough-like fluid in a single screw extruder (Dhanasekharan & Kokini, 2000). No finite element modeling of viscoplastic materials was found for either screw elements or kneading elements.

Finite element studies performed on mixing block design such as Alsteens *et al.* (2004) and Ishikawa *et al*. (2001) offer positive hypotheses about which designs are likely to promote better mixing performance for simple fluids, but often with no experimental verification. Instead, attempts to quantify mixing performance within extrders experimentally remain limited and are often constrained to simple Newtonian fluid flows. Low resolution visual techniques involving the addition of coloured dyes into model Newtonian fluids chosen for their visual clarity have been applied by Brod & Liesenfelder (2004) and Bigio & Wang (1996). Of the few authors that have attempted to quantify extruder mixing in industrial materials, rather than simple model fluids, the most common approach appears to be the addition of a tracer within the extruder. Examples were found where the concentrations of tracers in extrudates have been determined spectrophotometrically in a chemical granulation process (Van Melkebeke *et al.*, 2008)

and conductively in a glucose syrup extrusion (Van Zuilichem *et al.*, 1999) in order to establish variation from a target concentration and residence time distribution respectively.

Of the experimental studies referenced above, little of the knowledge learned is transferable to the extrusion processing of crumb paste as three of them relate to the mixing of Newtonian fluids only. The work of Van Melkebeke is most relevant to this study as it begins to consider the quantitative mixing performance of a granular material with liquid addition in geometries similar to those studied here. Unfortunately however, little insight into the evolution of mixing inside the extruder is gained from this work as only final extrudates were considered and the analysis used showed little variation between any of the processing conditions considered.

2.3.2 Extrusion processing of foods

The heavy bias towards the modelling of purely viscous fluids is likely to have been caused by the fact that the majority of modeling to date has been driven by the polymer plastics industry. Consequently, efforts have been largely focused on viscous fluids that are assumed to be homogenous throughout the section being modeled. The fact that these models are not always particularly relevant to the food industry is highlighted by Van Zuilichem *et al.* (1999) reporting that although a lot of knowledge has been gathered concerning mixing elements in the plasticating industry, incorporating this into the production of food products and other biopolymers (polymers produced by living organisms such as starch and proteins) is not always successful. Reasons cited for this include a drastic difference in feed composition, with oils, water and the presence of multiple solids which often interact strongly, melt indices that are less well defined than their chemical counterparts and finally, the degradation reactions that occur simultaneously

when a biopolymer is subjected to a temperature and stress field, changing the physical and chemical properties drastically from location to location.

In recent years, a number of authors have started to look at the effect of extruder operating conditions on various food products using Response Surface Methodology (RSM) such as De Pilli *et al.* (2008) and Pansawat *et al.* (2008). Here, primary (independent) extrusion variables such as barrel temperature, screw speed and feed moisture are used to examine the effect on secondary extrusion variables such as product temperature, die pressure, motor torque, specific mechanical energy and mean residence time as well as some physical properties of the extrudates. Second order polynomials models in the form of (7) are then used to generate contour plots of the experimental response of secondary variables with respect to independent variables:

$$Y = \beta_0 + \sum \beta_i X_i + \beta_{ii} X_i^2 + \sum \beta_{ij} X_i X_j \qquad (7)$$

where Y = experimental response of secondary variable, β_0, β_i, β_{ii} and β_{ij} are constants and regression coefficients and X_i and X_j are uncoded values of independent primary variables. Whilst this black box model approach is undoubtedly informative in an industry context, it offers little information on the mixing mechanisms and structural changes occurring within the extruder itself as is the additional subject of this study.

2.3.3 Internal effect of screw profile

Some of the key work most relevant to this project has been published after the commencement of this study. As was the observation of this author, Lertwimolnum & Vergnes (2007) reported the existence of only a few studies looking at the influence of screw profile and configuration on material properties in twin screw extrusion, as compared to the many studying the effects of processing conditions. It is encouraging to

see that one of the suggested methods of this study – stopping the extruder screws dead, before removing them to obtain samples along the entire extruder length – has already successfully been used by Lertwimolnum & Vergnes to investigate the influence of screw profile on the microstructure of a polymer nanocomposite. Whilst some clear observations on how the morphology evolved during extrusion were made in this work, the conclusions drawn relate specifically to polymer specific characterisations.

Following this, the earlier referenced work of Van Melkebeke *et al.* (2008) was published with a similar aim of documenting the influence of screw profile on a pharmaceutical wet granulation process, however this only considered the final properties of extrudate and dried tablets. It is hoped that work in this area can be extended by this study to the determination of multiphase food paste microstructures along extruder lengths.

2.3.4 Field of research

The field of research relevant to this project has been reviewed above and is also articulated well by Cheyne *et al*. (2005) who state that key mechanical parameters required for equipment design and operation principally involve the response of the material to deformation via shear, while key product quality parameters are related to the microstructure of the final form. Linking these two groups of data is not always straightforward, owing to the difficulties in quantifying the rheology and in measuring appropriate microstructural features. A lack of studies which aim to document quantitatively the statistics of the microstrucural distributions of industrially important materials and relate them to rheological behaviour is reported by Kalyon *et al*. (2006). The complexity of many naturally sourced materials means that these relationships can rarely be predicted in advance and facilitating the determination of these relationships for a

complex material for which no form of characterisation exists appropriately describes the scope of this work.

The first key challenge is to determine an obtainable and suitable form of rheological measurement for crumb paste which is capable of capturing the wide range of consistencies reported. As Cheyne *et al*. (2005) go on to say, many approaches to characterising soft solids require some kind of decision on the relative importance of yield and shear rate effects. Stiffer materials can be modelled as engineering plastics, while strongly shear rate dependent materials are often described using visco-plastic constitutive equations found in fluid mechanics. For intermediate behaviours, or processes which can display a wide variety of product consistencies from differing processing conditions, it is not always obvious which approach is most suitable for a given material on an *a priori* basis and will be one of the key considerations for this project.

The second challenge of this project will be to determine suitable methods of visualisation in order to determine paste microstructure, such that crumb paste evolution during the extrusion process may be better understood and microstructure may in turn be related to paste rheology.

Chapter 3 Off-line characterisation of crumb paste

This chapter presents the results of off-line studies on crumb paste using cone penetrometry and double cup density measurements. The goal of material characterisation studies on crumb paste is to develop characterisation tests which can provide insight into the process, whilst also offering the potential of a quality control measurement. With no existing characterisation methods for crumb paste available in either the reported literature or internally within the sponsor company, a preliminary attempt at characterisation is first required in order to gain a feel for basic material behaviour, such that a fuller characterisation may be considered. In particular, a hardening of crumb paste post extrusion has been reported by the company. If confirmed, the time scale of any such behaviour will have a significant impact on the approach and implementation of any future characterisation methods and is consequently of great interest here.

In this chapter, the use of cone penetrometry is proposed and discussed as a relatively quick and simple technique to perform a preliminary investigation of material consistency. Section 3.1 introduces the concept of cone penetrometry and describes the experimental method used in these preliminary investigations. Section 3.2 presents the preliminary results of penetration tests on crumb paste, whilst Section 3.3 considers dimensional analysis of the penetrations in order to obtain the fundamental material parameter of shear yield strength. Section 3.4 presents some observations about the

behaviour of crumb paste before finally discussing their implications for further characterisation in Section 3.5.

3.1 Cone penetrometry

Cone penetrometry is a rapid, yet empirical, method used in the assessment of soil samples and in the evaluation of food texture (De Man, 1983). It is designed to measure variations in firmness or consistency and in the context of food, has most typically been used in determining the firmness of fats. These fats have been assumed to display plastic behaviour, characterised by a minimum stress or yield value which must be exceeded to cause flow (Fearon & Johnston, 1989). As shown in Figure 3.1, the penetrometer consists of a cone, of angle α and vertical shaft assembly that is allowed to penetrate into a sample under the force of gravity for a standard time, after which the depth of penetration, p, is measured (Bourne, 2002). During penetration of the cone assembly, the cone moves into the sample until the stress exerted by the increasing contact surface of the cone is balanced by the hardness of the sample (De Man, 1983) and the kinetic energy of the falling cone absorbed by deformation of the sample. An empirical formula relating shear yield strength values to penetration depths was determined by Haighton (1959) for a wide range of margarine fats and shortenings, using a range of cone angles and weights. Successful correlation has often been reported between cone penetrometry data and both the rheological properties of butter and margarine (Haighton, 1959 ; Vasic & De Man, 1968) and sensory evaluations such as firmness (Dixon & Parekh, 1979) and spreadability (De Man *et al.,* 1979).

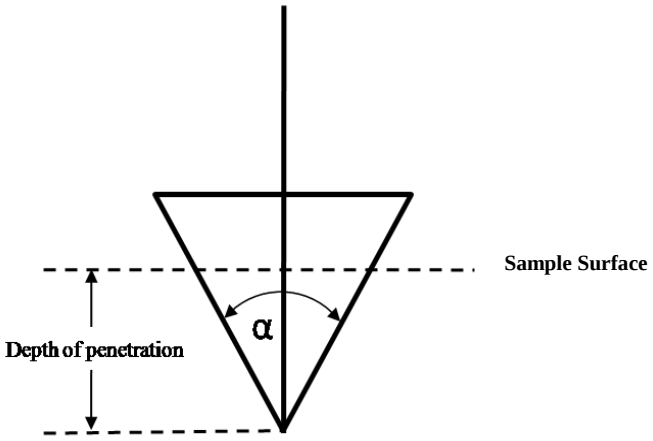

Figure 3.1 Cone penetrometer geometry showing depth of penetration, p and cone angle, α

The performance of cone penetrometry and the use of Haighton's formula as a gauge for determining butter spreadability was assessed by Fearon & Johnston (1989). When comparing the method to probe penetration and texture profile analysis, they reported that cone penetrometry successfully coped with the widest range of butter consistencies and was undoubtedly the most rapid and simple procedure to carry out.

The notion of a yield shear stress which must be exceeded in order to cause flow is one which is often used to describe the deformation behaviour of pastes. Coussot (2007) defines the yield shear stress, τ_y, to be the minimum shear stress making it possible to reach a deformation larger than the critical shear strain, γ_c, after which the initial configuration is irreversibly broken and the material has undergone the transition from solid regime to liquid regime. This results in observable flow with no *a priori* memory of the initial configuration.

Although the existence of a "true" yield stress in pastes is a widely debated topic within the literature, based on observations of extremely slow Newtonian flows with very large viscosities below apparent yield stresses (Barnes & Walters, 1985), many argue that the flows are negligible within time scales of observation and the use of yield as a parameter for paste characterisation is widespread (see Section 2.2.1). Consequently, a

deformation test of this nature was considered to be a suitable starting point for preliminary crumb paste characterisation. The moderate fat content in crumb paste and the practical success of cone penetrometry as a quality test for butters and margarines suggest that the assessment of crumb paste consistency may be a potential application of cone penetrometry.

3.1.1 Laboratory made (LM) crumb paste method

In order to assess the suitability of cone penetrometry as a form of consistency characterisation for crumb paste, tests have been performed on a range of laboratory made (LM) crumb pastes. LM paste is used by the company to replicate extruded crumb paste (detailed in Table 1.1) in smaller quantities for research purposes using a batch planetary mixing process.

The standard recipe for 2 kg batches of LM paste is shown in Table 3.1. With the exception of water content, all of the ingredients appear in the same relative proportions as extruded paste. The added water content is increased from 6% to 8% in order to try to compensate for the lower shear and temperatures experienced in an open planetary mixer.

Table 3.1 LM recipe by mass

Ingredient	Mass (%)
Sugar	51
Cocoa Mass Natural	10
Cocoa Butter (CCB)	2
Skimmed Milk Powder (SMP)	18
Lactose	6
Whey	5
Water	8

Dry ingredients were received from the company pre-blended in the correct proportions in sealed 25 kg sacks and are hereafter referred to as "blend". Once opened, blend was stored in sealable plastic containers away from heat or moisture. With the exception of water, materials added to the mixing bowl were added directly until the appropriate mass was achieved. No measuring into intermediate containers was made as significant residues made mass measurements inaccurate if not added directly.

The liquid ingredients of cocoa mass and cocoa butter were received from the company in solid form and melted in an oven at 65 °C, stirring periodically until smooth. The water used was Oxford tap water used at room temperature and weighed into a pouring cylinder before beginning the mixing process.

The mixing routine used to generate LM paste is shown in Figure 3.2 and was used in conjunction with a Crypto Peerless Industrial Planetary Mixer as shown in Figure 3.3. The water was added over thirty seconds to encourage uniform distribution. The final thirty seconds of mixing on the higher speed setting is designed to homogenise the paste.

Since added water content has been reported by the company to be one of the most significant factors affecting crumb consistency, it has been used here as the variable parameter in this preliminary work. Early attempts at making LM paste in the Oxford laboratory using the method in Figure 3.2 showed that the water content could be reduced no lower than 7% before forming a crumble rather than a paste. Since the purpose of the preliminary work is to devise a test capable of detecting consistency variations in the range likely to be experienced by the company, pastes with water contents ranging from 7% - 11% were investigated. Quantities of water to be added during mixing were determined by mass and the quantity of all other ingredients was fixed.

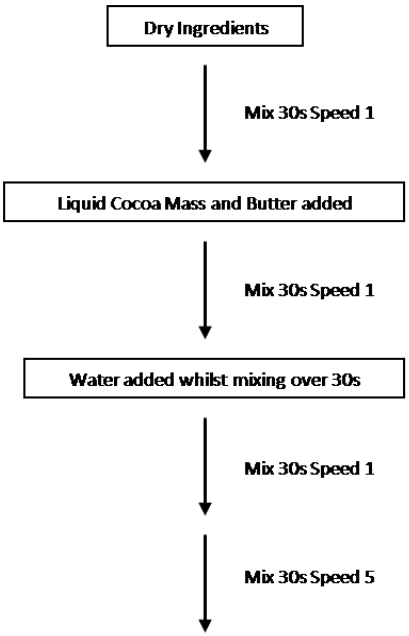

Figure 3.2 Mixing procedure for LM paste

Figure 3.3 Crypto Peerless planetary mixer

3.1.2 The penetrometer

The penetrometer used in this work was made by the Central Ignition Company, London and is shown in Figure 3.4. The 60 mm deep base made for use with this penetrometer has a 160 mm diameter and sits on a central locator upon which it can be rotated. The error in the vertical penetration depth calibration has been verified using vernier callipers to be within 1% for the full dial range.

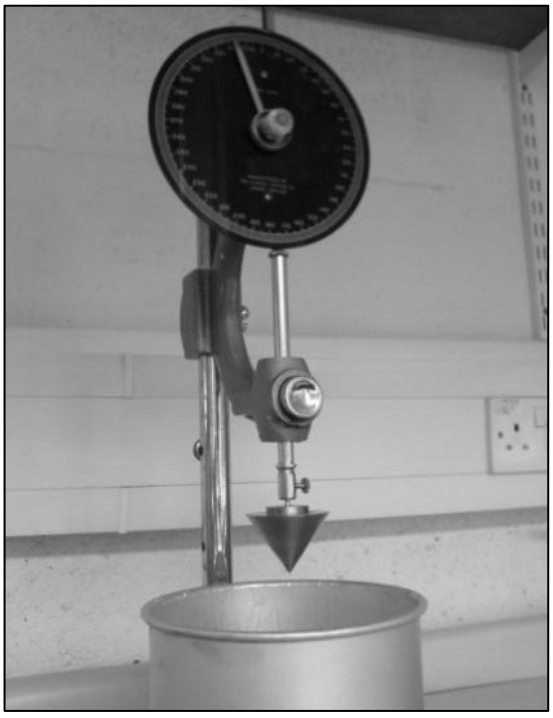

Figure 3.4 Central Ignition Company cone penetrometer

3.1.3 The penetration cones

A range of penetration cone angles and weights were used to investigate the most sensitive and repeatable assembly. The cone angles used and the corresponding cone assembly mass including the rod are shown in Table 3.2. The masses have been adjusted to provide the same assembly mass for two differing cone angles by filling the hollow penetration rod with appropriate amounts of lead shot.

Table 3.2 Cone angles & corresponding cone assembly mass used for cone penetration tests

Cone Angle (Degrees)	Cone Mass with Rod (g)
10°	80
30°	80
50°	251
70°	251

3.1.4 Experimental method

In the same way that the routine used to mix the paste must be performed consistently, so must the handling of the paste prior to and during testing. Once formed in the planetary mixer, the paste was immediately transferred into the metal base of the penetrometer where it was lightly compacted using a manual fixed weight press to create a flat and uniform surface. Whilst the penetration test would ideally be performed on samples that have undergone no compaction, the compaction was necessary in order to provide a flat and consistent surface from which accurate penetration depths may be determined. The consistent application of a fixed weight press to create this surface ensured that the same force history was experienced by all samples prior to testing. The paste samples were then left for 120 seconds to allow any residual stress from the compaction to dissipate before testing.

The tip of the penetration cone was first positioned at the material surface, ensuring it was away from the base wall and any previous penetrations to reduce end effects. Once positioned, the vertical measuring rod was lowered to the top of the cone assembly and the dial zeroed. At the point when a penetration reading was taken, the cone release button was pressed and held for twenty seconds. Haighton (1959) describes the use of penetrometry with butters and solid fats and suggests a penetration time of five seconds. However, early experimentation suggested the cones had not always stopped penetrating for the softer samples after five seconds and so twenty seconds was used instead. Upon

release of the cone release button, the cone becomes clamped in place restricting any further vertical movement. The measuring rod was then lowered to the new position of the cone assembly and the vertical penetration depth determined from the dial.

The penetration readings taken in this preliminary work were made at various time intervals in an attempt to observe the reported hardening of the paste after mixing and were taken at 150 s, 210 s, 270 s, 390 s, 510 s and 690 s. Six separate readings were therefore taken on each sample and were achieved by rotating the base after each penetration and positioning the cone tip on a fresh penetration site away from the wall and previously used sites. A fresh batch of LM paste was required for repeats of each water content and cone angle.

3.2 Preliminary results

3.2.1 Penetration-water content relationship

From the preliminary penetrations, profiles of penetration depth, p (mm), versus added water content, w (%), were constructed for each cone and time interval – an example of which is shown in Figure 3.5. Despite the extended release time of 20 s, for some of the heavier and sharper cones used on the wetter pastes, it was not always evident that the cones had reached an equilibrium position and so these data points were neglected.

These preliminary profiles suggested a non-linear relationship between penetration depth and water content. Whilst all data sets suggested the relationship was non-linear across the full range of water contents considered, this could not be confirmed measuring only four water contents. More refined profiles were consequently required in order to confirm the non-linear nature of the relationship.

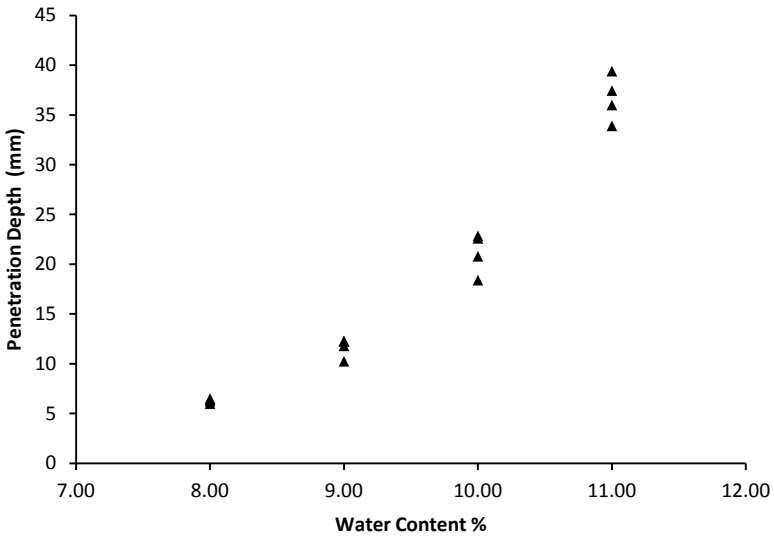

Figure 3.5 Penetration depth versus water content during cone penetration tests on LM crumb pastes at 690 s after mixing using 70° cone (251 g)

Time restraints limited further investigation to just one angle of cone and so the selection of a best performing cone assembly was made. Evaluation criteria dictated that a test setup should be sensitive and provide consistent, well correlated results. The sensitivity of each profile has been evaluated by taking the gradient value of a least squares linear fit to the data fit. Although the data does not correlate in a linear fashion, it is an arbitrary method from which a consistent numerical value indicating the average sensitivity can be obtained. The consistency of results and correlation were evaluated here by making the assumption of a power law fit (verified later) and taking the R^2 value.

In order to simultaneously assess the sensitivity and correlation of the differing cone assemblies and time intervals, an evaluation factor has been used:

$$Cone\ Evaluation\ Factor = \frac{S}{1 - R^2} \qquad (8)$$

where S is the sensitivity of the profile taken from the gradient of a linear fit and R^2 is the coefficient of determination from a power law fit. The arrangement of this factor means

that higher values indicate the most sensitive and well correlated data. Using this assessment, the 70° cone was the best performing of the four cones for all time intervals and was consequently used to produce a more complete penetration curve of water contents increasing in 0.25% increments. A more complete set of penetration curves was compiled using this cone at time intervals of 390 s, 510 s and 690 s only since equilibrium penetrations depths were not obtainable on the wettest samples before this time. The resulting penetration profiles appear to confirm the initial assumption of a power law relationship across the full range of water contents considered. Whilst the sensitivity of these profiles decreased with time interval, the consistency and correlation increased with time such that consistent cone evaluation factors were obtained for all three time intervals, ultimately suggesting that the overall robustness of the test did not increase or decrease significantly after 390 s. The more complete penetration profile for 690 s, confirming the power law relationship is shown in Figure 3.6.

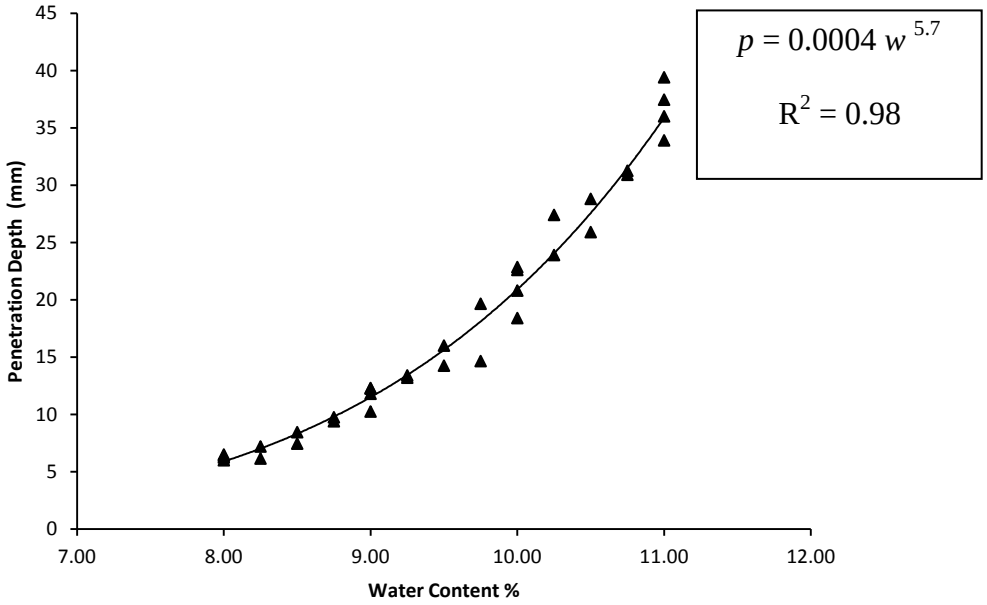

Figure 3.6 Penetration depth versus water content during cone penetration tests on LM crumb pastes at 690 s after mixing using 70° cone (251 g)

3.2.2 Reproducibility

Whilst reproducibility of penetrations obtained was generally good, there were cases of noticeable variation (see data points for 9.75% and 10% added water content in Figure 3.6 for examples). It was suspected that the variations lie in the somewhat inconsistent nature of making paste in an open planetary mixer – a view shared by the experience of the company. In order to assess the reproducibility of the test under an alternative set of controlled conditions, a day was spent taking fifteen sets of penetrometer readings on extruded paste from the main factory. Throughout the day, the paste was extruded at a fixed recipe in order to represent a control paste. Readings were taken at 180 s, 390 s and 510 s after extrusion with the 70° cone. Initial penetrations on the extruded paste using the 251 g cone assembly mass (used on LM paste) resulted in impractically low penetration depths, even before the paste had hardened significantly. Since the object of this investigation was to assess reproducibility of the test over a range of penetration depths, the mass of the cone assembly was increased from 251 g to 290 g in order to increase the early penetration depths. The results of the day are shown in Figure 3.7.

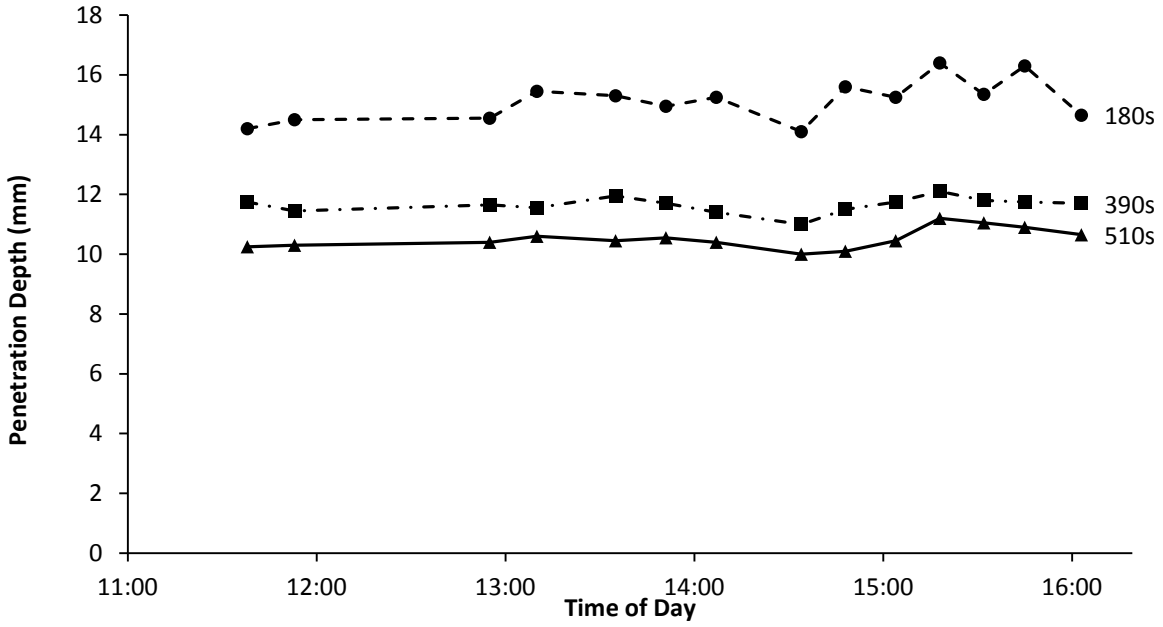

Figure 3.7 Cone penetration depths on factory extruded paste during working day using 70° cone (290 g), at 180 s, 390 s and 510 s after extraction

Although the extruder was run on a fixed recipe throughout the day, known variations in extruder feed and motor settings can occur. As such, printouts of the extruder diagnostics were retained in order to monitor operating condition fluctuations. Figure 3.7 shows the relative stability of penetration depths throughout the day for each time interval, with little variation in readings taken before 14:15 and an apparent increase in variability after this time. Inspection of the extruder diagnostics revealed steady conditions before 14:15, followed by an unusual spike in the milk powder feed rate to a value approximately 33% higher than the set level. Following this, significant fluctuations were observed from the otherwise stable motor current, suggesting either a changing consistency of extruded material or the build up and subsequent clearing of blockages within the extruder. Given this notable period of unstable paste extrusion, the penetration readings after 14:15 have been omitted as there is not sufficient confidence that the extruded paste represented an effective control during this time.

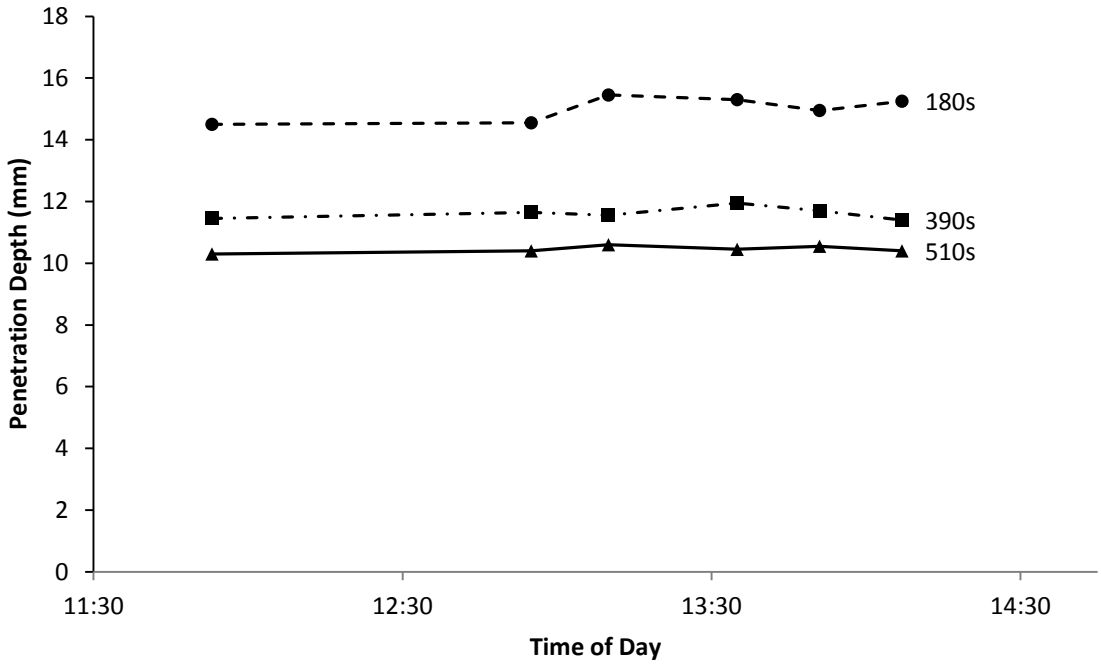

Figure 3.8 Cone penetration depths on factory extruded paste during period of stable extrusion diagnostics using 70° cone (290 g), at 180 s, 390 s and 510 s after extraction

Variability in experimental data is a common difficulty in characterising paste materials. This can often be attributed to material inhomogeneities that result from known paste phenomenon such as air pockets, agglomerates, phase migration, ageing, uneven packing, temperature sensitivity and drying (Cheyne *et al.*, 2005). Experimental variations from the mean as large as 10% are not uncommon (Amarasinghe & Wilson, 1999) and in this application have the potential to be further compounded by the inherent variability of natural food products.

For the data shown in Figure 3.8, the maximum deviation from the mean for six repeated penetrations at 180 s, 390 s and 510 s was 4.2%, 2.4% and 1.7% respectively. The consistent nature of these results show the method devised here is sufficiently robust to provide reproducible data for nominally identical systems. As such, the larger variation shown in some of the LM paste experiments is attributed to the variability of mixing powders and liquids in an open mixing system, rather than unsuitability of the

penetrometer method. As with LM paste, the degree of scatter in the data was noticeably lower on the readings taken at extended time intervals after preparation.

3.3 Determining paste shear yield strength from penetrometry data

The results so far have successfully shown that cone penetrometry tests have provided an observable correlation between cone penetration depth and crumb paste water content, implying that this simple method may be useful for observing variations in structural consistency. An empirical power law correlation between cone penetration depth and paste water content has been observed, however informed comparative analysis relies upon characterisation outputs which represent fundamental material parameters.

3.3.1 Haighton's formula

An empirical formula relating cone penetration depths to material shear yield strength values was determined by Haighton (1959) after plotting the yield values of a wide range of margarine fats and shortenings, as determined by unspecified independent instrumentation, against cone penetration depths on a double logarithmic plot for a range of cone angles and weights. His plot is reproduced as Figure 3.9.

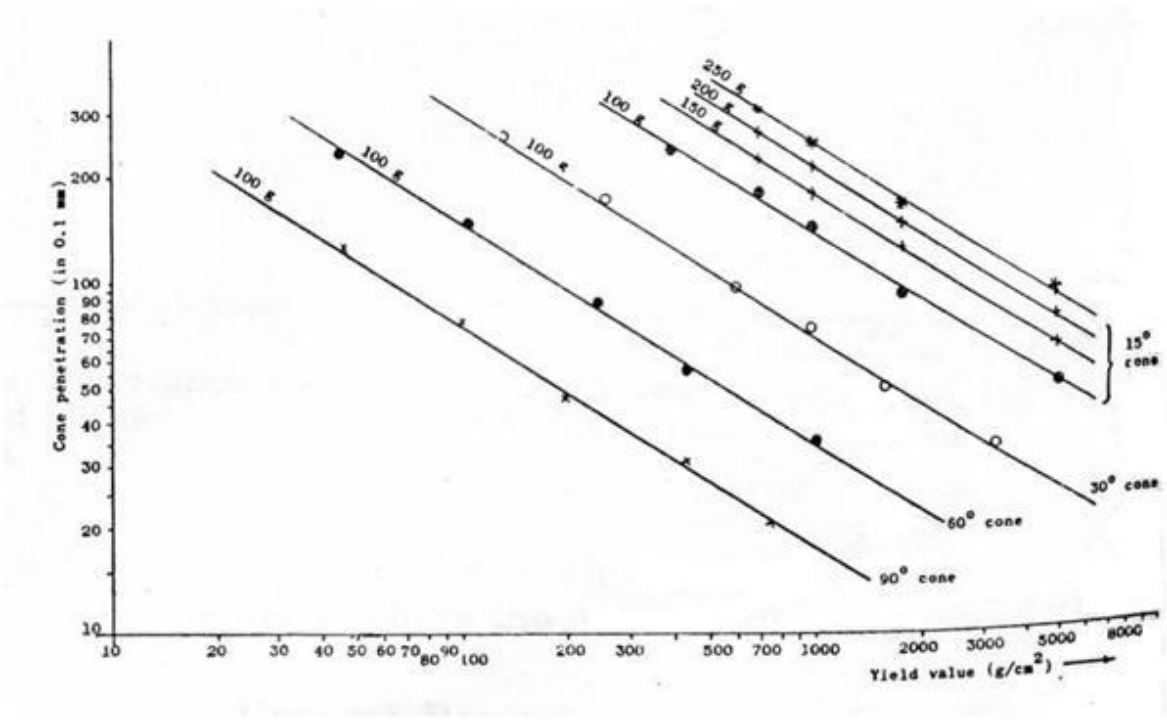

Figure 3.9 Double logarithmic plot of penetration depth versus shear yield strength for cone penetration tests on butters (Haighton, 1959)

From the straight and parallel lines evident in Haighton's plot, he inferred a relationship of the form:

$$Y = \frac{KW}{p^m} \tag{9}$$

using somewhat inconsistent units where Y = shear yield strength (g/cm^2), K = constant dependent on cone angle only, W = mass of the moving cone assembly (g), p is the penetration depth (0.1 mm) and m = a constant. Considering this relationship in the form:

$$log(p) = -\frac{1}{m}\, log(Y) + \frac{1}{m} log\,(KW) \tag{10}$$

allows for the calculation of a fixed value of m and K values for each cone assembly using gradients and intercepts, provided a sufficient number of cone angles and masses are used.

Haighton published mean values of his graphically determined values of the constant *K*, but reported large scattering in these values when using extremely soft and extremely hard samples. Haighton also reported *m* to equal 1.6.

3.3.2 Crumb paste shear yield using Haighton formula

When applying Haighton's formula to the crumb paste penetrometry data, the results were not viable. By considering all of the data collected and not just that of the 70° cone assembly, shear yield calculations were made according to Haighton's formula for each paste using the penetration depths of the 30°, 50° and 70° cones (Haighton did not publish a value of K for a 10° cone). In order for the calculations to be viable, yield calculations for similar pastes (i.e. the same water content and time interval) should be consistent, regardless of the cone assembly used. The large variation in calculated yield values using the differing cone assemblies is shown in Table 3.3 and is quantified using the relative standard deviation (RSD %) as given by Equation (11). The average RSD across all paste consistencies when considering the yield calculated by each cone assembly is 61.9%.

$$RSD\ (\%) = \frac{Standard\ Deviation}{Average} \times\ 100 \qquad (11)$$

Whilst some allowance can be made for the fact that planetary mixing did not generate identical pastes in each batch, this enormous variation in calculated yield renders them redundant and clearly shows that Haighton's formula is not transferable to crumb paste penetrometry.

Table 3.3 Shear yield strength calculations of similar pastes using cone penetrations depths obtained using three cone angels and the Haighton formula

Water content (%)	Time after mixing (s)	Shear yield calculation using Haighton Formula (kPa)			Relative standard deviation (%)
		30° cone	50° cone	70°cone	
8	150	101.1	34.9	-	68.9
8	210	133.0	42.3	-	73.1
8	270	158.6	48.3	37.2	82.5
8	390	205.7	60.0	47.1	84.5
8	510	261.6	72.7	55.6	87.9
8	690	315.1	88.1	70.4	86.4
9	150	27.5	12.9	-	51.2
9	210	36.2	15.9	-	55.0
9	270	43.8	19.1	12.0	66.8
9	390	56.9	25.3	15.4	66.6
9	510	72.9	29.1	19.3	70.6
9	690	92.6	36.4	26.3	69.0
10	210	12.4	6.9	-	40.3
10	270	15.7	7.5	5.4	57.0
10	390	21.2	13.4	6.9	52.0
10	510	25.7	11.7	8.1	61.5
10	690	30.8	14.9	10.1	58.2
11	390	5.84	-	3.2	40.3
11	510	7.05	5.3	3.7	31.5
11	690	8.57	5.9	4.2	35.4

3.3.3 Independent determination of shear vane yield strength

It was hoped that paste shear yield strength values would be obtainable directly from the rapid and simple technique of cone penetrometry. However since Haighton's formula has generated unviable results, an alternative method of yield strength determination was required to obtain paste yield strengths and re-assess any correlation with cone penetration depths. To achieve this, paste yield strengths were subsequently obtained using shear vane rheometry.

Shear vane rheometry records yield values by inserting a vane into the sample and applying an increasing torque at constant rotational speed. As the sample yields, the torque on the vane will peak and can be converted to a maximum stress based on the geometry of the vane. This represents the dynamic shear yield stress, τ_y, as the point where the structure of the paste begins to break down and flow in the fluid regime has been initiated according to the definition of shear yield in Section 3.1 Shear vane rheometry causes minimal disturbance to the sample when penetrating the probe and eliminates any possible wall slip effects from multiphase pastes since shearing occurs within the body of material (Barnes & Nguyen, 2001).

The shear rheometer available in this study was a Torvane hand held vane shear device which is used for the determination of shear strengths in cohesive soils and clay and is shown in Figure 3.10. The TORVANE includes three vane sizes in order to measure a wide range of shear strengths using a calibrated dial that records the maximum torque and converts it directly to a shear strength.

Before a reading is taken, the zero on the dial is reset and the TORVANE is pressed into a flat surface of the sample, at least two inches in diameter, to the depth of the blades. Maintaining a constant vertical pressure, the knob is turned at a constant rate of rotation such that failure develops in five to ten seconds. Once failure has developed, the spring tension is released slowly whilst the index mark remains in position to indicate the maximum shear value.

Of the three vane sizes available, the largest, most sensitive was used since most of the crumb paste was sufficiently soft. However, some of the harder paste samples were at the top end of the range for this vane and so for water contents 8% - 8.5%, yield strengths were additionally obtained using the intermediate vane size - intended for somewhat stiffer

soil samples - in order to verify that the larger vane measurements remained accurate when approaching the maximum range on the instrument.

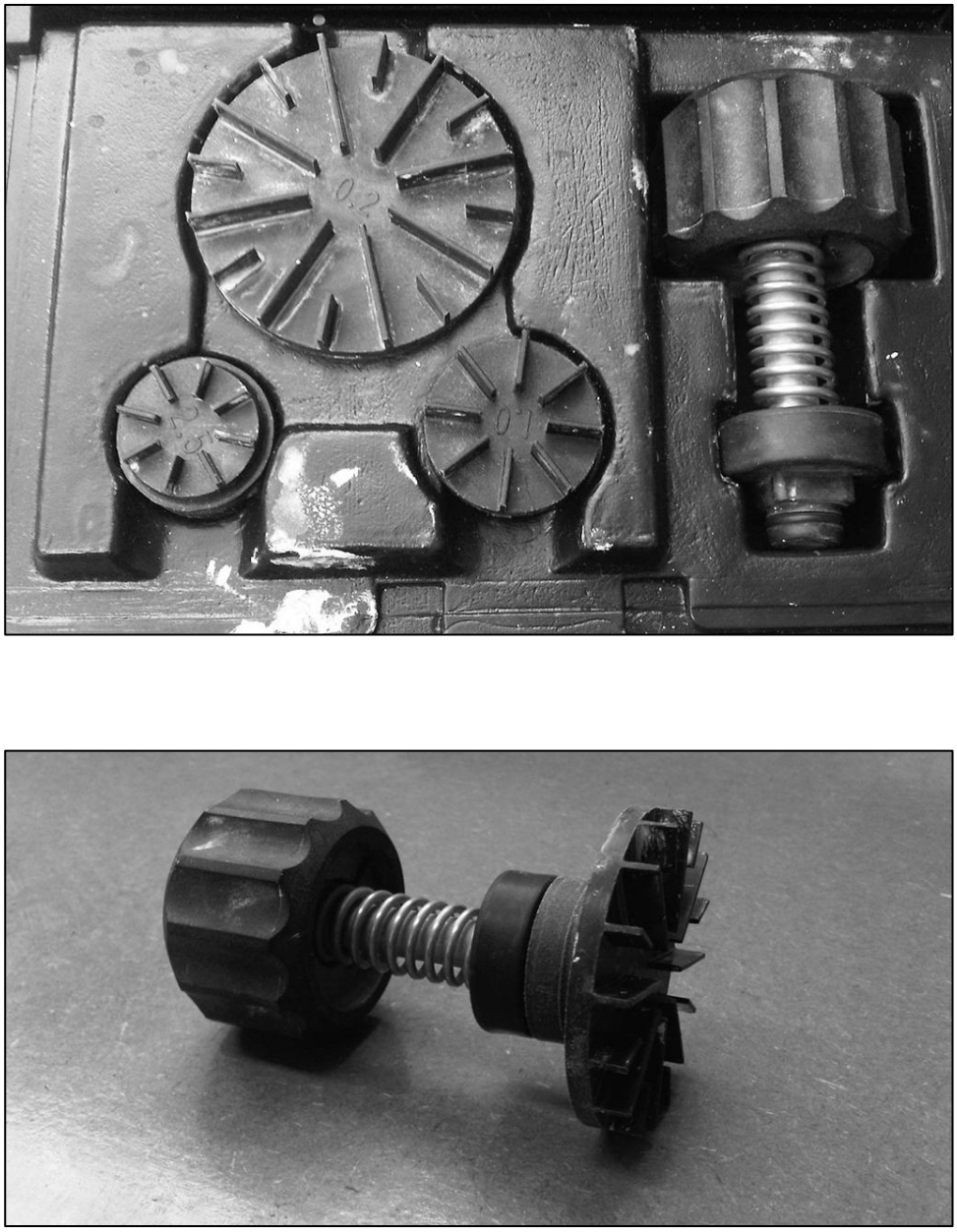

Figure 3.10 TORVANE Handheld shear vane with three different vane sizes

3.3.4 Independent observation of penetration-shear yield correlation

The double logarithmic plot of penetration depth versus shear yield strength using shear vane determined values of yield, rather than Haighton's calculated values, is shown

in Figure 3.11. The plots are somewhat similar in appearance to those obtained by Haighton (see Figure 3.9) with straight and almost parallel fits for each cone assembly. Despite the grossly different yield values calculated from the penetration depths using Haighton's formula (shown by the dashed dot lines in Figure 3.11), this suggests that the overall form of Haighton's formula may be appropriate to crumb paste, but with different constants or the inclusion of additional variables. This is investigated further using dimensional analysis in Section 3.3.5.

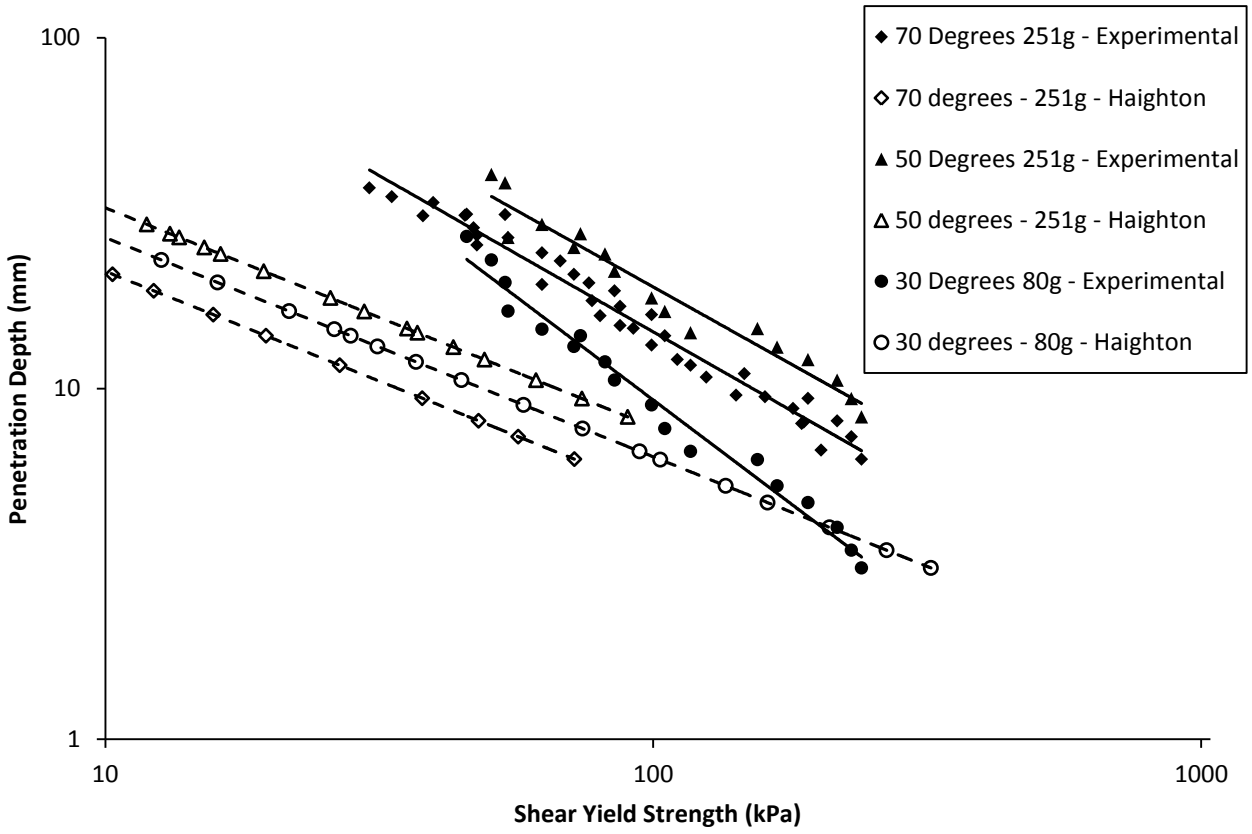

Figure 3.11 Double logarithmic plot of penetration depth versus shear yield strength for cone penetration tests on LM crumb pastes showing the large discrepancy between penetration depths predicted by the Haighton formula for each cone assembly and those found experimentally

The shear vane method used to obtain yield strengths could be used as a superior direct alternative to cone penetrometry. However, the equipment available for this study required practice to generate accurate, repeatable results and leaves too much margin for

experimental error with multiple operators. In comparison, cone penetrometry offers a more robust experimental method.

3.3.5 Dimensional analysis of shear yield-penetration correlation

The variables considered for a dimensional analysis of the shear yield-penetration correlation are shown in Table 3.4. Surface roughness of the cone will also be a relevant factor, but is not considered here since the stainless steel cones were cleaned before each penetration (as were Haighton's) in order to reduce the influence of friction as much as possible. Another source of influence will be the duration of penetration since with soft samples and small cone angles, penetration can go on for hours (Haighton, 1959), however only penetrations where the cone had appeared to have reasonably reached equilibrium are considered here.

Table 3.4 Variables in dimensional analysis of shear yield-penetration correlation

Variable	Symbol	Unit	Dimensions
Shear Yield Strength	Y	N/m^2 (Pa)	$ML^{-1}T^{-2}$
Cone Mass	W	kg	M
Cone Angle	θ	Degrees	-
Penetration Depth	p	m	L
Paste Density	ρ	kg/m^3	ML^{-3}
Acceleration due to gravity	g	m/s^2	LT^{-2}

In order to reduce the number of variables and consequently the number of dimensionless groups considered, a deep wide basin is assumed such the volume of paste displaced does not cause a rise in the surface level and the penetration depth is equal to the depth submerged. The penetration depth, p and cone angle, θ, can be combined into the volume of cone submerged, V_s by considering:

$$V_s = \frac{\pi}{3} r^2 p \qquad (12)$$

where *r* is the radius of the cone at surface level (see Figure 3.12).

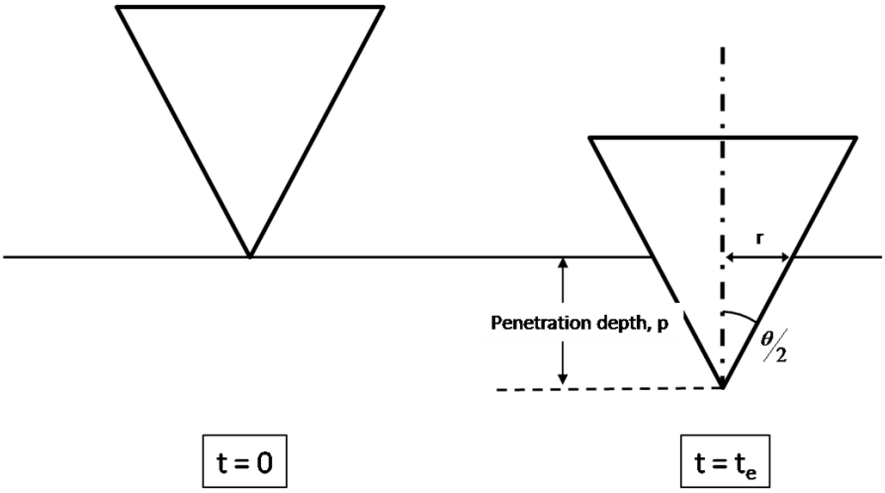

Figure 3.12 Cone geometry and positioning at time zero (t = 0) and time of equilibrium (t = t_e)

From Figure 3.12:

$$r = p\left[tan\left(\frac{\theta}{2}\right)\right] \qquad (13)$$

Substituting (13) into (12) then gives:

$$V_s = \frac{\pi}{3} p^3 tan^2\left(\frac{\theta}{2}\right) \qquad (14)$$

This combination of variables reduces the analysis to five variables with three dimensions, giving only two dimensionless groups to be considered. By choosing ρ and V_s as non-repeating variables, the two dimensionless groups shown in Equation (15) are the result with each an as yet unknown function of the other.

$$\frac{V_s Y^2}{gW^2} = \emptyset\left(\frac{Y^2}{\rho g W}\right) \qquad (15)$$

Assuming a function of the form:

$$\frac{V_s Y^2}{gW^2} = \propto \left(\frac{Y^2}{\rho g W}\right)^{\beta} \quad (16)$$

V_s can be expressed as:

$$V_s = \propto \left(Y^{2\beta-2}\rho^{-\beta}g^{-\beta+1}W^{-\beta+2}\right) \quad (17)$$

Then by substituting for V_s from (14), Y can be expressed in terms of all other measurable variables:

$$Y = \left(\frac{3 \propto}{\pi tan^2\left(\frac{\theta}{2}\right)}\right)^{\left(\frac{1}{2-2\beta}\right)} \rho^{\left(\frac{-\beta}{2-2\beta}\right)} g^{\left(\frac{-\beta+1}{2-2\beta}\right)} W^{\left(\frac{-\beta+2}{2-2\beta}\right)} p^{\left(\frac{-3}{2-2\beta}\right)} \quad `(18)$$

All that remains is to determine the constants ∝ and β, in order to define the relationship between dimensionless groups.

3.3.6 Paste density

In order to plot the dimensionless groups determined in Section 3.3.5, values of paste density are required. Little information on factory or LM paste densities was available from the company due to the common difficulties associated with accurately determining the sample volume of pastes of this nature for use in the standard density equation where ρ is density (g/cm^3), m is mass (g) and V is volume (cm^3) :

$$\rho = \frac{m}{V} \quad (19)$$

Consequently a method first presented by Campbell *et al*. (2001) for measuring the density of dough has been utilised in this work. The method eliminates the need to

measure the sample volume directly, by weighing samples both in air and whilst submerged in a fluid of known density.

Considering the force balance on a sample weighed in air (Figure 3.13), the apparent weight in air, w_{air} (N), measured by a balance is the downward force due to gravity minus the upwards buoyancy force caused by the displaced volume of air:

$$w_{air} = mg - \rho_{air} V g \tag{20}$$

As is common practice, the sample mass, m , is measured as the apparent mass in air, m_{air}, by considering the buoyancy force in air to be negligible due to its low density:

$$m_{air} = m \tag{21}$$

In contrast, the apparent weight of the same sample immersed in a reference fluid, w_{ref}, of known and significant density, ρ_{ref}, is given by:

$$w_{ref} = mg - \rho_{ref} V g \tag{22}$$

which simplifies to:

$$m_{ref} = m - \rho_{ref} V \tag{23}$$

By substituting for V from Equation (19) and m from Equation (21) the density of the sample can be accurately determined using m_{air} and m_{ref} :

$$\rho = \frac{m_{air} \rho_{ref}}{m_{air} - m_{ref}} \tag{24}$$

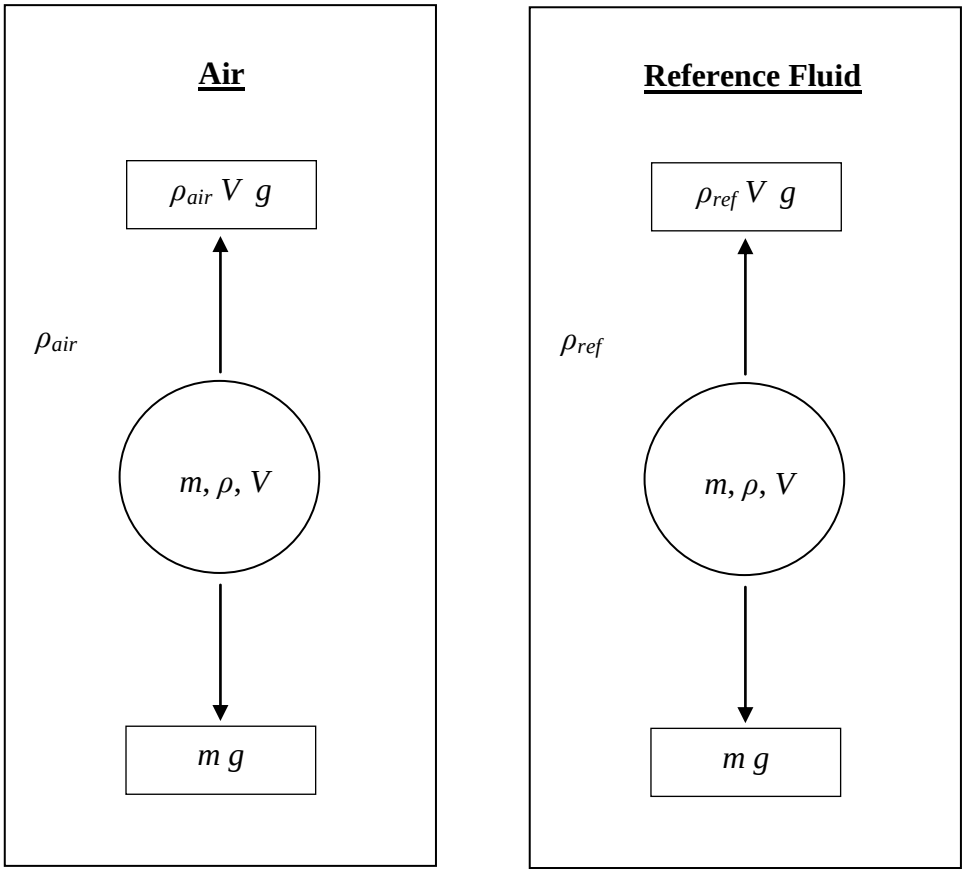

Figure 3.13 Force balance on sample in air and a reference fluid of known density used to determine paste densities using the double cup density measurement

The apparatus used to implement this form of density measurement is shown in Figure 3.14. A beaker of reference fluid was bridged across the balance plate of an Ohaus Corporation Adventurer precision balance without making contact. A wire frame with hanging double cup cone attachment was connected to the balance plate, which surrounded the beaker and allowed samples to sit in air or submerged in the reference fluid and transmit their apparent weight to the balance plate without contacting the beaker.

In this study, the reference fluid used was commercial vegetable oil as it was readily available and non-dissolving of the crumb paste samples. The density of the reference fluid was determined as 0.917 g/cm^3 using a Paar DMA 45 Calculating Digital

Density Meter which uses the highly accurate oscillating u-tube method for calculating the density of viscous fluids.

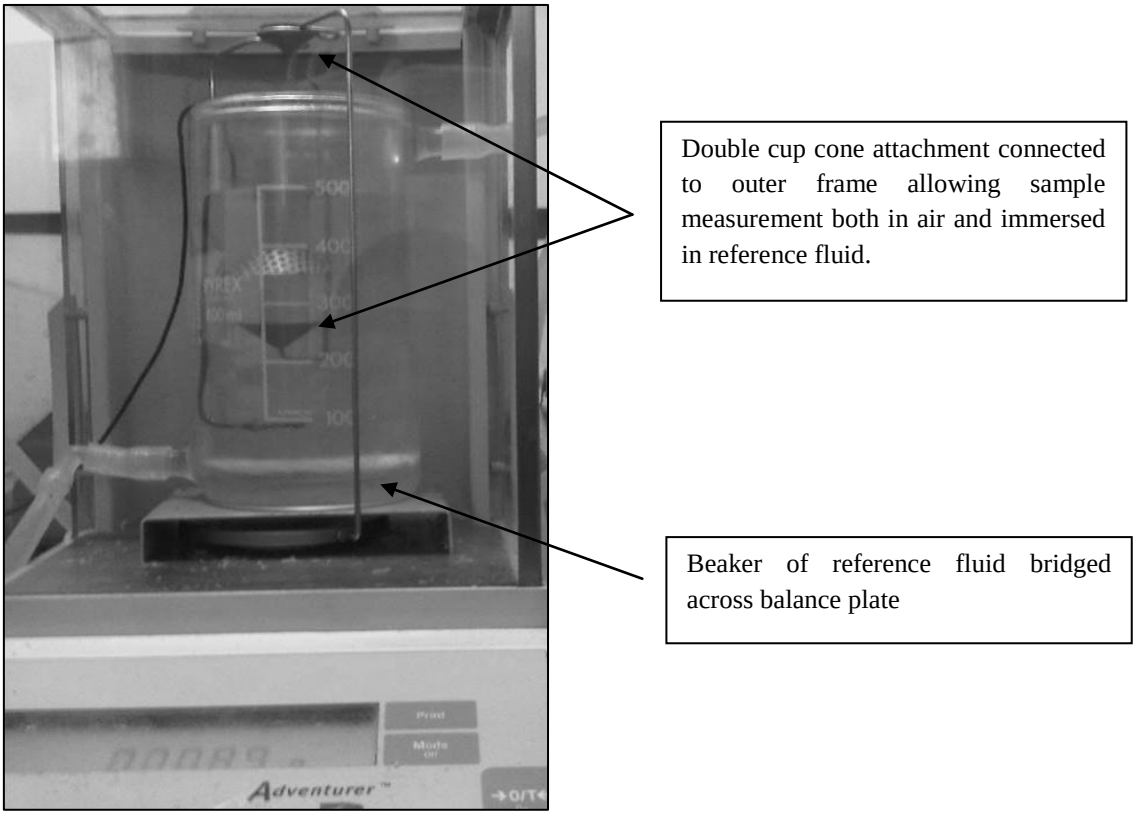

Figure 3.14 Double cup density measurement apparatus

Due to time constraints, obtaining density values for all LM paste water contents was not possible. Instead, three measurements were taken for 8%, 9%, 10% and 11% water and averaged. This data is shown in Figure 3.15. A quadratic polynomial fit with R^2 = 0.99 has been applied to estimate the density of the pastes with the remaining water contents.

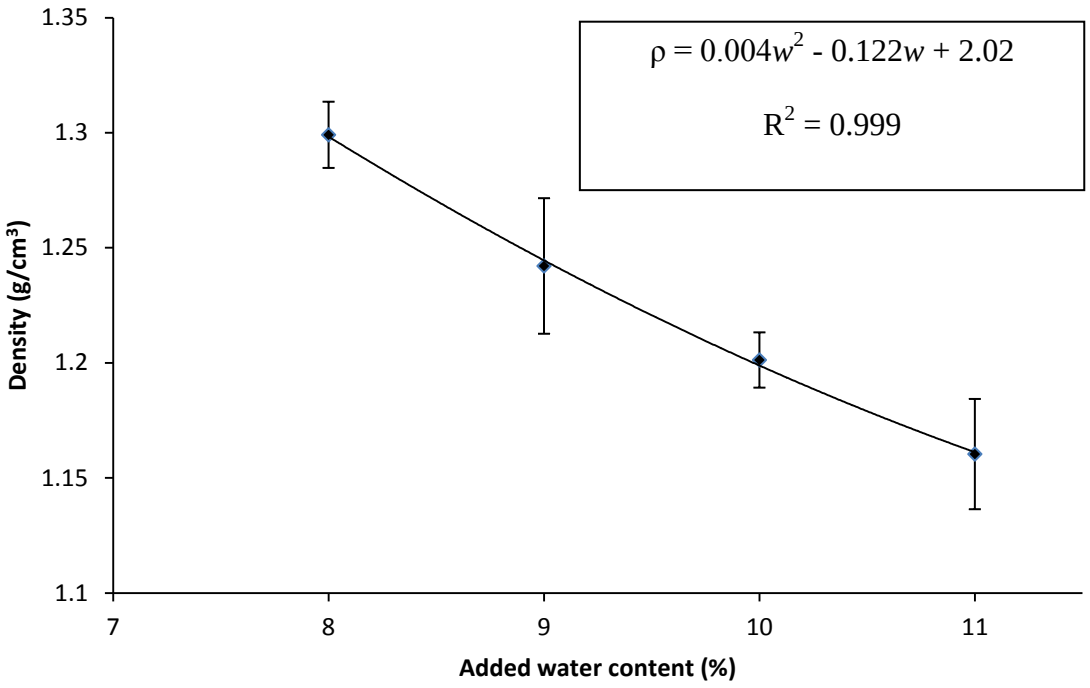

Figure 3.15 LM paste density variation with added water content as measured using double cup technique (error bars show standard deviation)

A plot of the dimensionless groups, based on the complete yield-penetration and density data is shown in Figure 3.16. All variables have been converted to base SI units. Recalling the assumption of a relationship between groups of the form given in Equation (16), a power law fit applied to the data gives the coefficient, $\propto$ =3.57 x 10^8 and the index, β= -0.66 with an R^2 value of 0.77. Assuming g to be constant, this gives:

$$Y = K(\theta)\,\frac{\rho^{0.2}\,W^{0.8}}{p^{0.9}} \qquad (25)$$

where

$$K(\theta) = \left(\frac{3.41\,x\,10^8}{tan^2\left(\frac{\theta}{2}\right)}\right)^{0.30}\sqrt{g}$$

In contrast to Haighton's formula, Equation (25) is presented in SI units.

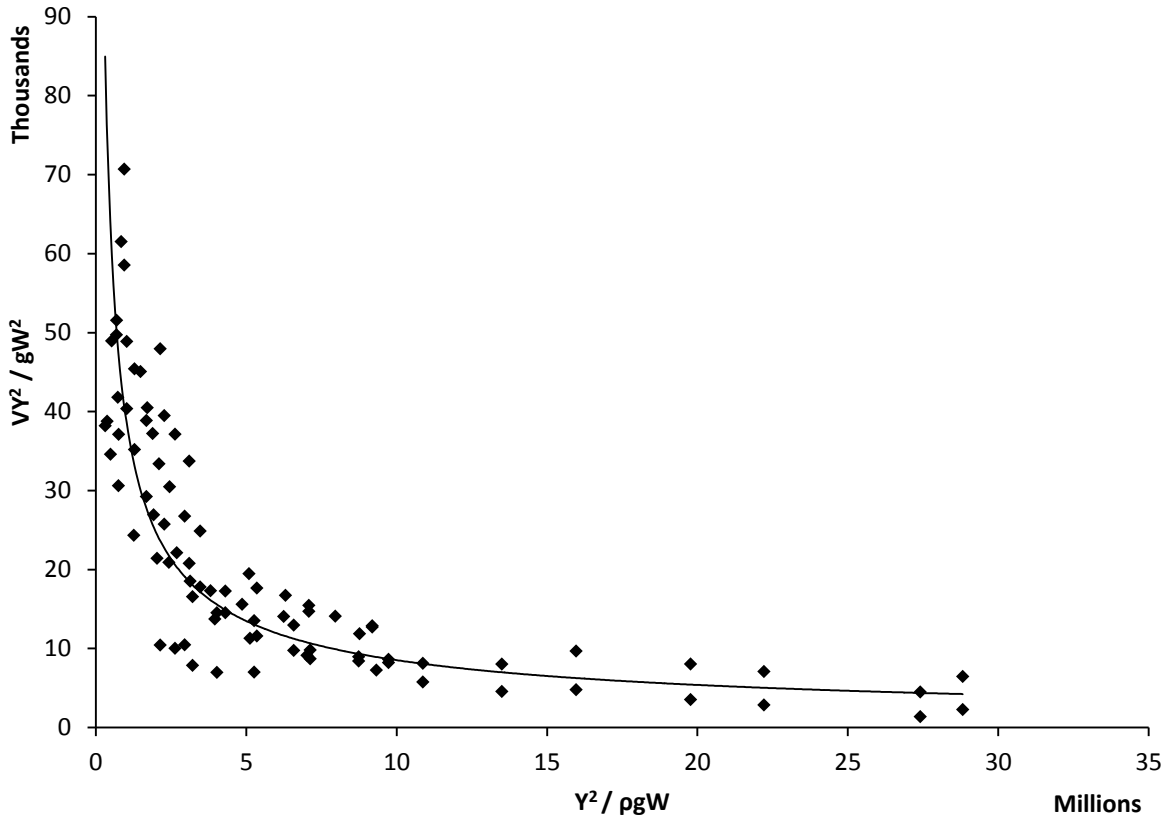

Figure 3.16 Plot of dimensionless groups used in analysis of shear yield-penetration correlation

3.3.7 Improving on Haighton's formula

Shear yield-penetration plots are shown for the four cones in Figure 3.17 - Figure 3.20, comparing experimental plots with those modeled by Equation (25) and the original Haighton formula. These plots are now plotted on linear scales in order to show the effectiveness of each model more clearly. Whilst the values of yield measured are orders of magnitude higher for crumb paste, these plots are similar in shape to those determined by Bauer *et al.* (2007) who plotted shear-yield penetration plots for mortars, having also determined shear yield using vane tests. The plots for the 10° cone (Figure 3.17) do not include Haighton calculations as he did not publish K values for a cone this sharp.

Equation (25) predicts the yield strengths closely for all cone assemblies used and provides a significant improvement on those calculated by Haighton's formula. The largest deviations from the semi-empirical model of Equation (25) occur on the softest samples using the 10° cone (Figure 3.17). The over-prediction of penetration depth for a given yield strength of the softer samples using the 10° cone would suggest that the cones used in the penetration experiments had not yet reached their equilibrium position. This is not surprising since it relates to the softest samples and the sharpest cone. As was demonstrated with the use of Cone Evaluation Factors in Section 3.2.1, the two flatter, heavier cone assemblies appear to have been the more robust assembly over the entire range of yield when compared to their sharper, lighter counterparts.

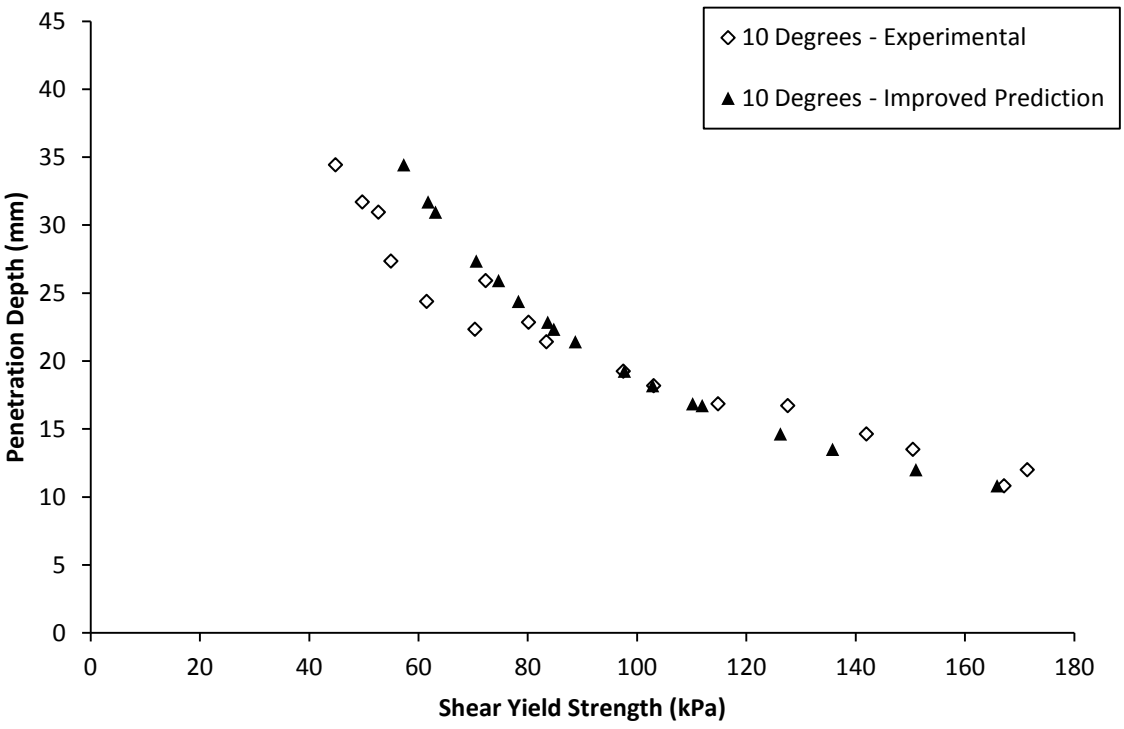

Figure 3.17 Experimental and modeled shear yield-penetration plots for 10° cone penetration tests on LM crumb paste

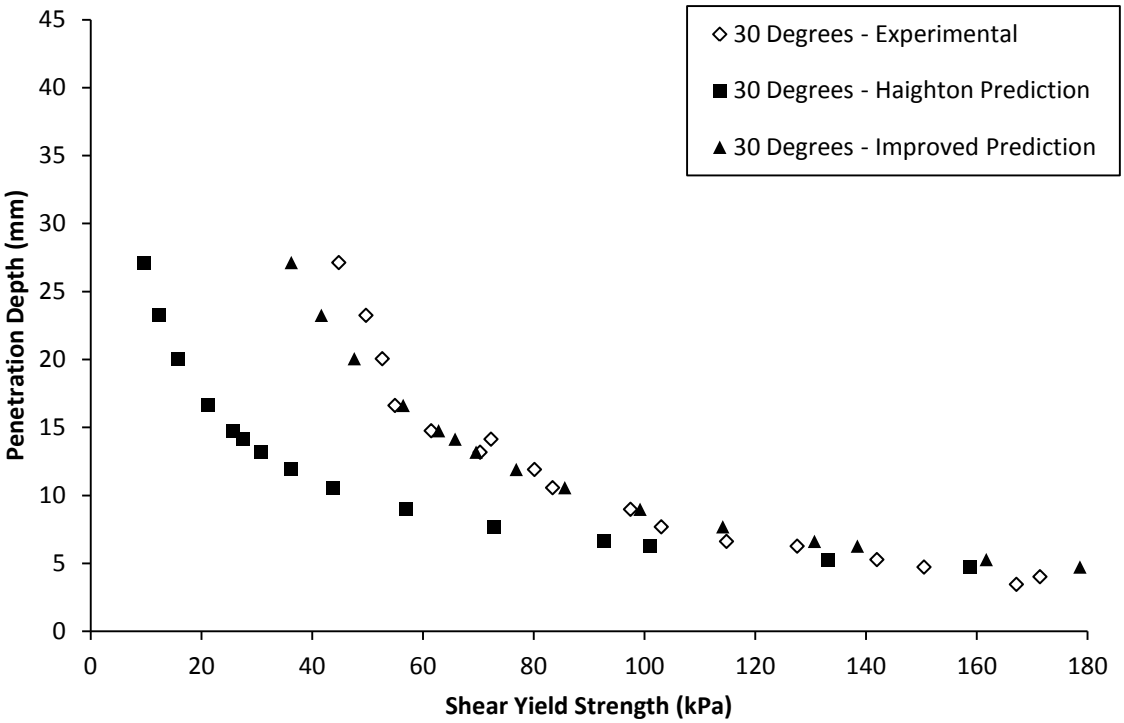

Figure 3.18 Experimental and modeled shear yield-penetration plots for 30° cone penetration tests on LM crumb pastes

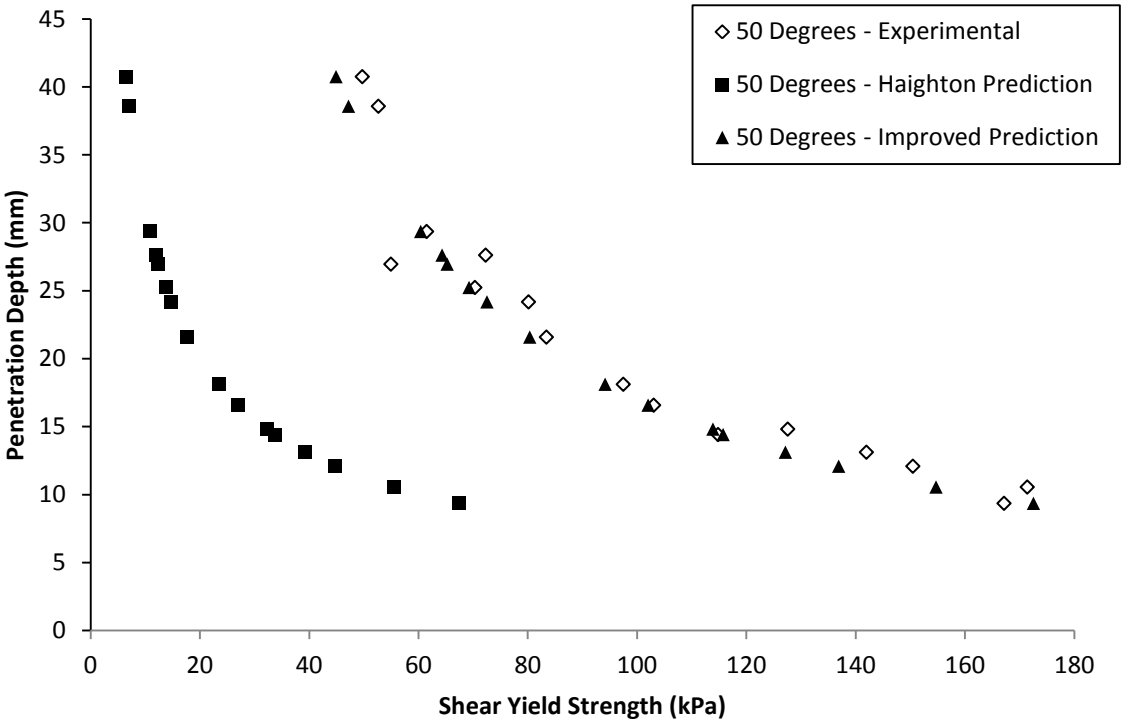

Figure 3.19 Experimental and modeled shear yield-penetration plots for 50° cone penetration tests on LM crumb pastes

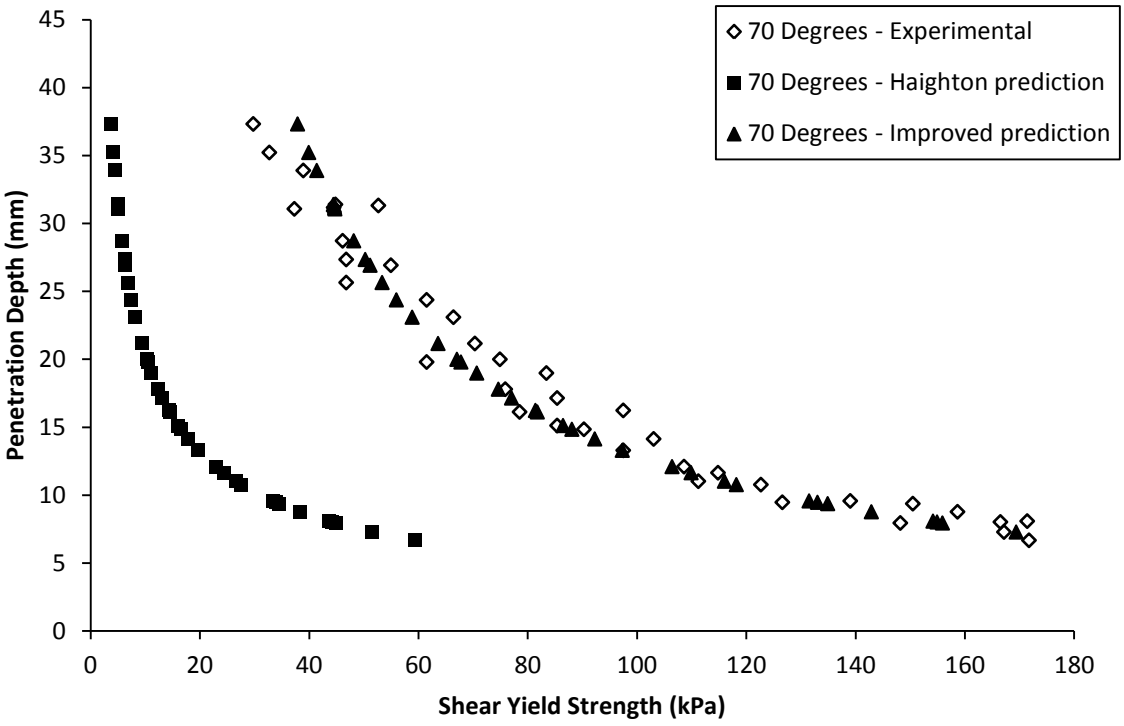

Figure 3.20 Experimental and modeled shear yield-penetration plots for 70° cone penetration tests on LM crumb pastes

3.3.8 Accounting for discrepancy between Haighton's formula and experimental values

Equation (25) and Haighton's formula (9) show similar forms of equation, albeit with a slight variation in the mass index and a significantly different penetration index (value of *m*). A simple evaluation of *m* as a variable material parameter might account for the large discrepancy between Haighton's prediction of yield and those obtained experimentally. However, altering the Haighton's formula to m = 0.9, as determined in Equation (25) only serves to over-predict yield values so greatly that they do not appear on the scale of the shear yield-penetration plots shown above.

Further exploration of cone penetrometry analysis revealed a review of interpretations for cone penetrometry consistency measurements of fats conducted by

Hayakawa and De Man (1982). Of the studies available to them (Rebinder & Semenenko, 1949 ; Haighton, 1959 ; Mottram, 1961 ; Vasic & De Man, 1968 ; Walstra, 1979 ; Dixon & Parekh, 1979) they surmised that although each of the suggested expressions for hardness was unique, each could be expressed in the general form of:

$$H = C\,\frac{M}{p^n} \qquad (26)$$

where H = a value of hardness or yield, C = a constant depending on cone geometry, M = mass of penetrating assembly, p = depth of penetration and n = an exponent.

Dimensional analysis for crumb paste penetrations has produced a shear yield-penetration correlation that for the most past conforms to the general expression of Equation (26). However the exponent of mass was determined here to be 0.8 rather than 1. In addition to cone angle and mass, this analysis has considered the possible influence of sample density on the shear yield-penetration correlation and has shown it to be a potentially relevant variable, appearing in the final form of Equation (25). Haighton makes no reference to the density of the butters and margarines used in his study, but an unconfirmed source claims butter density to be approximately 0.87 g/cm^3 (Densities of miscellaneous solids, 2011). If the density values of crumb paste (approximately 1.2 g/cm^3) are therefore assumed to be substantially higher than the butters used by Haighton and yield is assumed to be proportional to a positive exponent of density as found in this analysis, then values of yield corrected for density from Haighton's formula would be higher than those originally calculated, shifting them closer to those values found experimentally. It is impossible to say how much this hypothesis would account for the under-calculated values of yield from Haighton's formula without density data for Haighton's experiments, however it is unlikely to account for the full discrepancy.

3.4 Crumb paste observations

3.4.1 Crumb paste shear yield variation with water content

The first observation to be made from this preliminary work is the high sensitivity of paste yield to added water content. Figure 3.21 shows approximately a 75% decrease in shear yield strength for only a 3% increase in water in LM pastes tested 390 s after mixing. This demonstrates the potentially large range of consistencies that is likely to need characterising when considering the range of operating conditions used and investigated by the company.

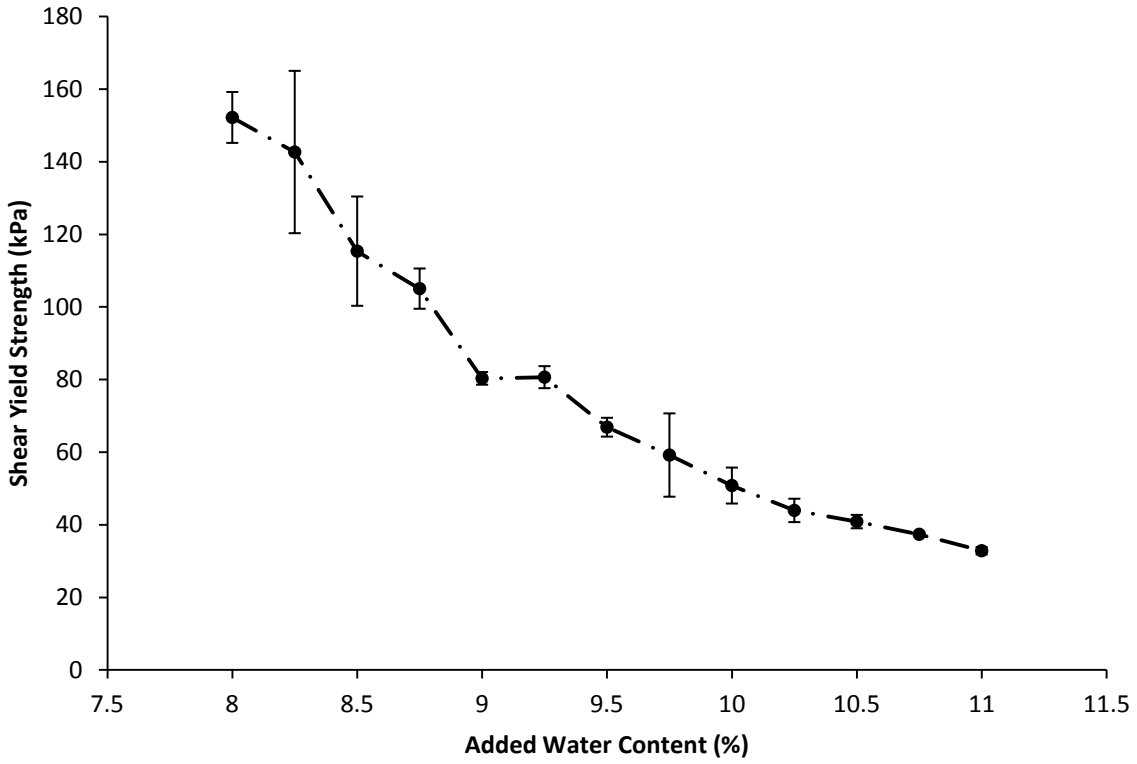

Figure 3.21 Shear yield strength determined by cone penetrations versus added water content for LM pastes at 390s after mixing (error bars show standard deviation)

3.4.2 Crumb paste hardening

Figure 3.22 shows an increasing shear yield strength with time after mixing for a range of LM pastes and confirms the existence of significant post mixing hardening as

reported by the company. This time dependent hardening is significant, with the standard 8% water LM paste showing a near doubling of shear yield strength after only 11 minutes.

Although the finite transfer time of samples to the penetrometer means there is no data to show it conclusively, the trend of hardening suggests that the rate of change may be most significant immediately after mixing. This has significant implications for the use of methods employed for further characterisation that are discussed in Section 0.

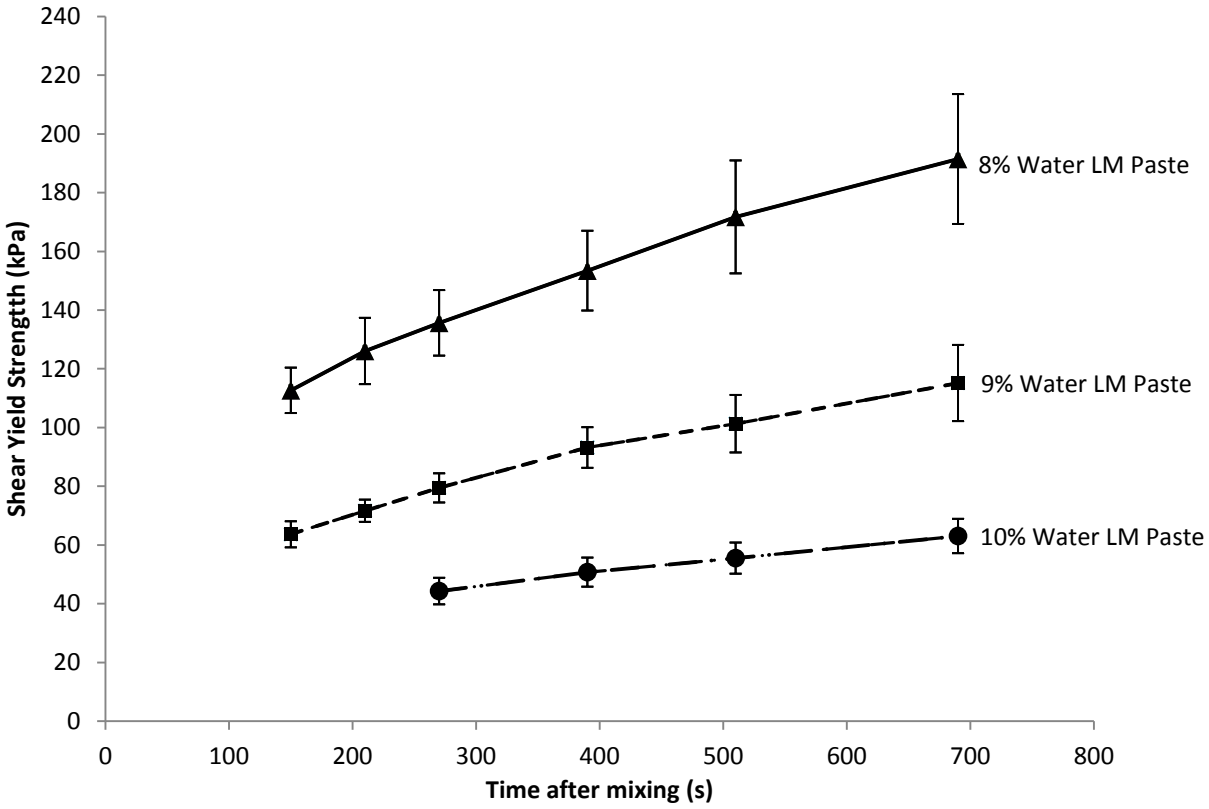

Figure 3.22 Shear yield strength determined by cone penetrations versus time after mixing for LM pastes of differing water content (error bars show standard deviation)

The exact cause of this hardening effect is unknown and it is unclear whether it relates simply to the crystallisation phase change occurring in the molten cocoa fats or whether there is a more complex interaction taking place between ingredients. In order to determine whether the onset of paste hardening was temperature dependent and could therefore by prevented for the purposes of characterisation testing, a sample was left at

room temperature and tested periodically for thirty minutes. A similar sample was then tested in the same fashion, but returned to a container in an 80 °C water bath between penetrations to replicate the approximate temperature of crumb paste as it leaves the extruder. The results of this are shown in Figure 3.23 and clearly show the onset of hardening irrespective of temperature, albeit at a possibly slower rate.

Due to the lack of repeat samples in this data, the maximum standard deviation in results obtained throughout all of the earlier cone experiments has been applied as error bars to each of the room temperature data points. As almost all of the 80 °C held samples sit approximately on or just below the maximum standard deviation bound, the lower bound on the confidence that the temperature held sample hardened at a slower rate is approximately 70%.

It would be expected that the crystallisation of molten cocoa fats would be prevented, or if already initiated, reversed by increasing the temperature to 80 °C. This would not necessarily be the case if the crystallisation of any dissolved sugars from solution made a significant contribution to hardening

These results serve to show that the hardening effect may well be a combination of a crystallisation phase change of the fats (potentially explaining the slower rate of hardening for the water bath sample) and also of non-reversible crystallisation or ingredient interaction/reaction, however it would appear that non-reversible crystallisation or ingredient interaction/reaction is the dominant cause of hardening, shown by the continued onset of paste hardening when maintained at 80 °C.

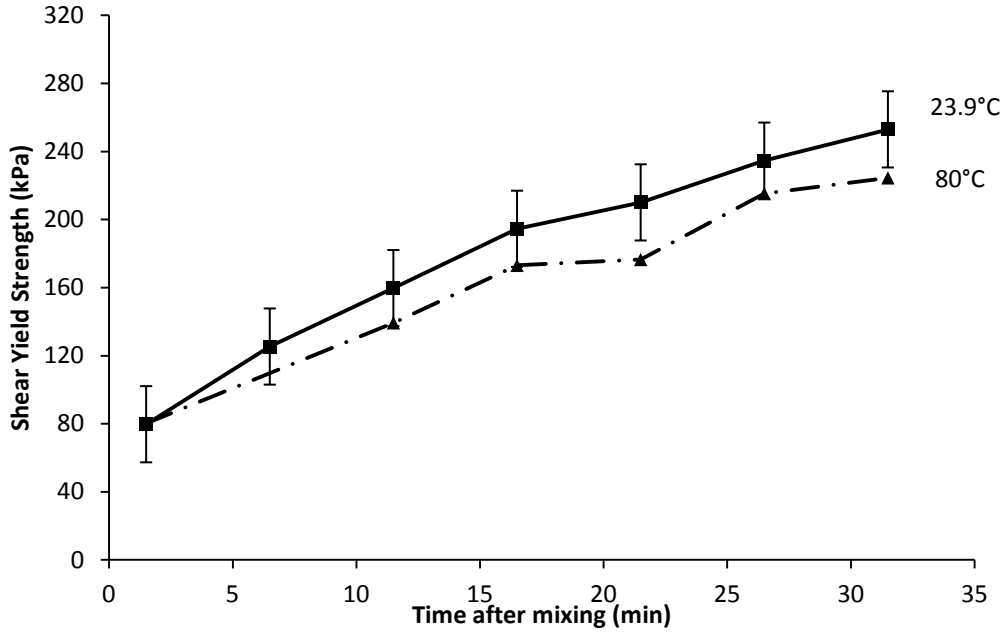

Figure 3.23 Shear yield strength determined by cone penetrations versus time after mixing for LM paste kept at room temperature (23.9°C) after mixing and in an 80 °C water bath after mixing

During the removal of paste samples from the penetrometer base after testing, it was also observed that seemingly less hardening had occurred on the sample surfaces which were unexposed. An example of the differing surface appearances is shown in Figure 3.24 and suggests that one of two things may be occurring:

1. Paste drying caused by free water disassociation at surface.
2. Interaction/reaction between ingredients that requires or is accelerated by air.

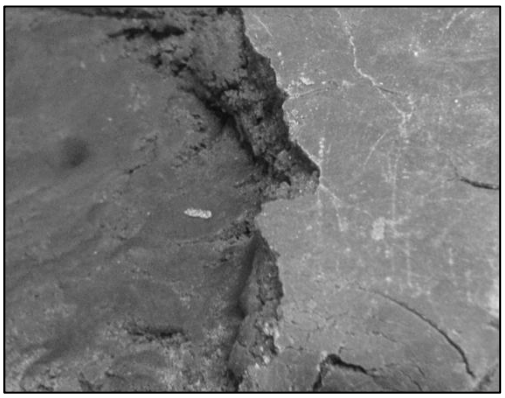

Figure 3.24 8% water LM paste appearance showing soft internal bulk and hardened surface exposed to air (width of image 100 mm)

Alternatively, the first suggestion above could be a consequence of the second. It is of interest that throughout preliminary cone penetration experiments, a temperature probe was placed into the paste samples in order to ensure a consistent temperature from mixing. On completion of each mixing routine, the LM paste temperature was dependent on water content, but remained approximately 30 °C. However it was noticed that the temperature near to the surface continued to rise by a few degrees long after mixing, despite being in cooler, room temperature surroundings.

In order to confirm this observation, sixteen minute temperature profiles were taken in the bulk of LM paste and factory extruded paste after mixing. These profiles confirmed the original observation, with LM paste rising approximately 1.5 °C and still continuing to rise at the end of the sixteen minutes. A similar test performed on the much hotter factory extruded paste (≈70 °C) showed a similar trend, rising 3 °C and taking approximately nine and a half minutes to peak.

These modest, but extended temperature rises post mixing suggest the possibility of an exothermic interaction/reaction occurring within the paste once mixed, however further work to determine the exact nature of crumb paste hardening is beyond the scope of this project. Instead, the post mixing hardening will be regarded as a complex material phenomenon that must be considered when designing and implementing characterisation methods. Suggested work to further investigate the observations made here could include the use of a wireless temperature probe to investigate rising paste temperatures. Here a probe, the size of a small coin, would be inserted into the paste where it responsively records the bulk temperature experienced for a predetermined length of time. The probe is then removed and the temperature data downloaded to a computer, which would provide more accurate and reliable information about this apparent prolonged temperature rise.

The potential air dependence of hardening could be investigated by placing paste samples in an inert gas chamber (a vacuum would draw moisture out of the paste), before conducting penetrometry tests and comparing them to a control paste left out in air. The development and application of an imaging technique which is capable of imaging crystal structure in real time and immediately after a sample is mixed would also likely provide insight into any structural changes occurring during this initial period of hardening.

3.4.3 Factory extruded paste

Cone penetrometry was also used to provide evidence of significant and rapid post extrusion hardening in standard 6% water factory extruded paste. The increasing yield strength with time is shown in Figure 3.25. In this preliminary work, the factory extruded crumb pastes were more fluid than the model LM paste showing lower values of yield, but demonstrating a similar rate of hardening. The comparison between extruded crumb paste and replicated LM crumb paste is discussed in more detail in Chapter 7.

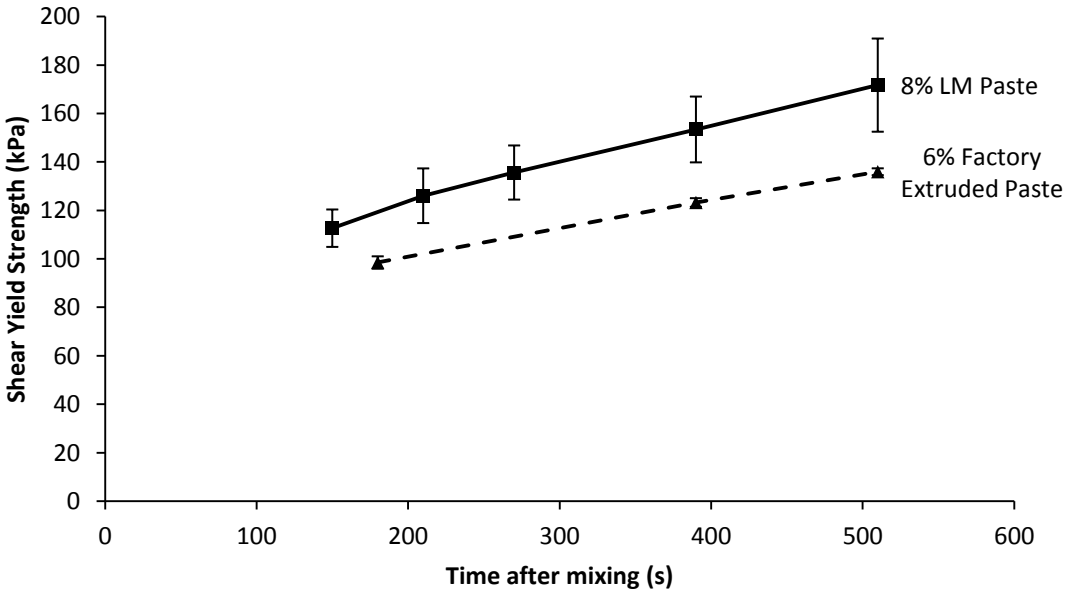

Figure 3.25 Shear yield strength as determined by cone penetrations versus time after mixing for 6% water factory extruded paste and 8% water LM paste (error bars show standard deviation)

3.5 Conclusion

It has been shown in this preliminary work that Haighton's formula for obtaining shear yield strength from cone penetrometry data is not applicable to crumb paste and its use in stiff paste applications is therefore not universal. An alternative, semi-empirical model for the shear yield-penetration correlation in crumb pastes has been developed and yield values are now reliably obtainable using the simple and repeatable method of cone penetrometry.

Cone penetrometry has confirmed the existence of significant hardening in crumb pastes post mixing, both in LM crumb pastes and factory extruded pastes. If attempts to model this hardening were made, it is likely that the methods surmised by Coussot (2007) would find some relevance. These macroscopic models consider the general shear stress versus shear rate relation described in Section 2.2.1, but include a structural parameter (λ) which describes the current state of the structure and evolves with the flow history. Determining the properties of such a structural parameter for crumb paste are beyond the scope of this project, however the existence of significant hardening must be carefully considered as this potentially reactive hardening of crumb paste post mixing poses a significant obstacle to its rheological characterisation.

In this project, a characterisation technique is sought that will allow the rheological comparison of crumb pastes extruded under a range of processing conditions and with a variety of modular twin screw configurations, such that the effect of extruder mixing conditions on paste formation may be better understood.

The standard approach for extrusion analysis of this kind is to take extruded samples and place them in an off-line rheometer in order to determine the flow curve of the sample. However, the procedure required to construct these flow curves, using either rotational rheometry or capillary rheometry, requires that material parameters remain

constant throughout the duration of the tests (usually in the region of 10 minutes or more), as a number of steady state data points are required at several stress states in order to observe the material's deformation response.

By considering the single parameter of shear yield strength, cone penetrometry has shown that crumb pastes cannot be considered time independent over the necessary measurement time scales, with a 100% increase in yield strength after only eleven minutes post mixing. Additionally, the hardening effect cannot be prevented or reversed by maintaining the sample at elevated temperatures, as is the case with polymer melts that set following extrusion (Narkis *et al.*, 2004 ; Haba & Narkis, 2004).

Dynamic oscillatory measurements (described in Section 2.2.1) offer an alternative rheological characterisation for viscoelastic materials by applying an oscillating sinusoidal displacement to a sample and observing the magnitude and phase difference of the stress response. The phase angle of the resulting complex modulus is considered to be an attractive way of characterising the solid-fluid behaviour of crumb pastes, since a wide range of consistencies were observed which were highly sensitive to added water content. Given that one of the key areas of research by the company is variations in added water content, it is anticipated that any characterisation test must be able to cope with a wide range of microstructures and consistencies.

The time required to obtain a measurement of the complex modulus, G^*, can be significantly shorter than that of capillary rheometry or rotational rheometry. However, the range of displacements over which the measurements are valid (the linear viscoelastic range) must first be determined on a sample by performing an amplitude sweep. This requirement is time consuming and prevents immediate testing of a material without prior knowledge of its behaviour.

As with all off-line testing procedures, both of these approaches require a finite time to transfer a sample to a rheometer following mixing or extrusion. Despite limited available data at short times after mixing (limited by this very transfer time), there is a suggestion that the rate of hardening is most significant immediately after mixing. This additionally serves to show that samples characterised after extraction are not representative of the material in process, making any rheological measurements performed on extracted samples unsuitable when considering process design. The importance of on-line extrusion characterisation was confirmed by Covas *et al.* (2008) who found that for a twin screw extruded polymer melt, G' and G'' appeared to increase along the extruder length when measured off-line, whilst on-line measurements showed the opposite. Their use of integrated dynamic oscillatory rheometry along the length of the extruder overcame the need to extract and transfer samples to an off-line rheometer for the main characterisation test, however still required an off-line determination of the linear viscoelastic range over which the measurements were valid This highlights the need for an in-situ rheological measurement technique for continuous extrusion analysis where the extruded material is not extractable and is also strongly time dependant. This is explored further in Chapter 4.

Chapter 4 In-line characterisation of crumb paste

As part of this project, a rheological characterisation technique is sought that will allow the comparison of crumb pastes mixed under a range of processing conditions such that the effect of mixing conditions on paste rheology may be better understood. Any testing procedure must be suitable for use on the variety of extruded crumb pastes to be explored in the extruder trials of Chapter 7.

Cone penetrometry studies in Chapter 3 have shown that a time dependent hardening of crumb paste once mixed or extruded poses a significant obstacle to its rheological characterisation. The finite time required to transfer extracted samples to an off-line rheometer means that traditional rheometer based techniques are unsuitable as samples characterised after extraction are not directly representative of the material in process. This highlights the need for an in-situ rheological measurement technique for continuous extrusion analysis where the extruded material is time dependent and not extractable.

This chapter considers the potential application of shear wave propagation and reflection techniques for future use as in-line characterisation methods for extruded crumb paste. A short summary of existing in-line techniques for monitoring the rheology of extruded materials in presented is Section 4.1, followed in Section 4.2 by a more detailed discussion of shear wave propagation in viscoelastic materials and a proposed concept for the testing of pastes such as extruded crumb. The implementation of the proposed concept

on a model dough material is presented in Section 4.3 and is followed finally by an introduction to a shear wave reflection method which is investigated experimentally in the extruder trials of Chapter 7.

4.1 In-line extrusion monitoring techniques

A number of in-line extrusion monitoring techniques currently exist, including ultrasound/Doppler profiling, MRI and slit/capillary style rheometry, however none are particularly suited to the stiff paste consistency and time dependent nature of crumb paste. Ultrasound and MRI are typically used on more fluid like materials to generate velocity profiles within the laminar flow of a pipe, from which viscosity measurements are obtainable. Alternatively, slit/capillary rheometry routes off a sample stream of material from the process and forces it through a slit or capillary of known dimensions at different pressures in order to create a number of stress-shear rate conditions in a similar fashion to off-line rheometers. Both allow the generation of flow curves in near real time for suitable materials, however they give little information regarding the solid-liquid microstructure of the extruded material and can suffer from technical difficulties when considering stiff and sometimes particulate pastes.

4.2 Shear wave propagation

Shear wave propagation has the potential to act as an in-line process for monitoring the rheology of stiff pasty materials and to the author's knowledge is yet to be developed fully for this purpose. The principle of this method involves monitoring the propagation characteristics of shear waves (or transverse waves) that are transmitted through a medium.

From theoretical considerations, it is then possible to compute various material parameters using the quantitative characteristics observed.

By considering the propagation of plane shear waves in a viscoelastic medium of density ρ, it may be readily shown (Whorlow, 1980) that:

$$G^* = -\frac{\rho\omega^2}{\Gamma^2} \tag{27}$$

where ω (=$2\pi f$) is the angular frequency (rad/s), f is the cyclic frequency (Hz) and Γ is the complex wave propagation constant expressed as:

$$\Gamma = \frac{1}{x_0} + i\frac{\lambda}{2\pi} \tag{28}$$

where λ is the shear wave length (m) and x_0 is the distance in the direction of wave propagation over which the wave amplitude decreases by a factor e (m). Thus, the individual components of G' and G'' of the complex modulus G^* can be conveniently written as (Ferry, 1980):

$$G' = \frac{\rho v^2(1 - r^2)}{(1 + r^2)^2} \tag{29}$$

$$G'' = \frac{\rho v^2 . 2r}{(1 + r^2)^2} \tag{30}$$

where $r = \lambda/(2\pi x_0)$, λ = shear wave length (m), v is the shear wave phase velocity (= ω/k, m/s) and k is the angular wave number (=$2\pi/\lambda$, m^{-1}). Consequently for linear viscoelastic systems, G' and G'' may be obtained from (29) and (30) by measurement of v and attenuation for a known frequency and density. It should be noted that as shear wave

attenuation tends to zero, characteristic of a perfectly elastic material, *G''* tends also tends to zero and *G'* simplifies to the elastic rigidity modulus.

4.2.1 Bender elements

In the last twenty-five years, bender elements have been developed to generate and detect shear waves in materials for the purpose of determining shear wave propagation characteristics, such as velocity and attenuation. Bender elements consist of two thin piezo-ceramic plates, which are bound together with a non-conducting surface around and between them. The polarisation of these plates means that when a driving voltage is applied to the bender element, one plate elongates and the other shortens, leading to a net bending displacement which in turn displaces the surrounding medium. Conversely, when an element is subjected to an external bending displacement by its surroundings, one plate is in compression whilst the other is in tension and a detectable voltage signal is generated. This dual functionality of bender elements allows an element to be used for either shear wave generation or detection.

A common application for the use of bender elements is the determination of shear wave velocities in soil tests. Here, the elements are traditionally encapsulated and mounted into inserts which are fixed into the pedestal and top cap of a triaxial cell. They protrude edge first into the soil by a few millimetres and create a shear wave which propagates through the sample until it is detected at the opposite end of the sample. Soils are typically considered to behave elastically at small strain amplitudes and the maximum elastic modulus, G_{max} (Pa) is calculated using equation (31) once the shear wave velocity has been determined.

$$G_{max} = \rho v^2 \tag{31}$$

4.2.2 Pulse propagation and shear wave dispersion

The simplest and most common technique used for determining shear wave velocity is known as 'pulse propagation' or 'time of flight' measuring. A simple pulsed driving voltage (usually a voltage step, a single square wave or a single sine wave) is applied to the transmitting element, causing the generation of a shear wave which propagates through the sample until it is detected at the receiver element. The time delay between the driven signal and the appearance of a signal at the receiver element is considered to be the time of flight and is used simply to determine the propagation speed over the known distance separating the two elements.

Whilst simple in principle, the key requirement of this method is the reliable identification of the received signal's first arrival. In an ideal elastic system, characterised by a constant coefficient of elasticity, shear waves propagate at a constant phase velocity, regardless of their frequency. However, in a non-ideal system, which exhibits a degree of viscoelasticity, dispersive effects mean that wave components of differing frequencies can travel at different speeds and are subject to varying levels of attenuation. As a result, a significantly transformed waveform is detected at the receiving element with features which no longer map to the original waveform. Voltage step inputs or square sine waves are particularly susceptible to these dispersive effects as signals of this form carry a broad spectrum of frequencies. It should also be noted that even pulsed sinusoidal signals of a single harmonic frequency are subject to this dispersion, as the inertia of any mechanical transducer means that instantaneous accelerations and decelerations are not possible and a range of peripheral frequencies is present in the signal in addition to the central harmonic. As a consequence of these dispersive effects, the determination of exact arrival times in the time domain can be a difficult and often subjective task - an observation which is heavily supported in the literature with many authors reporting difficulties of this kind (Dyvik &

Madshus, 1985 ; Brignoli *et al.,* 1996 ; Viggiani & Atkinson ,1995a, 1995b ; Nakagawa *et al.* 1996).

The experimental difficulties reported extensively in the literature have been replicated analytically by Williams & Williams (1994), who used the Maxwell model of viscoelasticity to analyse potential errors. It was demonstrated that viscoelastic dispersion severely restricts the validity of most wave based rheometry which utilises pulse propagation techniques. This analysis was also extended to the wave based rheometry of cohesive sediments under water waves (a material not dissimilar to crumb paste in consistency) by Babatope *et al*. (1999), who concluded that due to viscoelastic wave dispersion, measurements of shear wave velocity by pulse techniques are unsuitable as a basis for in-situ rheometry. It is for these reasons the determination of shear wave velocity in recent years has taken steps into the frequency domain.

Greening & Nash (2004) recognised the difficulties of trying to determine the shear wave velocities of soils using time domain techniques with bender elements and instead determined velocities using the frequency domain. In this work, the phase shift between the transmitted and the received signal was observed and the phase velocity calculated from:

$$v = L\,\frac{2\pi f}{\phi} \qquad (32)$$

where ϕ is the phase difference between the two signals (rad), f is the frequency (Hz) and L is the distance over which the wave is propagated (m). Comparisons made with time domain techniques indicated that time domain techniques significantly underestimate travel time, thus overestimating shear wave velocity. An attractive component of this work was the use of a spectrum analyser to analyse broadband spectrum signals and simultaneously determine the phase shift of multiple shear wave frequency components

using bender elements. The concept of this multi-wave analysis is explored further in Section 4.2.4.

4.2.3 The virtual gap rheometer (VGR)

Some of the most pioneering work in frequency domain methods for calculating shear wave propagation speeds in dispersive viscoelastic materials was the development of the principles used to create the 'Virtual Gap Rheometer' (Williams & Williams, 1992). This technique, for the measurement of dynamic moduli at high frequencies, was presented and verified on a dispersion, based upon the properties of a virtual gap formed by two unequal shear wave path lengths. Their method is summarised here.

Let A, B and C be parallel plates in a linear viscoelastic medium (see Figure 4.1). A undergoes continuous forced harmonic displacement in its own plane, generating plane shear waves which travel towards B and C. B and C are at distances x_1 and x_2 from A such that $x_1 > x_2$. Thus a "virtual gap" CB' of width Δx is created where $\Delta x = x_1 - x_2$ and $\Delta x << x_1, x_2$.

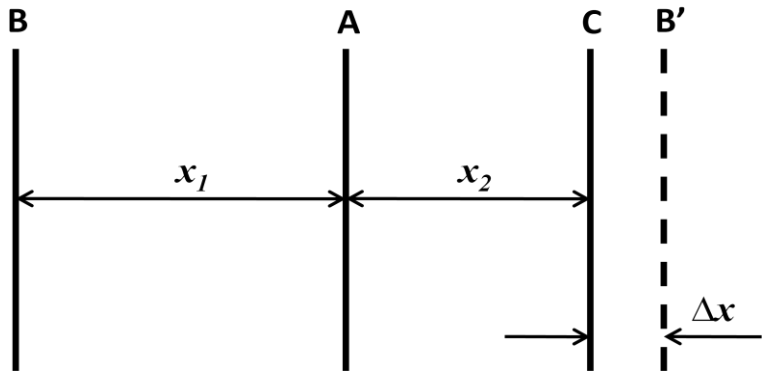

Figure 4.1 The virtual gap geometry

Plates B and C may function as linear force sensing devices, producing voltage signals in response to the harmonic motion of A, the common source of the shear waves. The displacement of A may be measured, for example by a non-contacting displacement transducer. Under steady state conditions, the time-varying form of the stress response at B and C (also harmonic for a linear viscoelastic material) will be as shown in Figure 4.2, which also shows the determination of δ.

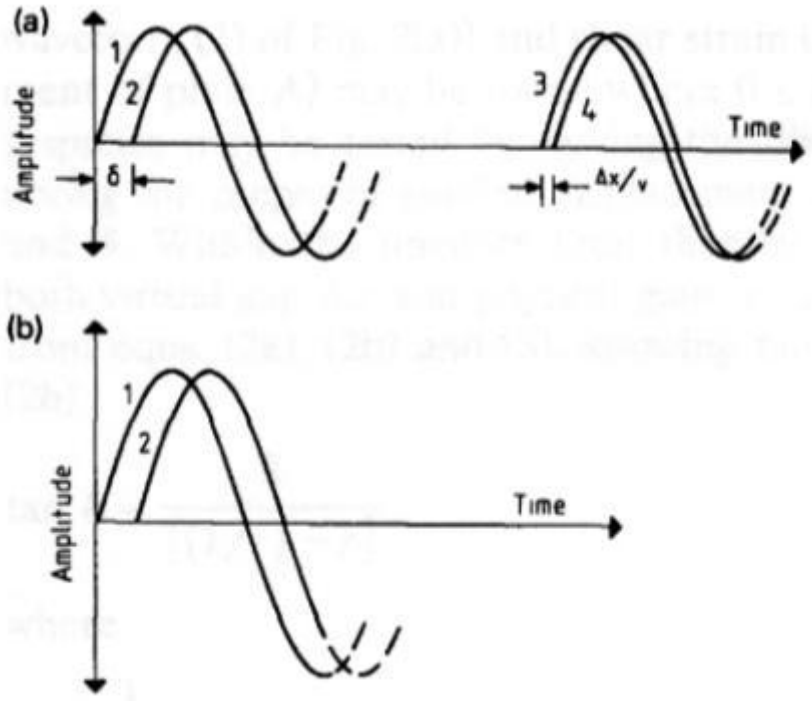

Figure 4.2 Virtual gap rheometer signal response (Williams & Williams, 1992)

(a) The determination of v and δ using the virtual gap geometry: curve 1- stress at plate A (calculated); curve 2 - displacement of plate A (measured); curve 3 - stress at plate C (measured); curve 4 - stress at plate B (measured). (b) The determination of maximum local shear strain amplitude (γ_{max}); curve 1, displacement of plate A, x = 0, (measured); curve 2, stress at x = x', (calculated)

The shear wave velocity in terms of the virtual gap is given by (33) which is notably similar in form to (32) used independently by Greening & Nash (2004):

$$v = \Delta x \left(\frac{\omega}{\phi}\right) \qquad (33)$$

where ϕ is the phase angle between the stress measured at B and C and $\lambda = 2\pi\Delta x/\phi$. Linearity of viscoelastic response may be tested by varying the displacement amplitude of A and noting the range of applied displacement which produces no change in ϕ and δ. Within the linearity limit thereby established for the medium in both the virtual gap and physical gaps x_1 and x_2, tanδ and λ are known. By combining (29) and (30):

$$tan\delta = \frac{G''}{G'} = \frac{2}{[(1/r) - r)]} \tag{34}$$

where

$$r = \frac{\lambda}{2\pi x_0} \tag{35}$$

Equation (34) may then be solved for x_0 and thus G' and G'' may be calculated from (29) and (30). The VGR principle has not only been used successfully on dispersions, but also as an in-situ technique for the measurement of dynamic mechanical properties in non-rigid mud beds under wave pressure (Babotope *et al*., 2005). This viscoelastic material, which was considerably denser than a dispersion and included the presence of large particles up to 27 μm exhibited marked linear viscoelastic wave dispersion and highlighted the applicability of the principles on a dense viscoelastic material similar to crumb paste.

4.2.4 Multiwave analysis

Discussion of wave rheometry techniques such as this for time dependent materials was first made by Holly *et al*. (1988), who commented that if techniques were to be applied to time dependent viscoelastic systems e.g. in reacting systems or gel-point studies, it is desirable that $v(\omega)$ be determined in a single measurement. For equations (29) and (30)

to be valid, it is a further requirement that the attenuation corresponding to each frequency component also be determined (Williams & Williams, 1994).

Advances in signal processing techniques have led to the development of 'multiwave' spectral analysis, in which the sine wave history can be replaced by superimposed harmonics. By doing this, experiments may be carried out simultaneously at several discrete frequencies, generating harmonics of the nominated fundamental frequency within the time given by the reciprocal of the longest (Ross-Murphy, 1994). Naturally, this technique is particularly well suited to the investigation of properties on time dependent systems as the individual responses to each frequency can be recovered by Fourier methods.

The virtual gap rheometer principle serves as an ideal basis for implementing this experimental technique, as it is an instrument that can be used to measure the phase velocity and corresponding attenuation of the component frequencies of multiple frequency waveforms (Williams & Williams, 1994). The phase velocity v_j, corresponding to a frequency component ω_j is therefore given by:

$$v_j = \Delta x \left(\frac{\omega_j}{\phi_j} \right) \qquad (36)$$

where ϕ_j is the phase angle between stress measured at B and C. The ϕ_j components are readily found by sequential FFT based cross correlation analysis of appropriately bandpass-filtered signals from the spatially separated surfaces B and C (Brigham, 1988), thereby allowing the determination of $G^*(\omega)$ from a single measurement.

This multiwave analysis was successfully applied to the VGR by Williams & Williams (1994) on a viscoelastic colloidal suspension using sinusoidal voltages over a frequency range of 100-800 Hz. Williams & Williams (1996) then went further by investigating the propagation of multiplexed frequency groups containing 22 frequencies

between 400 Hz and 1800 Hz in an experiment system as it underwent gelation and was analysed using the FFT based cross correlation techniques described by Brigham (1988).

The potential application of these techniques to crumb paste extrusion are immediately apparent. It was reported by William & Williams that the VGR multiwave analysis was currently being developed as the basis of an in-line process rheometer for reacting systems, but to the author's knowledge, no such system currently yet exists. It is hypothesised that this may in part be due to the circular parallel plates used by Williams & Williams (1992) to generate and receive shear waves which are immersed wholly within the sample chamber. It is felt that this configuration of transducers would be awkward to implement for use on a continuous in-line process.

4.2.5 Bender element configurations

After reviewing the literature on shear wave propagation rheometry, it is hypothesised here that bender elements, which need only protrude into the sample by a few millimetres may offer an altogether more convenient implementation of the basic VGR principles for use as in-line rheometry. In order to implement the virtual gap using benders, the need for three elements (one transmitter and two receivers) means there is an implicit requirement for benders to be mounted along the side of a vessel rather than the end mounted elements traditionally seen with soils (one transmitter and one receiver).

Clayton *et al*. (2004) successfully used side mounted bender elements to transmit and receive pulse propagated shear waves along the length of a sample (configuration reproduced in Figure 4.3). Although this work continued to use a time domain technique for determining shear wave velocity, it used a configuration which created a gap over which the same energy packet is sampled by two separate receivers. The benefit of this arrangement was presented on the grounds that in a conventional bender element

arrangement, the couplings between the (driven) transmitter and the soil can be expected to differ and vary with frequency. Because of unknowns in mechanical coupling between the transmitter and the specimen, the true waveform input to the soil must remain unknown and it is therefore desirable to use two separate receivers over a known distance where possible.

The side mounted bender elements used by Clayton *et al*. (2004) were similar to those described by Pennington *et al*. (2001), were 10 mm wide and protruded only 2 mm into the specimen. As described in Section 4.2.2, the authors continued to report difficulties in determining time of flight measurements due to frequency dependent dispersion.

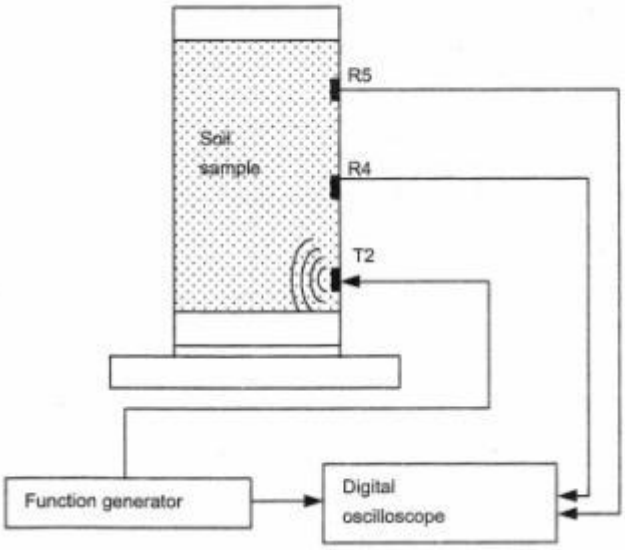

Figure 4.3 Layout and instrumentation of side mounted bender elements (Clayton et al., 2004)

T1, side mounted transmitting bender element, R4, R5, side mounted receiving bender elements

4.2.6 Proposed concept

It is proposed here that the frequency domain use of benders by Greening & Nash (2004) could be significantly extended by applying the principles of virtual gap rheometry

(Williams & Williams, 1992) to bender elements. By combining the principle of the virtual gap rheometer with the instrumentation of bender elements and multiplexed shear waves, it is thought that the in-line determination of dynamic moduli for time dependent, reactive and non-extractable extruded paste materials could be possible.

It has already been shown by Clayton *et al*. (2004) that side mounted bender elements may be used to generate and detect shear waves, meaning that in principle, it should be possible to create the virtual gap required for signal detection by the VGR method of Williams & Williams (1992). The use of the frequency domain for shear wave velocity determination derived independently by Greening & Nash (2004) is already notionally similar to that used by Williams & Williams (1992). This phase shift technique was however, used not over a 'virtual gap', but directly between the transmitted signal and a single received signal. By applying the same technique over a virtual gap, the added benefits of detecting the signal at two separate receivers described by Clayton *et al*. (2004) would also be realised.

To the author's knowledge, the use of benders is currently restricted to analyses which consider elastic materials only, meaning that only the shear wave velocity is required for the determination of G_{max}. Using benders in the way proposed here would extend their use to viscoelastic materials and would consequently require the consideration of the viscous damping factor required by equations (29) and (30) for the determination of the viscoelastic parameters G' and G''. In the long run, it is suggested that this might be achievable by strain gauging the transmitting bender element, or integrating a laser velocimeter to accurately observe the phase angle between signal and displacement, thereby obtaining x_0 in a similar manner to Williams & Williams (1992). In the short run however, it is envisaged that x_0 should primarily be obtained by measuring the attenuation of signal magnitudes directly over known distances.

4.3 Shear wave propagation using play dough

In order to test the concept of using virtual gap bender rheometry as a form of in-line rheological characterisation for time dependent systems, it was first decided to establish the necessary signals on a similar, but simpler time stable viscoelastic material. For this purpose, a play dough paste was selected as the chosen material as it contains soluble solids, water and fats, all similar phases to those present in crumb paste. Whilst play dough is known to dry out over long periods of time when exposed to air, it is time stable over the necessary periods of testing and therefore a suitable choice for trialling the bender element rheometry setup.

The standard 42% liquid play dough recipe used is shown in Table 4.1. All dry ingredients were first mixed together by hand before adding the water and stirring until smooth. The oil was then added and the mixture transferred to a pan for cooking on a medium heat. The mixture was stirred continuously until the dough left the sides of the pan into a cohesive, but pliable paste with a consistency typical of commercially available play dough. On the electric hob used, this process required three minutes of heating.

In order to test a range of paste consistencies, it was decided that the liquid content of the play dough samples could also be varied. Experimentation showed that by keeping a fixed ratio of solid ingredients, a liquid content range of 32% - 62% gave doughs with a range of consistencies which were similar to those experienced using LM crumb paste - ranging from very stiff to almost fluid. Each of the doughs with liquid contents which differed from the standard 42% recipe was subjected to the same three minutes of cooking. Samples were then stored in sealed bags and refrigerated until required. Each sample was used within one week of mixing.

Table 4.1 Standard 42% liquid play dough recipe by mass

Ingredient	Mass (%)
Flour	26
Salt	23
Cream of tartar	9
Water	39
Vegetable oil	3

4.3.1 Bender element equipment

The equipment required for testing the bender element rheology principle was kindly made available for use by Dr David Nash at the Civil Engineering Department, University of Bristol. Each element used was produced by the University of Bristol using a specifically designed mould to coat the piezoceramic plates with epoxy resin. Each pair of coated plates was then placed inside a stainless steel casing pot with a second mould and epoxy filling to fix the plates orthogonally in place. Dimensions of the benders used are shown in Figure 4.4 along with the plane of shear wave propagation that is generated if connected to a function generator and used as a transmitting element.

The experimental arrangement used to create a bender element virtual gap is shown in Figure 4.5. A continuous sinusoid signal was generated using a Thurlby Thandar TG1010 function generator and was emitted from the transmitter element at position T. The two receiver elements are placed at positions R_1 and R_2 at a distance of x_1 and x_2 from T to create the virtual gap $\Delta x = x_2 - x_1$. The received signals at each receiver were than fed to a Tektronix TDS 3014 oscilloscope via a x8 amplifier.

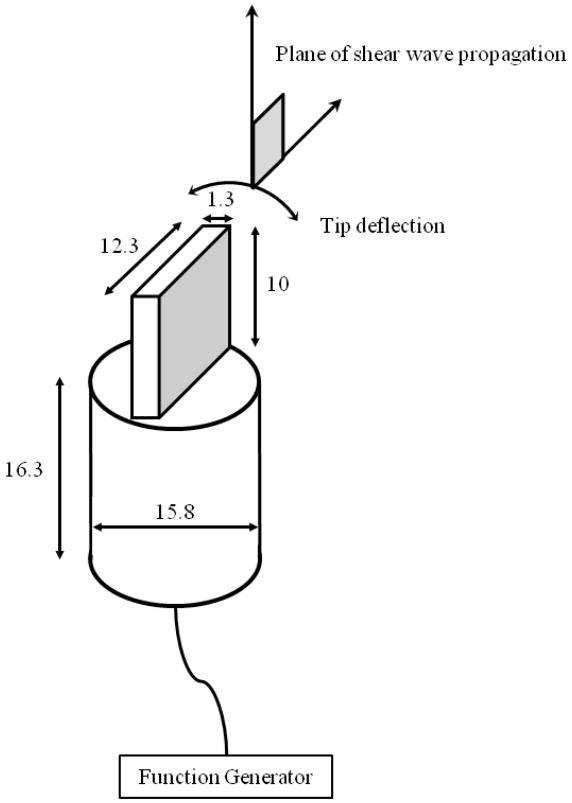

Figure 4.4 Potted bender element dimensions (mm) and plane of shear wave generation (transmitter)

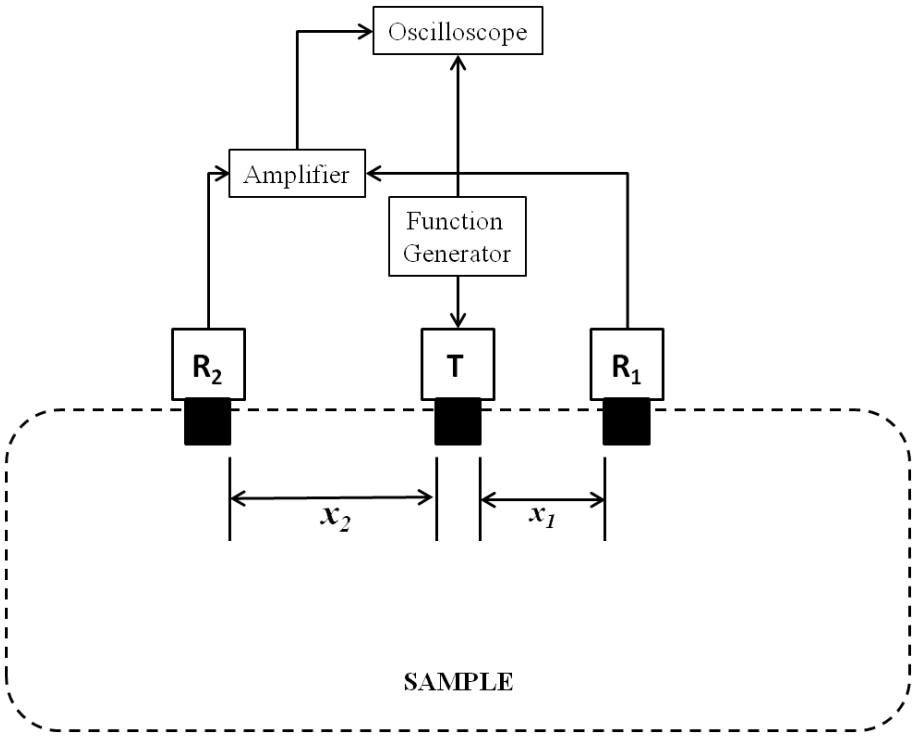

Figure 4.5 Schematic of virtual gap bender element arrangement

4.3.2 Virtual gap signals in play dough

In order to try to detect the anticipated signals for virtual gap rheometry, the arrangement shown in Figure 4.5 was applied to a large free standing mass of 42% liquid play dough. The mass of sample was compressed lightly to produce a flat surface and elements T, R_1 and R_2 were aligned and inserted manually with x_1 = 68 mm and x_2 = 72 mm to give Δx = 4 mm.

Figure 4.6 shows the signals received by R_1 and R_2 (steady state was achieved after approximately one second) when a 10 kHz continuous sinusoid input signal of magnitude 11 V_{pp} was applied to T. A continuous sinusoid of the same 10kHz frequency was detected at both R_1 and R_2 and as anticipated, a phase shift exists between the two signals with the R_2 signal more highly attenuated than the R_1 signal having propagated over a longer path length.

Although it is encouraging that the desired signals have been transmitted and received in the dough paste using the bender element virtual gap arrangement, the magnitude of the received signals shows there to be high levels of shear wave attenuation - producing received signals of only 6 mV_{pp} and less for an 11 V_{pp} input signal over approximately 70 mm. High levels of attenuation are expected due to the viscous component of the dynamic modulus, however given such small magnitudes it was found that the received signals were highly sensitive to the rotational orientation and alignment of the elements, making the magnitude of signals from bender elements which have been inserted by hand susceptible to large errors. It was also the case that benders simply pushed into the material had a tendency to be unstable, causing tipping and fluctuations in coupling which was otherwise strong before tipping had taken place. This effect became more exaggerated as the liquid content of the doughs increased. The results presented here demonstrate the existence of the necessary signals to implement virtual gap rheometry

using a side mounted bender element arrangement, however the sensitivity of the arrangement to transducer alignment and coupling have shown that any further work in this area requires the construction of a test cell which can ensure the accurate and stable alignment of transducers.

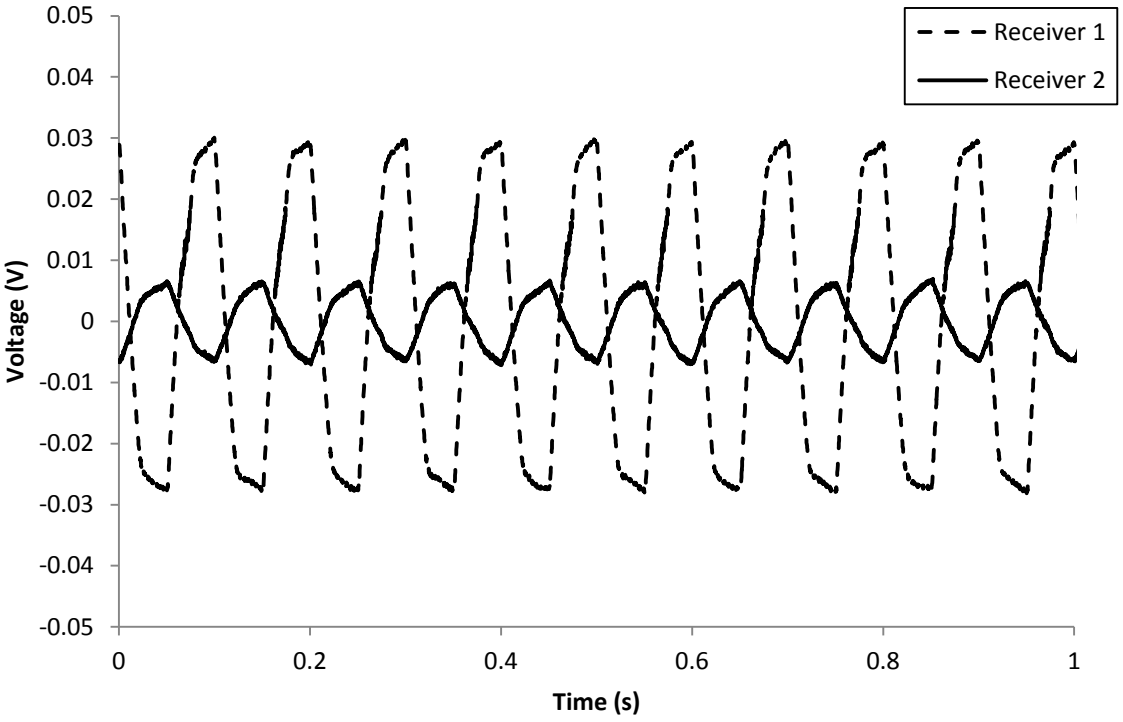

Figure 4.6 Received signal from side mounted bender elements

R_1 and R_2 when applying an 11V_{pp} 10 kHz signal to transducer T in a 42% liquid play dough

4.3.3 Test cell

For the purpose of further testing the concept of virtual gap bender rheometry, the design and construction of a Perspex test cell was attempted which would allow the accurate and stable alignment of transducers. The cell, shown in Figure 4.7, includes multiple portholes for the insertion of the potted bender elements into the module lid leaving only the element itself protruding into the material. The positioning of each of the

receiving sites is off-set in relation to the transmitting site so as to create the virtual gap Δx. Multiple portholes were included so that the distance of the virtual gap could be varied and so that for the testing of non-time dependent materials only, the attenuation of signals could be obtained more accurately using the same receiving element consecutively placed closer to the transmitter.

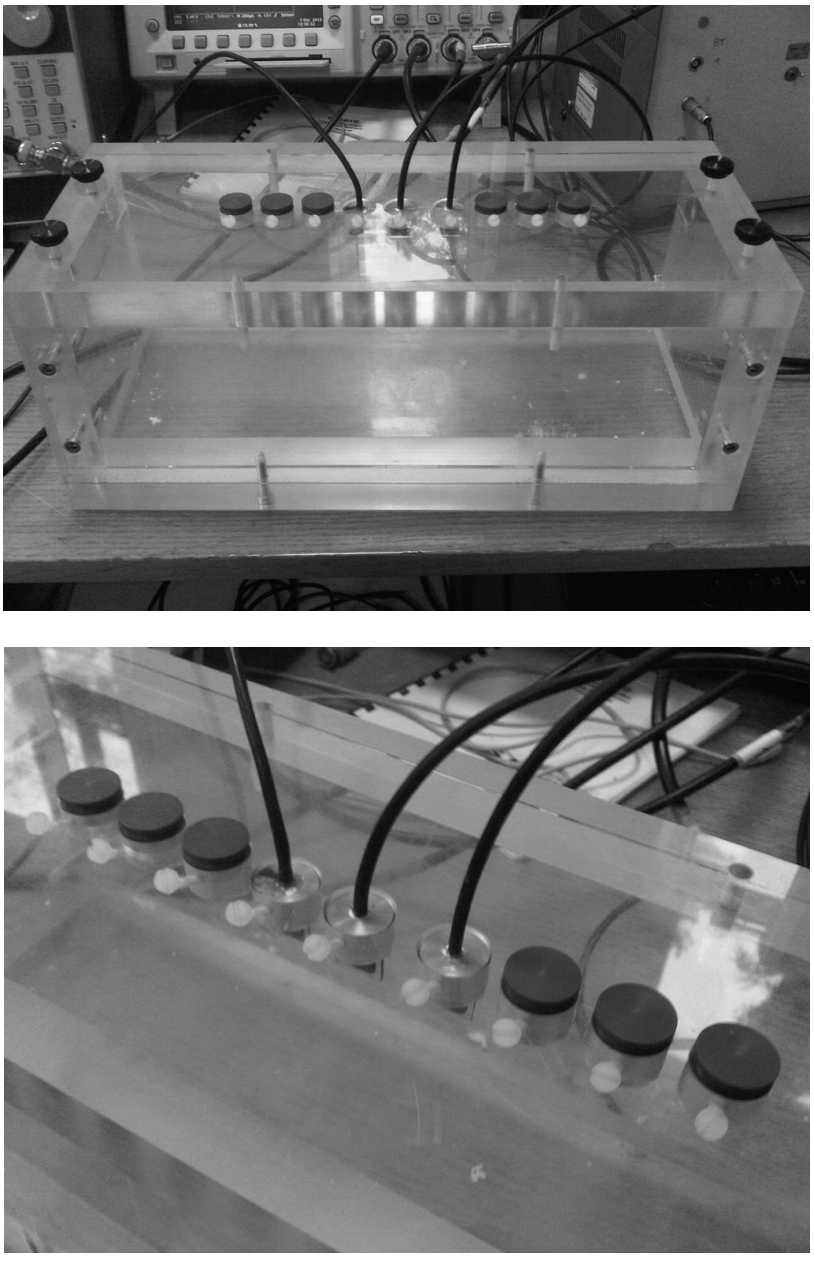

Figure 4.7 Perspex test cell showing virtual gap arrangement of side mounted bender elements

The test cell was designed such that the direct path length between transmitter and receivers was significantly less than those available from reflected paths. Given the viscoelastic nature of the materials being considered and the high levels of associated attenuation shown in Section 4.3.2, signals from the direct path were considered to dominate.

Due to the strong dependency of the received signals on the rotational orientation of both transmitters and receivers, notches were used on bender pots and the module lid to ensure that elements would be accurately aligned. The alignment of these elements was then secured using angled nylon fixing screws. All transducers could be accurately aligned and fixed in position before inserting the lid onto the sample in one movement, ensuring an altogether more reliable and consistent alignment. Solid inserts were placed into the portholes not in use.

By considering the signals received at each of the receivers when the test cell was empty, Figure 4.8 shows that despite the cell being designed such that no contact existed between the elements themselves and the lid (only between the lid and the stainless steel pots), a significant level of vibrations was being transmitted and received via the lid. This was consequently discovered to be a fundamental flaw of the design, since inertia at the fixed end of the bender elements acting as cantilevers was sufficient to cause vibrational interference to be transmitted via the pots and Perspex. Waves passing through a solid material such as Perspex will be subjected to significantly less attenuation than those passing through a paste like sample, resulting in vibrational noise signals from the rig which are orders of magnitude larger than the targeted signals propagating through the sample. It is therefore clear that the Perspex cell designed here is not suitable for its intended use in its current form.

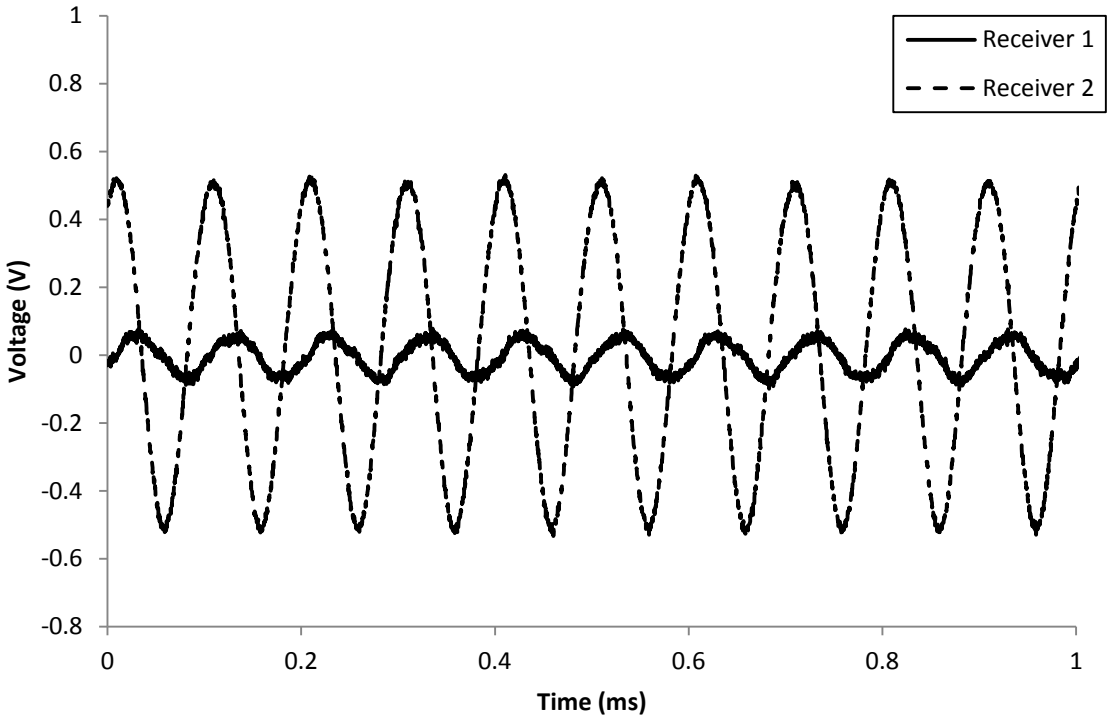

Figure 4.8 Noise vibration received at receiver elements when applying an 11V_{pp} 10kHz signal to transducer T in empty test cell.

4.3.4 Further work

Limitations of time and resources meant that it was not possible to take this line of work any further and it is left as further work to make the necessary modifications and further develop this implementation of the virtual gap principle. This work has encouragingly shown that it is possible to transmit and receive the anticipated signals required for using virtual gap rheometry on a viscoeleastic material using a side mounted bender element arrangement. However, any further work in this area would require the isolation of the transmitting element from the receiver elements such that no direct path is available from transmitter to receiver and vibrational interference through the test rig is eliminated.

If future work was able to achieve this, suggested work would begin with a verification of the method on a time stable viscoelastic material as originally intended in this work. It is suggested that either of the manual frequency domain determinations of shear wave phase velocity described fully by Greening & Nash (2004) and Rio (2006) be used to plot a response phase delay curve for each sample, plotting the unwrapped phase difference between two signals against frequency. The main distinction between this work and the work that was intended here is that the phase shift between the two received signals over the virtual gap would be considered rather than the phase shift between a transmitter and a single receiver. This phase delay curve can be achieved with the bender element arrangement using either the continuous signal method of pre-selecting the frequency of the signals and recording the phase difference of the corresponding responses, or by the pi-points method where the phase differences are pre-selected (usually multiples of π) and the frequencies at which they occur are recorded.

The attraction of this pi-points method is that unlike measuring the phase difference between two signals, which requires a small amount of calculus, the pi-points method can be determined directly from an oscilloscope reading (Rio, 2006). This would be achieved by connecting R_1 and R_2 to the oscilloscope and observing the "Lissajous" plots which superimpose the magnitudes of the two signals and represent them as an ellipse which changes in shape depending on the relative phase difference between them. As the signals pass perfectly in or out of phase, a straight line of positive or negative gradient appears on the Lissajous plot and the corresponding frequency can be recorded.

The travel time of a wave can be determined from the gradient of the phase delay response curve measured between two points (Rio, 2006):

$$\frac{\Delta\, phase}{(2\pi)\,\Delta frequency} \equiv \frac{rad}{(2\pi)Hz} \equiv s \qquad (37)$$

As described by Greening & Nash (2004), the phase travel time is determined from the secant of the curve and the group travel time is determined from the tangent of the curve. This phase travel time over the known distance Δx then gives the phase velocity of the wave, with a linear curve representing a non-dispersive system and a non-linear curve representing a dispersive system as anticipated for viscoelastic materials.

In addition to the phase velocity of the wave, which is all that is required for work on soils, consideration of the damping factor must also be made for the determination of *G'* and *G''* in viscoelastic materials as described in Section 4.2.6, where it has been established that this can be achieved either by direct measurement of the attenuation, x_0 or by direct measurement of δ. It is suggested that in the first instance when establishing the technique, this could be most simply achieved by measuring x_0, recording the magnitude of received signals at varying distances from the transmitter. This approach would be suitable for time stable materials, but would become unsuitable for time dependent materials whose properties changed significantly over the time of measurement. In this instance, it is suggested that strain gauging the bender element to determine the phase angle δ between the stress applied to the transmitting transducer and its corresponding strain is a more suitable approach and one that is similar to that employed by Williams & Williams (1992). Strain gauging of a bender element has been conducted successfully by Greening & Nash (2004), albeit for a different purpose of determining the resonant behaviour of a bender element, by mounting a strain gauge directly onto the biomorph prior to encapsulation. It is proposed that by utilising the signal from a strain gauge element in this way, the bender element arrangement of the virtual gap could be fully utilised to deliver the dynamic moduli of viscoelastic materials over a range of frequencies using equations (29) and (30).

If all of this can be achieved manually on a stable viscoelastic material, there is then the scope to extend the method to time dependent viscoelastic materials by incorporating the use of a spectrum analyser on the two received signals to simultaneously determine the phase shift and hence phase velocities of multiple frequencies. As described by Greening & Nash (2004), instead of applying only a single harmonic signal, a broadband signal containing many frequency components is used. A spectrum analyser which typically splits the frequency range into 800 spectral lines, takes $800/f_{max}$ seconds to determine the transfer function between two signals. Thus for a frequency range of say 20 kHz, the sampling time is 0.16 seconds. A similar analysis would also be required for the determination of δ at multiple frequencies when considering the strain gauged transmitter. If implemented successfully up to this point, the attraction of developing this arrangement into an in-line testing module for use on time dependent viscoelastic materials in process is clear to see.

4.4 Shear wave interface reflection

In addition to the shear wave propagation methods using bender elements described above, the use of ultrasonic shear wave reflection at the material interface as described by Kulmyrzaev & McClements (2000) was also considered as a potential method of in-line rheological characterisation. In this work, the complex shear reflection coefficient of honey was determined over the frequency range 5-15 MHz by measuring the phase and amplitude of ultrasonic shear waves reflected from its surface. This was achieved using a single transducer which both transmitted the driving signal and received the reflected signal after passing through a quartz delay line. This complex shear reflection coefficient was then used in conjunction with the density to calculate high-frequency dynamic shear moduli using the analysis reproduced from Kulmyrzaev & McClements (2000).

The complex reflection coefficient at the delay-line/sample interface was calculated at each frequency using the following formula:

$$R_S = R_C \frac{M_S}{M_C} \frac{[cos(\theta_S) + isin(\theta_S)]}{[cos(\theta_C) + isin(\theta_C)]}$$

$$= R_C r[cos(\Delta\theta) + isin(\Delta\theta)] \quad (38)$$

where R is the reflection coefficient, r the magnitude ratio (M_S / M_C), $\Delta\theta$ the phase difference (θ_S - θ_C) (degrees) and the subscripts S and C refer to the sample and calibration material respectively. The value of R_C can be calculated from the known acoustic impedances of the calibration material and the delay line: $R_C = (Z_{DL} - Z_C) / (Z_{DL} + Z_C)$, where the subscript DL refers to the delay-line. In general, the sample reflection coefficient is a complex number, but it becomes real when $\Delta\theta$ is zero, i.e. for an ideal liquid, which is incapable of supporting shear waves.

The complex shear impedance of the sample can be calculated from the measured reflection coefficient using:

$$Z_S = Z_{DL} \frac{(1 - R_s)}{(1 + R_s)} \quad (39)$$

where Z_{DL} is the shear impedance of the delay line (N.s/m^3) and Z_S is the shear impedance of the sample (N.s/m^3) which contains a real and imaginary component: $Z_S = Z_R + iZ_I$. The dynamic shear rheology of the sample can then be determined from the following relationships (Harrison & Barlow, 1981):

$$G'(\omega) = \frac{(Z_R^2 - Z_I^2)}{\rho} \quad (40)$$

$$G''(\omega) = \frac{2Z_R Z_I}{\rho} \qquad (41)$$

Surprisingly, this approach has not found widespread use in the food industry, despite the fact that it has certain advantages over conventional rheology techniques (McClements, 1997 ; Povey, 1998). The key advantages of this technique advocated by the authors are that the technique is non-destructive and non-invasive, giving it the potential to continuously measure the rheology of samples flowing through a pipe without disturbing them. It was also suggested that following the successful demonstration of the technique for determining the rheological characteristics of a homogenous fluid, it would be useful for future studies to consider its applicability to the study of multiphase materials - an application relevant to the crumb paste extrusion process. To the author's knowledge, no such further work has been performed and the technique has yet to be developed into an in-line testing system.

Due to the simplicity of the transducer arrangement and the mobility of equipment required for this method, it was felt that that the potential application of this technique to monitor the rheological characterisation of crumb paste was best tested directly on extruded samples. In this way, the single transducer required could be brought into contact with extruded paste to collect data at very short time periods after extrusion. This technique is therefore considered further in Section 7.5.

Chapter 5 Distributive mixing of crumb paste

Chocolate crumb extrusion is one of many industrial processes which rely on the mechanical mixing of multiple components. Many such processes, be they continuously mixed or batch mixed, often require that a product be mixed to a minimum degree of homogeneity. For crumb paste, there is currently no known degree of mixedness which must be achieved at the extrusion stage in order to facilitate successful downstream processing of chocolate.

This chapter investigates whether it is possible to quantitatively characterise the extent of distributive mixing evident within crumb paste. Such a characterisation would allow the comparison of mixing performance between one mixing process and another. Additionally, the capability to reference the quality of distributive mixing in crumb paste against characteristics in the final chocolate would be highly desirable.

In this chapter, the use of thermogravimetric analsysis (TGA) to quantify distributive mixing in crumb paste is explored. Section 5.1 begins with an introduction to distributive mixing in industrial processes and analysis currently used to quantify such behaviour. The use of TGA on crumb paste is explored in Section 5.2 and highlights why conventional analysis cannot be used confidently in the same fashion for crumb paste. A novel alternative analysis is therefore presented in Section 5.3 along with results of this analysis in Section 5.4. Finally, conclusions on the suitability of using TGA to quantify distributive mixing in crumb paste are drawn in Section 5.5.

5.1 Distributive mixing

Distributive mixing is the mechanism by which mixtures containing two or more components become increasingly homogenous and can be described as the convective transport and distribution of phases and components over the total volume. This is in contrast to dispersive mixing which relates to changes in the physical characteristics of components and the breakup of agglomerates. Figure 5.1 shows a clear change in the physical appearance of LM crumb paste as the mixture becomes more homogenous with mixing time once water has been added to the mix. The objective of this chapter is to quantify this. Further areas of interest are: Do some ingredients distribute more efficiently than others? Is a certain level of mechanical energy required in order to achieve a set level of homogeneity? How much is distributive mixing affected by the screw profile used to extrude it? Does LM paste exhibit the same level of homogeneity as extruded paste? These are all questions that can be investigated if it becomes possible to quantify the distributive mixing within crumb pastes.

Attempts in the literature to physically quantify distributive mixing in batch and extrusion mixing appear to have been limited to Newtonian fluids and suspensions. Brod & Liesenfelder (2004) successfully quantified distributive mixing efficiency for differing extruder designs by imaging inert tracer dies injected into transparent Newtonian fluids and observing the contrast of die in the extrudate using image inalysis, however this approach is not transferable crumb paste, or indeed many other industrial materials, due to their inherent opacity.

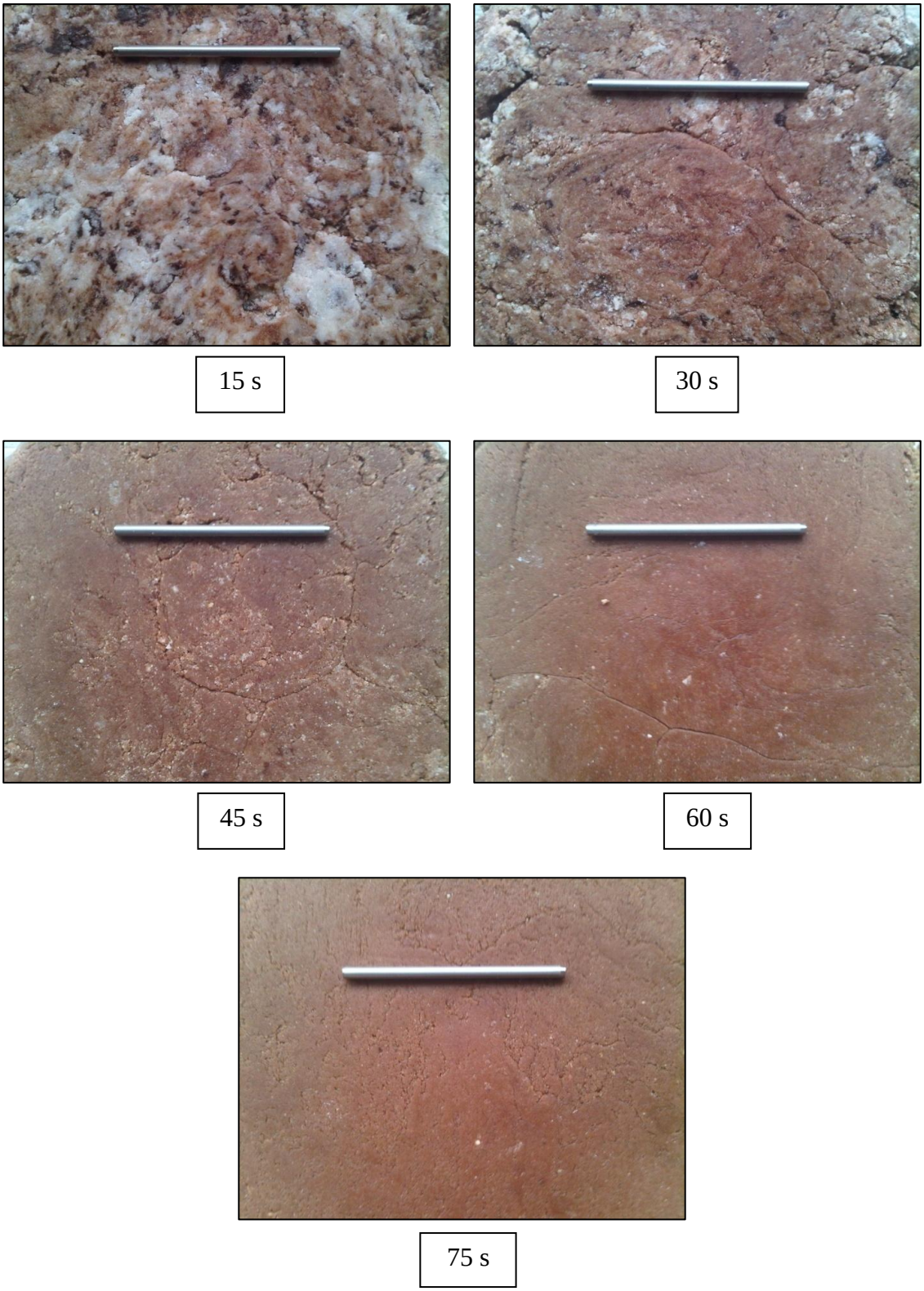

Figure 5.1 Changing 8% water LM paste appearance with increased batch mixing time (scale bar 70mm)

Kalyon *et al*. (2006) studied the characterisation of the degree of mixedness in graphite filled polymer suspensions processed using batch and continuous processes and under differing operating conditions were characterised quantitatively using X-ray diffraction and thermogravimetric analysis. Using these techniques, the statistics of concentration distributions within samples were successfully analysed to provide a quantitative index of mixing.

The same techniques and analysis were then adopted by Ozkan *et al*. (2007) to analyse the statistics of concentration distributions within nano-alumina based gels processed with a twin-screw extruder as well as conventional processing methods. These results were then corroborated with microscopy in a similar fashion to this study.

The use of thermogravimetric analysis (TGA) for quantifiying distributive mixing in dense complex pastes as well as polymer suspensions and nano particle gels has been investigated. The mixing analysis used by both Kalyon *et al*. (2006) and Ozkan *et al*. (2007) and the starting point for use on crumb paste, relies upon the ability to determine the concentration of components in samples of the mixture. In turn, the distribution statistics of these concentrations are then analysed to produce a quantitative mixing index. The key areas of this analysis are reproduced in Section 5.1.1.

5.1.1 Degree of mixedness analysis (measure of concentration distributions)

If N measurements of the concentration, c_i, of a component in the mixture are made, then the mean, $\bar{c}$, and the variance, σ^2, of the concentration distribution of this component are calculated from:

$$\bar{c} = \frac{1}{N}\sum_{i=1}^{N} c_i \qquad (42)$$

$$\sigma^2 = \frac{1}{(N-1)} \sum_{i=1}^{N} (c_i - \bar{c})^2 \qquad (43)$$

The variance, σ^2, arising from the distributions of individual concentration values i.e. c_i measurements, provides the most basic measure of the concentration homogeneity of a mixture (Tadmor & Gogos, 1979). Thus, the determination of the statistics of the extent to which the concentration values at various regions within the volume differ from the mean concentration can be used as an index to quantitatively assess the "degree of mixedness" (McKelvey, 1962).

A small variance would suggest that the mixture approaches the behaviour of a homogenous system, where most of the samples yield c_i values that are approaching the mean concentration, $\bar{c}$. On the other hand, if the components of a mixture are completely segregated, the maximum variance occurs. The value of the maximum variance, σ_0^2, (or the square of the between-sample standard deviation) for a completely segregated system, can be defined by assuming that the samples are taken from either one component or the other without crossing a boundary (McKelvey, 1962):

$$\sigma_0^2 = \bar{c}\,(1 - \bar{c}) \qquad (44)$$

The variance of the distribution of the concentrations of a given component can be normalised with its maximum value and the resulting parameter provides a measure of the degree of mixedness i.e., one possible mixing index for that component. This parameter, σ^2/σ_0^2, would be equal to one for completely segregated ingredients and would decrease toward zero as the homogeneity of the mixture improves.

For no other reason than simplified interpretation, both Kalyon *et al*. (2006) and Ozkan *et al*. (2007) used a slightly modified index for a component by subtracting the

above parameter from unity. This alternative mixing index, *MI*, would exhibit a value of zero for a completely segregated sample and its value would approach one for a completely mixed, random distribution of the concentration of its ingredients.

$$Mixing\ Index = 1 - \frac{\sigma}{\sigma_0} \qquad (45)$$

5.1.2 Effect of number of samples and sample size

It is well established in the literature that sample size (Schofield, 1976 ; Yazici & Kalyon, 1993) and the number of samples analysed (Kalyon *et al*., 2006) will affect the value of mixing indices. The difference between the mean concentration of samples, $\bar{c}$, and the actual overall concentration, ϕ, of an ingredient (be it a minor or major component) is indicative of the quality of the sampling technique (Tadmor & Gogos, 1979).

The difference between $\bar{c}$ and ϕ diminishes as the number, *N*, of characterised samples increases, making it desirable to include as many samples as possible, though this must of course be considered against time restraints and practicalities. The measured concentration values of a component in the mixture will also depend upon the sample size. These concentration values approach the overall concentration of the component in the mixture, ϕ, as the sample size (or the "scale of the examination") is increased. On the other hand, as the scale of the examination is reduced, the concentrations of the ingredients deviate significantly from their mean values and in the limit, the variance of the concentrations measured would reach the variance of a segregated sample (Ozkan *et al*., 2007).

A simple analogy to illustrate this concept is the visual appearance of countryside satellite images when observed at different scales. At a very large scale of observation, a field may appear homogenously green with no distinguishable features, whereas at a

medium scale of observation a field may appear mostly homogenous with large trees becoming observable. At much smaller scales of observation, heterogenous features such as localised areas of buttercups may feature. Cheyne *et al.* (2005) observed characteristics such as these when attempting to characterise the extrusion behaviour of starch potato pastes, noting that while water was evenly distributed at the macro scale, at the micro scale there was a highly uneven distribution of water due to the uneven competitive adsorption of water between three powders. *N*-point probability distribution functions have been successfully used to model the material properties of heterogeneous materials (Gokhale *et al.*, 2005 ; Belvin *et al.*, 2009 ; Jefferson *et al.*, 2005). Given suitable images of phases or material properties in 2D or 3D space, an *n*-point polyhedron having *n*-vertices at random locations is mapped into the microstructure or material properties of a multiphase material. The probability that all *n* vertices are contained within one phase or range of material property values is then calculated as a function of distance and orientation between vertices and provides a rigorous formalisation of the "scale of observation" concept described above.

In summary, it can therefore be possible to classify the same multi-component mixture as both homogenous and segregated by changing the scale of observation. This illustrates the point that any mixing analysis of this kind is arbitrary and that for comparative purposes, a scale of observation must be selected that is relevant to the application or process being considered.

5.2 Thermogravimetric analysis (TGA) of LM crumb paste

Thermogravimetric Analysis (TGA) measures the mass change of a sample as it is heated at a controlled rate and can be used to determine the concentration of individual components which thermally decompose at known temperatures. The standard deviation,

σ, or variance, σ^2, of individual component concentrations observed from multiple samples can then provide a basic measure of homogeneity in a mixture as described in Section 5.1.1.

This technique and analysis was used successfully by both Kalyon *et al*. (2006) and Ozkan *et al*. (2007) on a three component polymer composite and a four component nano particle alumina gel respectively. An example thermogram obtained by Kalyon *et al*. (2006) is reproduced in Figure 5.2 and shows how easily and accurately the concentration of the individual components can be made when each component has a discrete and narrow temperature range over which it thermally decomposes.

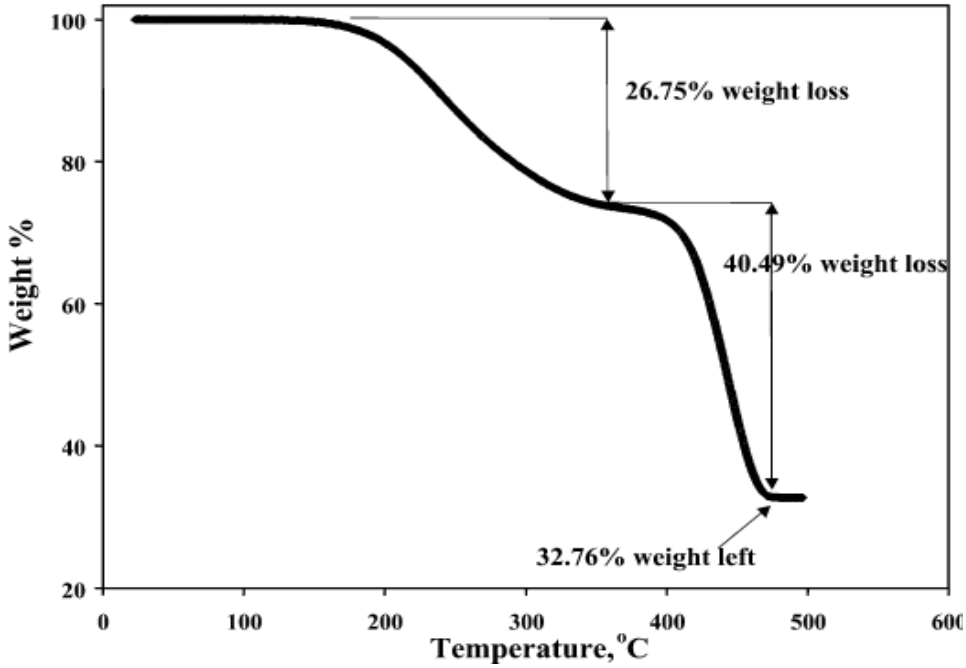

Figure 5.2 Well defined TGA thermogram for a three component mixture (Kalyon et al., 2006)

In this trial, the potential for applying the same mixing analysis using TGA to crumb paste has been investigated. In order to assess the potential of the technique, standard 8% water LM crumb pastes were sampled at various times of mixing, where a visual improvement in homogeneity is known to occur (see Figure 5.1). All pastes have been mixed according to the LM crumb mixing routine described in Section 3.1.1 and

times of mixing are referenced against the point at which all water has been added to the mixer (see Figure 5.3).

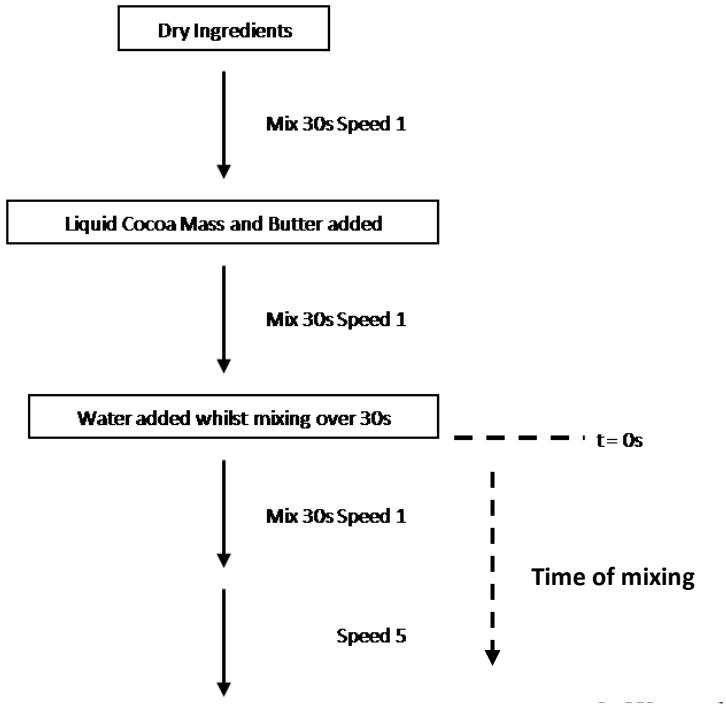

Figure 5.3 Mixing routine for LM crumb paste showing point of reference for time of mixing

5.2.1 Sample size

Cylindrical samples of LM crumb paste were cut for use in this trial using custom made sample cutters. As discussed in Section 5.1.2, sample size and spacing will affect the value of any mixing index measured and therefore the "scale of examination" must be consistent and appropriately chosen for the process and material in question. For the purposes of this trial, two sample length scales, $L1$ and $L2$, have been examined and the dimensions for these are shown in Figure 5.4, where L is both the diameter and height of the cylindrical samples.

Analysis of the pre-processed powdered ingredients has been conducted by the company and is shown in Figure 5.5, although no such information is available for fully

mixed crumb paste. The largest particle size of raw ingredient is approximately 200 μm whilst the majority lie in the region of 10-100 μm. This means that the characteristic length, *L*, of the largest sample being examined is approximately ten times the size of the largest particle size present. It should however be noted that this selection of examination scale would ideally have been based upon knowledge of the largest particle or droplet size in processed crumb rather than the initial powdered ingredients.

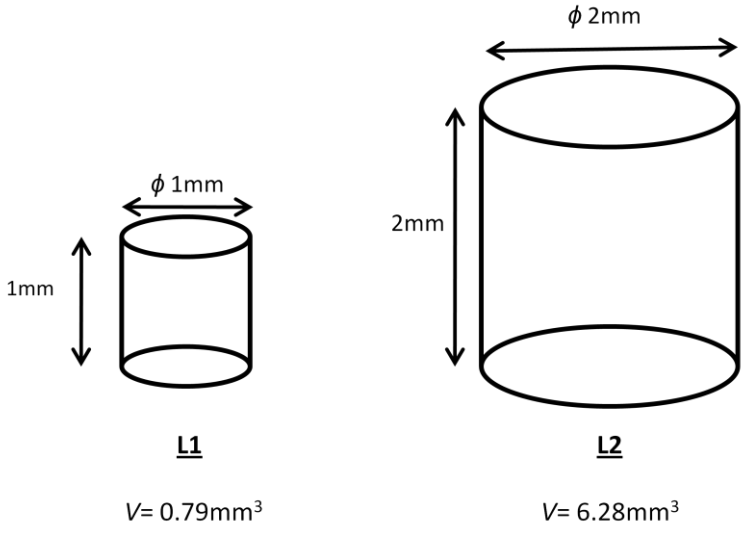

Figure 5.4 TGA sample dimensions for length scales L1 and L2

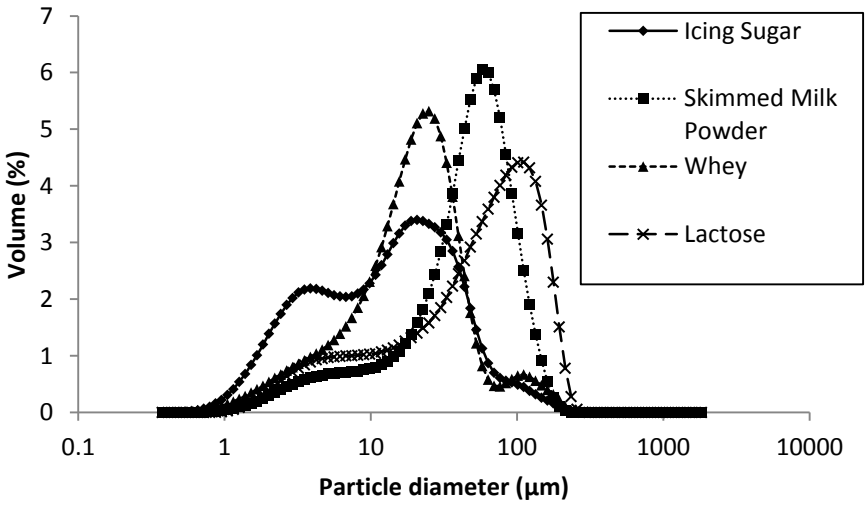

Figure 5.5 Particle size distributions of dry ingredients (provided by Mars UK Ltd)

In order to achieve cylindrical samples with the dimensions shown in Figure 5.4, two custom samplers (an example of which is shown in Figure 5.6) were designed and machined with sharp edged casings of diameter 1mm and 2mm respectively. The cylinder height was then achieved by inserting a plunger of adjustable length. The combined plunger assembly, shown in the right hand image of Figure 5.6, was then inserted into the paste. With the sampler filled with crumb paste, the insert is then removed and the cylindrical sample of paste pushed out of the open end to leave a cylindrical sample of the correct size, as shown in Figure 5.7.

The location of sampling must ensure that an entirely random selection of samples is achieved and that the distance between sample sites is larger than any localisations of segregated ingredients. Experience of handling the material and consideration of the paste images shown in Figure 5.1 suggested that a separation distance of ten times the characteristic sample length would be sufficient. As such, sampling site templates to place over batches of LM crumb paste were also produced with dimensions also illustrated in Figure 5.6. The standard deviation between thermograms of 10 samples was used for each mixing index data point.

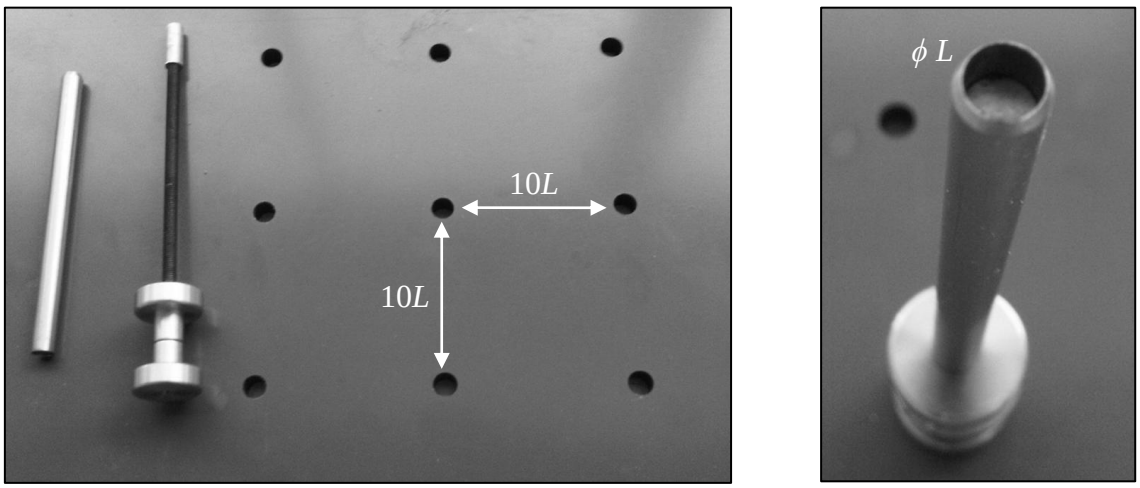

Figure 5.6 One of two sets of custom sample cutters and sampling template showing relative dimensions in terms of the length scale, L

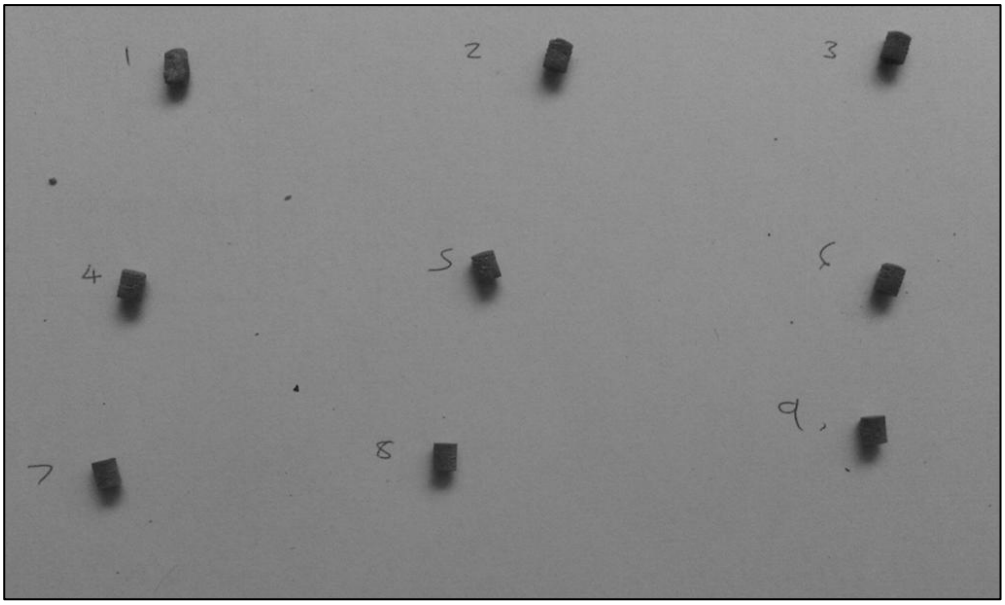

Figure 5.7 Example of nine L2 8% water LM crumb paste samples for use in TGA

5.2.2 Method

A Perkin Elmer Pyris 1 thermogravimetric analyser was used for the thermal decomposition characterisation of cylindrical LM paste samples subjected to various mixing times. Preliminary runs showed that all decomposition that takes place in well mixed LM crumb paste within the thermal range of the TGA (1000 °C) occurs below 600 °C. A residue remains above 600 °C, but exhibits no further decomposition between 600°C and 1000 °C. Consequently all further samples were then run between 30 °C and 600 °C. *L*2 samples were heated at a rate of 30 °C/min and in an attempt to maximise the "resolution" of the technique on the smaller scale, *L*1 samples, heating was performed at a slower rate of 20 °C/min. This decrease in heating rate has a negative effect on the total processing time of samples.

Whilst processing the preliminary samples, a systemic variation in the percentage mass remaining between 150 °C and 200 °C was apparent as the age of the sample increased and was likely indicative of drying out in the samples. Systemic variations of

this kind would be erroneous for mixing analyses which assess the statistics of variation between samples. In order to confirm this observation, "well mixed" samples, where compositional variations were assumed to be small, were heated after various times of ageing to record the percentage mass remaining at 190 °C, at which point any free water within the samples is assumed to have evaporated. Figure 5.8 shows a significant increase in the percentage mass remaining at 190 °C as the age of the sample increases, indicating that the concentration of free water is decreasing with time and that the samples are drying out. This effect appears to stabilise somewhat after approximately 620 hours (25 days). All samples were therefore run after at least 25 days of stabilisation after mixing. Figure 5.8 also shows that keeping samples in a sealed container containing desicant does not accelerate the stabilisation significantly.

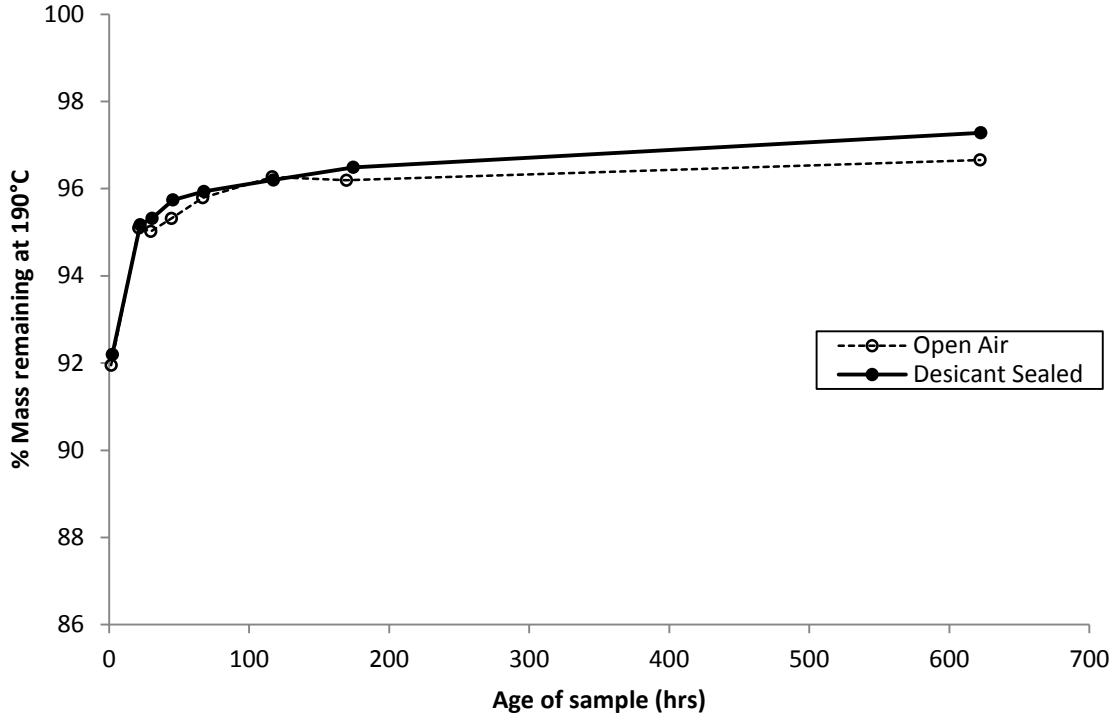

Figure 5.8 Mass remaining at 190°C during TGA versus age of L2 sample (8% LM paste) for samples stored both in air and sealed containers with desicant

Figure 5.9 shows a typical TGA thermogram for *L2* LM crumb paste samples. Whilst there are temperature regions of the thermogram which show significant rates of thermal decomposition, the definition of individual components is poor in comparison with thermograms such as those obtained by Kalyon *et al.* (2006) in Figure 5.2. In these cases, where the material is simple with relatively few ingredients, of high purity and discrete decomposition temperatures, it is possible to accurately determine individual component concentrations. However, for complex materials such as crumb paste, comprised of complex organic ingredients which do not decompose entirely within discrete temperature regions, individual component concentrations are indeterminable with any degree of accuracy.

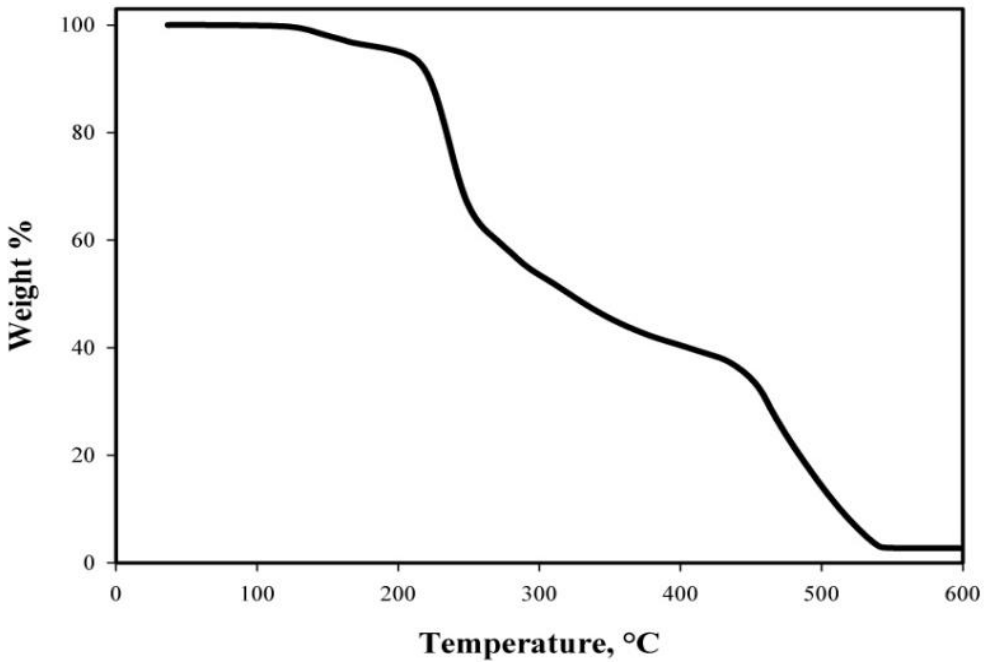

Figure 5.9 A typical TGA thermogram for L2 samples of LM crumb paste obtained during preliminary TGA tests at 30°C/min

Figure 5.10 and Figure 5.11 show preliminary TGA data for seven *L2* samples of LM crumb paste after fifteen seconds of mixing and sixty seconds of mixing respectively. The clear reduction in thermogram variation between samples shown after sixty seconds of

mixing when compared to fifteen seconds of mixing demonstrates that TGA of these samples has managed to detect the increased homogeneity that was evident visually from the images in Figure 5.1. This observation supports the work of Kalyon *et al*. (2005) who found that TGA was able to detect a reduction in the breadth of variation of component concentrations as batch mixing time increased for graphite filled polymer suspensions.

However, poor thermogram definition displayed by LM crumb paste means that the intended mixing analysis described in 5.1.1 to quantify these changes in the degree of mixedness is not possible. Instead, an alternative analysis for quantifying distributive mixing within complex multicomponent pastes such as this with TGA must be considered. A novel alternative analysis is therefore presented in Section 5.3.

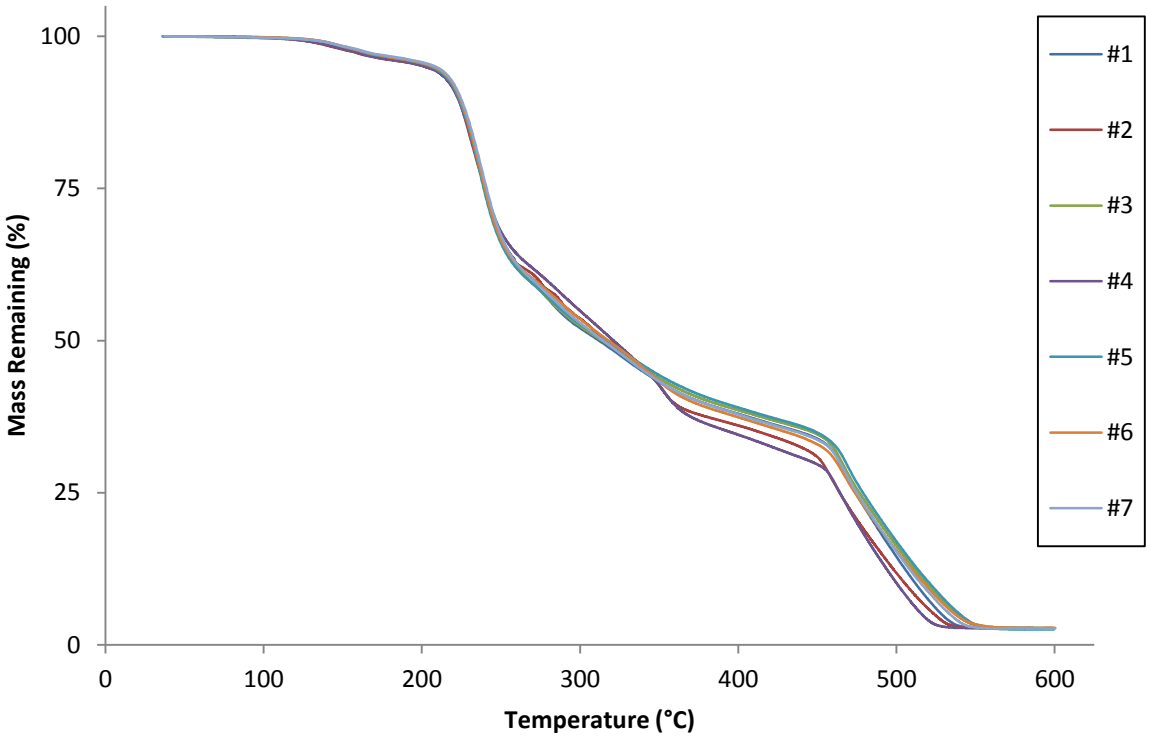

Figure 5.10 Thermograms of 7 L2 crumb samples (heated at 30°C/min) which have undergone 15 seconds of mixing

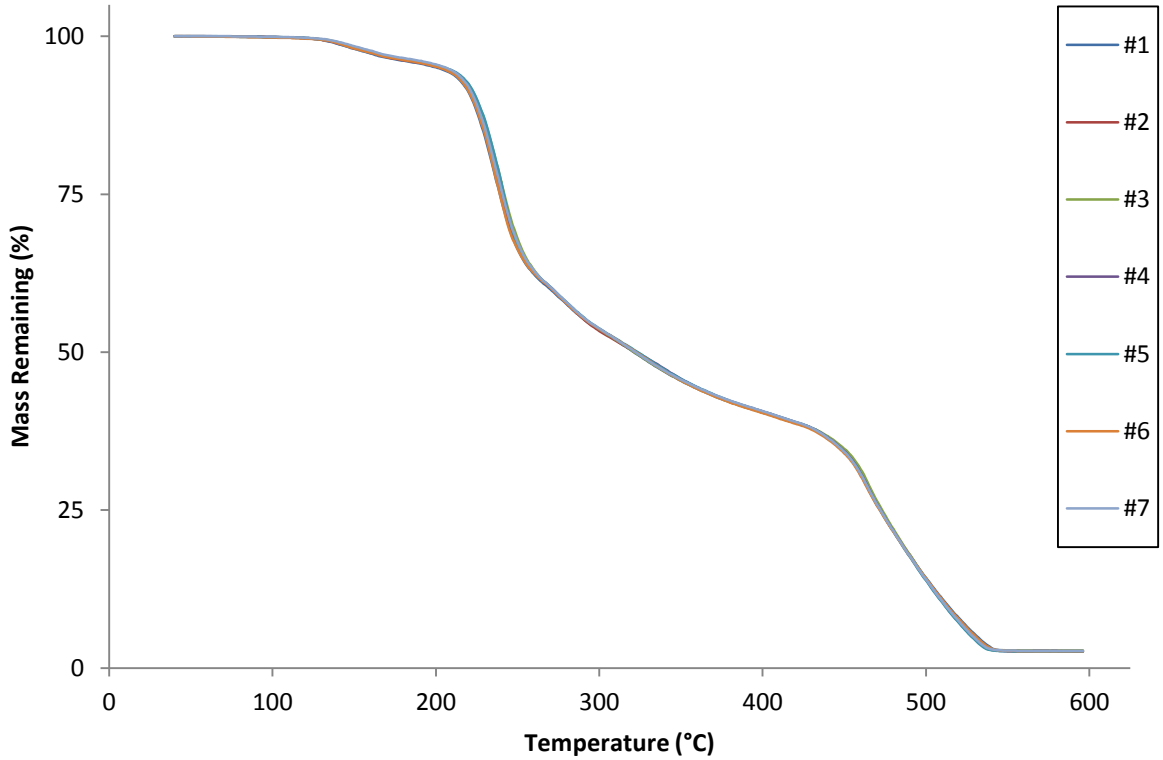

Figure 5.11 Thermograms of 7 L2 crumb samples (heated at 30°C/min) which have undergone 60 seconds of mixing

5.3 Alternative TGA analysis

Consider each sample, *j*, as being composed of an infinite number of components, *i*, which all thermally decompose within a temperature range between $T_{\min}$ and $T_{\max}$. Each of the components, *i*, in sample, *j*, decompose over a temperature range of dT at $T = T_i$ and is present in the quantity dM_i. The gradient of a thermogram, $-\left.\frac{dM_i}{dT}\right|_{T=T_i}$, therefore gives the mass concentration present in the sample for each component decomposing at temperature, T_i, as shown in Figure 5.12.

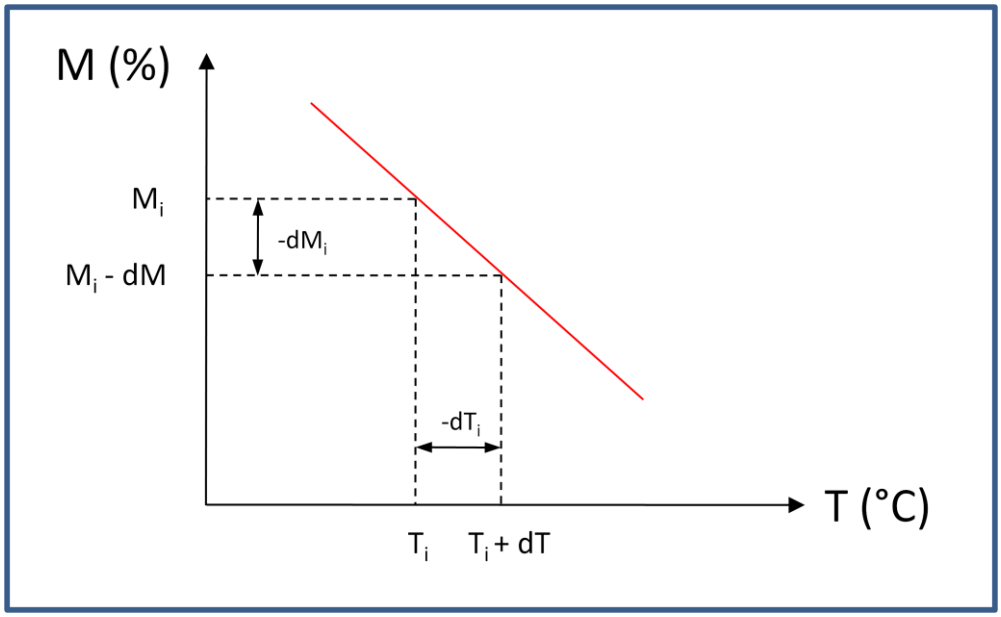

Figure 5.12 Thermogram gradients for alternative TGA analysis

When considering the homogeneity of component i in N samples, the standard deviation, σ_i, between thermogram gradients at temperature T_i provides a measure of the variation in concentration of component, i, and is given by:

$$\sigma_i = \sqrt{\frac{1}{(N-1)}\sum_{j=1}^{N}\left(\left[\left.\frac{dM_i}{dT}\right|_{T=T_i}\right]_j - \overline{\left[\left.\frac{dM_i}{dT}\right|_{T=T_i}\right]}\right)^2} \qquad (46)$$

Plotting σ_i against temperature will then display the temperature distribution of any compositional inhomogeneities between samples. By integrating this distribution in the range T_{min} to T_{max}, an overall mixing index of sample homogeneity can be obtained without the need to accurately determine the concentration of any one component. Larger integral values will represent significant overall variations in composition between samples whilst smaller values represent lower compositional variations indicative of improved homogeneity.

$$MI = \int_{T_{min}}^{T_{max}} \sigma_i(T)\, dT \qquad (47)$$

If inhomogeneities are localised i.e. appearing as sharp peaks in the temperature distribution of standard deviation and these peaks occur at temperatures corresponding to peaks in the thermal decomposition rate of individual ingredients furnaced alone, the magnitude of the inhomogeneity peaks may be used to track the mixing behaviour of individual ingredients, or parts thereof. This concept is explored further in Section 5.4.

5.4 Results

Figure 5.13 shows the results of the mixing index analysis devised in Section 5.3 for LM crumb paste TGA samples at various times of mixing. An approximately exponentially decreasing mixing index is shown for increasing mixing time using both $L1$ and $L2$ length scales. This decreasing integral mixing index indicates an increase in compositional homogeneity during batch mixing and is the anticipated result given that mixing time was the only variable between sample sets and the images shown in Figure 5.1. As such, this shows that the technique and proposed analysis has successfully characterised the most basic trend of a relative improvement in the distributive mixing of LM crumb paste subjected to increasing degrees of batch mixing.

As would be expected from the discussion of sample size in Section 5.1.2, both length scales display a similar pattern of distributive mixing, with a high initial rate of mixing which approaches a steady value. However the $L1$ samples generate wholly larger values of integral mixing index than the $L2$ samples since the scale of observation is reduced and the apparent inhomogeneities are larger, offering potentially higher resolution if trying to distinguish between similar samples.

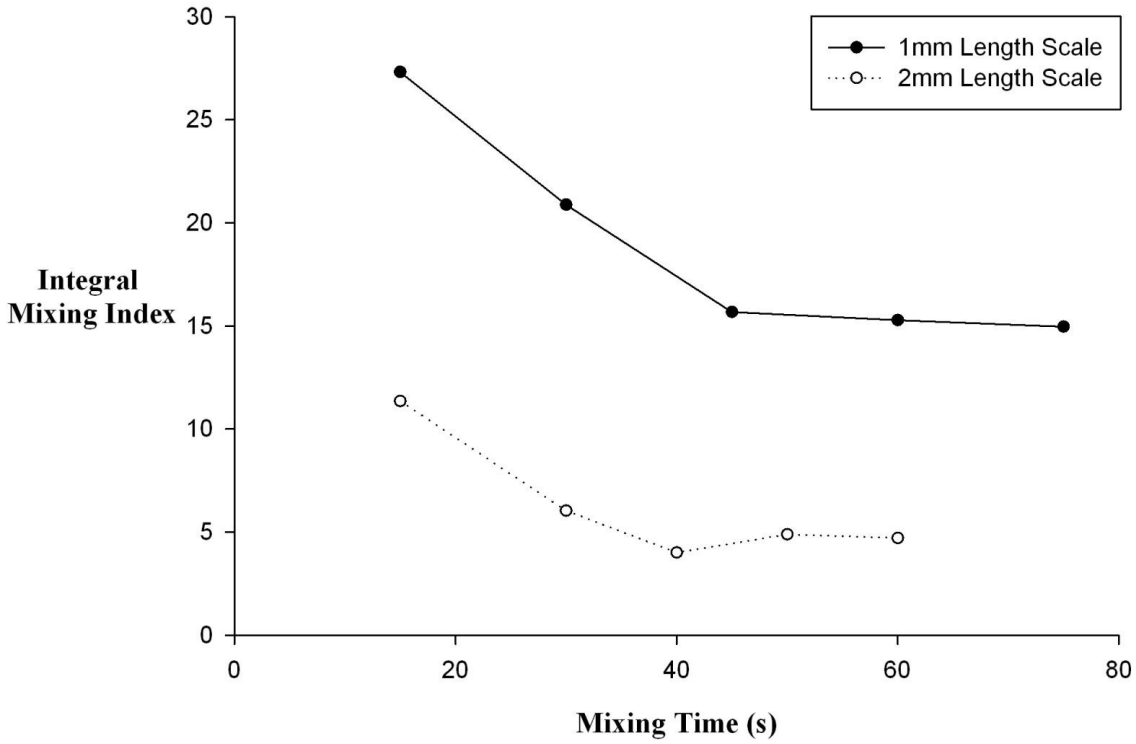

Figure 5.13 Integral mixing index versus mixing time for 1 mm (L1) and 2 mm (L2) length scale samples

Figure 5.14 shows an example of a waterfall plot of the changing temperature distribution of *L*2 inhomogeneities with mixing time. The apparent reduction in the overall area under the standard deviation distributions with mixing time has been characterised by the decreasing integral mixing index shown in Figure 5.13 above. Within the distributions themselves, the sharp peaks of variation appear to be localised to consistent temperature ranges between sample sets, as illustrated by the colour coded peaks. As these peaks appear approximately in the same temperature regions across all sample sets, it was hypothesised that the temperature ranges at which the largest inhomogeneities appear are characteristic of the material and ingredients in question.

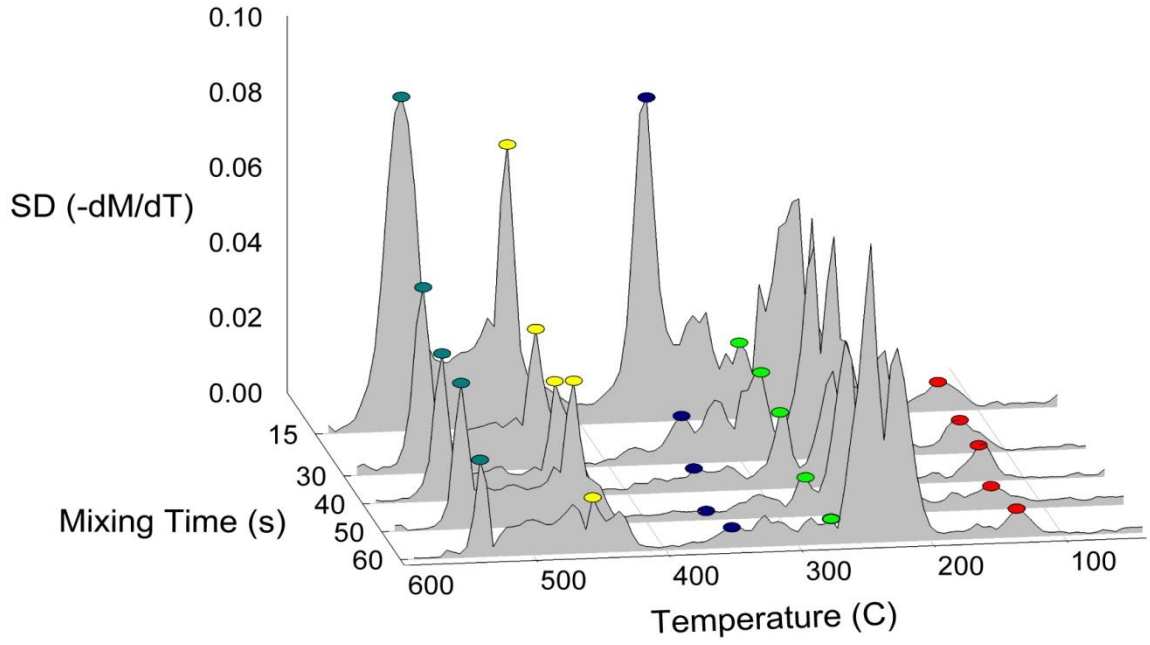

Figure 5.14 Waterfall plot to show the changing temperature distribution of thermal decomposition rate inhomogeneities obtained using TGA for sample sets which have undergone increased mixing time

Although it has been shown in Section 5.2 that the thermal decomposition temperatures of the ingredients making up crumb paste were not discrete enough to allow the determination of individual ingredient concentrations, it was hypothesised that the temperature zones of some inhomogeneity peaks may be attributable to a particular ingredient (or at least a subcomponent of). If this is the case, then the magnitude of the inhomogeneity peaks may be used to provide insight into the relative distributive mixing of some individual components.

In order to confirm or disprove this hypothesis, thermograms of each of the individual ingredients in crumb paste were obtained and plotted as the rate of mass change against temperature in order to determine the most significant decomposition temperatures. Where clearly identifiable, peaks of thermal decomposition rate for the individual ingredients were then matched to peaks in the inhomogeneity distributions across the

sample sets. An example of this peak matching is shown in Figure 5.15 where an inhomogeneity peak (shown most clearly in the sample set taken after fifteen seconds of mixing) is shown to correspond well with the thermal decomposition peak of cocoa mass alone.

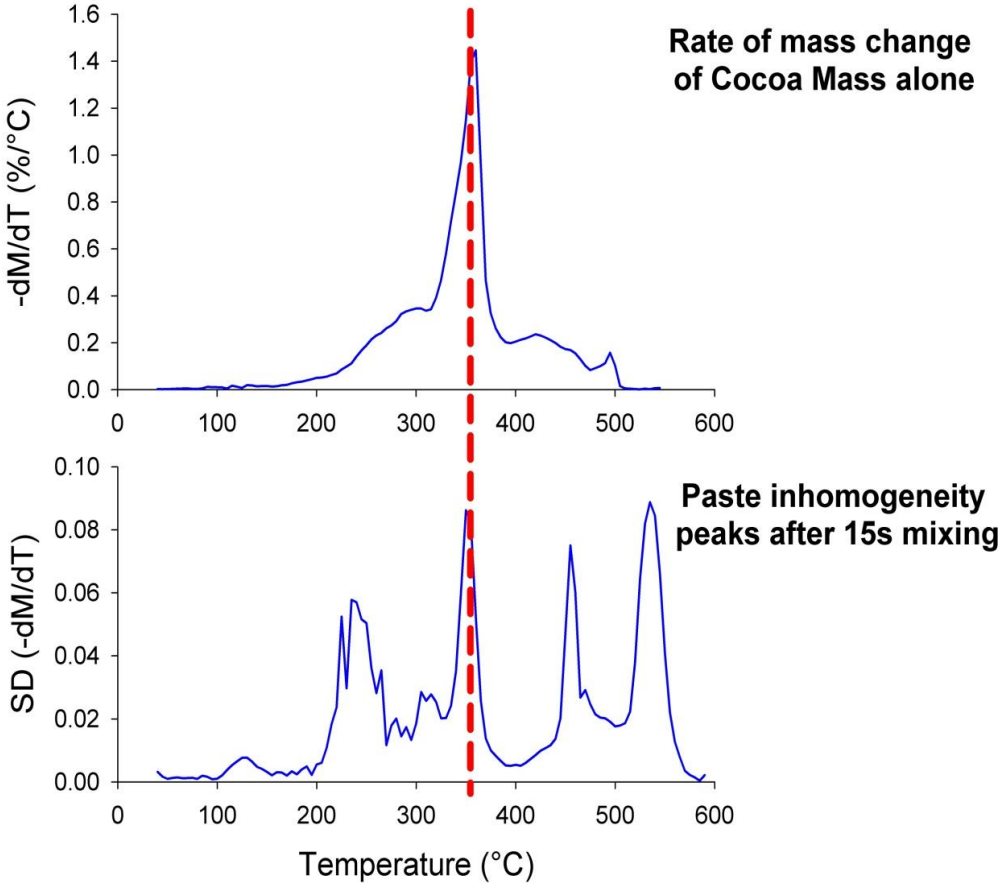

Figure 5.15 Inhomogeneity peak (bottom) matched to cocoa mass decomposition peaks (top) using TGA

In some cases, such as icing sugar, multiple peaks exists, which is representative of the complex nature of these natural ingredients which contain sub components or multiple phases of structure within themselves. Where multiple peaks for an ingredient exist, confident matching of a single peak to a TGA inhomogeneity peak means only part of that ingredient is being matched, however this may then act as a "tracer" element to indicate the presence of that ingredient.

For some ingredients, two separate ingredients may exhibit thermal decomposition peaks of the same temperature. This may be coincidental if each ingredient contains different components or phases which happen to decompose at the same temperature. If this is the case, it is not possible to distinguish between the behaviour of the two ingredients by considering the evolution of the single inhomgeneity peak. However the incomplete separation of ingredients within the dairy industry means that sometimes the coexistence of peaks between two ingredients can be explained by the presence of one ingredient within the other. For example whey powder often contains some lactose as well as whey proteins.

Where possible, ingredient peaks have been matched to the most identifiable peaks apparent in Figure 5.14 (those marked by the coloured dots) in order to produce the 2D plot in Figure 5.16 to illustrate the changing magnitude of each matched inhomogeneity peak with mixing time. As the magnitude of an inhomogeniety peak decreases, the variation in concentration of the ingredient which decomposes significantly at that temperature (or at the very least, a subcomponent or phase of) within each sample set decreases indicating that particular ingredient is becoming more evenly distributed throughout the volume.

In this simple batch mixing geometry, the identifiable liquid ingredients intuitively appear to be distributed more readily than powdered ingredients. At the first sample set of fifteen seconds, the distribution of water appears to have already reached a steady homogeneity whilst cocoa mass is relatively localized, before mixing well between fifteen seconds and thirty seconds on the low mixing speed. The increased mixing speed after thirty seconds results in a further improvement in the distribution of cocoa mass throughout the volume, albeit at a less significant rate. It is anticipated that the difference in distributive mixing demonstrated between water and cocoa mass can be attributed to

their significantly different viscosities, with low viscosity water penetrating the powdered ingredients much more readily than viscous cocoa mass.

Tracer elements of some of the solid ingredients then appear to distribute at differing rates and is expected due to the differing quantities of each ingredient and the range of particle size distributions possessed. Time restraints did not permit further investigation of the mixing dynamics within this process, however the results of these trials have demonstrated the technique has the potential for exploring the mixing dynamics of such systems.

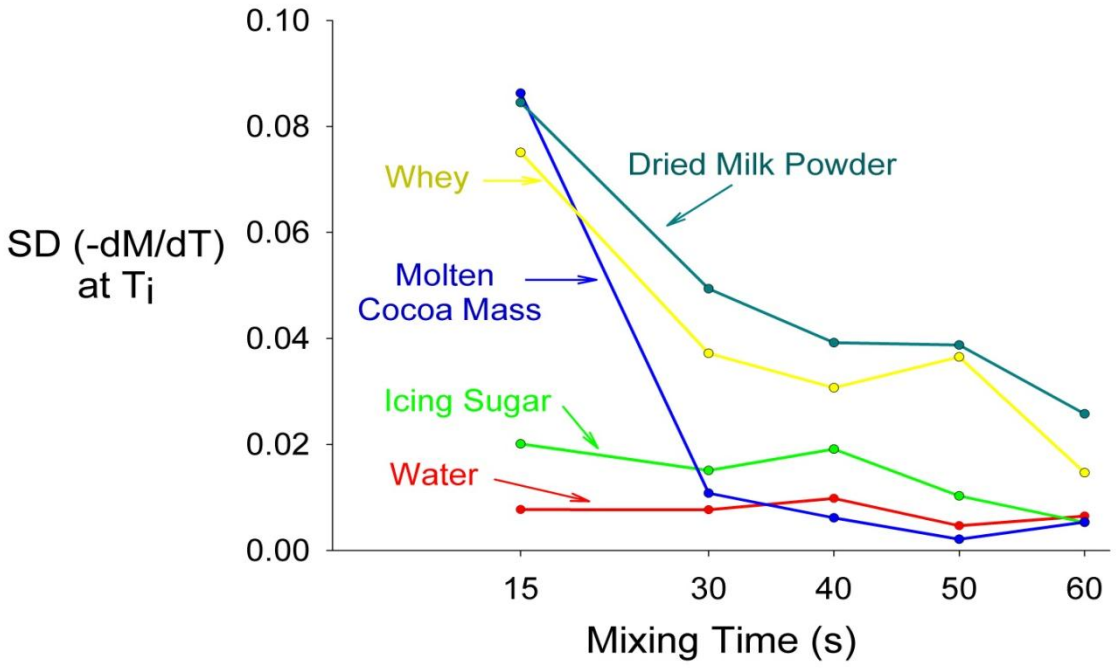

Figure 5.16 Individual ingredient mixing versus mixing time for LM crumb paste using TGA analysis

5.5 Conclusion

In this chapter, a novel analysis of thermogravimetric data for batch mixed LM crumb paste has been developed to quantitatively observe the relative distributive mixing of both the bulk and individual components with mixing time. LM crumb is a complex, multi-phase paste containing seven organic ingredients with similar and relatively non

discrete decomposition temperatures. For this reason, the determination of individual component concentrations from TGA thermograms is not possible, making the use of standard TGA mixing analyses that assess the variance of discrete component concentrations within a sample set unviable.

Instead, the standard deviation of rates of mass change between samples have been plotted as a function of temperature for each sample set. From these standard deviation distributions, it has been possible to observe peaks in variation between samples and determine which temperature ranges contain the largest inhomogeneities. These peaks appeared to occur within temperature ranges that were characteristic of the peak decomposition temperatures of individual ingredients, allowing peak magnitudes to provide insight into the relative distributive mixing performance of individual ingredients.

Whilst the relative magnitudes of peaks within the standard deviation distributions have provided information about the relative mixing of individual components, it was also possible to integrate these functions to provide a quantitative index of bulk mixing and homogeneity. As was expected, this numerical index successfully showed improved homogeneity in LM crumb paste with increased batch mixing time for both sample length scales considered.

Intuitive observations regarding both the bulk homogeneity of LM crumb paste and the distributive mixing behavior of individual components provided confidence that that the technique and analysis have been robust enough to accurately capture anticipated behaviours in this simplified version of the process. Given this successful application of TGA and the novel analysis to batch mixed LM crumb pastes presented in this chapter, their use has been proposed for the investigation of distributive mixing with the extruder itself. The results of this work as a part of the extruder pilot plant trial are presented in Chapter 7.

Chapter 6 Dispersive mixing of crumb paste

Attempts to characterise the rheological behaviour and distributive mixing of crumb paste have been presented in Chapters 3 to 5. In addition to these forms of characterisation, it is also necessary to develop a method from which it is possible to visualise the paste microstructure. If achieved successfully, it may then be possible to track the microstructure and the extent of dispersive mixing at various stages of crumb paste production and under various processing conditions.

In this chapter, attempts to visualise various aspects of crumb paste microstructure using three techniques are presented. Section 6.1 begins with an introduction to dispersive mixing and an overview of the visualisation techniques presented in this chapter. Section 6.2 presents visualisations of LM crumb paste obtained using scanning electron microscopy and is followed by images and a novel analysis of protein networks using optical microscopy staining in Section 6.3. The novel application of multiphoton microscopy for the mixing analysis of food pastes is presented in Section 6.4 and conclusions about LM crumb paste microstructure and the suitability of the various techniques for use in the extruder trials are drawn in Section 6.5.

6.1 Dispersive mixing and paste visualisation

Dispersive mixing is the extent to which agglomerates are broken down and changes in the physical properties of material constituents occur. The operative mechanism for this form of mixing is the existence of elongational forces and/or shear stresses (Van Zuilichem *et al.*, 1999). In a general context, dispersive mixing is generally of great significance in all extrusion or batch mixing which involves the processing of powders or granules. For example, poor dispersive mixing in many pharmaceutical applications can lead to undesirably high concentrations of poorly water soluble drugs when granules have not been dispersed and broken down sufficiently (Van Melkebeke *et al.*, 2008).

In the context of crumb paste extrusion, the build up or dispersion of powdered ingredients and sugars is likely to have a direct effect on the uptake of water in the process. Given the large range of potential microstructures that can occur during the formation of a paste, as water and fluid phases interact with soluble and non-soluble solid phases (see Section 2.2.2) the extent of dispersive mixing occurring during crumb paste formation is likely to bear significance on the form of microstructure present at any stage of the mixing process. Given the difficulties in modelling that occur from a lack of clear microstructural classification in pastes (described further in Section 2.2), the importance of being able to visualise and classify paste microstructure is clearly evident.

The physical characteristics of particles and agglomerates in the final form of chocolate are well documented to have a significant effect on the taste and the perception of texture, however the relationship between crumb paste microstructure and chocolate microstructure is currently unstudied. Therefore the ability to benchmark the extent of dispersive mixing taking place within respective crumb mixing processes is highly desirable for further development of crumb mixing.

The difficulty of the problem is highlighted by Kalyon *et al*. (2006), who when considering the extrusion of graphite filled polymer suspensions stated that for industrial suspensions there is no easy way to determine the changes in the particle cluster dimensions as a function of the mixing process. This is indeed the challenge that is being considered as part of this project and the three techniques outlined have been tried on crumb paste in order to try to achieve visualisation of crumb paste microstructure and dispersive mixing.

6.1.1 Scanning electron microscopy (SEM)

Scanning electron microscopes have been used extensively from around the mid nineteen sixties to provide high magnification and high resolution images of specimen topography using electron signals rather than light. Using this technique, specimens are primarily imaged by focusing and raster scanning a narrow beam of accelerated electrons through a high vacuum and onto the surface of a sample. Secondary electrons are ejected from atoms at the surface of the specimen following their interaction with primary electrons in the beam. These ejected electrons are then collected by a detector with signal intensities strongly dependent on the surface topology of the sample resulting in high resolution images (as low as 2 nm) with sharp topological contrast giving a three dimensional appearance to the images obtained.

Whilst images obtained using standard SEMs provide an excellent quality of highly magnified images, there are restrictions on the sorts of samples that can be viewed under a normal SEM due to the high vacuum environment that is required by the operation of the electron beam. Samples are also required to be dry and electrically conductive to prevent charging. For non-conductive samples, this requires a thin conductive film of gold to be sputter coated onto the sample surface. Such sample restrictions then led to the

development of environmental scanning electron microsopes (ESEMs) in the nineteen eighties which now permit the imaging of wet, non-conductive samples by separating the electron beam column from the sample environment using pressure limited apertures. This removes the constraint of having a vacuum in the sample chamber as well as the need to coat non-conductive samples since ionisation in the sample chamber prevents charging artefacts in images. This type of imaging is now highly attractive for food samples due to their typically large water contents and the lack of sample preparation now required in order to obtain an image for non-conductive samples.

If the electron microscope being used is also fitted with an EDAX X-ray detector system, it can be possible to perform Energy Dispersive Spectrometry (EDS) to assist in identifying objects within images, by providing as estimate of their elemental composition. Energy Dispersive X-ray Analysis (EDAX) works by bombarding the specimen (or part thereof) with a tightly focussed electron beam, knocking off electrons from the outer shells of the elements being targeted. If an electron is displaced from the outer shell of an atom, an electron from one of the inner shells will seek to replace it. In doing this, it must make an energy jump and a burst of X-ray energy is emitted as a result. The precise amount of energy released in this form is characteristic of the element being bombarded and the shell transition being made. From this, it is possible to estimate the elemental composition of a targeted area on the specimen by counting the frequency of each magnitude of X-ray that is received by the detector and building an EDS spectra. The use of ESEM to visualise the morpohology of crumb paste on a micro scale is considered in this chapter and images of LM crumb paste obtained using an ESEM are presented in Section 6.2.

6.1.2 Optical microscopy

Traditional optical microscopy techniques are an obvious potential source of information for microstructural studies such as this, provided that meaningful and robust images can be obtained. A successful example of this is Potluri *et al.* (2006) who were able to use optical micrographs of extruded polymer blends sampled from various points within a counter rotating twin-screw extruder to show that the size of polystyrene fragments remained constant throughout the length of the extruder after initial fracturing.

Protein staining techniques used in conjunction with traditional optical microscopy are well established and the significant concentration of proteins present within the ingredients of crumb paste suggests that their dispersion or aggregation may be observable using such techniques. The dense opacity of crumb paste means that any optical techniques involving the transmission of light require thin sections of sample.

An optical protein staining technique adopted by the company has been used widely on final form chocolate and briefly on small "lumps" of chocolate crumb to qualitatively observe protein distribution, but has so far not been used to draw any quantitative conclusions. The technique, which involves staining proteineous volumes of sample with ethanolic Eosin Yellow, can be used to observe protein distribution across a sample when viewed under brightfield transmitted light. Additionally, due to the birefringent nature of anisotropic crystals, any crystalline material can be selectively viewed under polarised light and it may be possible to observe the interaction between protein formations and sugar crystals as a function of mixing.

In this chapter, the use of this technique on crumb paste is explored further to determine whether or not a robust enough method and analysis can be used to draw quantitative conclusions about the extent of protein network formation and their

microstructural interaction with sugar crystals. The results of this investigation are presented in Section 6.3.

6.1.3 Multiphoton microscopy (MPM)

In addition to scanning electron and optical microscopy, the scope of using multiphoton microscopy (MPM) on crumb paste is also considered. MPM is a powerful technique which enables the 3-D imaging of fluorescent particles or structures. A pulsed laser generates two beams of photons, which on their own have insufficient energy to cause fluorophore excitation. At the point of focus however, multiple low energy photons can be absorbed simultaneously with a combined energy of sufficient magnitude to induce an electronic transition. Consequently, only at the point of focus will fluorophore excitation occur, thereby eliminating out of focus fluorescence. MPM is accomplished by raster-scanning this tightly focused beam within a specimen and thereby optically selecting an axially isolated plane of fluorescence information and achieving optical sectioning (Williams *et al.*, 2001).

Although similar in principle to conventional confocal fluorescence microscopy, multiphoton microscopy possesses two main advantages. Whilst confocal microscopy captures fluorescence illumination and then filters out-of-plane signals in order to create a section (McNally *et al.*, 1999), multiphoton microscopy restricts the excitation to a finer volume, reducing out-of-plane noise at the source as well as reducing the effects of photobleaching. Secondly, due the use of longer wavelengths in the lasers (typically red to infrared >700 nm), the depth of penetration into specimens is greater and in optically favourable specimens can be as great as a few hundred microns (Centonze & White, 1998).

Some materials can demonstrate natural fluorescence, which can be very attractive when considering that little sample preparation is then required, however if materials do not demonstrate this behaviour, then the staining of individual elements with fluorophores is widely used. Proteins are again particularly well suited to this staining as demonstrated by Hughes *et al.* (2006a).

MPM is currently used most widely in the Biological Sciences, for which there is wealth of published work analysing tissue samples and living cells, but has also begun to be used in applications such as the monitoring of cake formation on microfiltration membranes (Hughes *et al.*, 2006b). At the time of writing, the author is unaware of the use of MPM for visualising mixing processes and ingredient dispersion and believes that crumb paste analysis could be a novel application of this technique.

6.2 Scanning electron microscopy (SEM) of LM crumb paste

Environmental scanning electron microscopy (ESEM) images were obtained using an FEI Quanta 200 ESEM fitted with an EDAX/Genesis X-Ray detector system kindly made available by the School of Chemical Engineering and Analytical Science, University of Manchester. To provide some perspective of the physical form of the pre-processed ingredients mixed together in crumb paste, ESEM images were taken of dry blend, cocoa mass and cocoa butter, using EDAX on each to help identify components from their EDS spectra. In order to then obtain a visualisation of crumb paste topography, fractured samples of 8% water LM crumb paste (mixed using the routine described in Section 3.1.1) were imaged both fifteen minutes after mixing and ninety minutes after mixing. For comparative purposes, images of unfractured crumb paste were obtained by sampling the outer surface of the paste mass once removed from the mixing basin.

6.2.1 Pre-processed ingredients

Figure 6.1 shows a typical image of the dry blend powders (skimmed milk powder, sucrose, lactose and whey) when imaged using ESEM. A variety of shapes and sizes are evident amongst the powder particles and EDAX analysis was used to assist in identifying the type of ingredient associated with each particle shape. The EDS spectra for both the angular particles (Figure 6.2) and the "whispy" particles (Figure 6.3) show strong concentrations of predominantly carbon and oxygen atoms in an approximate ratio that suggests these particles may represent the various forms of sugar present in blend. Since both sucrose and lactose possess the molecular formula, $C_{12}H_{22}O_{11}$, differing only in molecular structure and arrangement, an EDS spectra showing only carbon and oxygen would be expected from these forms of sugar since hydrogen atoms do not have sufficient atomic weight to be detected using the EDAX detector system used here.

The detectable spectra of the angular particles contains only carbon and oxygen, from which it is inferred that this material is likely to be the purer form of sugar present in blend, sucrose. Conversely, the spectra for the whispy particles contains traces of a number of other elements present in dairy ingredients, from which it is inferred that this is likely to be a form of lactose containing traces of dairy elements from the incomplete separation known to occur during lactose production.

Finally, the EDS spectra of the rounded particles within Figure 6.1 shows strong concentrations of the elements present in sugars, carbon and oxygen, as well as many of the elements present in dairy ingredients, phosphorus, sulphur, chlorine, potassium and calcium. It is with a high degree of confidence that these particles can be labelled as skimmed milk powder particles as the vacuoles created by the spray drying process are also evident in the images.

The ESEM images and EDS spectra for cocoa mass and cocoa butter alone are shown in Figure 6.5 - Figure 6.8, however no discernible features of microstructural topography were observed from ESEM images of these materials. As expected, a notably more complex EDS spectra was obtained for cocoa mass than cocoa butter.

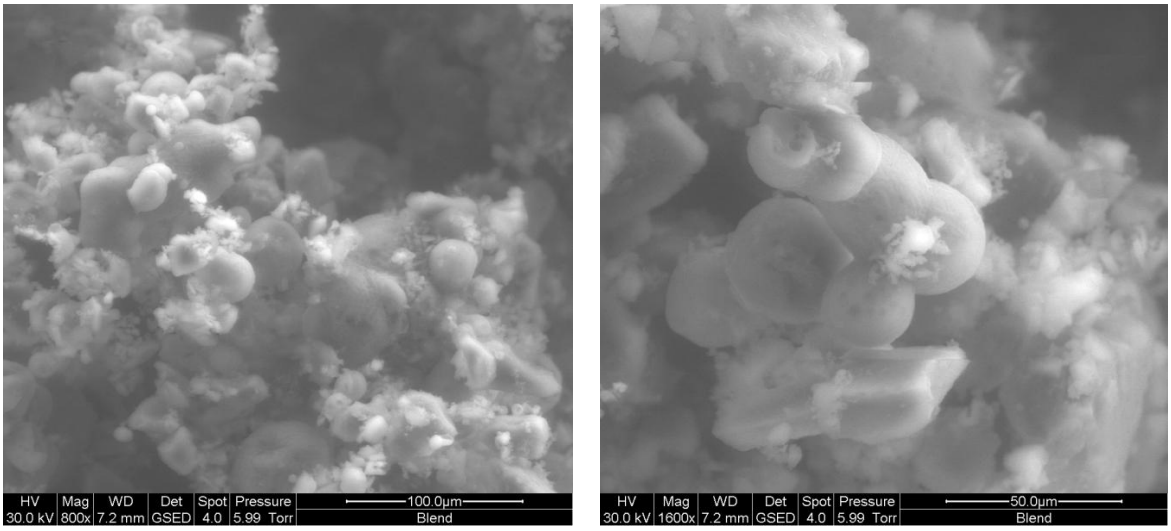

Figure 6.1 ESEM images of powdered blend pre-processing (x800 left, x1600 right)

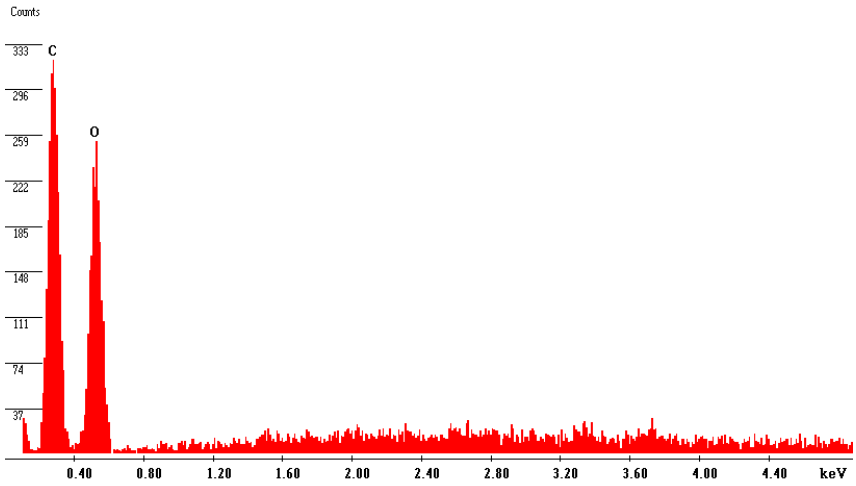

Figure 6.2 EDS Spectra of angular volume in blend (believed to be sucrose)

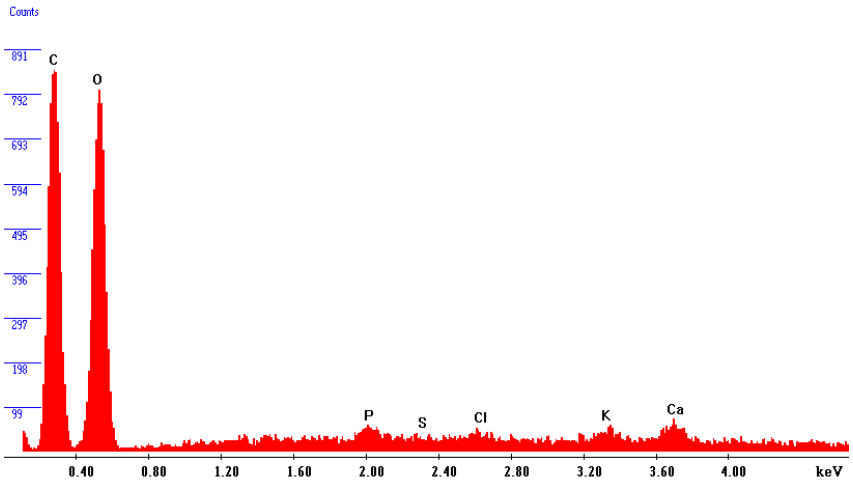

Figure 6.3 EDS spectra of "whispy" volume in blend (believed to by lactose)

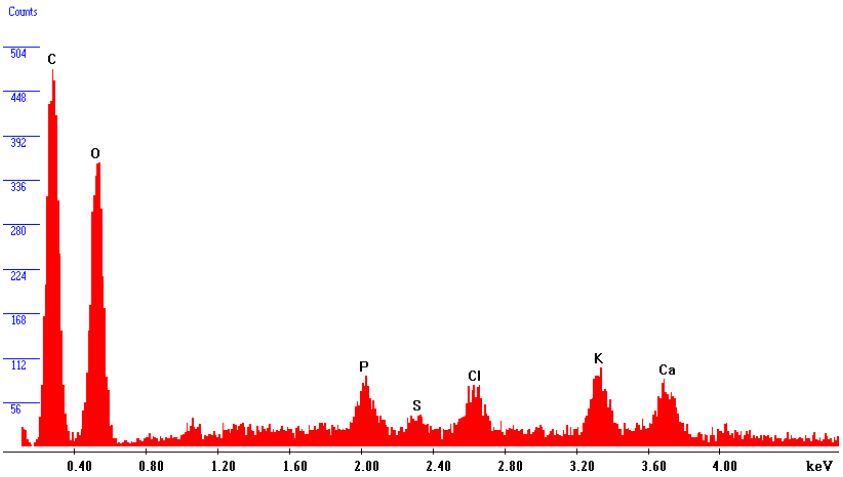

Figure 6.4 EDS Spectra of spherical particles in blend (believed to be SMP)

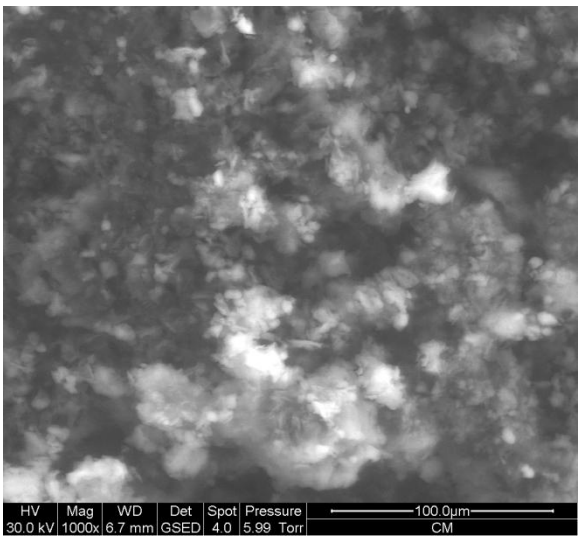

Figure 6.5 ESEM image of cocoa mass (x1000)

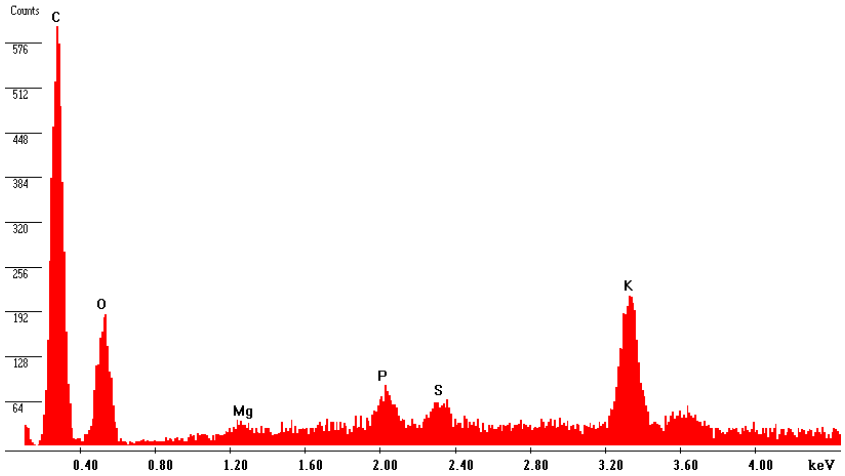

Figure 6.6 EDS spectra of solid cocoa mass

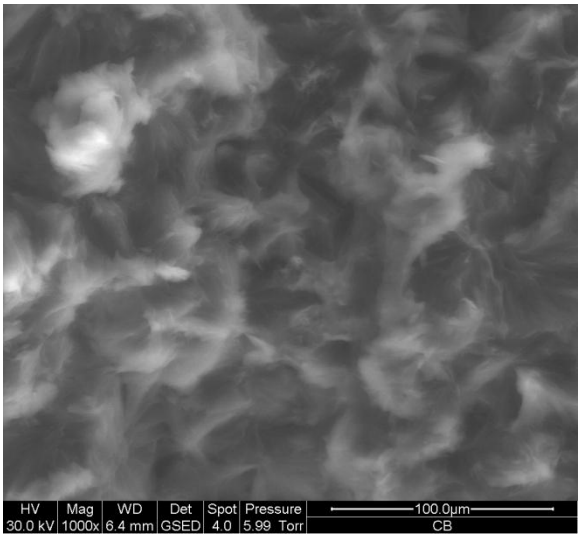

Figure 6.7 ESEM image of solid cocoa butter (x1000)

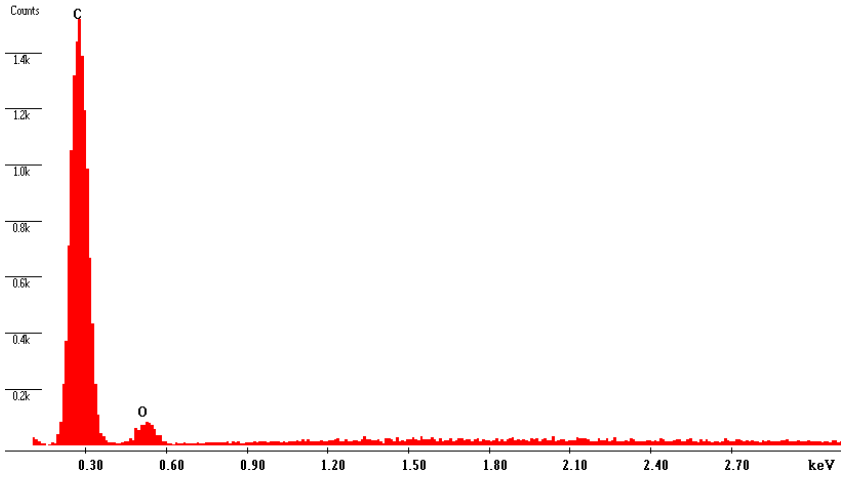

Figure 6.8 EDS spectra of cocoa butter

6.2.2 Fractured LM paste topography

Figure 6.9 shows the topography of a homogenous region of fractured LM crumb paste taken fifteen minutes after mixing. One of the most striking initial observations is the continuous nature of the paste and the lack of porosity. It was initially anticipated that air bubbles would be prevalent throughout the paste, however this does not appear to be case. Although there appears to be a number of dark holes across the image which resemble air pockets, closer inspection of the images using EDAX whilst under the microscope revealed that these were in fact not voids, but flat localised regions of a phase believed to be cocoa mass. In this image, the cocoa mass phase appears to be dispersed evenly amongst a binding medium which covers and supports an unknown network of solids.

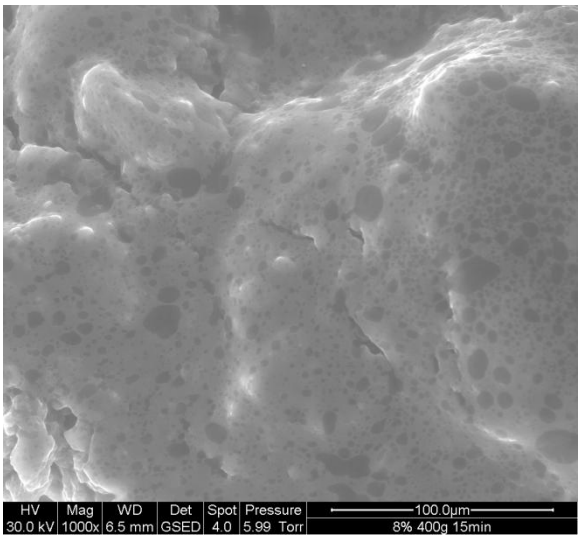

Figure 6.9 ESEM image of 8% water LM crumb paste fractured 15 minutes after mixing (x1000)

From the same batch of paste as Figure 6.9, Figure 6.10 shows various images of increasing magnification of a less homogenous region of the paste. In this region, a large agglomerate of solid material is apparent, which with increased magnification in the lower image, shows a part rounded particle with a jagged angular face. This is similar in size and appearance to what was believed to be a dried particle of one of the powdered dairy ingredients in Figure 6.1, suggesting this to be an ingredient particle which has only been

part dispersed. This image additionally shows a localised region of more angular topography than that shown in Figure 6.9. The angular nature of this material suggests a region of crystalline material most likely to be associated with the sugar content of the paste. The multi angled shape and size of this region when compared to the sugar crystals observed in Figure 6.1 suggests the formation of a secondary crystalline network, rather than a large sugar crystal undisturbed by the mixing process.

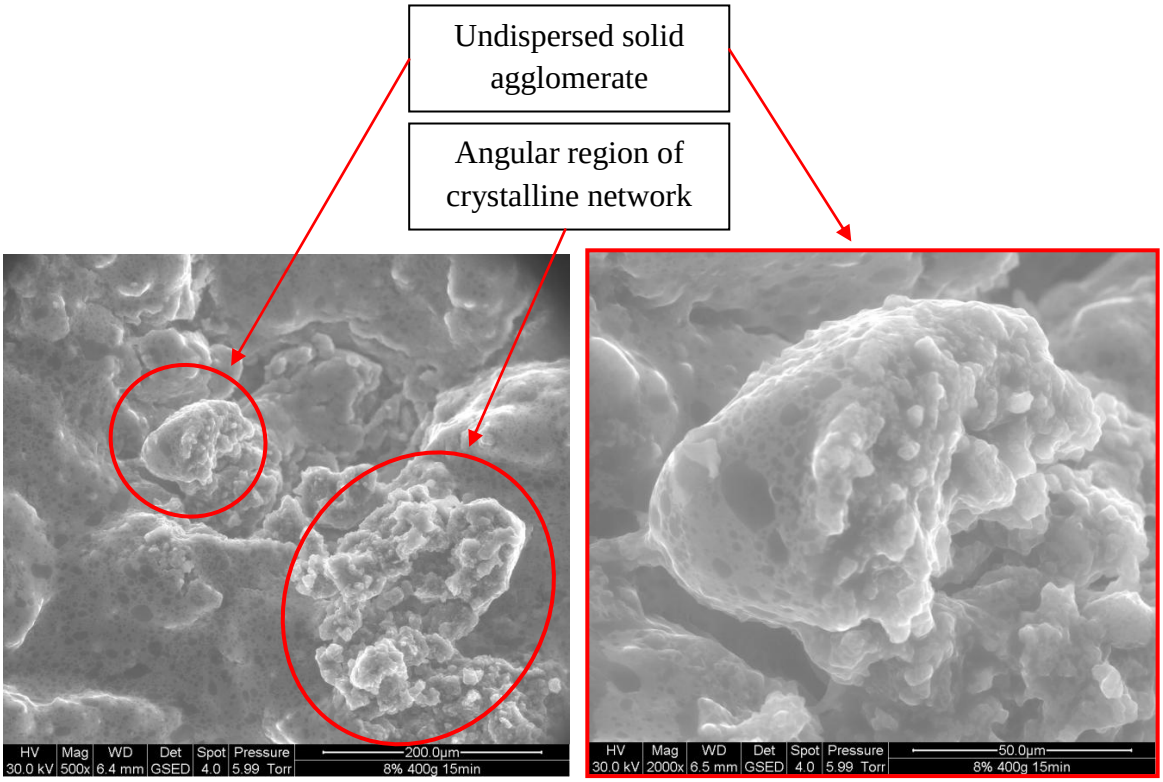

Figure 6.10 ESEM images of 8% water LM crumb paste fractured 15 minutes after mixing (x500 left, x2000 right)

For comparative purposes, images of samples that were allowed to harden for ninety minutes before fracturing are shown in Figure 6.11. When compared to the pastes imaged after only fifteen minutes in Figure 6.10, the topography of the paste is considerably more angular in nature, suggesting a more extensive crystalline network has developed between fifteen minutes and ninety minutes.

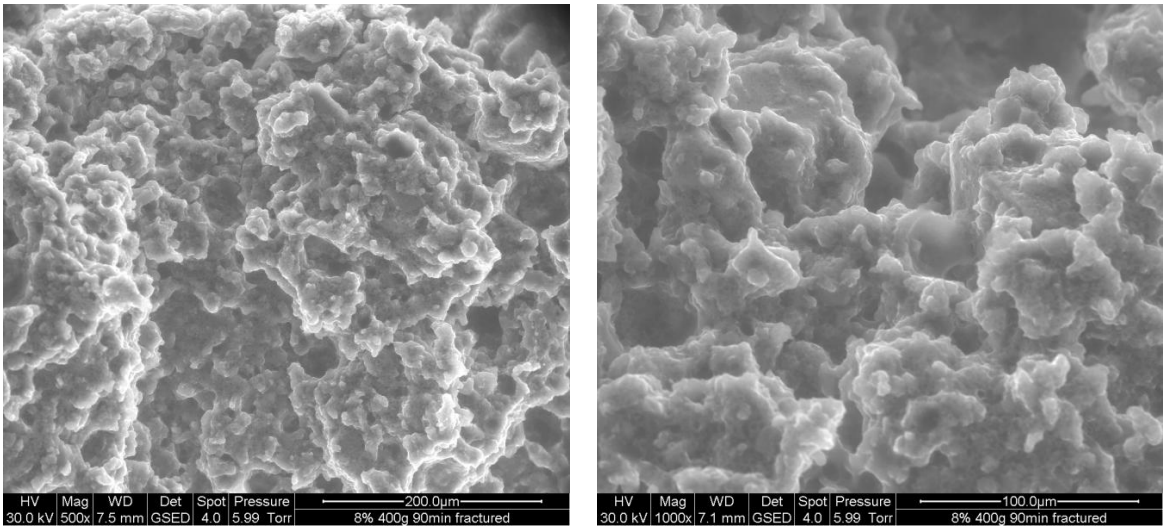

Figure 6.11 ESEM images of 8% water LM crumb paste fractured 90 minutes after mixing (x500 left, x1000 right)

A possible hypothesis from this observation is that a contributing factor to the hardening of crumb paste is prolonged crystallisation of sugars out of solution post mixing, forming an ever more rigid network until the paste exhibits a solid like structure with bound water and crystallised fats, rather than the original paste structure of solid bound by a continuous medium of fluid phases. Notably larger voids were visible in the fractured surfaces of the hardened samples (shown in Figure 6.12), however this is attributed to the more rigid fracture taking place to create the surface.

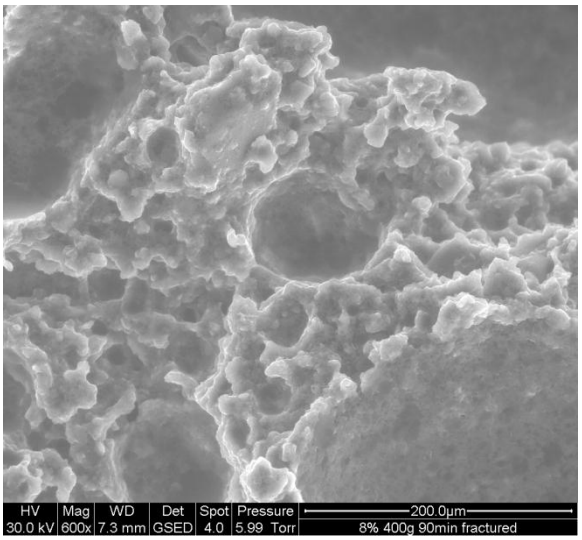

Figure 6.12 ESEM image of 8% water LM crumb paste fractured 90 minutes after mixing (x600)

6.2.3 Unfractured LM paste topography

In comparison to the previous images showing the internal topography of the bulk paste created by fracturing, Figure 6.13 shows a representative image of the outer surface of unfractured paste as it comes out of the mixer. Images taken seventy-five minutes after mixing showed a predominantly smooth outer surface where the presence of cocoa mass and its orientation were clearly visible.

The strongly aligned orientation and stretched shape of the cocoa mass suggests that areas of cocoa mass are affected not only by shear forces, but also by elongational forces and that in this image, it is these forces which have dominated their final alignment. In the few areas of the outer surface where protruding agglomerates of solid are visible (see the bottom half of Figure 6.13 (left) and Figure 6.13 (right)), undispersed regions of cocoa mass appear to surround the agglomerated or undispersed solids, suggesting regions that have been subjected to comparatively less shearing and dispersion.

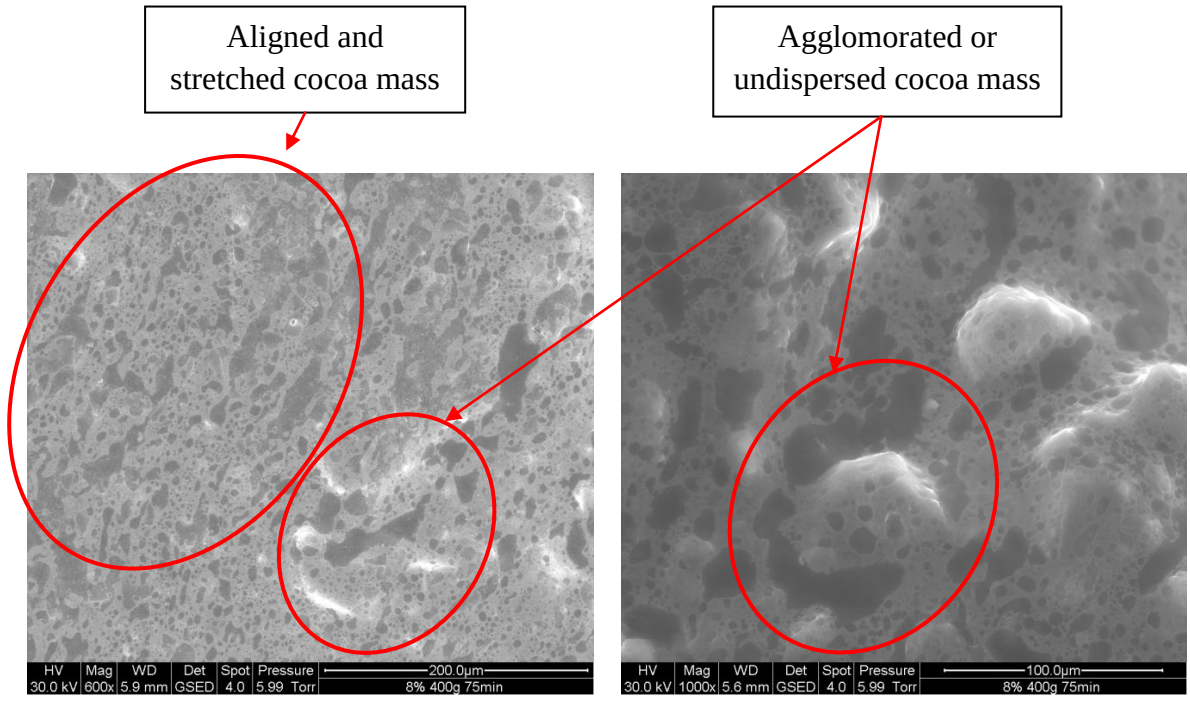

Figure 6.13 ESEM image of 8% water LM crumb paste surface (unfractured) 75 minutes after mixing (x600 left, x1000 right)

6.2.4 ESEM remarks

ESEM has been successful in providing high resolution images of powdered crumb paste ingredients and a visualisation of fractured and unfractured LM crumb paste topography on a micro scale. From this, it has been possible to infer qualitative observations about the microstructural features of LM crumb paste, observing both well dispersed and undispersed material.

Whilst the images obtained have been useful in observing some variations in the general form of paste microstructure, without tracers or stains, the number of components makes it difficult to distinguish between components confidently. Consequently many of the images obtained do not lend themselves to any obvious avenues of constructive image analysis and it is felt that a robust and quantitative analysis of differing crumb pastes would not be forthcoming from the type of images obtained here on LM paste.

6.3 Optical microscopy of LM crumb paste

In this section, experiments have been focused on assessing the viability of using optical microscopy as a means of observing paste microstructures produced under varying operating conditions. To achieve this, it was decided to attempt the imaging of lab made paste samples that varied both in the degree of mixing experienced and the quantity of water added.

6.3.1 Experimental design

The mixing routine used for these experiments (standard LM paste procedure), along with marked sample points to illustrate the degree of mixing is shown in Figure 6.14. Full details of the six pastes sampled are then shown in Table 6.1.

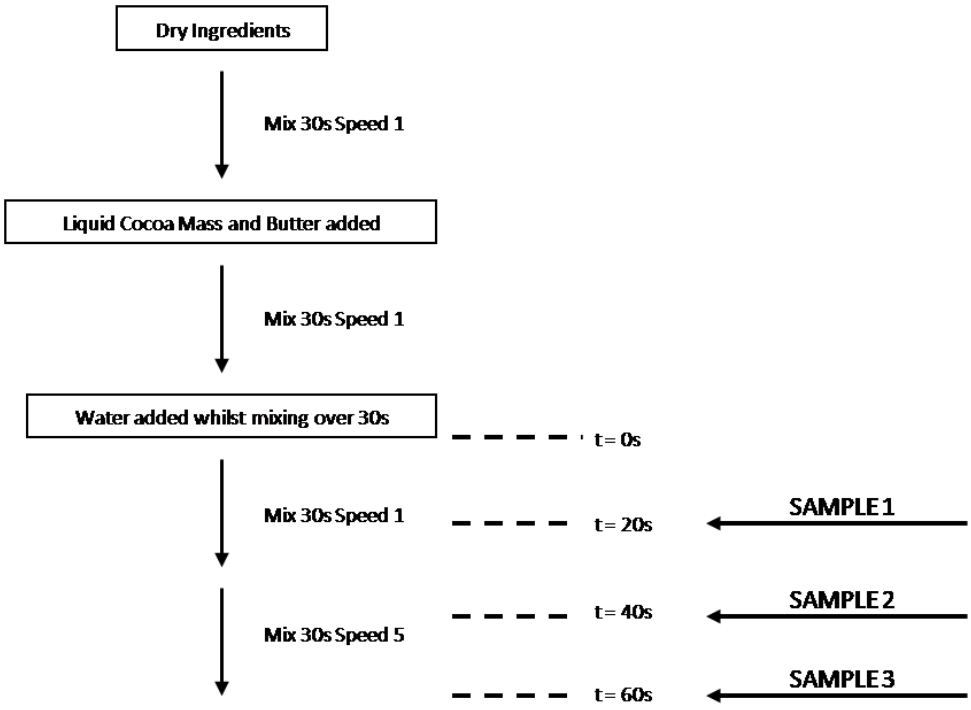

Figure 6.14 LM paste micing routine with marked sample points for degree of mixing study

Table 6.1 Sample properties of six LM pastes imaged

Sample	Added Water (%)	Degree of Mixing post water (s)
1	8	20
2	8	40
3	8	60
4	6	60
5	8	60
6	10	60

6.3.2 Slide preparation & section staining

When sampling paste from the mixing bowl, large portions were removed using a sharp edged spoon. These oversized samples were then made smaller by removing the outer volume using a sharp blade, to leave an inner cube of approximately 1 cm^3. Thin sections of 16 μm thickness were then generated from the centre of the sample cube using

a Clinicut Cryostat microtome (kindly issued on loan by the School of Chemical Engineering and Analytical Science, University of Manchester), having left the sample to equilibrate at -34 °C for 1 hour. Section thicknesses were set at 16 μm as it was not possible to create consistent slices any thinner without folding the section.

So as not to damage or contaminate the sections when transferring from the microtome blade to the slide, each was lifted using a sticky slide. A sticky slide was made by placing a small amount of Evostick Impact adhesive onto one slide, pressing it against a second slide to create a thin film between the two and then quickly sliding them away from one another, leaving two slides each with a flat, thin adhesive surface. This sticky surface can then be used to pick up sections directly onto the slide.

The protein stain used here was eosin yellow, made up as a 5% solution in ethanol hydroxide. Prior to preparing the stain stock solution, the ethanol was dried by adding magnesium sulphate to the bottle and when needed, 20-30 ml of stock solution was filtered in a coplin staining jar. To stain samples, each section was left in the staining jar for eight minutes, before being twice rinsed with fresh, dry ethanol hydroxide. Each stained section was then further rinsed with Histoclear, before finally mounting in paraffin oil and adding a glass cover slip.

6.3.3 Interpreting micrographs

Figure 6.15 (top) shows an example of a stained section viewed under brightfield light. The red/pink stained areas clearly indicate protein (both casein and globular) and other components are visible such as crystal outlines (sucrose and lactose) and brown regions of cocoa mass. Furthermore, the larger regions of protein with black dots in them can reliably be interpreted as undispersed SMP particles. Since air bubbles show up as

black, the spots visible in the highly proteinous areas are indicative of vacuoles generated during spray drying. The bright white areas simply represent holes in the section.

Figure 6.15 (bottom) shows the corresponding image of the same section viewed instead under polarised light. Due to the birefringent nature of the anisotropic sugar crystals in paste, imaging under polarised light highlights only the crystalline structures. Although crystalline fats would also be expected in the mixture, the size and degree of the birefringent behaviour of sugar crystals means they are the predominant feature of such a mixture under polarised light. It should be noted that the microscope used to take these images ordinarily outputs black and white images. In order to obtain the colour images shown here, a colouring filter card is used which unfortunately has a partial polarising effect. This explains why some of the crystals and spectrum colours, which are not visible when viewed directly down the microscope, also appear in the brightfield image. The polarising effect of the colour filter card varies from image to image and for accurate images of the crystalline structure, the polarised image taken using the controlled polarising filter should always be used.

Care is also required when interpreting the red colour that appears in the polarised image. This red colouring can also be a side effect of the birefringence which can generate a spectrum of colours due to the prism effect and may not represent stained protein. In order for red areas in the polarised image to represent protein covered crystals, the corresponding area must also appear red in the brightfield image. An example of a misleading red zone in the polarised image is shown with its corresponding area in the brightfield image.

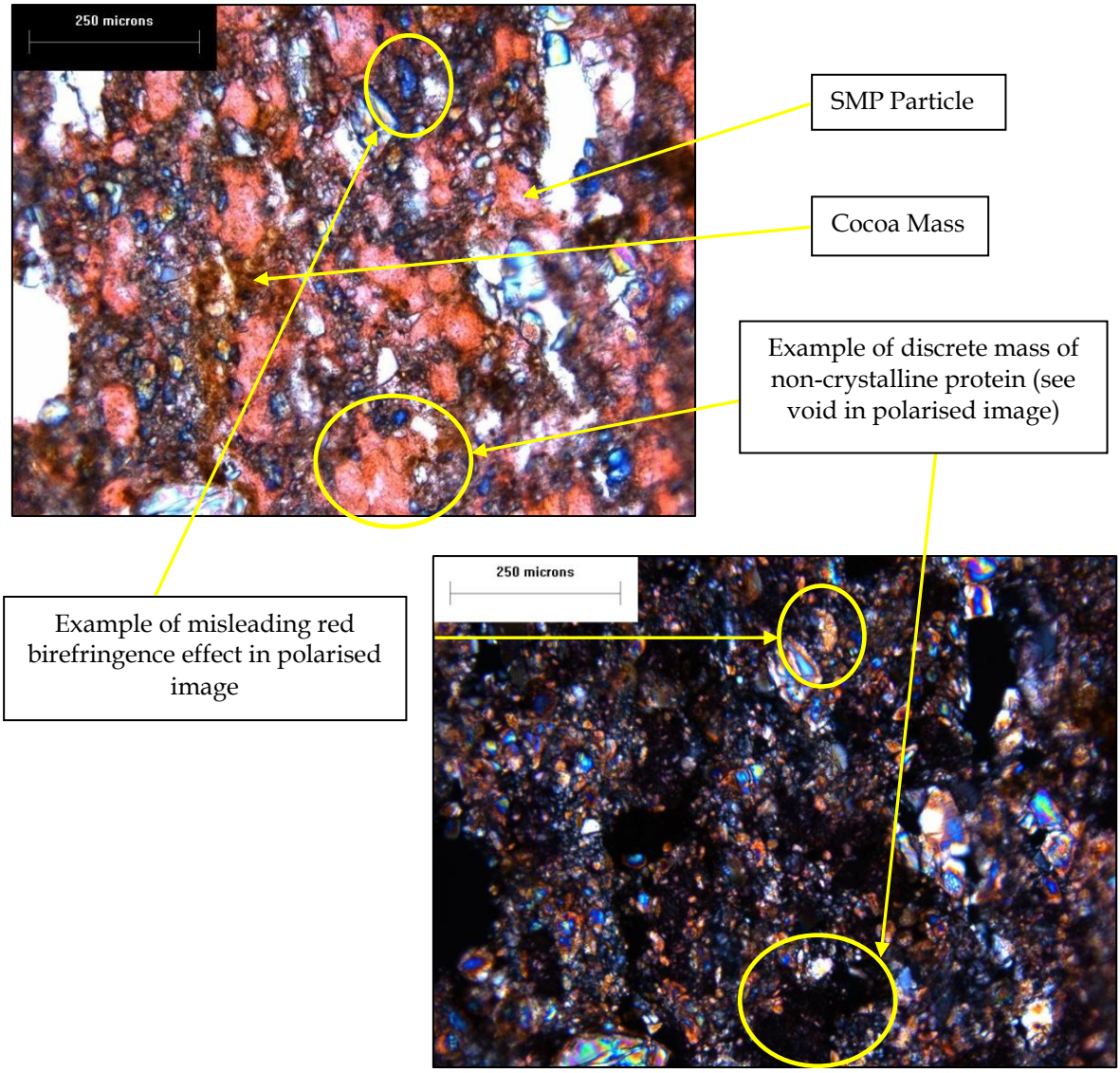

Figure 6.15 Key features of stained microtome sections of 8% water LM paste subjected to 20s mixing as viewed under an optical microscope – x10 brightfield (top) x10 polarised (bottom)

6.3.4 Visual observations – degree of mixing

When first considering the brightfield image of the paste after twenty seconds of mixing post water addition (Figure 6.16 (*i*)), it is clear that there are many discrete regions of protein as shown by the visible red stain. Whilst there are a few small areas of continuous protein, the vast majority of the visible protein is concentrated in localised pockets identifiable as SMP particles. There are also some discrete regions of brown

cocoa mass and in some areas it is possible to see clear boundary interfaces between protein, cocoa mass and sugar crystals.

The matching polarised image (Figure 6.16 (*ii*)) shows a large number of black voids which correspond to the protein rich areas on in the brightfield image. Whilst the polarised image seems to show large amounts of red stained protein covering the visible crystals, this is unfortunately a bad example of the red birefringence effect, as little or none of these red areas appear red in the brightfield image. At this early stage of mixing, it seems that very little ingredient dispersion has taken place, with pockets of undisturbed SMP, discrete regions of cocoa mass and very little crystal distribution amongst the protein.

The brightfield image of Figure 6.16 (*iii*) shows paste after forty seconds of mixing. There are still discrete areas of red, but less so, as the proteinous regions start to mix with each other and begin to form a network. The cocoa mass is somewhat better dispersed with fewer localisations. The two big areas of brown that appear in the top right and bottom left of both the brightfield and polarised images should be ignored as they are caused by thick layering of the section. Although the proteins are beginning to mix into each other, the sugar crystals are still not being distributed into the protein network as shown by the large areas of void in the polarised image (Figure 6.16 (*iv*)) and the lack of red crystals with matching zones of red in the brightfield image.

Looking lastly at the brightfield image of the paste subjected to sixty seconds of mixing (Figure 6.16 (*v*)), a more widespread network of protein is clearly visible with far fewer discrete zones of protein or undisturbed SMP particles. Where protein has become wetted and fully dispersed, a stronger red colour is seen.

Finally, the polarised image of Figure 6.16 (*vi*) shows a far greater mixing of the lactose and sucrose crystals amongst the protein mass by comparing the relatively smaller

area of non-crystalline voids with that of the twenty second mixed paste (Figure 6.16 (*ii*)). This is supported by the even colour of red crystals showing in the polarised image (i.e. less birefringent red) and the greater degree of matched red in the brightfield image.

In conclusion, the mixing process timeline seems to tell a story of discrete, undispersed ingredients in the early stages of mixing, followed by a partial dispersion of the protein and cocoa mass in the intermediate stages without interaction with crystalline material. Towards the end of the mixing period, a more continuous protein network appears to have formed, beginning to engage with and cover some of the crystalline material. This purely visual hypothesis is discussed further in the image analysis work conducted in Section 6.3.6.

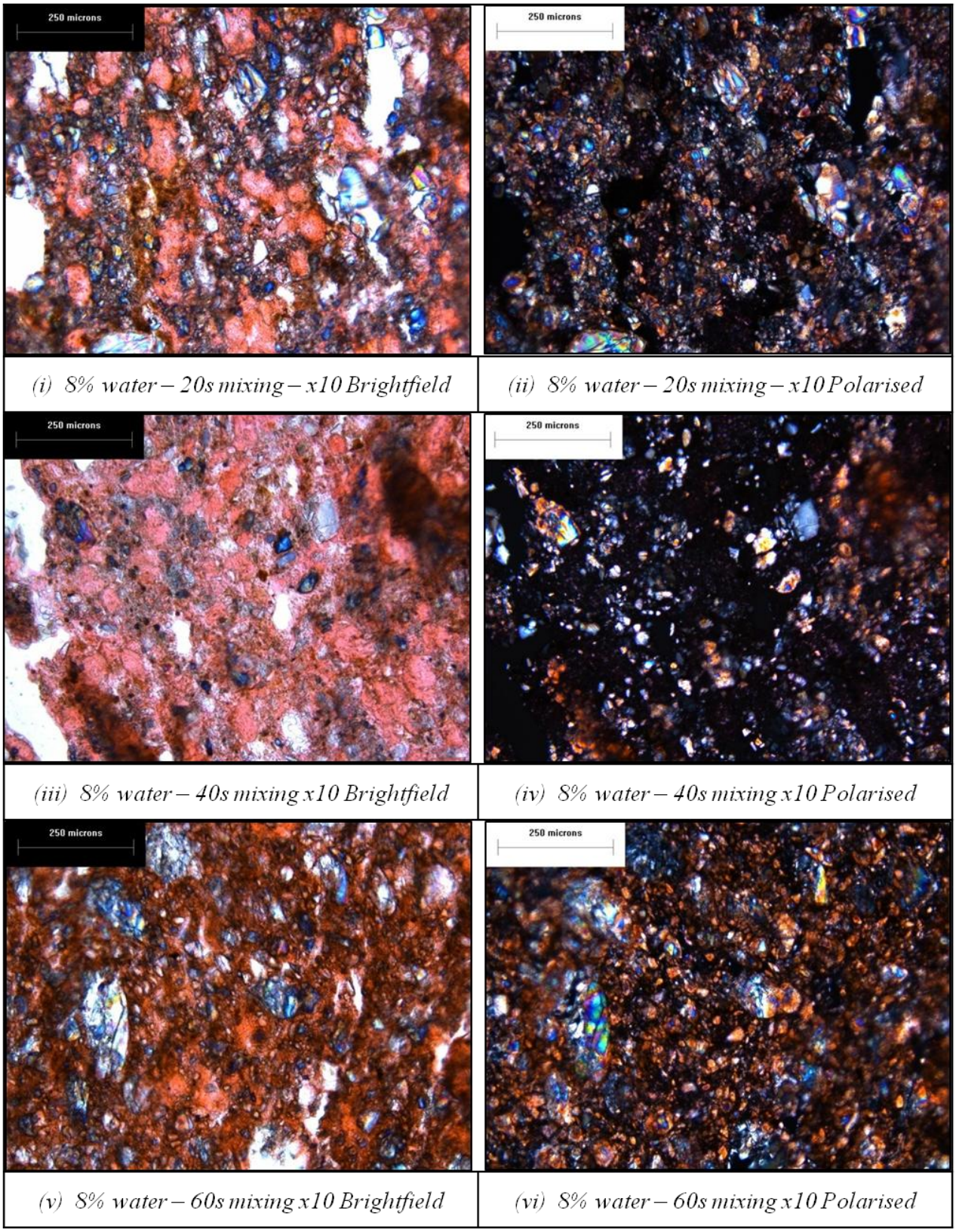

Figure 6.16 Optical micrographs of 8% LM crumb pastes after varying degrees of mixing. Shown in brightfield light with the corresponding image under polarised light (scale bar 250 μm)

6.3.5 Visual observations – added water content

In addition to viewing pastes subjected to varying degrees of mixing, images were also generated from samples receiving the full sixty seconds of mixing time, but with differing quantities of water addition in order to examine the effect of water content on mixing in lab made paste. The 6% added water sample showed similar characteristics to that of the poorly mixed samples seen in the 8% degree of mixing study, with discrete regions of protein and cocoa mass clearly visible in the brightfield image of Figure 6.17 (*i*). Just as with the poorly mixed 8% samples, the polarised image (Figure 6.17 (*ii*)) shows virtually no distribution of sugar crystals amongst the protein. The dryness of this mixture has clearly inhibited the dispersion of ingredients during mixing under these conditions.

This hypothesis is supported by the relatively improved ingredient dispersion and distribution shown in the 8% sample (Figure 6.17 (*iii*) and Figure 6.17 (*iv*)). As should be the case, these micrographs bear resemblance to the 8% 60 s mixed images taken in the degree of mixing study, although seem to contain more regions of discrete protein. In continuation of this trend, the 10% sample shows the greatest ingredient dispersion and distribution seen in any of the six samples imaged. Although difficult to pick out the brown of the cocoa mass on printed versions of the images, Figure 6.17 (*v*) shows the near homogenous distribution of protein and cocoa mass with very few localised regions.

The polarised image of Figure 6.17 (*vi*) then shows a near blanket distribution of protein covering the sugar crystals. The proteinous nature of this red colouring is easily confirmed on inspection of the brightfield image. In fact, the only crystals not showing a red protein coating appear to be the larger crystals which have been sliced though.

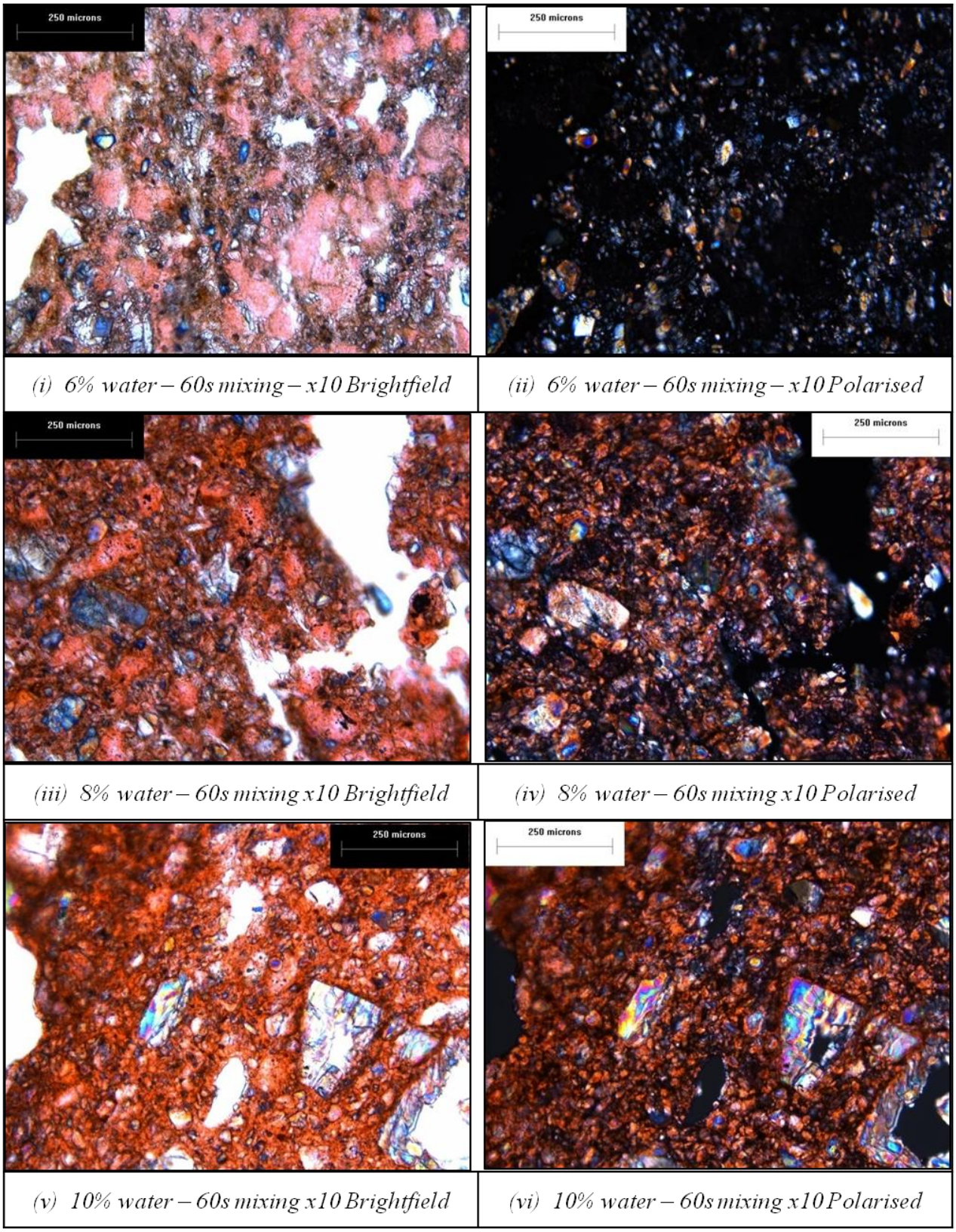

Figure 6.17 Optical micrographs of LM crumb pastes of varying water contents subjected to sixty seconds of mixing. Shown in brightfield light with the corresponding image under polarised light (scale bar 250 μm)

6.3.6 Quantitative image analysis

Qualitative observations of how the mixing time and water content affect LM microstructure have been presented in Sections 6.3.4 and 6.3.5. These hypotheses are based on visual interpretations of what have been shown to be difficult images to interpret accurately, requiring simultaneous consideration of paired images to draw meaningful conclusions. The visual observations made are adequate for a general feel of what is occurring, but must be confirmed with a more reliable quantitative analysis. This is particularly true of the red birefringence effect. For this purpose the images have been analysed using the ImageJ image processing software to determine discrete protein fractions and the percentage protein coverage of crystalline material in each image.

6.3.7 Particle analysis to determine undispersed protein fraction

In order to determine discrete protein fraction, the relevant brightfield image is first thresholded according to colour so as to pick out the pink areas of interest, since these have been shown to correspond well with unwetted and undispersed agglomerates of protein, whilst the strong red areas represent the opposite. The range of colours allowed to pass is determined by first sampling a selected area of the image which is representative of the colours required. The thresholding colour range is then manually adjusted at both ends to confirm that all desired colours are being allowed to pass. Figure 6.18 (ii) shows an example of colour thresholding to highlight undispersed proteinous regions performed on Figure 6.18 (i). Once thresholded, the image is then converted to a binary image (Figure 6.18 (iii)) where the thresholded regions appear as positive black and everything else as zero white.

This binary image can then be analysed for particles using a function within the ImageJ software. Figure 6.18 (iv) is the result, showing the outline of all particles found,

from which particle fractions are calculated as a proportion of the overall slice excluding voids. For illustrative purposes, Figure 6.18 (v) shows the identified particles superimposed on the original image.

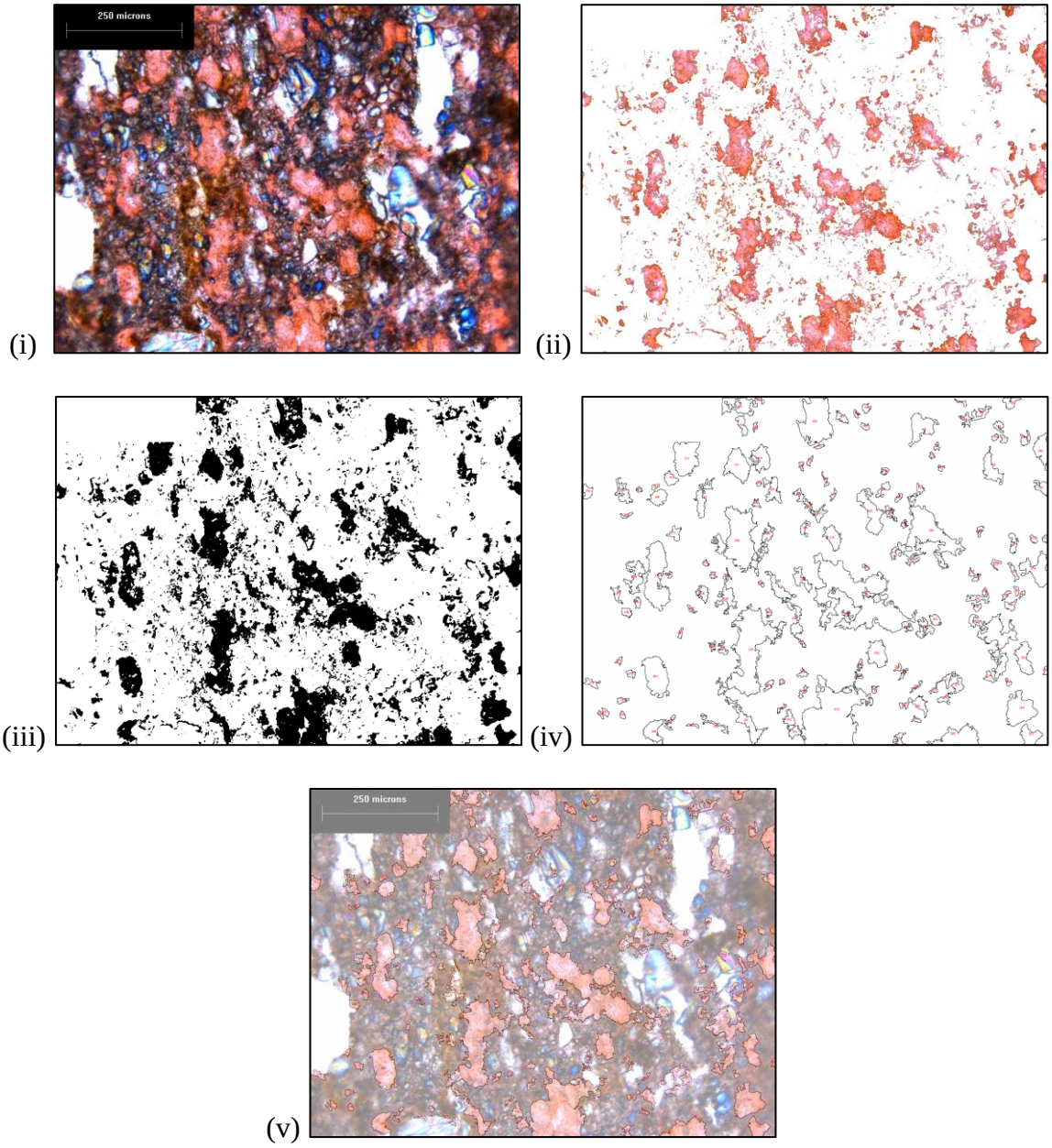

Figure 6.18 Undispersed protein image analysis segmentation algorithm

(i) Original brightfield image (ii) Colour thresholded image (iii) Thresholded binary image (iv) Resulting image from particle analysis (v) Overlay of particles found on original image

6.3.8 Determining percentage protein coverage of crystalline material

Determining the percentage protein coverage of crystalline material in each section is somewhat more complicated than identifying the discrete protein areas alone, due to the red birefringence effect. The consequence of this is that red appearing in the polarised images must also appear red in the brightfield image for it to represent protein covered crystalline material. The first step is to threshold both the red and pink areas of the brightfield image and its corresponding polarised image. Both are then converted to binary images that again show thresholded areas as positive black and elsewhere as zero white. To generate an image showing only the areas that appear positive black in both, the two are multiplied together as illustrated in Figure 6.19. Only pixels which are positive black in both images multiply to generate a secondary positive black pixel in the output image. Any other combination of positive black or zero white generates a zero white pixel.

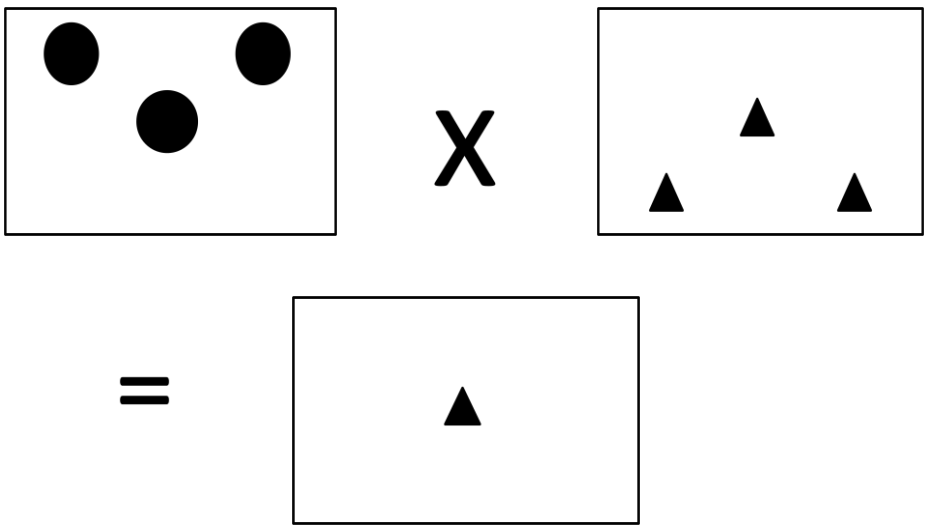

Figure 6.19 Schematic illustration of binary image multiplication with black pixels representing 1 and white pixels 0

Figure 6.20 illustrates the effect of the image multiplication process for samples 4 and 6 (6% and 10% added water respectively) and confirms the significance of the red birefringence artefacts. Whilst both samples appear to show large quantities of protein covered crystalline material in the polarised versions, the multiplied images of (v) and (vi) show these quantities are in fact greatly exaggerated and in the case of sample 4, the protein covered crystalline material is actually almost non-existent. For analytical purposes, the total area of confirmed protein covered crystalline material is considered as a fraction of the total crystalline area in the image (determined by blocking all dark colours from polarised images).

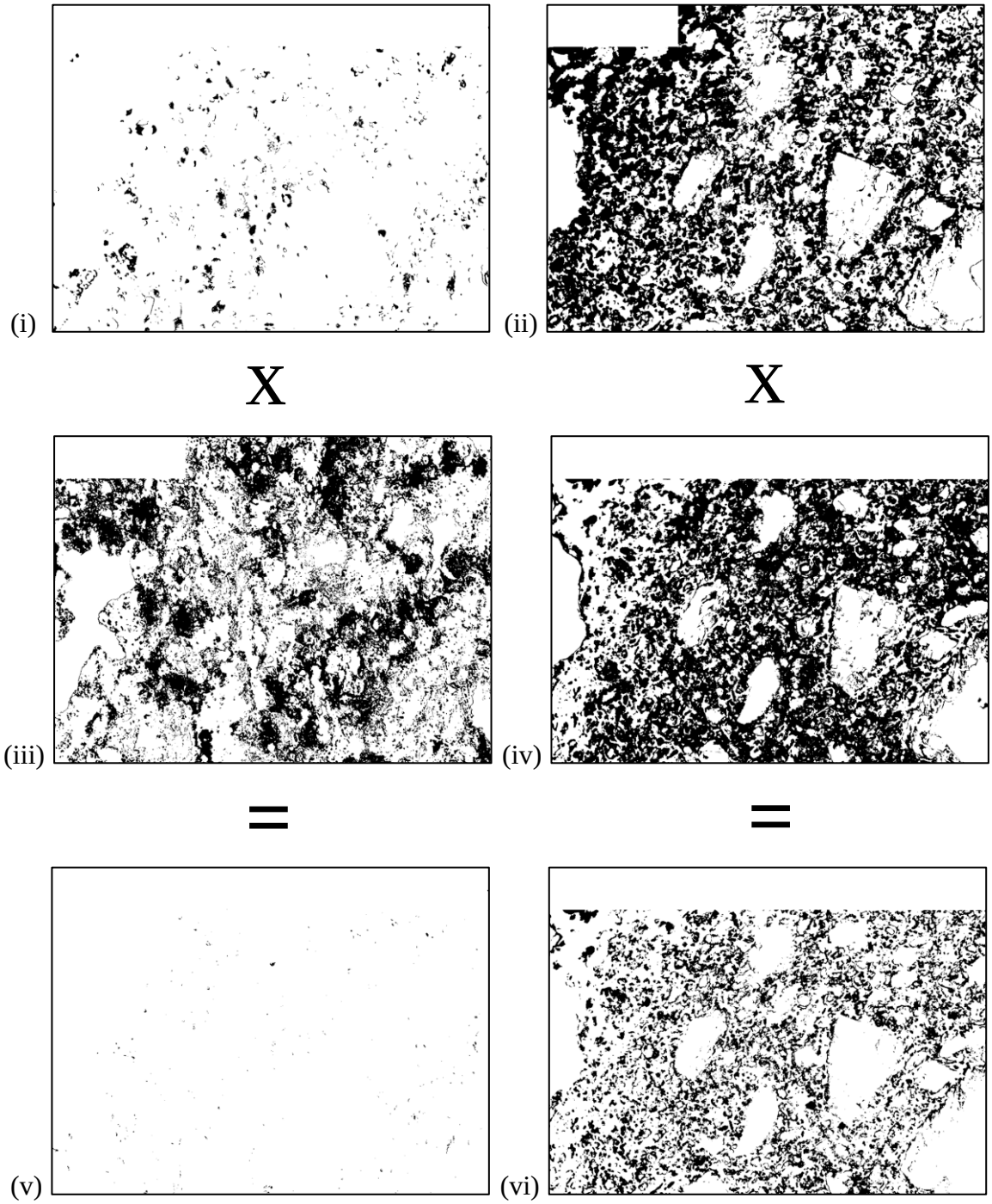

Figure 6.20 Binary image multiplication to determine actual protein covered crystalline material (i) Binary image of visible red in polarised image – 6% (ii) Binary image of visible red in polarised image – 10% (iii) Binary image of visible red in Brightfield image – 6% (iv) Binary image of visible red in brightfield image – 10% (v) Resulting image from binary multiplication – 6% (vi) Resulting image from binary multiplication – 10%

6.3.9 Image analysis results – degree of mixing

Hypotheses about the mixing processes occurring in LM paste have been made from visual observations of the micrographs (Sections 6.3.4 and 6.3.5) and so can now be assessed with the results of the image processing. The object of this exercise is to assess the potential use of image analysis on optical micrographs.

The first observation made in Section 6.3.4 was that the discrete and localised areas of undispersed protein were most apparent in the early stages of mixing and decreased with time mixed. The image analysis performed on the three images considered is shown in Figure 6.21 and appears to support this general observation. The fraction of discrete undispersed protein is initially high in the first forty seconds of mixing (20-35%), but as mixing progresses to the full sixty seconds, the results indicate a fuller dispersion, making up a significantly smaller fraction of the section (2%). An unintuitive rise in the fraction of undispersed protein visible is shown between twenty seconds of mixing and forty seconds of mixing. This uncertainty is explored further in Section 6.3.12.

The area where quantitative image analysis could perhaps be most useful is the determination of protein coverage across crystalline material. Due to the difficulties associated with the red birefringence effect, simple observation of the polarised images appeared to indicate some degree of protein coverage for all degrees of mixing. However, the results of the binary image multiplication, which show only the areas that appear red in both polarised and brightfield images (Figure 6.22), indicate otherwise. The proportion of crystalline material covered in protein is negligible up to forty seconds of mixing, potentially indicating that until this point, no infiltration of crystalline material into the surrounding protein network has occurred. However after sixty seconds, this fraction rises significantly to 16.2%. As hypothesised, Figure 6.22 supports the notion that in 8% added

water lab paste, crystalline material is the last thing to disperse amongst the protein network and occurs in the latter stages of mixing.

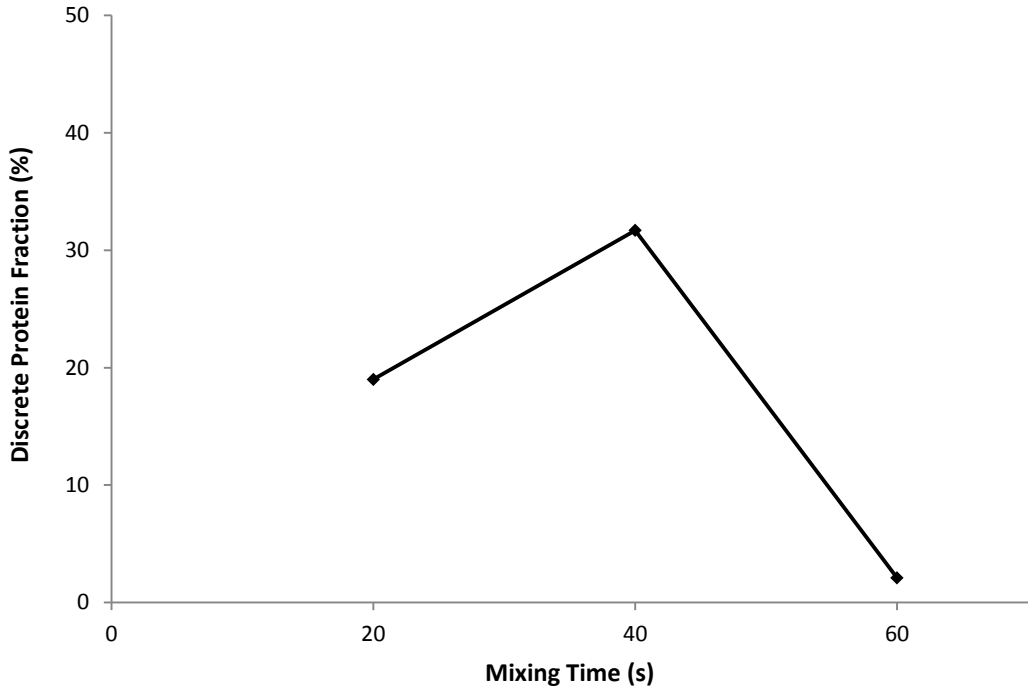

Figure 6.21 Discrete protein fraction versus degree of mixing (8% water LM paste)

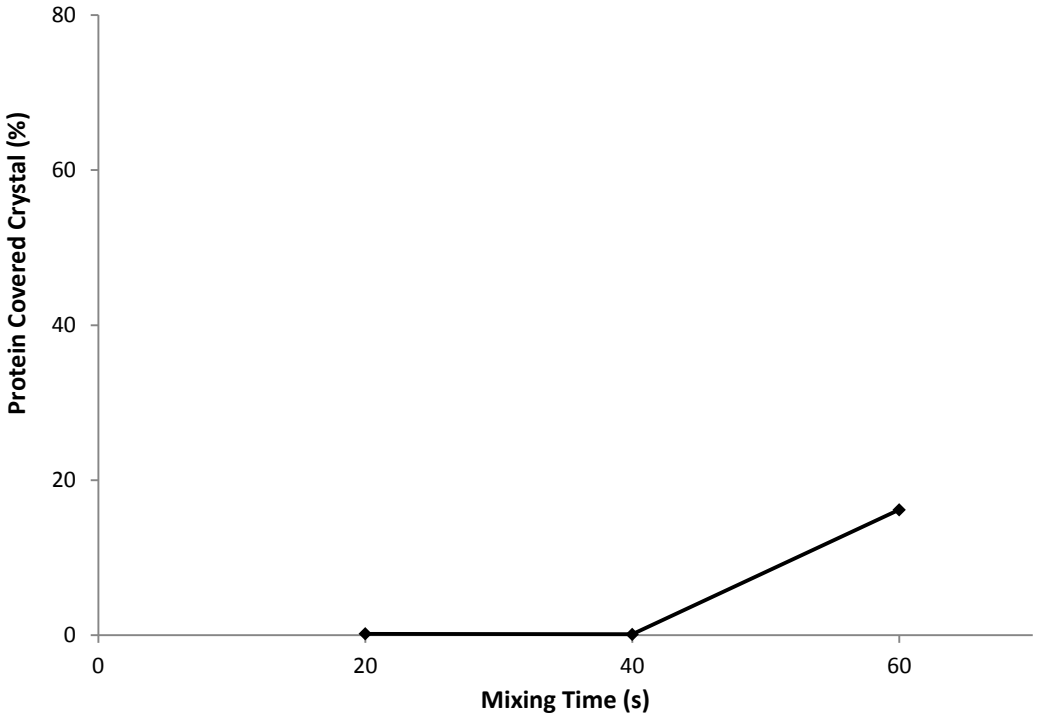

Figure 6.22 Protein covered crystal fraction versus degree of mixing (8% water LM paste)

6.3.10 Image analysis results – added water content

The same image analysis data is now presented as a function of added water content in Figure 6.23 and Figure 6.24. The general trend observed visually in Section 6.3.5 was that increased water content significantly increases ingredient dispersion and distribution under similar mixing conditions and the discrete protein fraction analysis performed on the three images considered (Figure 6.23) supports this well showing a drop in discrete protein fraction from 23% in the 6% water image to only 1% in the 10% image, indicating near complete protein dispersion.

The most significant data to come from the image analysis in this area of the study is the protein covered crystal fraction of Figure 6.24. As with a poorly mixed sample, there is little or no protein covered crystalline material in the driest 6% sample. As with the corresponding sample in the degree of mixing study, the 8% sample exhibits moderate coverage of approximately 20%. However, significantly improved levels of coverage are achieved by raising the water content to 10%. The high fraction of crystalline material covered in protein (here 69.3%) indicates almost full crystal distribution amongst the protein matrix since the images show that the only crystals not to be protein covered are the largest crystals, which are deep enough that they are simply sliced through when sectioning 16 μm films. This means that 100% coverage cannot be observed from 2D sections of this thickness in the presence of the largest crystals.

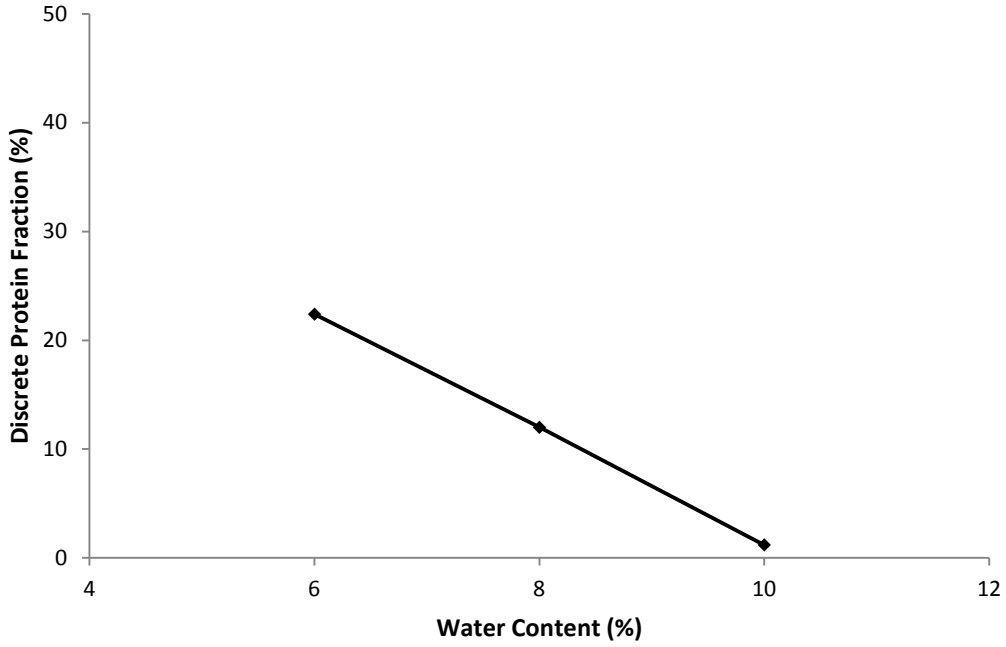

Figure 6.23 Discrete protein fraction versus added water content (60 s of mixing)

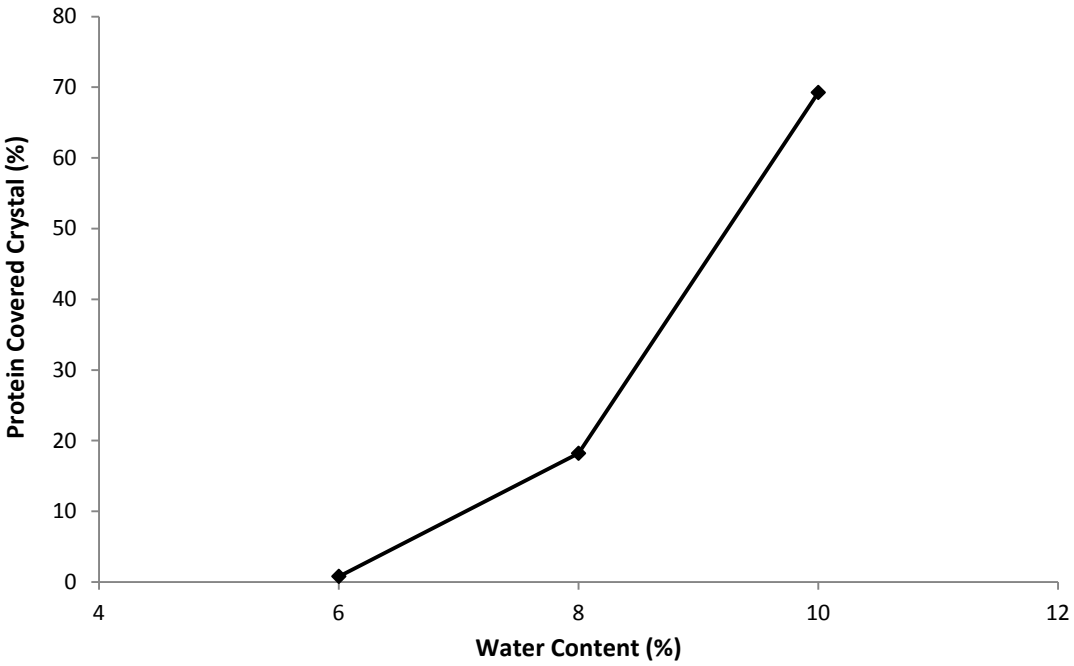

Figure 6.24 Protein covered crystal fraction versus added water content (60 s of mixing)

6.3.11 Numerical consistency between images

Although only a small sample of images were obtained, samples 3 and 5 represent control samples, since they both contain the same added water content and both experienced the full sixty seconds of mixing. Consequently, it would be expected that similar micrographs would be obtained for each. It is therefore encouraging to see that the brightfield images for each are visually similar. It is also encouraging to see the strong agreement in the protein covered crystalline material, perhaps the most important indicator of mixing quality, at 16.2% and 18.2%. There is however a larger variation in the discrete protein fraction of each sample (2.1% and 12%). When selecting regions of each section to image, it was attempted to pick the most representative areas, however an inherent variation between samples on a micro scale is anticipated as samples of varying homogeneity are being analysed before reaching an entirely homogenous state. As a result, further work is required to assess the variation between notionally similar samples using this technique and analysis, such that conclusions about the confidence of interpretations made in this section can be drawn.

6.3.12 Quantitative analysis of multiple sections

In an effort to consider the inherent variation between section samples that can be expected from the quantitative indicators of dispersive mixing considered here, the analysis used encouragingly on single sections has also been applied to a more complete data set. In this set, twelve to fifteen sections were cut, stained and imaged from 8% water LM pastes subjected to fifteen, thirty, forty, fifty and sixty seconds of mixing post water addition. The same sample preparation and staining procedure as described in Section 6.3.2 was used for all samples, but ensured that a fully representative range of sections were obtained within the mixing bowl.

Attempts to replicate the analysis on a wider set have data have been less successful, due to an inconsistent level of protein staining. An example of this inconsistency in shown in Figure 6.25 which shows a montage of the fifteen sections imaged and stained of relatively well mixed pastes after fifty seconds of mixing, after which time a relatively consistent distribution of protein would be expected. Sections were stained in batches of three to five and a good consistency of protein staining within batches is seen, just as was the case with the sections prepared together in the preliminary analysis. However for different batches, despite efforts to maintain a consistent submersion time and stain concentration, large systemic variations in the degree of protein binding and contrast of the staining between batches is seen, indicating that the contrast of staining is highly sensitive to the preparation conditions.

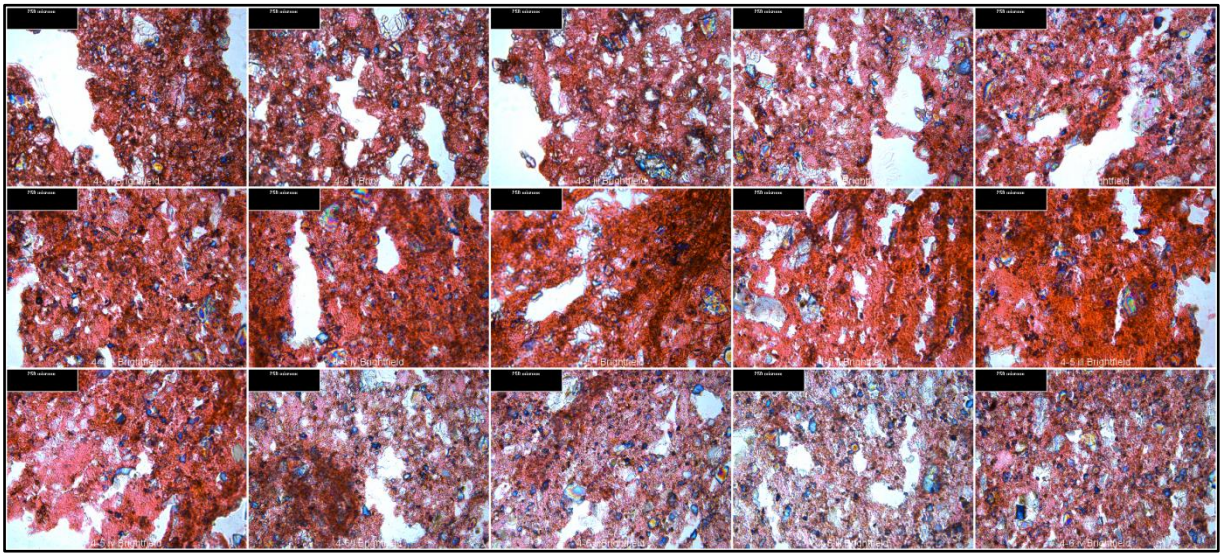

Figure 6.25 Inconsistent protein staining of 8% water LM crumb paste sections using Eosin Yellow after 50 seconds of mixing

In the first experiment, protein staining in the sections imaged was such that strongly red coloured areas were visible in dispersed regions of protein that had most likely become wetted. The lighter coloured pink areas were then visible only in the areas

of undispersed protein, such as unwetted milk particles. From this consistent contrast of staining, it was possible to distinguish undispersed protein from dispersed protein based upon a colour thresholding algorithm. However, in many of the images in this secondary set of images, such as that shown in Figure 6.26, pink areas of staining are visible both in regions of continuous dispersed protein as well as in localised areas of undispersed protein, meaning that image analysis algorithms based upon colour thresholding the pink areas are no longer able to successfully discriminate between dispersed and undispersed protein with any consistency.

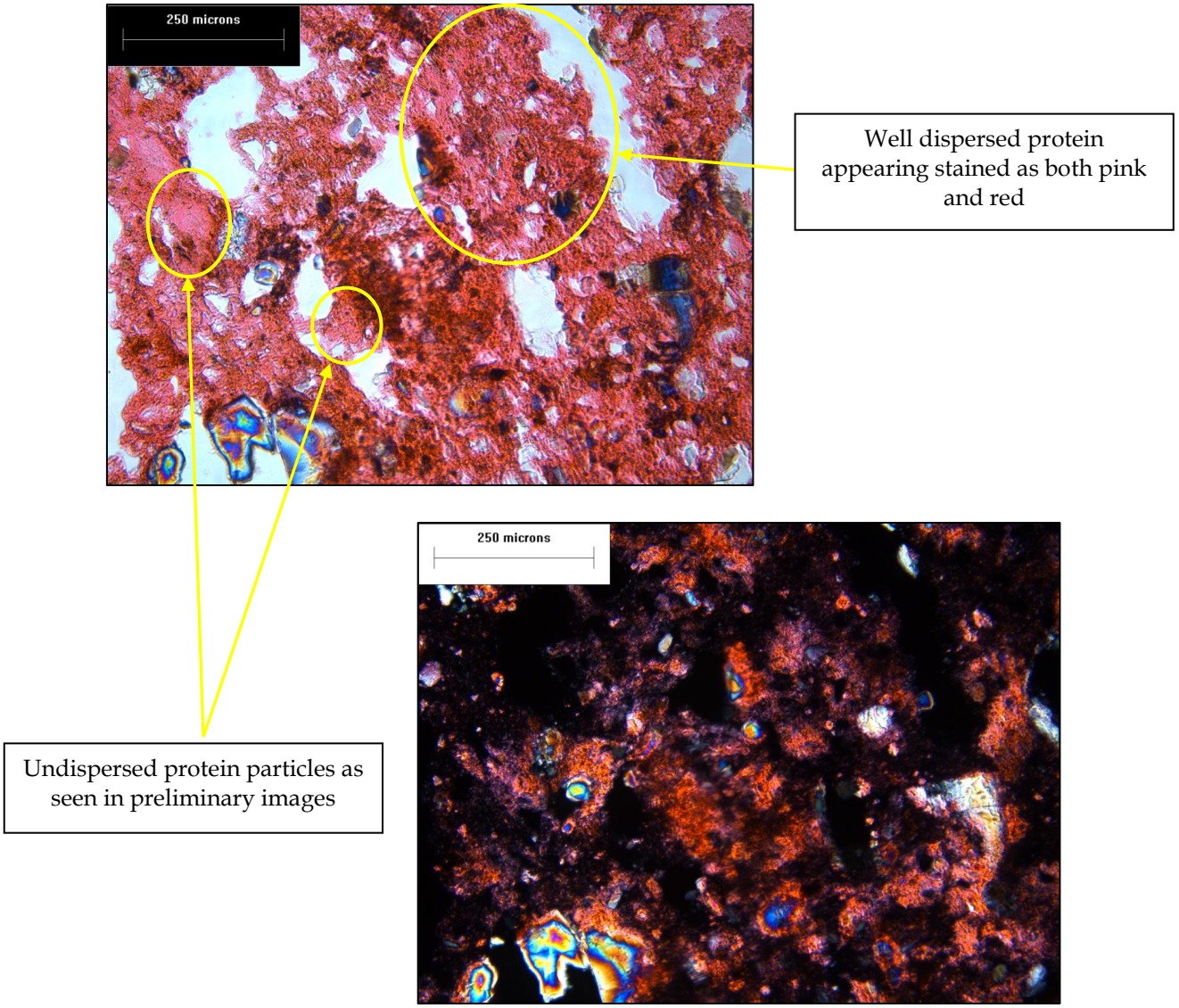

Figure 6.26 Indiscriminate nature of protein staining making it difficult to distinguish between dispersed and undispersed protein

As a consequence of this, Figure 6.27 shows the result that is achieved when the same algorithm for determining the discrete fraction of undispersed protein is applied to this data set. As the algorithm now detects a large proportion of dispersed protein as well as undispersed protein, the fraction now remains approximately constant for all times of mixing.

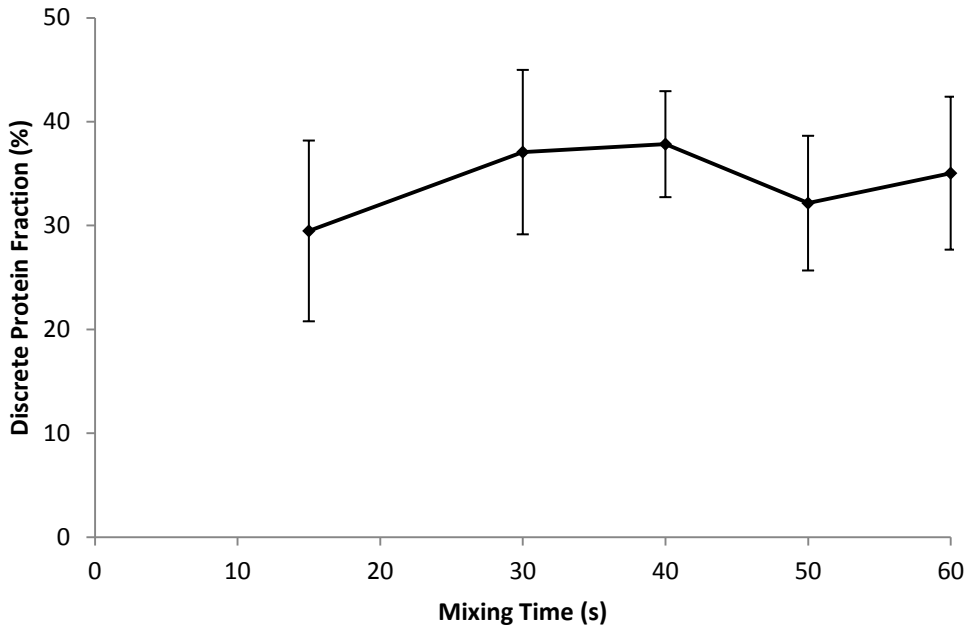

Figure 6.27 Discrete protein fraction (dispersed & undispersed) vs. mixing time for 8% water LM crumb paste using 15 microtomed samples for image analysis at each point (error bars show standard deviation)

The standard deviation within sample sets is shown in Figure 6.27 and shows that the variations remain consistent across all times of mixing. If variations in measured results were dominated by variations within samples due to distributive mixing inhomogeneities (see Chapter 5), it would be expected that the standard deviation of discrete protein fraction between samples would be largest after fifteen seconds of mixing and decrease with mixing time. As this is not the case and standard deviations remain consistent throughout, it is assumed that the length scale observed in these images (1 mm^2)

is sufficiently large to capture characteristics representative of the whole volume and that the degree of variation seen can be attributed to the preparation and staining of samples.

Despite the quantitative image analysis for determining the fraction of undispersed protein no longer being applicable, there is still the potential for determining the fraction of crystalline material covered in protein as the algorithm for this indicator thresholds both pink and red regions of staining and is not as sensitive to variations in contrast as the algorithm for determining undispersed protein in the brightfield images. The results of this algorithm applied to multiple images are shown graphically in Figure 6.28 and are tabulated in Table *6.2* showing the anticipated trend of increased coverage with mixing time. Given the variations within each data set, this data was analysed using the one-way analysis of variance (ANOVA) "F-test" to reject the null hypothesis of equal means, followed by Fisher's LSD method for a pairwise comparison of the means in order to determine which variations between means were statistically significant (α = 0.05). Analysis of the data gave an F value of 9.841 with $p<0.001$ confirming that the null hypothesis of equal means could be rejected and that at least one pair of points have a statistically significant difference in means. The results of the pairwise comparisons then show that the mean coverage of crystals after fifteen seconds of mixing is lower and statistically significant from all other points. Conversely the mean coverage after sixty seconds is higher than all other values and statistically significant from all points other than that after thirty seconds. No statistical significance was found between the differing means of images at thirty, forty and fifty seconds.

With the exception of the statistically inconclusive comparison between the mean after sixty seconds and the mean after thirty seconds, the data supports the hypothesis made in Section 6.3.9 that at the extremes, protein covered crystal increases with mixing time. Whilst a high confidence level could be placed on the overall trend, the precise

magnitude of coverage at any given time point was subject to average relative standard deviation between samples of 37%. The accuracy of the technique was not sufficient to provide any statistically significant differences between the protein covered crystal fraction of samples imaged between thirty and fifty seconds.

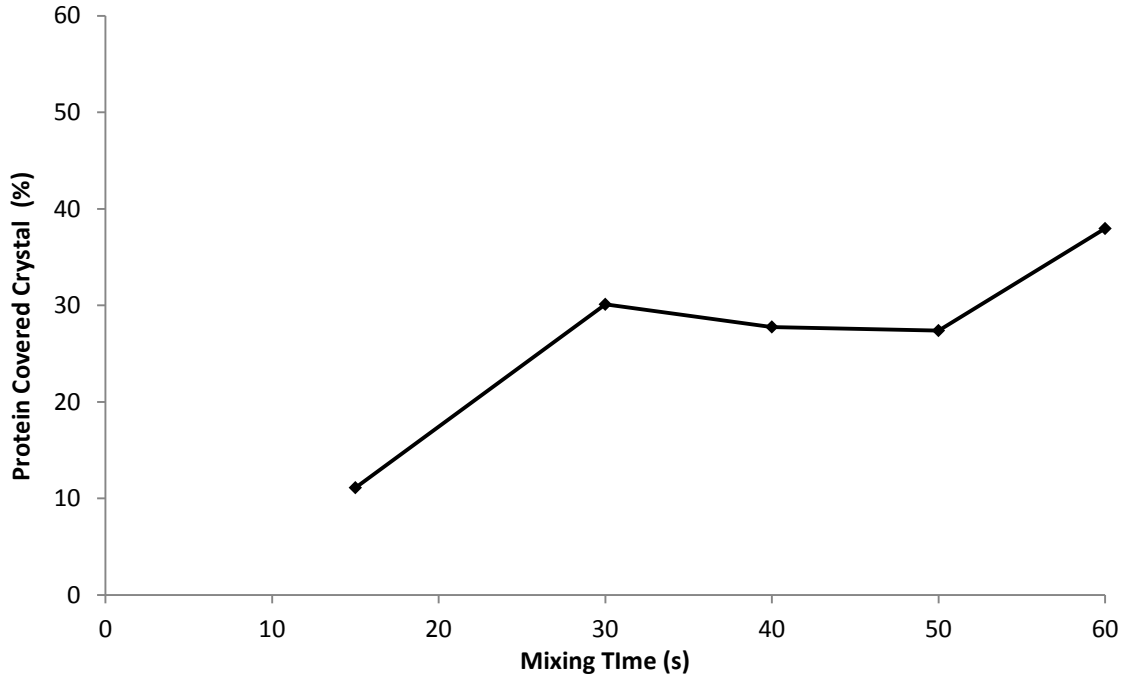

Figure 6.*28 Protein covered crystal fraction versus mixing time for 8% water LM crumb paste, using 15 microtomed samples for image analysis at each point*

Table 6.*2 Fraction of crystalline material covered by protein in response to mixing time for 8% water LM crumb paste, using 15 microtomed samples for image analysis at each point. Values represent mean ± standard deviation for duplicate determinations. Means with the same letter within columns are not significantly different (p> 0.05)*

Mixing time post water addition (s)	**Protein covered crystal (%)**	
15	11.11 ± 3.25	a
30	30.11 ± 10.76	b, d
40	27.77 ± 9.96	b
50	27.39 ± 13.99	b
60	37.97 ± 12.63	c, d

6.3.13 Remarks on optical microscopy

Optical microscopy and protein staining has successfully highlighted differences in the microstructure of varying LM crumb pastes with respect to sugar crystals and protein network. Primary sections prepared and stained consistently in a single batch have produced intuitive results when analysed using quantitative image analysis algorithms. However, the secondary samples have shown that images obtained using this technique are highly sensitive to the conditions in which the sample is prepared, making it difficult to prepare a large number of samples such that a robust quantitative analysis based upon colour thresholding may be performed.

It is therefore concluded that this technique and analysis are useful as an observational tool to assist in finding trends between samples, provided a consistent level of staining can be achieved. However in this work, this caveat has proved unmanageable for the analyses developed and their use as a robust technique for the quantitative comparison of large data sets, such as proposed in the extruder trials of Chapter 7, has proved unviable due to a large sensitivity to sample preparation conditions.

6.4 Multiphoton microscopy (MPM) of LM crumb paste

The experiments detailed here were also focused on assessing the viability of using multiphoton microscopy (MPM) as a means of observing paste microstructures produced under varying operating conditions. To investigate this, MPM images were obtained using a multiphoton microscope setup kindly made available by the Institute of Biomedical Engineering, University of Oxford. As described by Hughes *et al.* (2006), two photon images were obtained using a modified BioRad/Zeiss Radiance 2100 MP multiphoton laser scanning system (Zeiss, GmbH, Jena, Germany). The near-infrared (NIR) laser beams (λ = 800 nm) were obtained from a tuneable 76 MHz femtosecond Ti:sapphire laser

(Mira 900-F, Coherent, Ely, U.K.) pumped by a 7 W multiline argon-ion laser (Verdi, Coherent, Ely, U.K.). Appropriate mean laser powers were electronically regulated via the pockol cell of the BioRad beam-conditioning unit (BCU) and were recorded using the Fieldmaster FM power meter (Coherent, Ely, U.K.) interfaced between the BCU and the MPM scan head. The NIR femtosecond pulsed laser beams were focused to a diffraction-limited spot using a high-numerical-aperture (N.A. 1.3) 60_ Nikon water-immersion objective (with a working distance of ca. 1 mm).

6.4.1 Experimental design and sample preparation

As with the work conducted using optical microscopy in Section 6.3, the MPM technique has been applied to a variety of LM paste samples that varied both in the degree of mixing experienced and the quantity of water added, albeit with a smaller range of samples due to limited access to the microscope. All pastes were mixed using the standard LM crumb paste routine and details of the pastes sampled are shown in Table 6.3.

Table 6.3 LM crumb paste samples imaged using MPM

Sample	Added Water (%)	Degree of Mixing post water (s)
1	8	30
2	8	60
3	6	60
4	10	60

When sampling paste from the mixing bowl, large portions were removed using a sharp edged spoon. Given the general ability of the technique to image sections below the surface of a sample in optically dense specimens, it was not necessary to section thin slices

of sample using the Cryostat microtome as was necessary when imaging using optical microscopy. Instead, approximately 5mm thick were manually shaved from the outer surface and transferred to a sticky slide (as described in Section 6.3.2) such that the surface being imaged was undisturbed by the sample preparation. The only dimensional restriction for the sample was that it must be thin enough to fit under the microscope.

As discussed in Section 6.1.3, some material components can demonstrate auto-fluorescence when excited using MPM. If evident, this behaviour can be highly attractive for imaging as no form of staining is required. In this work, LM crumb pastes have therefore been imaged in their natural states to determine what components, if any, demonstrate auto-fluorescence.

6.4.2 Auto-fluorescence in LM crumb paste

Figure 6.29 shows a 2D MPM slice of 8% LM crumb paste obtained approximately 50μm below the surface of the highest topographical peak. It is apparent that a great deal of specimen matter is visible under MPM excitation, despite no fluorophore labelling of the specimens. This indicates that an encouraging level of auto-fluorescence exists within LM crumb paste, as strong signals are evident from all channels (red, green and blue). The large black regions of the image represent areas where no signal has been detected and given the density of signals received elsewhere, represent voids within the section caused by the topography of the sample surface. As the samples surfaces were prepared non-destructively and imaged in their natural state from the mixer, these voids are anticipated as the variations in depth of the surface topography are larger than the depth of imaging that could be achieved clearly (up to approximately 80 μm).

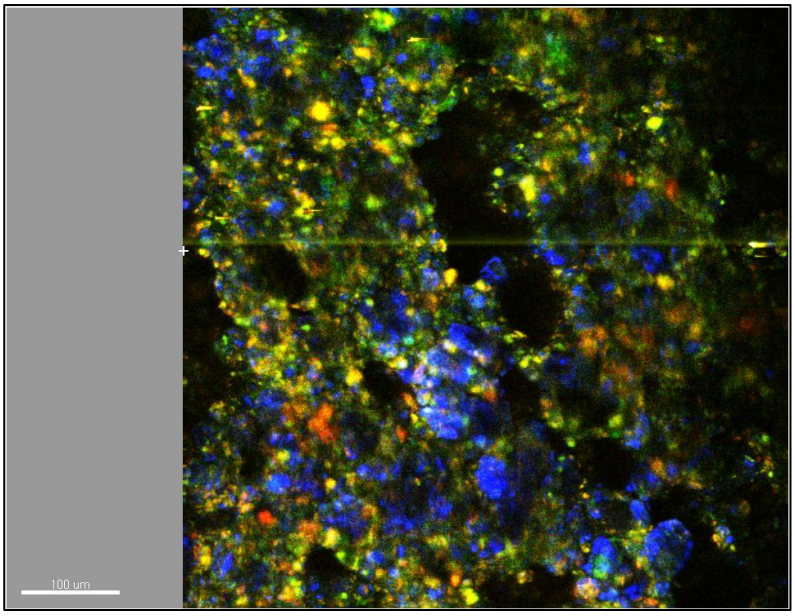

Figure 6.29 MPM section image of unstained 8% water LM crumb paste (approximately 50μm below surface) showing red, green and blue channels combined

Given the level of auto-fluorescence apparent within crumb, it is necessary to try to identify the source of each channel of signal. Figure 6.30 - Figure 6.34 shows the auto-fluorescence that is generated by excitation of the individual ingredients before mixing, demonstrating the strength of emitted signal in each channel as well as the overall image of the three channels combined. Figure 6.30 and Figure 6.31 show that both sucrose and lactose emit a strong blue channel signal, from which individual crystals are clearly visible. Only background noise is detected in the red channel of both sugars and whilst only background noise is seen in the green channel of sucrose, a small, but significant area of signal is seen in this channel of lactose. Conversely, Figure 6.32 and Figure 6.33 show that both skimmed milk powder and whey powder alone are dominated by emissions in the green channel, with only small areas of signal in the blue channel. Neither powder shows any significant signal in the red channel.

From these images, it is deduced that the dominant source of auto-fluorescence emissions in the blue channel is carbohydrate sugars (albeit with no way of distinguishing

between sucrose and lactose) and the dominant source of emissions in the green channel is dairy proteins. Under this assumption, relatively pure sucrose demonstrates fluorescence in the blue channel only, while lactose - a sugar obtained by a usually incomplete separation from whey, exhibits a strong blue channel signal as well as small areas of signal in the green channel from residual whey proteins. The converse argument is supported well by Figure 6.33 which shows whey powder particles, known to be made up of whey proteins and lactose, as predominantly proteinous particles with blue lactose tips. As would be expected, the same blue tips of lactose then also appear in the skimmed milk powder particles of Figure 6.32 which are otherwise mostly proteinous green.

Figure 6.34 shows cocoa mass to be the only unmixed ingredient to exhibit a strong signal of auto-fluorescence in the red channel, along with an equally strong signal in the green channel. No signal was visible in any channel when imaging cocoa butter alone and therefore as the only ingredient which exhibits any significant fluorescence in the red channel, any red signal in crumb paste images may be attributed to cocoa mass. Unfortunately, the equally strong green wavelength emitted by cocoa mass complicates the interpretation of the green channel in crumb paste images, as dairy proteins have been shown above to emit a signal of the same wavelength, making it impossible to distinguish between the two when considering the green channel only.

To summarise, in attempting to label the significant levels of auto-fluorescence demonstrated by crumb paste under MPM excitation, imaging of the individual ingredients has shown that the dominant source of signal in the blue channel is carbohydrate sugars, dairy protein and cocoa mass in the green channel and cocoa mass alone in the red channel. Areas of yellow visible in Figure 6.29 are the result of pixels which simultaneously co-fluoresce signals in the red and green channels.

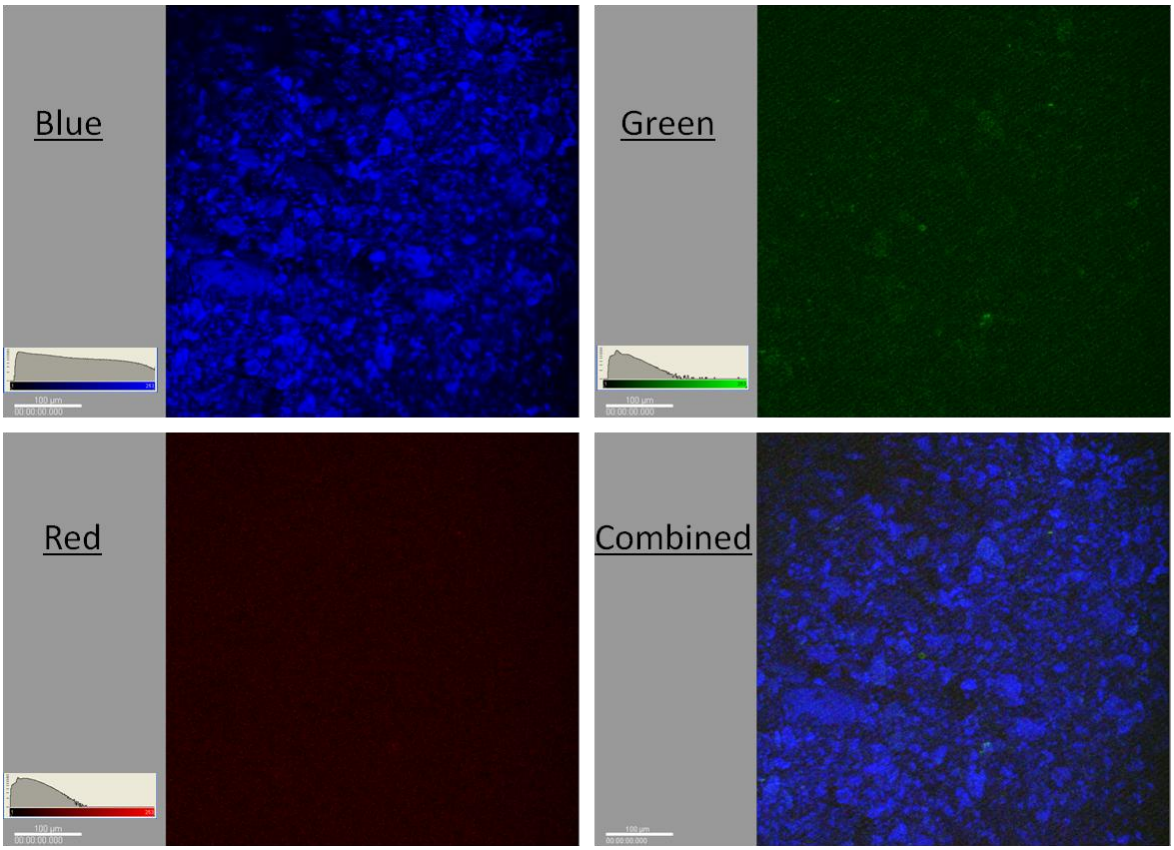

Figure 6.30 MPM channel images of section through sucrose (scale bar 100 μm)

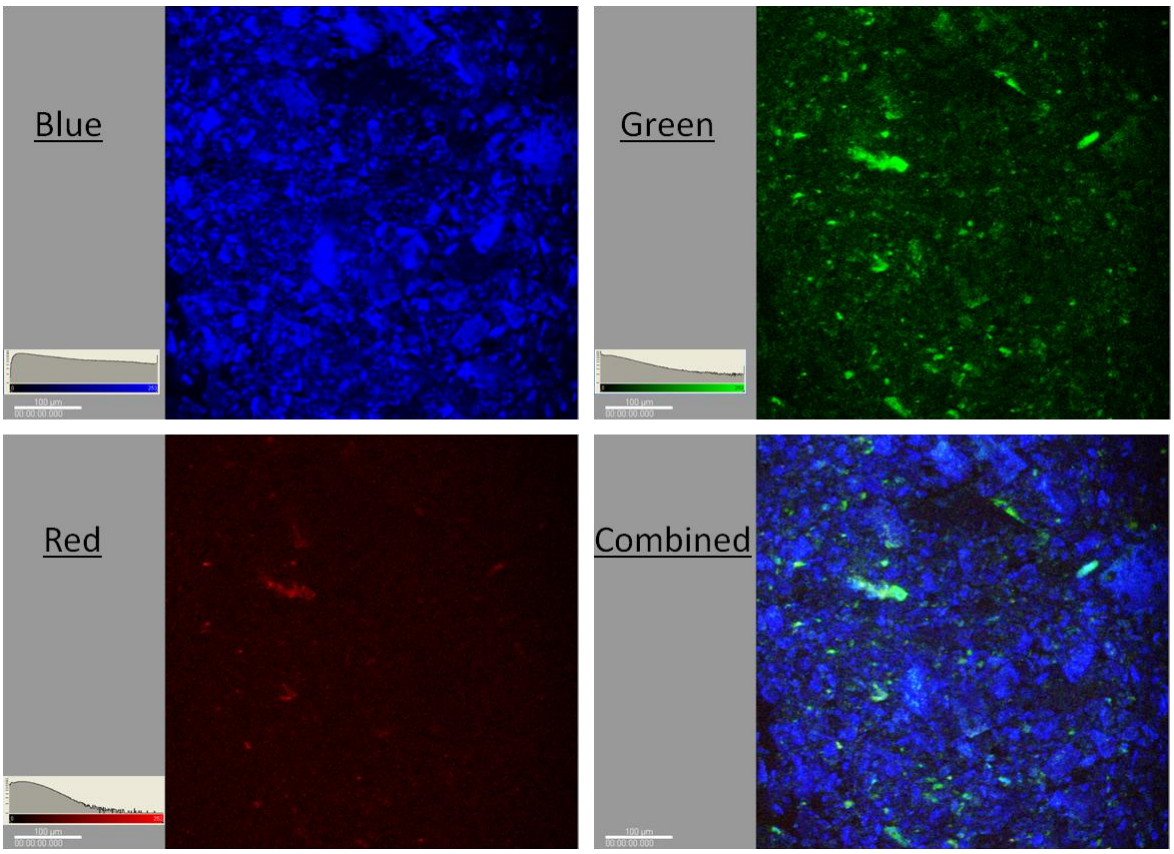

Figure 6.31 MPM channel images of section through powdered lactose (scale bar 100 μm)

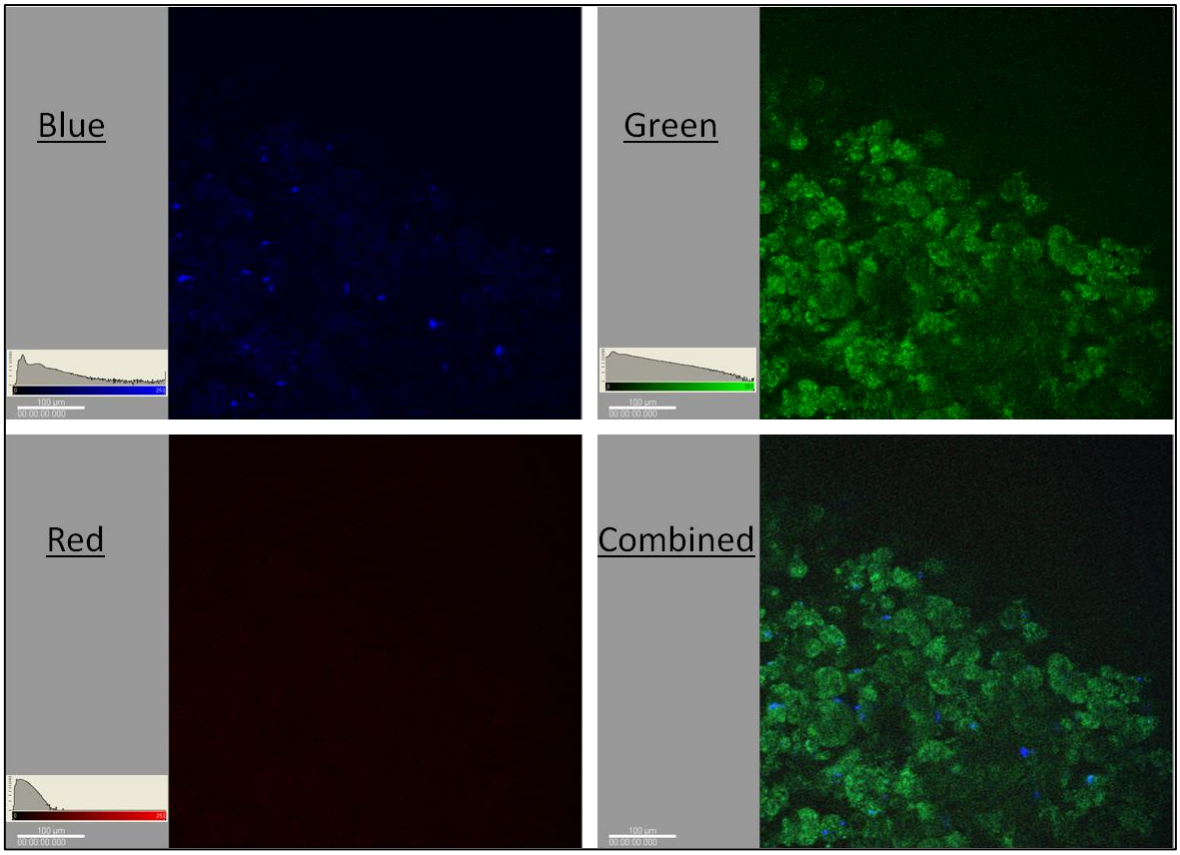

Figure 6.32 MPM channel images of section through skimmed milk powder (scale bar 100 μm)

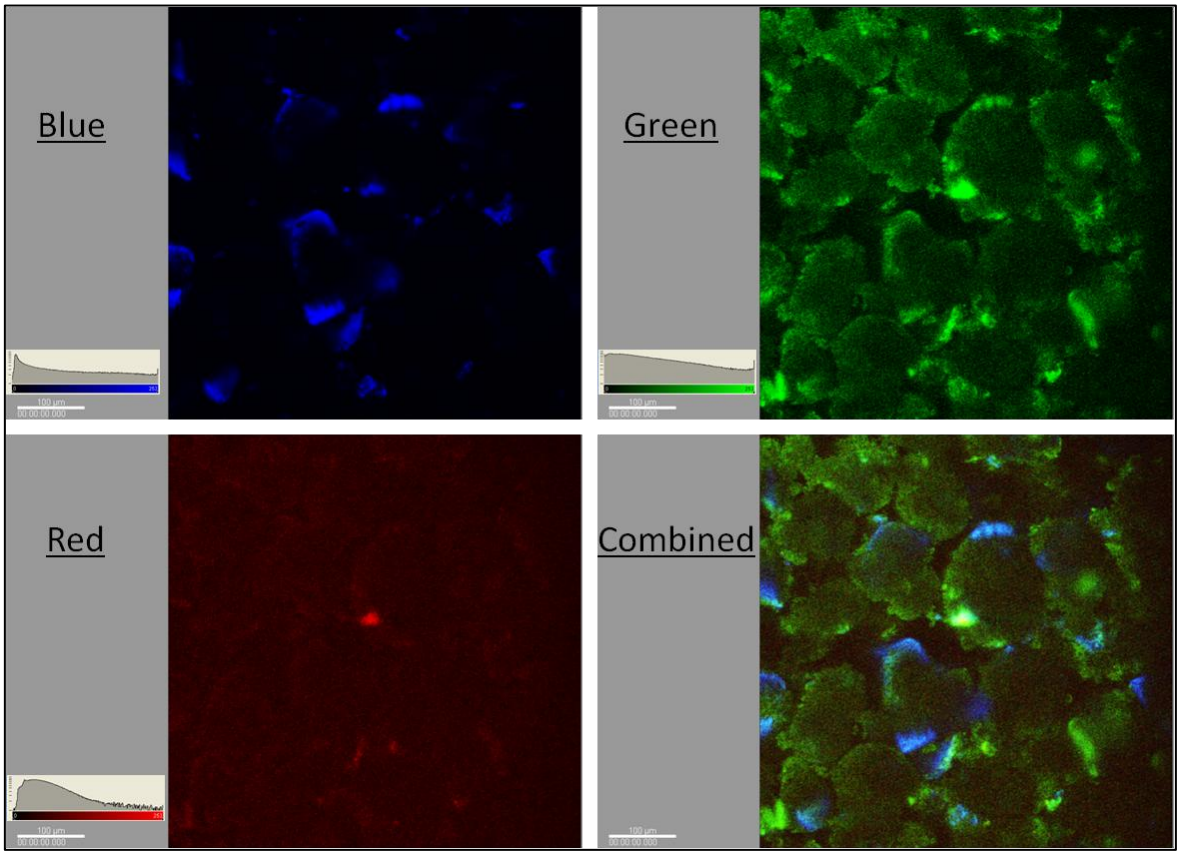

Figure 6.33 MPM channel images of section through whey powder (scale bar 100 μm)

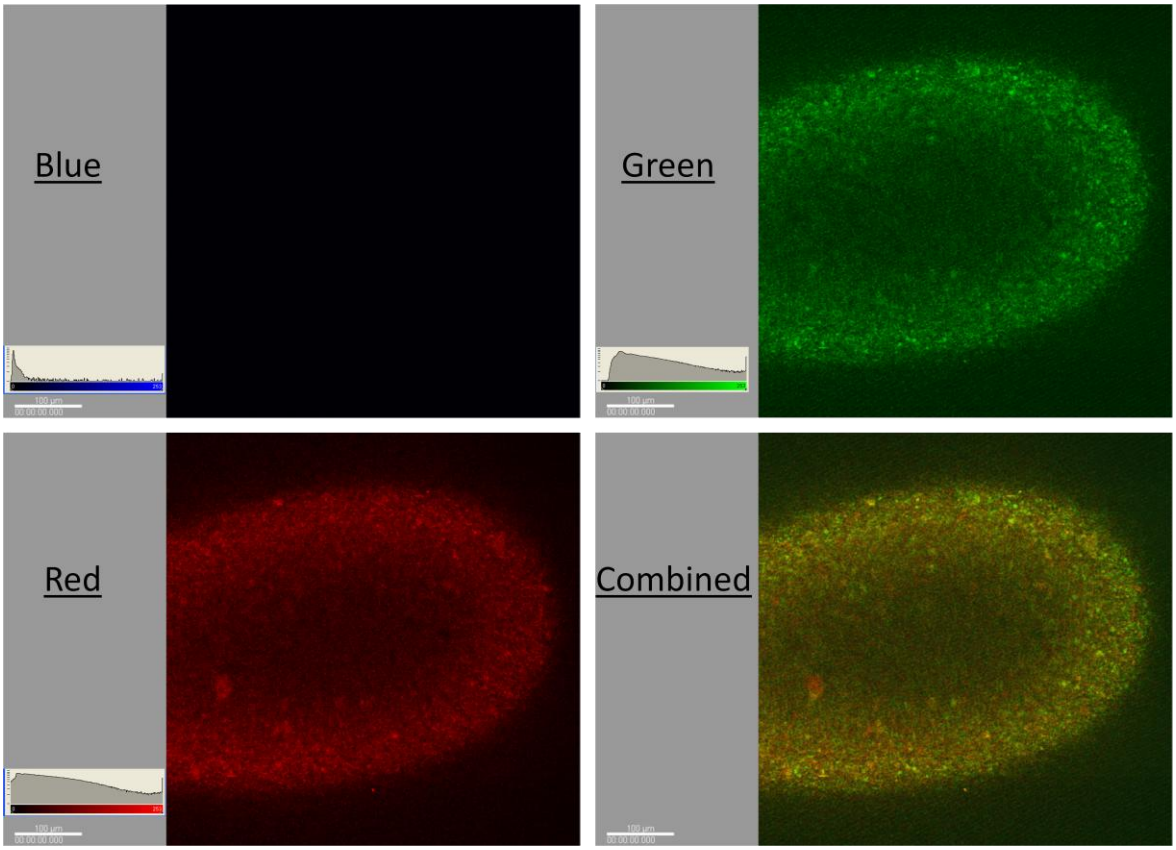

Figure 6.34 MPM channel images of section through solid cocoa mass (scale bar 100 μm)

6.4.3 3D imaging of LM crumb paste

One of the attractive aspects of MPM is its potential for non-destructively achieving multiple optical sections by raster scanning the point of focus at different depths. From this, it can be possible to construct a 3D volume without the need to destructively section and image individually. Attempts at the 3D imaging of LM crumb paste using MPM were made by manually observing peaks on the sample surface to select the depth at which to image the first section. From this depth, 664 sections were raster scanned with a depth interval of 0.22 μm to create a series of images corresponding to focal planes looking deeper into the sample along the *z*-axis. This form of data set, known as "z-series data" thereby achieved an imaging volume of 621 μm x 621 μm x 147 μm.

Despite impressive 2D resolution of the scans, the resulting 3D volume presented in Figure 6.35 shows there to be a significant degree of distortion in the depth, or *z*-

direction. Figure 6.35 shows the blue channel only for clarity, but is representative of the green and red channel. This comparison is further compounded by Figure 6.36 showing a clear 2D section of all channels and the corresponding distortion in the accompanying depth profiles.

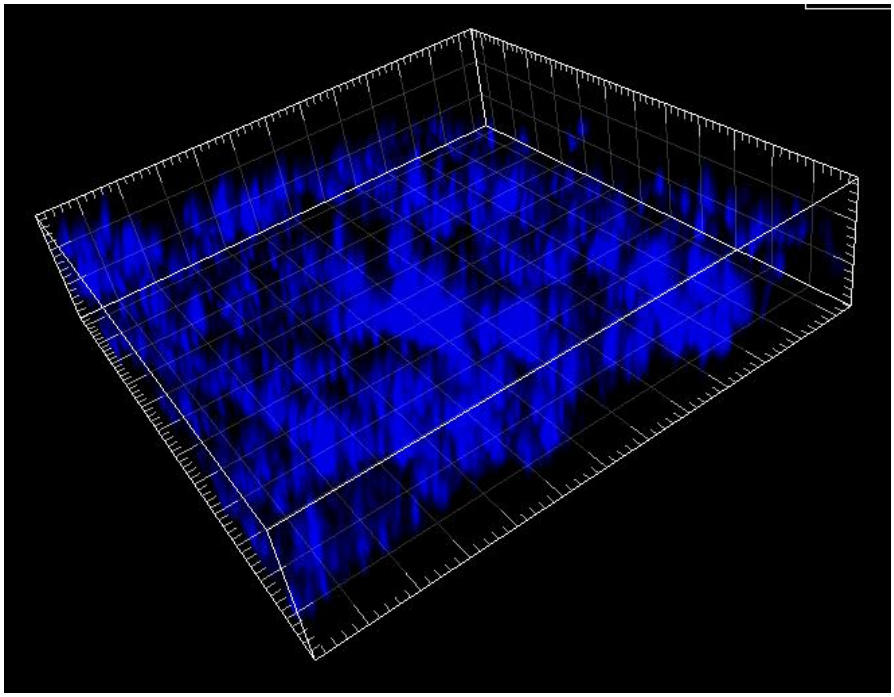

Figure 6.35 3D MPM of 8% water LM crumb paste showing blue channel only

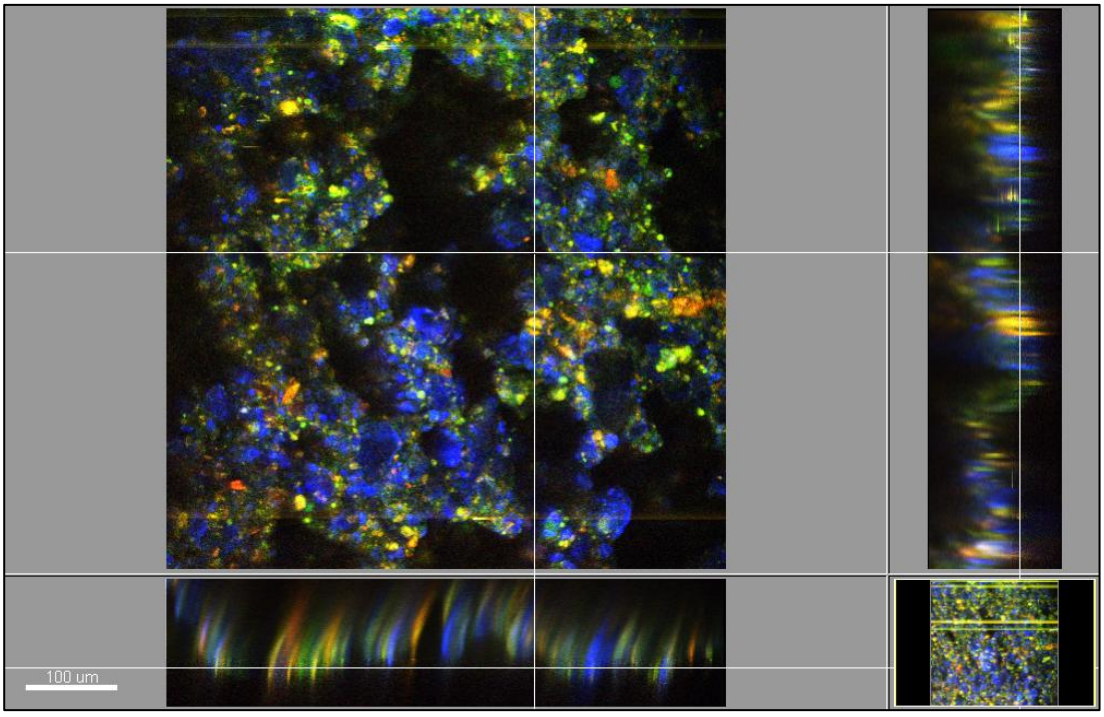

Figure 6.36 MPM section image of 8% water LM crumb paste showing depth profiles in z-direction

A pre-requisite for any future image analysis of 3D volumes is that registration errors between sections are minimal i.e. images are aligned and orientated correctly such that they all share a common coordinate system. The curved and consistent "lateral warping" evident in the depth profiles of Figure 6.36 indicates that consecutive image sections are appearing laterally shifted. Common causes of registration errors can be translational motion of the whole sample, or temporal variations within the sample during imaging which are common in living materials. Since crumb paste is not a live specimen and the microscope stage is assumed to be fixed and rigid, it does not seem likely either of these errors are causing the drift shown. A more likely explanation could be that a complex multiphase paste such as crumb is likely to contain a wide range of refractive indices and that large mismatches of refractive index between phases in the sample can lead to an effective focal point of the lasers which is different from that calculated by the imaging system. Image distortions of this nature are described by Doukoglou & Hunter (1995) for mismatches in the axial direction, but could equally apply in the radial direction.

In addition to distortions caused by refractive index mismatches, a common cause of volumetric distortion within confocal and laser microscopy is that caused by the point Spread Function (PSF) of the optical system, which describes the three dimensional diffraction pattern exhibited by light emitted from all point sources within the specimen. The resulting convolution of the PSF with the fluorescence of each specimen point then results in a blurring of the output image. The shape and contour of the PSF is dependent on the imaging mode being utilised, but is commonly bell shaped, or Gaussian in the x-y plane and hour glass shaped in the x-z plane. Because the point spread function is three-dimensional, blurring from the point spread function is an inherently three-dimensional phenomenon, as the image from any focal plane contains blurred light from points located

in that plane mixed with blurred light from points originating in other focal planes (Wallace et *al*., 2001). Example PSFs of optical imaging systems in the *x-z plane* with varying degrees of spherical aberration are reproduced from Wallace et *al*. (2001) in Figure 6.37 and show relative diffraction in the axial, *z* direction to be significantly larger than that in the radial direction in the *x-y* plane of the source.

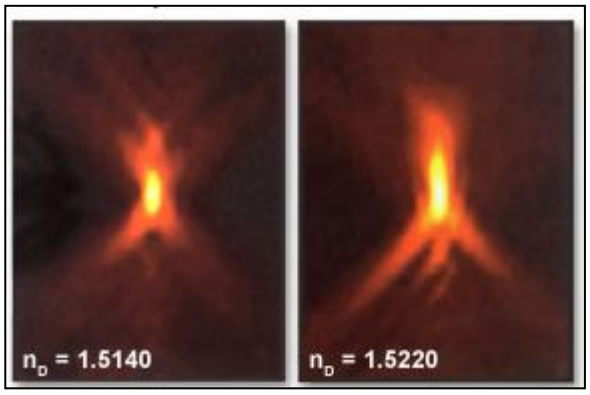

Figure 6.37 x-z projections of point spread functions with different degrees of aberration (Wallace et al., 2011)

The combined effect of the two imaging errors described above offers a viable explanation of the distortions seen in the 3D imaging, with little distortion in the *x-y* plane, registration errors from refractive indices mismatch and significant axial distortion from both refractive indices mismatch and the tendency of PSF distortion to be most exaggerated in the axial direction.

When reviewing the state of 3D microscopy, Cebollero (2009) concluded that automated methods of quantitative 3D microscopy are still very much in their infancy which primarily reflects the current lack of image analysis tools which are suited to the unique properties of microscope image volumes. Contributing factors to these inadequacies were that microscopy volume distortions are inherently anisotropic in

complex materials and that at a larger scale, contrast decreases with depth, both characteristics which were evident in the 3D imaging of crumb paste.

In order to try to correct for the registration errors described here, algorithms are widely used to align stacked images by mapping features of adjacent images to each other, but require an *a priori* knowledge of the features in the image for automatic segmentation and recognition, or a manual input for picking landmarks. Both of the considerations are difficult when considering the number of features seen in crumb paste sections.

Deconvolution techniques are used for trying to reverse PSF errors and blur, by taking a blurred image and reconstructing the specimen from an assumed knowledge of the PSF for the optical system used. Such algorithms require either a known empirical model of the PSF, or a theoretical model for the PSF which is often axially symmetric above and below the *x*-*y* plane and rotationally about the *z*-axis. However, many deviations from the ideal, symmetrical PSF (such as those seen in Figure 6.37) arise as a result of any irregularities or misalignment of any of the components in the optical system. It can be possible to measure the PSF of a system, by imaging a single fluorescent bead of known dimensions, however no such information was available for the microscope used.

In the absence of access to any well established deconvolution and registration algorithms, as well the expertise to implement them effectively, it was decided that the major and in-depth analysis required to obtain accurate three dimensional representations of the volumes imaged in crumb paste using multiphoton microscopy was beyond the scope of this project. Consequently, only two dimensional section images are considered for analysis from this point forward.

6.4.4 Possible 2D analysis of LM crumb paste

Given the decision to consider the undistorted 2D sections only, Figure *6*.38 and Figure *6*.39 show the spatial interactions that may be observable in a variety of pastes without the need for staining due to the auto-fluorescence that is exhibited by crumb paste. Figure *6*.38 shows only the red and blue channels of section images for each of the LM crumb pastes sampled in order to observe the relative spatial distribution of carbohydrate sugars and cocoa mass. For standard 8% water paste, a clear improvement in cocoa mass dispersion amongst sugar crystals is observed when comparing the sample subjected to thirty seconds of mixing with the sample that experienced a further thirty seconds of mixing at the higher mixing speed. After thirty seconds, large regions of clustered cocoa mass are observed without much interaction with the sugar crystals. After sixty seconds of mixing however, the regions of cocoa mass are finely dispersed amongst the sugar crystals. A similar effect is observed when comparing images from samples made with differing water contents. Whilst the cocoa mass appears well dispersed as fine clusters amongst the sugar network of the 8% and 10% water samples, the cocoa mass amongst the drier 6% water sample appears less well dispersed across the samples volume.

Figure *6*.39 then shows the same section images, but instead displays the blue and green channels. The interpretation of these images is severely limited by the fact that the green channel has been shown in Section 6.4.2 to highlight the presence of both dairy proteins and cocoa mass, making the two indistinguishable from the green channel alone. Unfortunately, it is not possible to simply subtract the pixels of green that also appear in the red channel, in order to isolate the signal showing dairy proteins, as a single pixel may be simultaneously occupied by both cocoa mass and protein.

Although difficult to interpret, a more continuous network of green appears in the 8% and 10% water samples than the thirty second mix sample or the drier 6% water

sample. This would be expected as a similar trend was shown for the cocoa mass alone in Figure *6*.38, however the effect appears more exaggerated when considering the green channel and suggests that the formation of a protein network is also more established after the complete mixing time and with higher water content. This effect appears particularly noticeable in the 10% water sample with a virtually continuous network of green surrounding the sugar crystals and corroborates well with protein distributions observed from optical microscopy in Section 6.3. It is however not possible to make conclusive remarks about the dispersion of protein agglomerates in crumb paste from these auto-fluorescent signals alone when cocoa mass is also present within the paste.

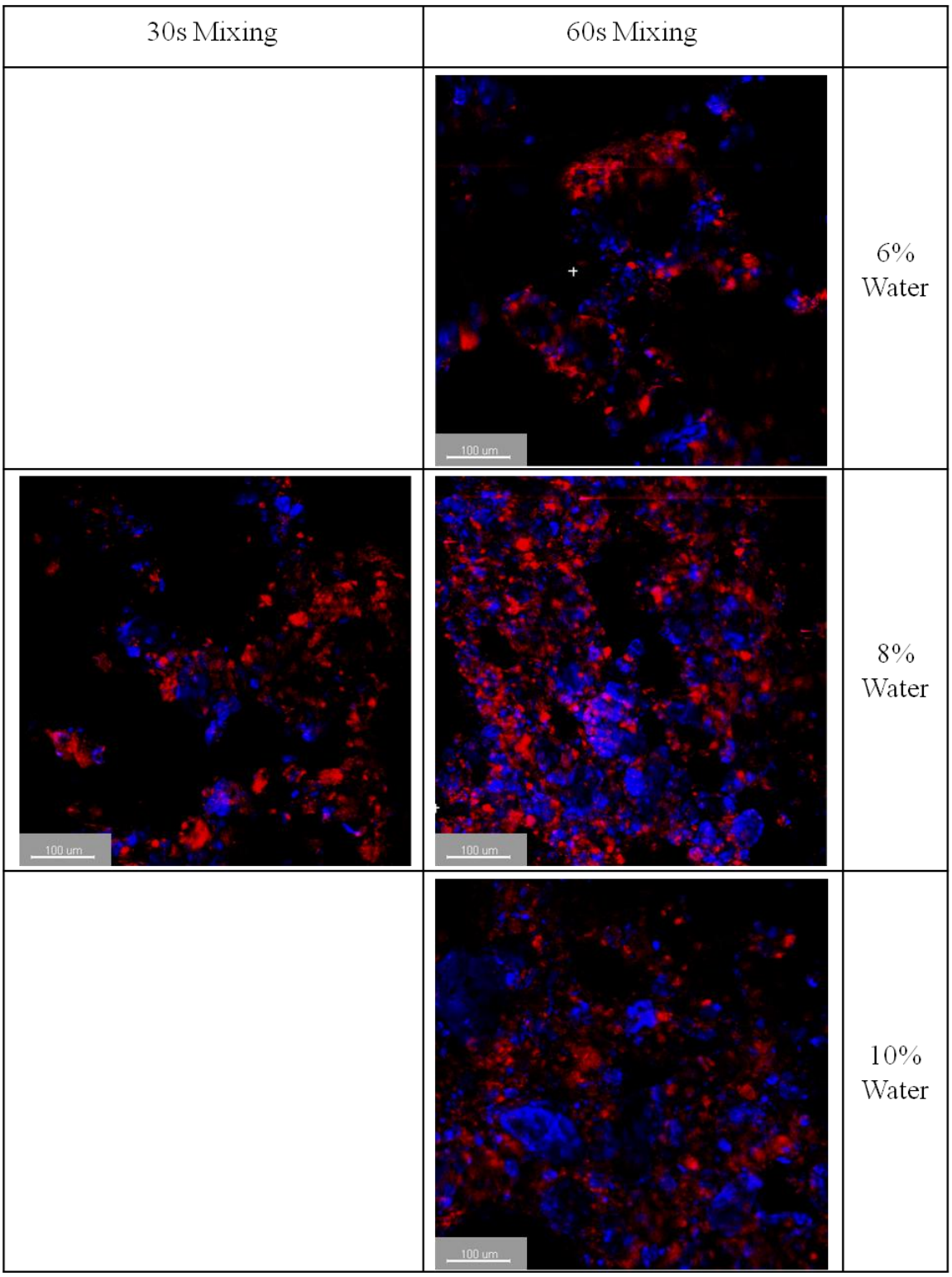

Figure 6.*38 MPM images of various LM crumb pastes showing red (cocoa mass) and blue (sugars) channels only (scale bar 100 μm)*

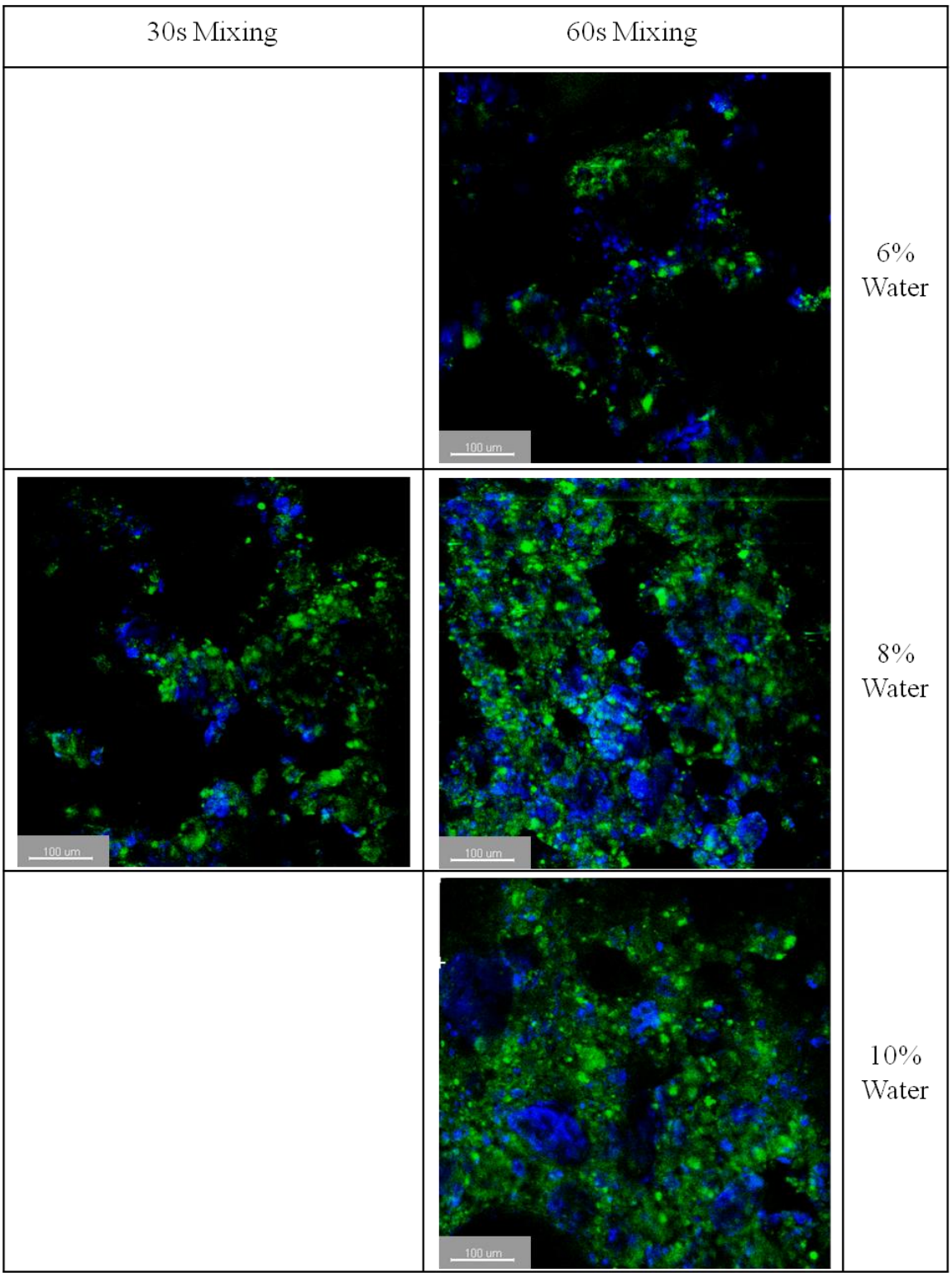

Figure 6.*39 MPM images of various LM crumb pastes showing green (cocoa mass & dairy proteins) and blue (sugars) channels only (scale bar 100 μm)*

6.4.5 Remarks on MPM

MPM has shown that it is possible to successfully visualise the internal microstructure of sugar, protein and cocoa mass in two dimensional sections, without the need to perform any sample preparation of fluorophore labelling. This therefore makes the technique highly attractive for use on the extruder trial in Chapter 7. However the major limitation of the technique seen in this chapter is the inability to isolate proteinous volumes due to the co-fluorescence of cocoa mass in the green channel.

Before the project began, protein interaction with sugar crystals in crumb was highlighted as an area of significant interest by the company, to ascertain whether the proteinous coating of sugar crystals was necessary for the successful processing of chocolate crumb. It is with this project aim in mind that a method for visualising the interaction between sugar crystals and protein is prioritised over the interaction between sugar and cocoa mass. It is therefore proposed that this interaction be investigated in the extruder trial by mixing crumb paste without cocoa mass and replacing it with additional pure cocoa butter. This mixture, known as "white crumb" is often mixed by the company as a model mixture for research purposes, maintaining a similar consistency and fat content to regular crumb paste, but without the presence of cocoa solids. Pure cocoa butter was shown to exhibit no auto-fluorescence when imaged using MPM in Section 6.4.2, thereby indicating that the red signal generated by cocoa mass was as a result of the cocoa solids in the cocoa mass and not the cocoa butter. Consequently, imaging white crumb paste using MPM without the presence of cocoa solids should mean that any green signal emitted is generated exclusively by the proteins such that the desired interaction can be observed. The results of such imaging are presented as part of the full extruder trial in Chapter 7.

6.5 Conclusions

In this chapter, the suitability of three techniques for determining dispersive mixing within crumb paste and visualising the resulting microstructure has been assessed. These have included environmental scanning electron microscopy (ESEM) of crumb paste surface topography, the staining of protein networks within microtomed paste sections observed through an optical microscope and the application of multiphoton microscopy (MPM) to non-destructively image paste volumes below the surface.

ESEM images were successfully obtained for LM crumb pastes in Section 6.2 and disproved a previous hypothesis that crumb paste contained a significant number of small air voids and was largely porous. Instead, crumb paste was shown to be mostly non-porous with a continuous surface of liquid and solid phases depending on the degree of hardening that had taken place when imaged. An increasing degree of angularity in the fractured surface with time after mixing led to the suggestion that crumb paste hardening may in part be attributed to an immediate but prolonged formation of sugar crystals out of solution post mixing. The orientated and stretched cocoa mass imaged on the unfractured crumb paste surfaces provided evidence that elongational, as well as shear forces, play a significant role in the final shape and positioning of cocoa mass. Whilst some interesting and useful observations were made about the general form of crumb paste at high magnification, the images were not suitable for use in directly comparing the dispersive mixing in differing pastes.

A visual protein staining method using optical microscopy was successfully applied to a small data set of 16μm sections in Section 6.3. Here, variations in the protein network of pastes subjected to varying times of mixing and of differing water contents were observed. Visual observations were made to suggest that both the dispersion of protein and the protein coverage of sugar crystals increased both with mixing time and

water content. When applied to a small number of samples that were prepared consistently, both of these observations were then supported quantitatively by a novel image analysis which simultaneously considered the images under brightfield light and polarised light to negate the effect of artefacts. A larger study of multiple samples was then conducted so as to perform an analysis of variance within the data. In this study, it was found that image contrast was highly sensitive to preparation conditions and that a systemic variation in the staining of images was seen for sections prepared in different batches despite efforts to apply a consistent procedure. Consequently the quantitative image analysis algorithm for determining the undispersed protein fraction fell down as it was no longer able to confidently distinguish between dispersed and undispersed protein. The algorithm for determining the protein coverage of crystals was still able to produce some intuitive results that supported the original hypothesis observed of increased coverage with mixing time.

Whilst a quantitative image analysis was successfully able to determine varying trends in the dispersion of protein within LM pastes using optical microscopy, a large degree of difficult sample preparation is required for imaging large sets of data and it has been shown the analysis conducted is highly sensitive to slight variations in sample preparation. It is therefore concluded that protein staining of microtomed sections is a useful observational tool for examining trends of protein distribution in the extremes, but for this material is too sensitive to preparation conditions to provide a robust quantitative analysis between large sets of data, such as is required on the extruder trials.

Finally in Section 6.4, multiphoton microscopy has proved successful at imaging a number of microstructural features within crumb paste up to 80 μm below the surface without any form of sample preparation, making this form of visualisation highly attractive for future use. Using this technique, it has been shown that it is possible to visualise the

interaction between cocoa mass, sugars and proteins in differing pastes via the channels of fluorescence that they each emit when subjected to focused multiphoton excitation. The major advantage of this technique is the lack of sample preparation required and that samples may be imaged non-destructively without the need to section or fracture. The disadvantages of this technique are that distortion has limited images to 2D optical sections when it was hoped that 3D images would be achieved and that the co-fluorescence of cocoa mass and proteins in the green channel mean that it is not possible to distinguish between the two when both are present in the mixture.

None of the visualisation techniques assessed in this chapter are capable of imaging within a timescale before the onset of crumb paste hardening, however this is a limitation of the techniques considered that cannot be avoided. As detailed in Section 6.4.5 multiphoton microscopy will be used to image extruded paste with cocoa butter only and without the presence of cocoa mass, such that the desired interaction between sugars and proteins may be observed in the extruder trial. The results of these images are presented in Chapter 7.

Chapter 7 Extruder study of crumb paste

It was established in Chapter 2 that despite the widespread use of twin-screw extrusion as a continuous form of mixing for industrial suspensions and pastes, relatively few studies exist which look to experimentally establish the influence of screw profile and configuration on extruded material properties or relate the statistics of microstructural distributions to rheological behaviour. This is despite the fact that in many cases, key mechanical parameters for equipment design and operation are principally related to the deformation response of the material under shear and key product quality parameters are principally related to the microstructure of the final form. It was also established that linking these two groups of data is not always straightforward, owing to the difficulties in quantifying the rheology and in measuring appropriate microstructural features.

This has certainly been the case with trying to characterise the complex behaviour of crumb paste, however work in Chapters 3 to 6 has sought to overcome these difficulties. In this chapter, the techniques and analysis developed in this work have been applied to the study of a pilot plant extruder available at the company's factory such that the effect of extrusion on the formation of crumb paste may be better understood and trends of ingredient mixing identified to facilitate the quantitative comparison of differing screw profile designs and mixing conditions.

This chapter begins in Section 7.1 with an introduction to the pilot plant extruder available for this study and the experimental design of data to be collected. Section 7.2

presents and discusses images of crumb paste evolution along the screw profile obtained from dead-stop screw extractions. Variations in extruded paste density are then determined in Section 7.3 as a pre-requisite for the analysis of crumb paste shear yield using off-line cone penetrometry which follows in Section 7.4. Section 7.5 then presents data obtained by shear wave reflection at the sample interface to discuss the potential for its use as an in-line rheological characterisation technique. Analysis of the distributive mixing mechanism within the extruder is detailed in Section 7.6 using thermogravimetric analysis (TGA) and is followed by analysis of the dispersive mixing mechanism using multiphoton microscopy (MPM) in Section 7.7. Section 7.8 discusses the microstructural evolution of crumb paste under various mixing conditions and is followed finally by a summary of the major findings in this extruder study in Section 7.9.

7.1 Pilot plant extruder

The pilot plant extruder used in this work was a Buhler BCTL-42 co-rotating twin-screw extrusion system (as shown in Figure 7.1). The system comprised of a 110 kw/700 Nm motor capable of rotating the screws at a maximum speed of 1500 rpm. The maximum temperature permitted in the extruder is 300 °C and seven discrete zones of temperature cooling were available along the barrel length with integrated water cooling units. The inlets/outlets for each water cooling region are shown in Figure 7.2, along with a number of available ports for the flexible positioning of any liquid feeds. The extruder barrel and die plate with circular die (shown in Figure 7.3) are capable of withstanding pressures up to 300 bar.

On this extruder, the screws and feeds can be halted suddenly and the screws ejected using two 31 kN hydraulic cylinders. Once ejected, the full length of the screws can be carefully removed to view material in the screw channels at the point of halting.

This therefore shows the evolution of the mixture along the length of the screw profile and thereby achieves the dead-stop sampling described in Section 2.3.3.

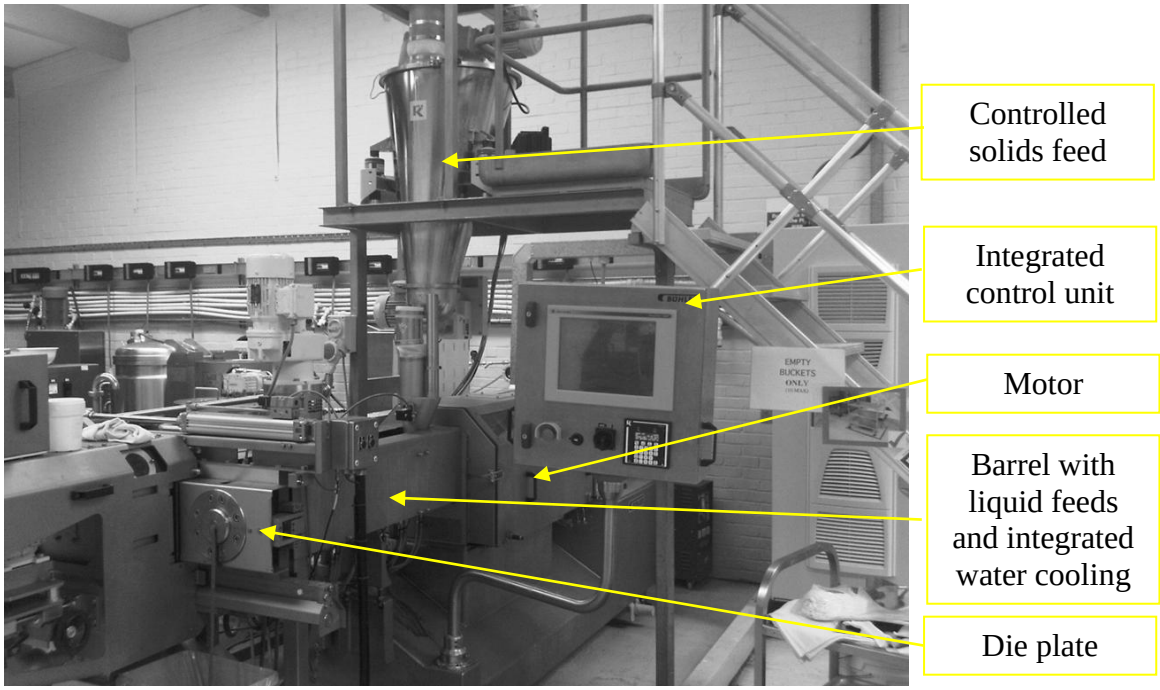

Figure 7.1 Buhler BCTL-42 Co-rotating twin-screw extrusion system

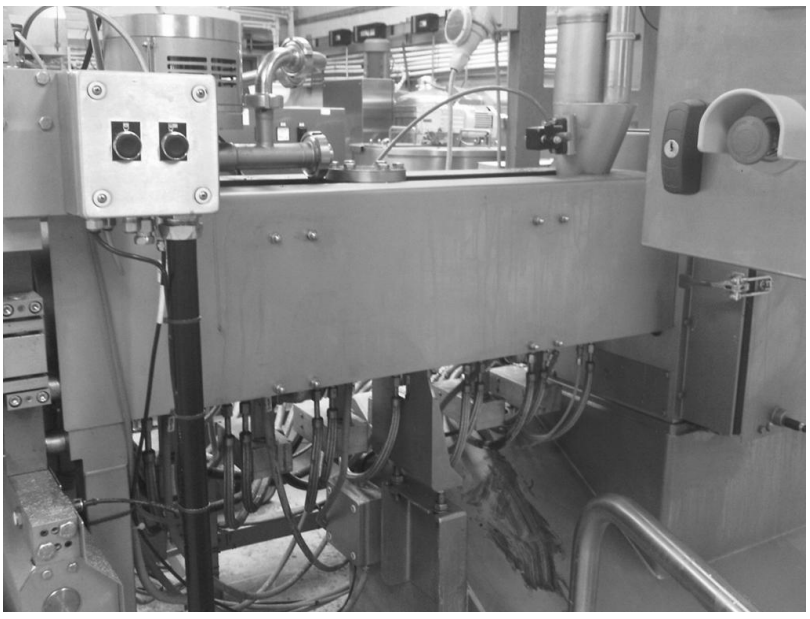

Figure 7.2 Extruder barrel showing integrated water cooling connections and liquid feed inputs

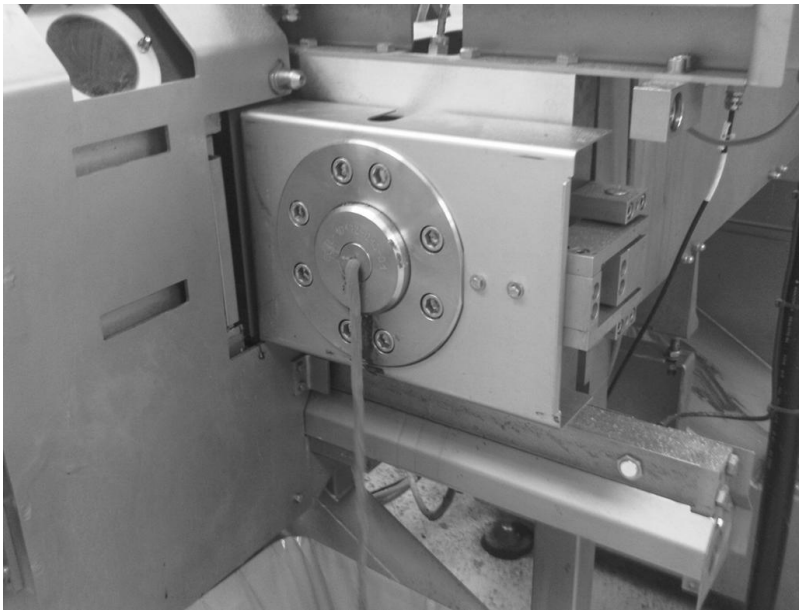

Figure 7.3 Extruder endplate with circular die

7.1.1 Screw profile

The screw length used in the barrel was 1182 mm with an outer diameter of 41.4 mm, an inner diameter of 24.6mm and a distance between the screw centers of 33.4 mm. The modular nature of the screw elements, which slide over common shafts as shown in Figure 7.4, mean a great deal of flexibility can be achieved in designing the screw profile. With the modular elements available, the screw profile design which best replicated that used in the factory extruder is shown in Figure 7.5. In this design, powdered and liquid ingredients are fed separately into a conveying zone of right-handed, double thread screws with a pitch of 60 mm (BCTL-10074-010). Paste then reaches a mixing or "kneading'' element with a four stage, right-handed polygon pack and stagger angle of 45° (BCTL-10102-010). Following the kneading element, a further conveying region of the same screw dimensions transports the paste into a compressional zone with a reduced pitch of 42 mm (BCTL-10073-010), followed by a further reduction in pitch to 28 mm (BCTL-10071-010) before finally reaching the die land.

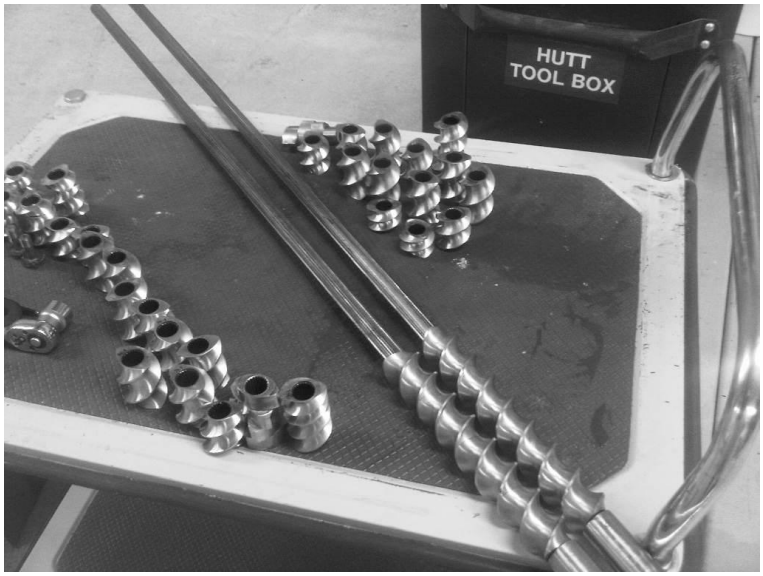

Figure 7.4 Modular elements that slide over common twin screw shafts

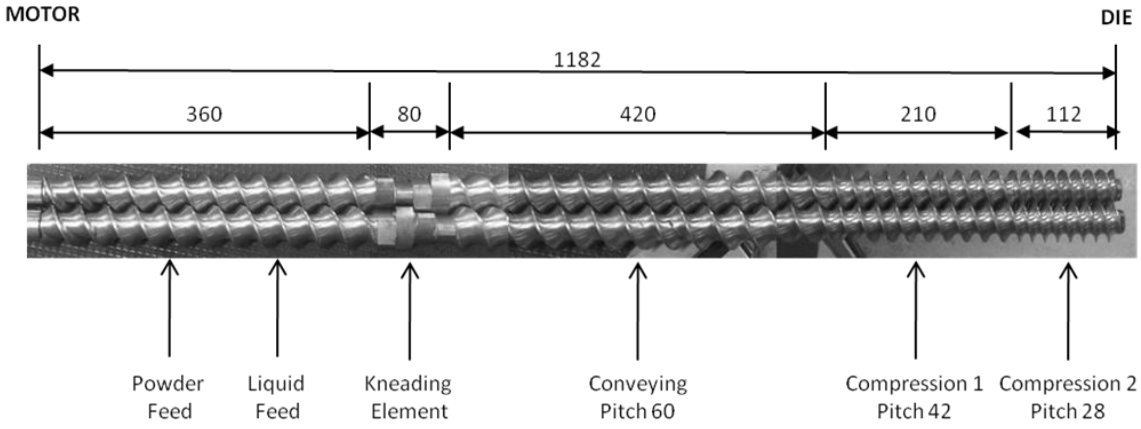

Figure 7.5 Standard pilot plant screw profile (dimensions in mm)

7.1.2 Experimental design

To utilise all the characterisation techniques succesfully designed and applied to LM paste in Chapters 3 to 6, the experimental design shown in Table 7.1 has been performed in these pilot extruder trials. Normal water content used when extruding crumb paste is 5% and this configuration is represented by operating condition S1. Preliminary trials showed that for regular 5% crumb paste, a throughput of 100 kg/hr was the highest that could comfortably be achieved without the risk of backing material up into the solids

feed. A screw speed of 300 rpm then maintained a paste temperature in the normal region of approximately 70 °C such is the case with factory extruded paste.

As described in Section 1.3, water is added at the crumb paste extrusion stage, only to be removed in the baking ovens immediately after, for which there is a significant associated cost. Water content therefore represents a significant variable in the overall efficiency of the chocolate making process and its effect on material properties at the extrusion stage is therefore of great interest. In order to observe and reference the effect of water content on paste characteristics at the extrusion stage, operating conditions S1 - S4 include a drier paste (2%) and two wetter pastes (8% and 11%). The extrudates of these pastes have been analysed for density using the double cup method described in Chapter 3, along with rheological characterisations using cone penetrometry (CP - described in Chapter 3) and shear wave reflection (SWR - described in Chapter 4). Due to the time intensive data aquisition required by the thermogravimetric distributive mixing analysis (TGA - described in Chapter 5), only samples S1 - S3 have been analysed in this way.

As was described in Chapter 6, analysis of dispersive mixing in crumb pastes using multiphoton microscopy (MPM) neccesitates the exclusion of cocoa mass from the mixture. The effect of water content on dispersive mixing is therefore observed on samples S6 - S8, which are otherwise identical to S1 - S3, but are made using “white crumb” where cocoa mass is substituted with cocoa butter only.

In order to quantify the effect of the mixing or “kneading” element in the screw profile, sample S5 has been extruded using the standard 5% water paste, but without the kneading element in the screw profile. This was instead replaced with additional conveying elements and the extrudate from these extrusion conditions was then characterised using TGA. A white crumb equivalent was then visualised using MPM as sample S9.

Table 7.1 Experimental design for pilot plant extruder trials

Extrusion Configuration						Tests				
No.	**Cocoa Mass**	**Water**	**Throughput (kg/hr)**	**RPM**	**Kneading Element**	**Density**	**CP**	**SWR**	**MPM**	**TGA**
S1	✓	5%	100	300	✓	✓	✓	✓	×	✓
S2	✓	8%	100	300	✓	✓	✓	✓	×	✓
S3	✓	2%	100	300	✓	✓	✓	✓	×	✓
S4	✓	11%	100	300	✓	✓	✓	✓	×	×
S5	✓	5%	100	300	×	✓	×	×	×	✓
S6	×	5%	100	300	✓	✓	✓	×	✓	×
S7	×	8%	100	300	✓	×	×	×	✓	×
S8	×	2%	100	300	✓	×	×	×	✓	×
S9	×	5%	100	300	×	×	×	×	✓	×

A key feature of this work is a desire to track the evolution of microstructural features along the length of the extruder profile. In pursuit of this, dead stop experiments have been performed on pastes S1 and S6, such that distributive (TGA) and dispersive (MPM) mixing analysis may be performed on samples collected along the length of the extruder. Sampling points along the screw are shown in Figure 7.6 and include points at the start of the kneading element (A), immediately after the kneading element (B), before the start of the compression zone (C) and the extrudate (D).

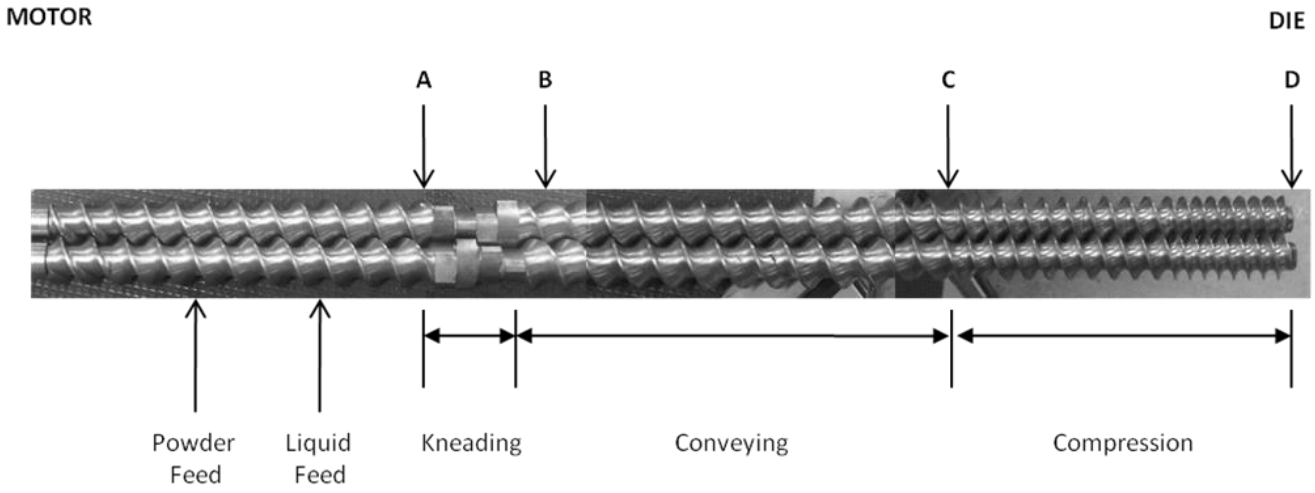

Figure 7.6 Sampling points along screw length for dead-stop experiments once screws are removed from the extruder

7.2 Dead-stop experiment images

Prior to this project, the internal appearance of crumb paste within the extruder had not previously been considered. The utilisation of dead-stop experiments has allowed the visualisation of crumb paste evolution to be made on extruded pastes S1, S2, S3 and S5 and images are shown in Figure 7.7 - Figure 7.10. It is noted that whilst every effort was made to remove the screws gently, some material was lost upon extraction of the screws. This was particularly true of any unmixed viscous fluids, however the volume of material

lost was a small fraction of what was retained in the screws and it can be said with confidence that the images shown are representative of the in-situ conditions within the extruder during extrusion.

Figure 7.7 and Figure 7.8 show that for normal and high water contents of 5% (S1) and 8% (S2), a cohesive paste appears to form at the start of the mixing element. From this point on, no visual change in appearance occurs within the conveying region as it is extruded through the die land. In the case of the drier 2% mixture (S3 - Figure 7.9), a more crumble like mixture is formed after passing through the mixing element and the screw channels appear less filled than those of S1 and S2. This is the case throughout the entire of the conveying zone until the last few screw revolutions before the die land. Within this short section, the paste appears to compact and a cohesive paste was observed passing through the endplate.

Interestingly, a similar effect was observed on the 5% water paste extruded without a mixing element, which despite the absence of the high shear mixing zone, generated a cohesive paste which resembled regular paste when visually observing the extrudate. Little, if any mixing is observed in the first half of screw where conveying elements of the largest pitch are situated. However, near the start of the region of conveying elements with reduced pitch (the start of compression zone 1), some degree of mixing appears to be occurring as strings of paste form. This mixing continues as the screw pitch reduces again and a higher degree of fill in the screw channels is noticeable. Further consideration of the distributive and dispersive mixing occurring within all of these pastes is made in Sections 7.6 and 7.7.

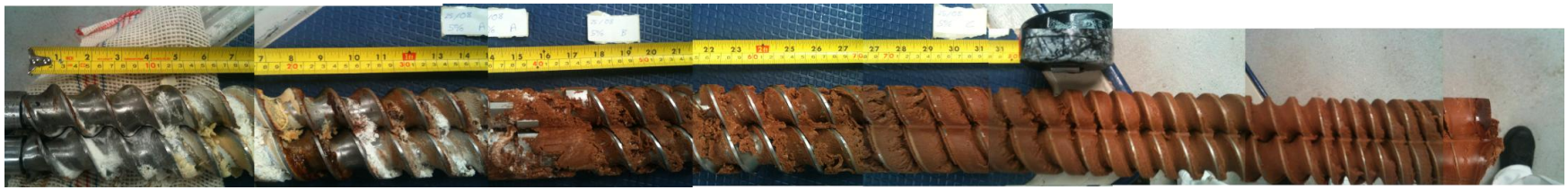

Figure 7.7 Dead-stop screw photo of paste S1 - 100 kg/hr - 300rpm - 5% water - with Mixing Element

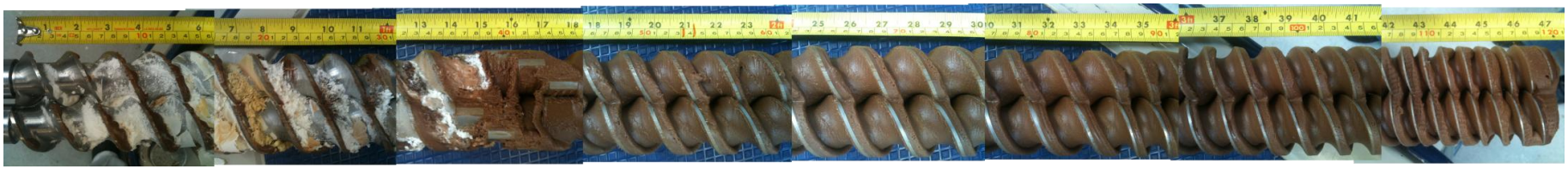

Figure 7.8 Dead-stop screw photo of paste S2 - 100 kg/hr - 300rpm - 8% water - with Mixing Element

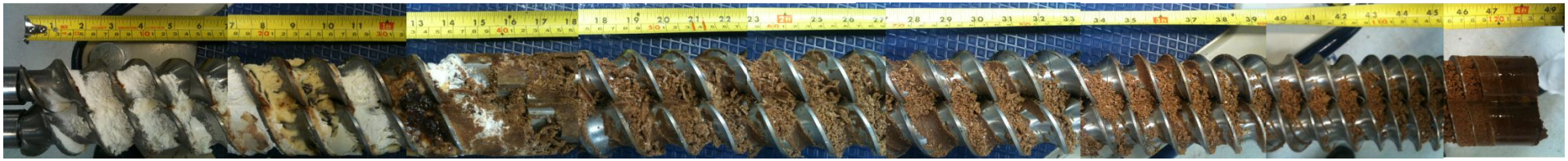

Figure 7.9 Dead-stop screw photo of paste S3 - 100 kg/hr - 300rpm - 2% water - with Mixing Element

Figure 7.10 Dead-stop screw photo of paste S5 - 100 kg/hr - 300rpm - 5% water – no Mixing Element

7.3 Density of extruded crumb pastes

Extruded paste densities were determined both for comparison with LM crumb paste and also as a required parameter for the analysis of cone penetrometry and shear wave reflection data. Each paste density was obtained using the double cup density method described in Section 3.3.6. Two samples were measured independently and averaged for each data point.

Figure 7.11 shows a small but steady increase in apparent density with time after extrusion (between 1% and 3.5% over ten minutes) for all samples obtained. It was considered that the apparent increase in density shown may be due to an increasing penetration of the reference fluid into the voids of the paste with time. This would cause the displaced volume of reference fluid to decrease, reducing the buoyancy force felt by the sample and an increase in the apparent density as determined by Equation (24). To confirm or reject this as a misleading source of error, two identical samples were taken from S5 extruded paste. The first was immediately placed into the reference fluid and the changing density observed with time. The second was used as a control sample left exposed to air. After twelve minutes, the first sample was removed from the apparatus and the control sample density measured. The result is shown in Figure 7.12 demonstrating that the control sample, which had not been immersed in the reference fluid for any significant length of time, exhibited a similar density value to the regular sample, which had been immersed for the duration of its increasing density over ten minutes. From this it is concluded that a small increasing density is not an artefact of the double cup density method, but a phenomenon apparent in extruded crumb paste as it hardens after extrusion. By considering the SEM images obtained in Section 6.2, showing an apparent increase in paste crystallinity with time, the increasing density shown here may instead be attributed to the formation of a growing crystal network into the voids of the paste.

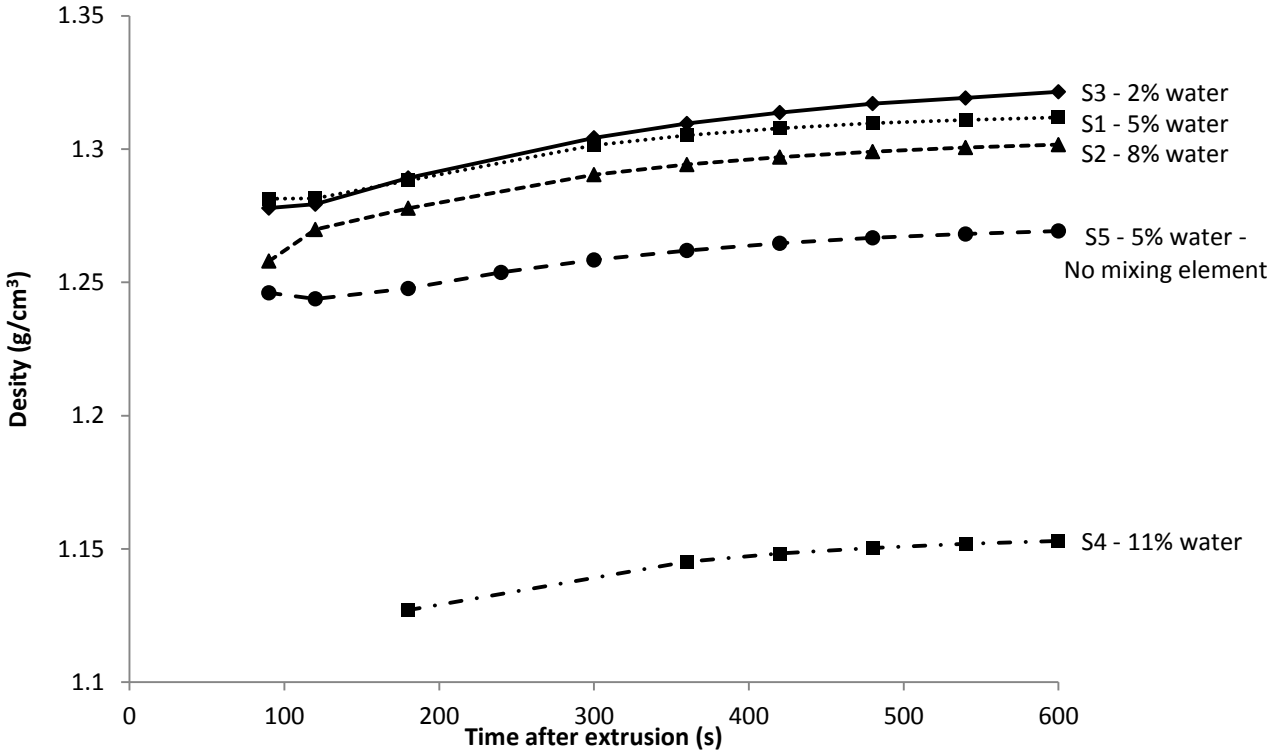

Figure 7.11 Extruded paste densities versus time after extrusion measured using double cup method

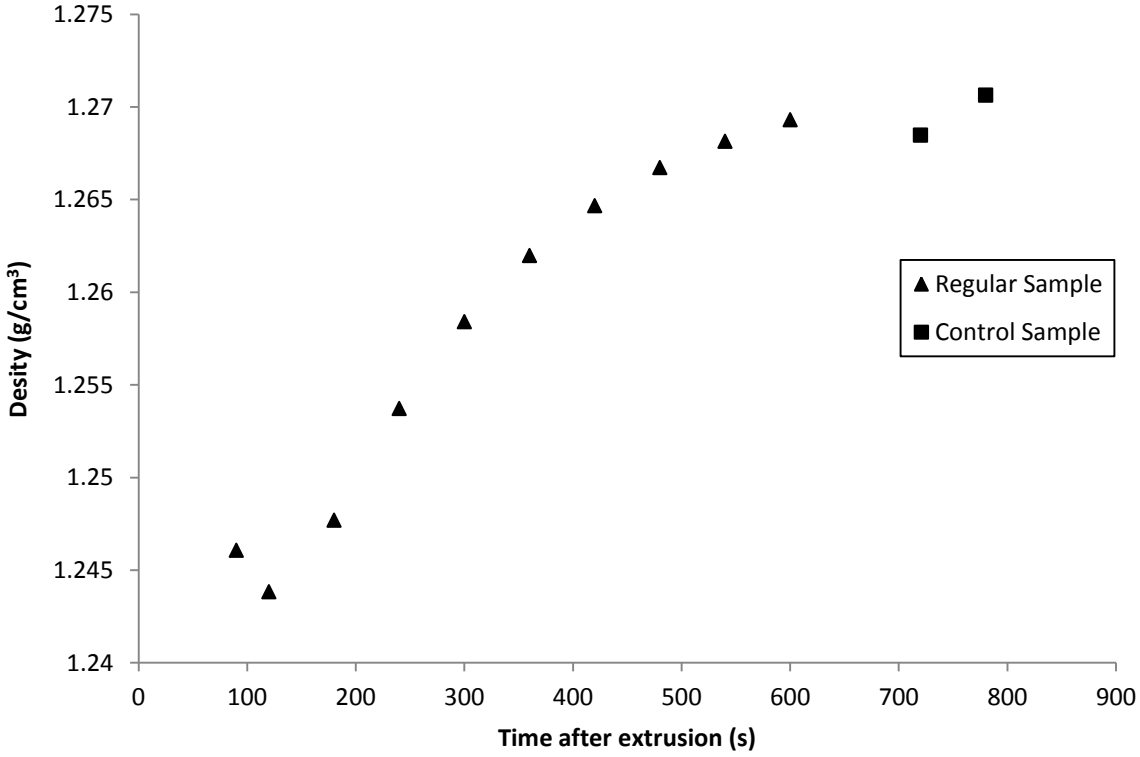

Figure 7.12 Density versus time after extrusion for paste S5 using double cup method with control sample immersed after 12 minutes

As expected with crumb paste density values greater than that of water, the density-time data shown in Figure 7.11 shows a decreasing trend in density with increasing water content (S1 - S4). Interestingly, the 5% paste extruded with a mixing element (S1) exhibited a density value which was 3.3% higher than that of the same paste extruded without a mixing element (S5). This intuitive result may in part be explained by the high shear dispersive effect of the mixing element leading to smaller particle sizes and an increased packing fraction of solids.

Although not shown in Figure 7.11 for clarity, 5% water white crumb paste extruded without cocoa mass for the purposes of MPM imaging (S6) did not show any significant difference in density to regular 5% water paste (S1). For future analyses requiring values of density as a parameter, a power law fit has been applied to the density-time data in each case.

7.3.1 Density comparison with LM crumb paste

Density data for extruded pastes (S1 - S4) after 180 seconds is compared with the density data obtained for LM pastes after 180 seconds in Figure 7.13. Data was not available for LM pastes below 8% water content, but largely show that in the range 8% - 11%, the densities of crumb paste made using the LM method are not significantly different from those subjected to extrusion mixing. The relatively weak dependence of extruded paste density on water content in the range 2% - 8% means that both standard LM crumb paste (8% water) and standard extruded crumb paste (5% water) demonstrate similar density values of around 1.3 g/cm^3.

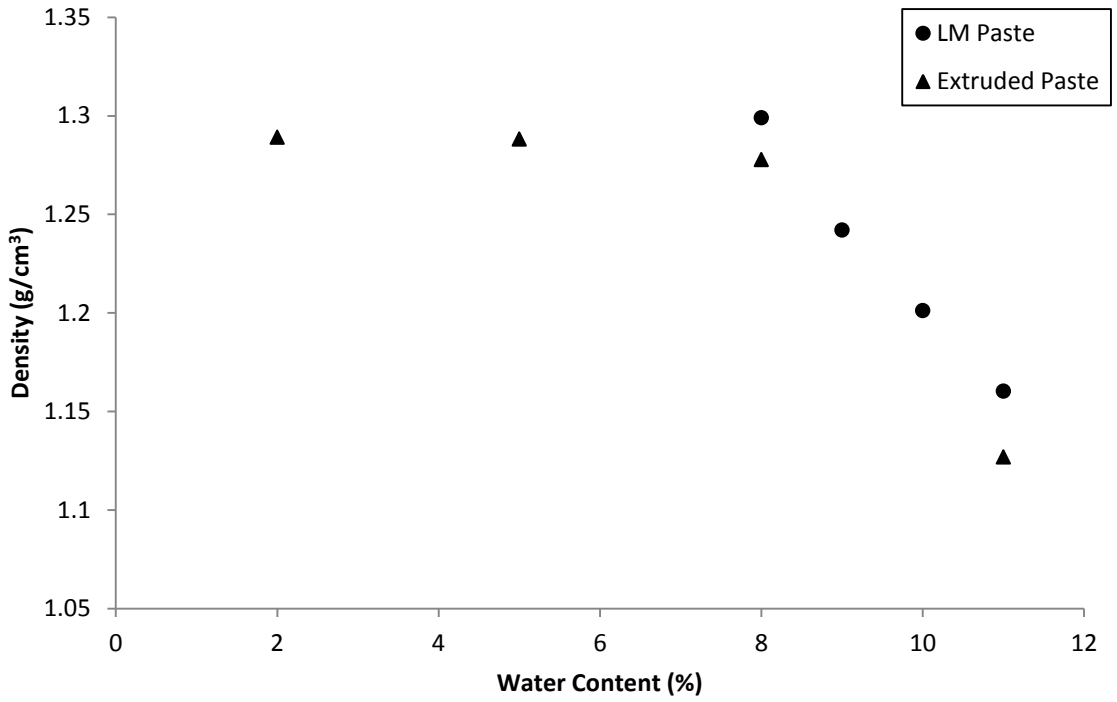

Figure 7.13 Densities for extruded crumb paste and LM crumb paste measured using double cup method 180 seconds after extrusion or mixing

7.4 Cone penetrometry of extruded crumb paste

As an offline characterisation of paste shear yield and hardening once extruded, cone penetrometry analysis (as presented in Chapter 3) was performed on the extrudates of pastes S1 - S4 with varying water contents as well as S6 - a white crumb paste. Given the large variation in paste consistencies over this range of water contents, it was necessary to vary the cone assemblies used for each paste, such that penetration depths within the range of the penetrometer were obtained. The cone assemblies used for each paste are shown in Table 7.2 and are accounted for in the analysis of paste shear yield according to Equation (25). Three readings were obtained for each paste and time point.

Table 7.2 Cone assemblies used for penetrometry on pilot plant extrudates

Configuration	Water Content	Cone Angle	Cone Assembly Mass
S1	5%	40°	393g
S2	8%	50°	251g
S3	2%	40°	393g
S4	11%	70°	286g
S6	5%	40°	393g

The results of this offline characterisation are shown Figure 7.14, plotting the average shear yield of the three readings versus time after extrusion. The statistical significance of each point is then presented in Table 7.3 following a one-way analysis of variance (ANOVA) test on each set of paste data to reject the null hypothesis that the means of shear yield strength at each time point are equal. Fisher's LSD method was then used to determine statistically significant differences between the means of duplicate determinations.

As was the case with LM crumb paste in Chapter 3, Figure 7.14 shows the shear yield strength of extruded crumb paste to be highly dependent upon both added water content and time after extrusion. The magnitude of yield is inversely dependent on the level of added water, with the strongest dependence at lower water contents. No data is shown for 2% water paste (S3), since despite using the sharpest and heaviest cone assembly available, the stiff and solid like nature of the paste meant that penetration depths beyond this point were too low to give accurate data. Conversely, even when using the flattest and lightest cone assembly for 11% water paste (S4), the low yield and fluid like nature of the paste meant steady state penetrations were not achievable until three minutes after extrusion. The fact that the full range of penetrations which can be recorded with this apparatus has been reached with extruded crumb pastes varying in water content from 2%

- 11% has again highlighted the large range of rheological behaviours apparent within crumb paste extrusion when considering a normal range of processing conditions.

The large dependence upon added water content is also true of the rate at which paste hardening occurs, with 5% water paste (S1) showing a 180% increase in yield over ten minutes, a 90% increase for 8% water paste (S2) and a 40% increase for 11% water paste (S4). One-way ANOVA shows that the null hypothesis of equal means can be rejected for each of the crumb pastes and therefore the yield of at least one time point is statistically significant from other time points for that paste with a confidence level of $\alpha = 0.05$. Although a few adjacent data points are not significantly different, the statistical significance of mean differences for time points on each paste shown in Table 7.3 strongly supports the hypothesis made from Figure 7.14, that significant paste hardening of shear yield has occurred post extrusion in all of the trial pastes considered.

It also appears the 5% water crumb paste extruded without cocoa mass (S5) has hardened at a slower rate than the regular 5% water crumb pate extruded with cocoa mass (S1). In order to confirm whether or not this hypothesis is significant within the statistical variance of the technique, a two-way ANOVA test was performed on the data for pastes S1 and S5, with time after extrusion and the inclusion of cocoa mass as the two factors considered. Results showed that with a high confidence level of α less than 0.01, paste yield is highly dependent on time after extrusion, an observation which was already known from the individual one-way ANOVA tests performed earlier. With a similarly high confidence level of α less than 0.01, the dependence of yield on the presence of cocoa mass was shown to be significant, supporting the hypothesis that crumb pastes without cocoa mass exhibited lower yield strengths. Finally, with a confidence level of α less than 0.03, the interaction between cocoa mass and the time after extrusion was also shown to be significant i.e. the exclusion of cocoa mass has reduced the rate at which the yield

increases, as seen by similar yield values in the first five minutes after extrusion followed by an increasing deviation with time.

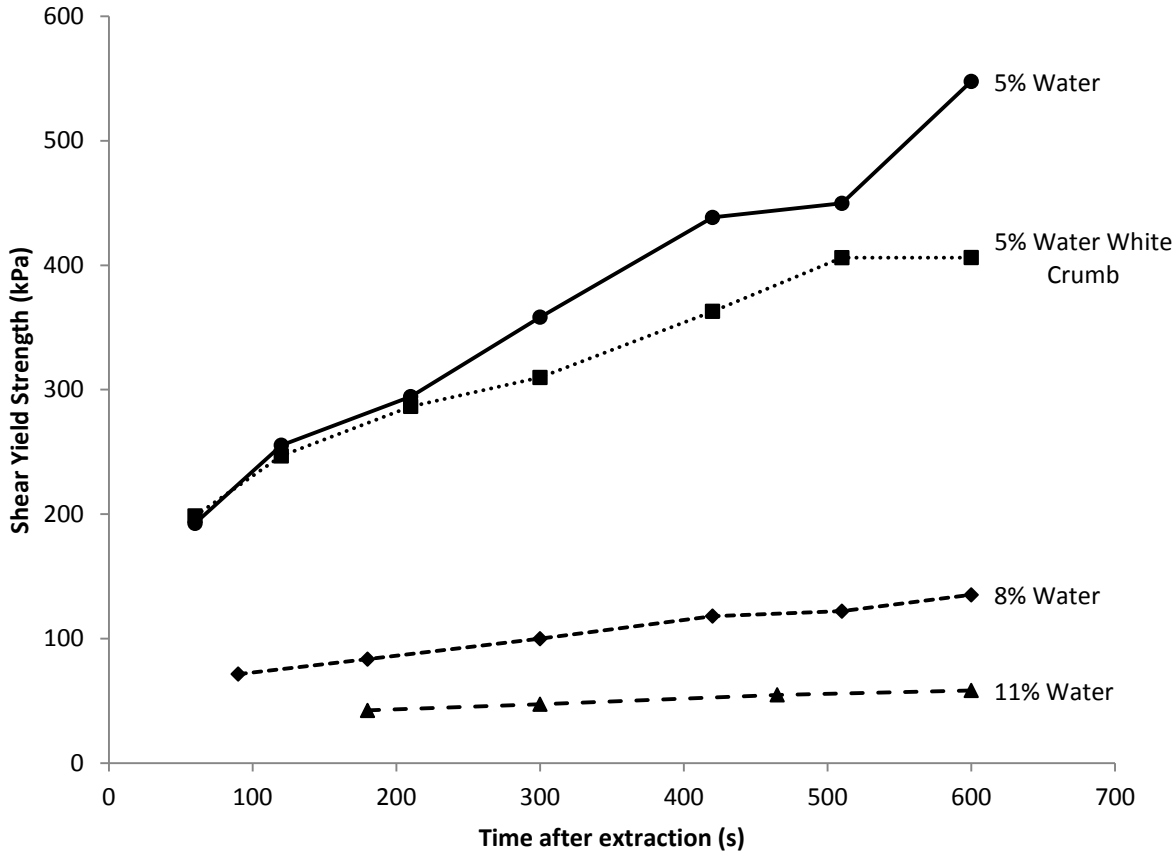

Figure 7.14 Shear yield strengths of extruded crumb pastes versus time after extrusion

Table 7.3 Extruded crumb paste shear yield strengths as determined by cone penetrometry. Values represent mean ± standard deviation for duplicate determinations. Means with the same letter within columns are not significantly different (p> 0.05)

Time after extrusion (s)	Crumb paste shear yield strength (kPa)			
	5%	8%	11%	5% White
60	192.6 ± 2.1 a			198.5 ± 8.8 a
90		71.5 ± 8 a		
120	255.4 ± 30.6 b			246.7 ± 0.9 a,b
180		83.5 ± 7.4 a,b	42.2 ± 1.3 a	
210	294.4 ± 35.2 b			286.6 ± 10.5 b
300	358.3 ± 0.9 c	99.9 ± 10.3 b,c	47.2 ± 1.1 b	309.8 ± 33.4 b,c
420	438.4 ± 1.6 d	118.1 ± 7.7 c,d		363.0 ± 28.1 c,d
465			54.8 ± 2.2 c	
510	449.8 ± 47.9 d	122.0 ± 9.3 d		406.1 ± 40.7 d
600	547.7 ± 15.9 e	135.1 ± 1.4 d	55.8 ± 1.8 c	406.2 ± 40.7 d

7.4.1 Off-line shear yield comparison with LM crumb paste

Figure 7.15 shows a comparison of the crumb paste shear yields obtained by extrusion mixing and LM mixing. Shortly after mixing, the standard 5% water extruded paste (S1) exhibits a shear yield stress of more than double that of the standard 8% water LM paste which is currently used as a laboratory made representation of extruded paste. This demonstrates that the model LM paste used currently is a poor representation of consistency when considering the off-line characterisation of shear yield strength.

It is noted that that the yield-time behaviour of 8% water LM paste bears a much closer resemblance to the yield-time behaviour of 8% water extruded paste (S2) and that for this level of water content, the LM mixing method produces model paste of similar

yield to extruded paste. Under the conditions of LM mixing however, it is the experience of both this work and the company that a cohesive paste is not formed within the planetary mixer if a water content of 5% is used.

Analysis of extruded paste shear yield using cone penetrometry has confirmed the difficulties associated with using off-line rheological characterisation techniques which were hypothesised in Chapter 3 following analysis of LM crumb pastes. In fact, the rate of hardening for pastes extruded under normal conditions is greater than that of any of the LM pastes considered. This validates yet further the ineffectiveness of rheological characterisation techniques which require lengthy transfer and loading times for samples and the assumption of time independent material over the period of measurement.

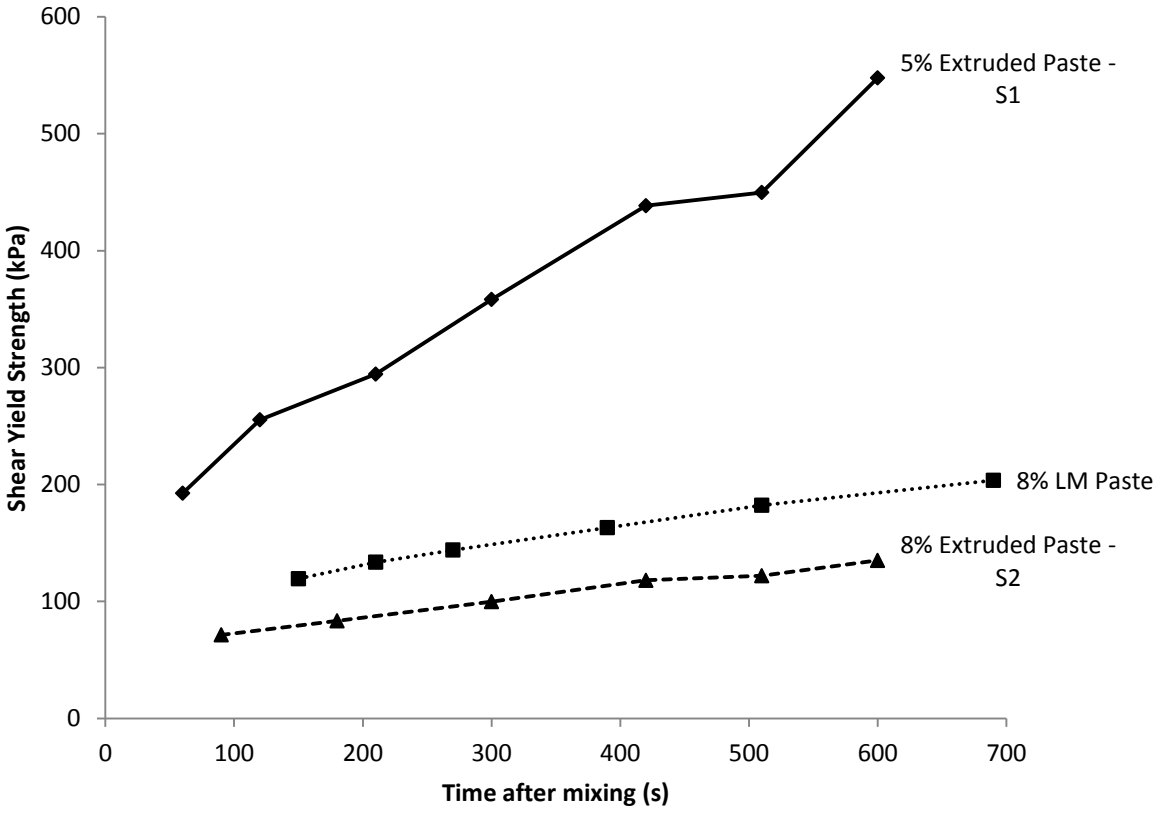

Figure 7.15 Off-line comparison of extruded and LM crumb paste shear yield strengths versus time after mixing using cone penetrometry

7.5 Shear wave reflection

It was described in Section 4.3 how a shear wave interface reflection method described by Kulmyrzaev & McClements (2000) may offer potential as a future method for the in-line rheological characterisation of extruded crumb paste. Kulmyrzaev & McClements called for future studies to consider the application of their method to multiphase materials and the extruder trials of this work present the perfect opportunity to trial obtaining the necessary signals.

7.5.1 Equipment

In order to consider the application of the method described in Section 4.4, a 10MHz broadband ultrasonic shear transducer (Olympus V221-BA-RM) with a 7 μs silica delay-line was brought into contact with extruded paste samples according to the arrangement shown in Figure 7.16. A broadband pulse was transmitted along the delay line and reflected from the sample interface back to the transducer where the magnitude, M and phase, θ of the 100 times averaged signal was computed as a function of frequency by the spectrum analyser. The real and imaginary parts of the reflection coefficient were recorded as calculated by Equation (38) and normalised against the reflection coefficient of the reference material (in this case air), which was measured prior to the intitiation of each data run.

The collaborative assistance of Richard Tweedie of Industrial Tomography Systems plc, Manchester, whose kind provision of the pulse generator, spectrum analyser and signal processing expertise were invaluable to the trialling of this arrangement. The mobility of the self-built pulse generator and spectrum analyser arrangement allowed for data to be collected from as little as twenty seconds after extrusion.

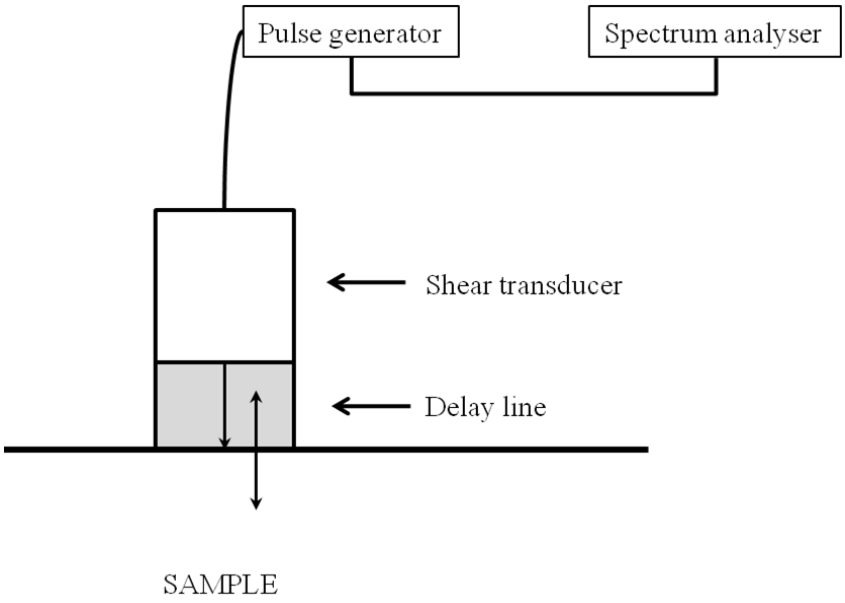

Figure 7.16 Shear wave reflection transducer arrangement

7.5.2 Results

Figure 7.17 and Figure 7.18 respectively show the real and imaginary components of the normalised reflection coefficient of extruded pastes S1 - S4 100 seconds post extrusion. Normalised components of any value other unity indicate that the transducer arrangement has successfully detected a different reflection coefficient (and by implication differing rheological properties) from that of the calibration material. Rapid hardening of the 2% water S3 paste meant that achieving sufficient coupling between the transducer and sample before hardening was not possible in this case post extrusion.

It is clear from these figures that both components of the reflection coefficient are complex functions of both water content and frequency. The hypothesis that the transducer arrangement is detecting variations in the rheological properties of the pastes is further supported by Figure 7.19 and Figure 7.20 which show the reflection coefficient components as a function of time for the 5% S1 samples as they undergo hardening post extrusion. The reflection coefficient is again shown to be a complex function of frequency and further supports the hypothesis made using cone penetrometry that the rate of change

of rheological properties as it undergoes post extrusion hardening is most significant immediately after extrusion.

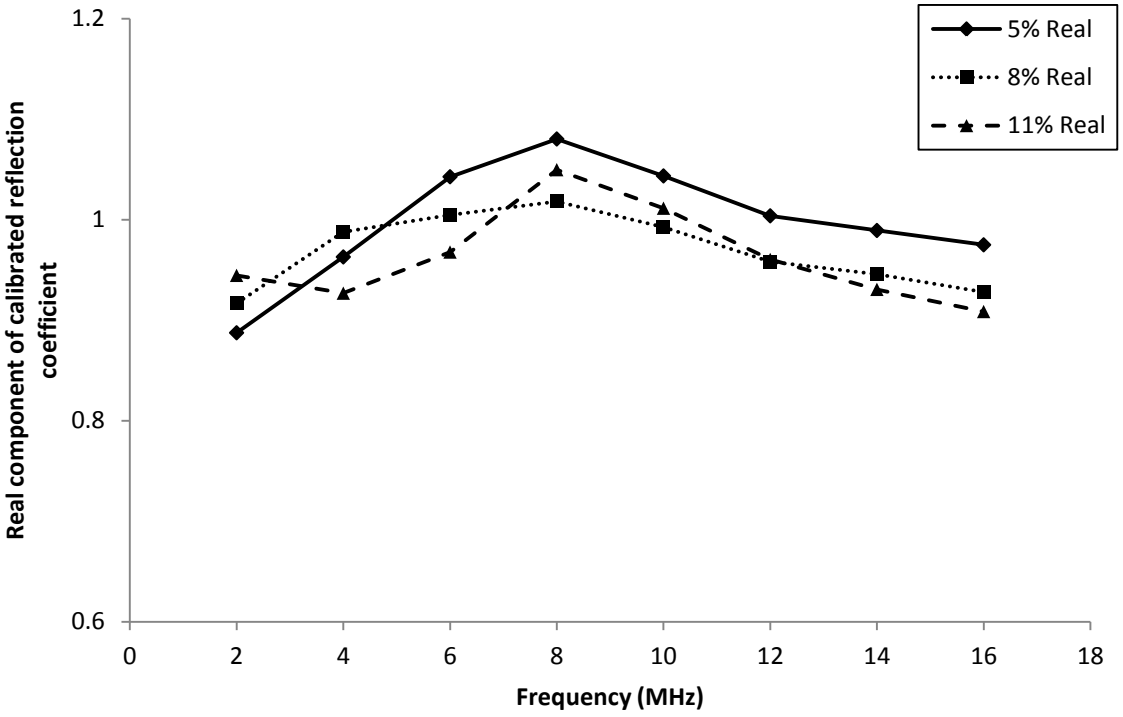

Figure 7.17 Calibrated reflection coefficient (real) of extruded crumb pastes versus frequency 100 s post extrusion

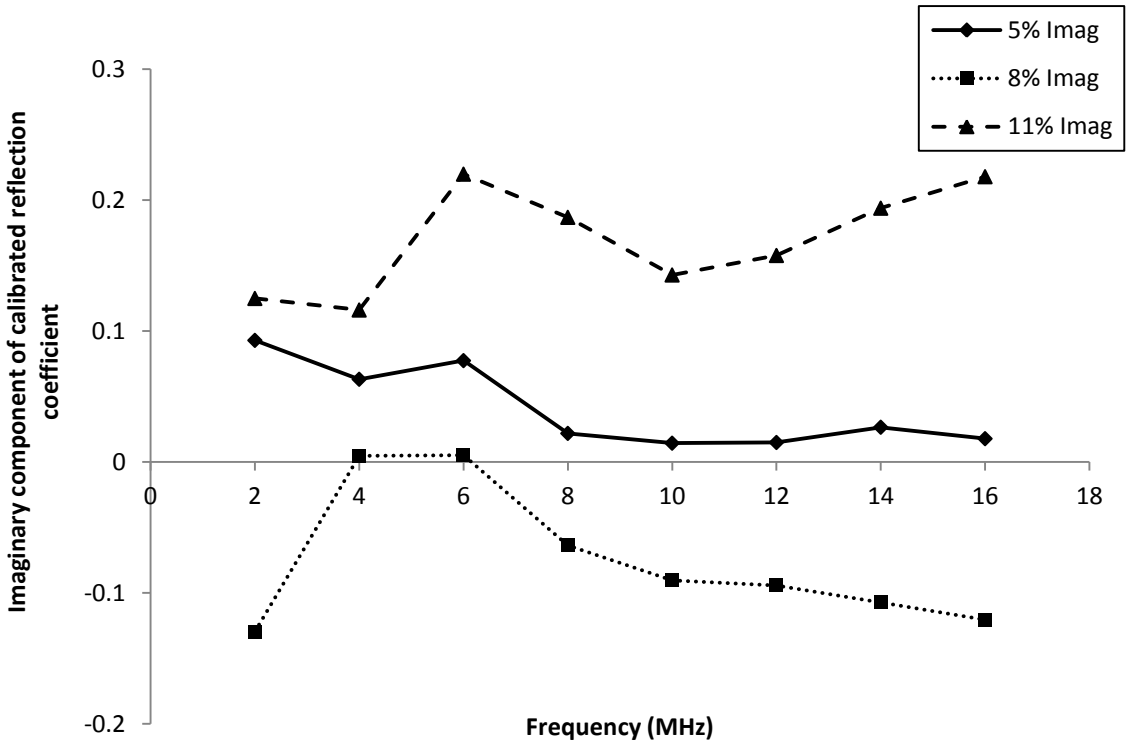

Figure 7.18 Calibrated reflection coefficient (imaginary) of extruded crumb pastes versus frequency 100 s post extrusion

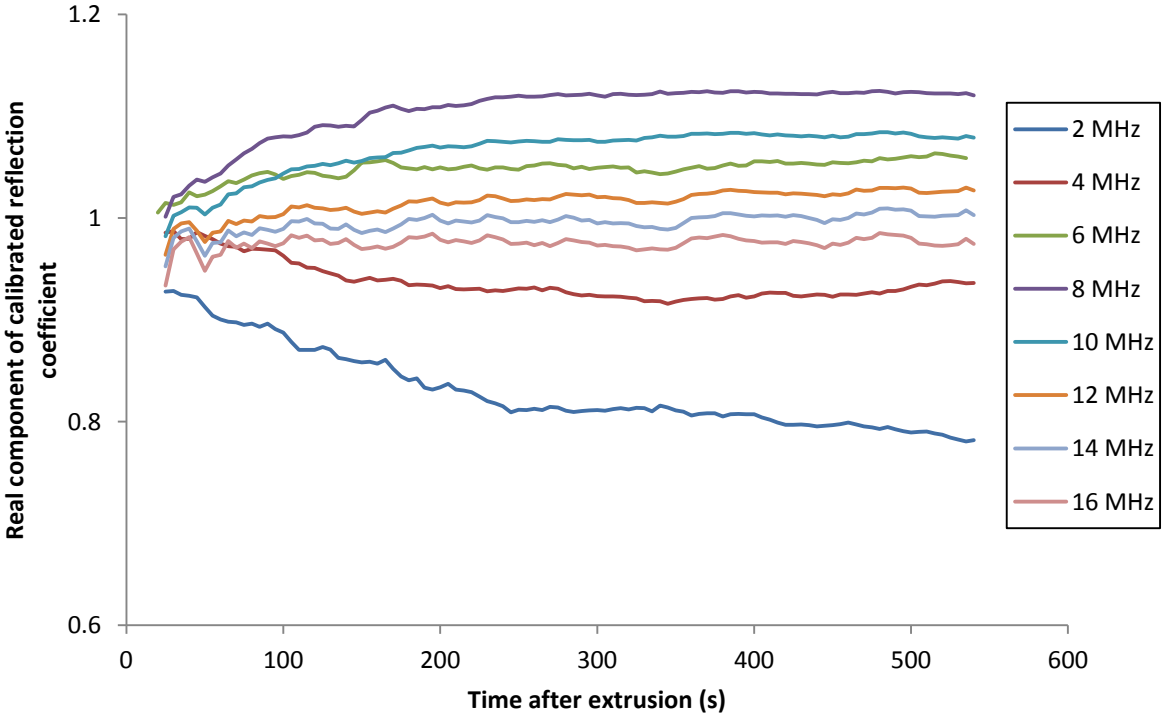

Figure 7.19 Calibrated reflection coefficient (real) of extruded crumb pastes versus time post extrusion

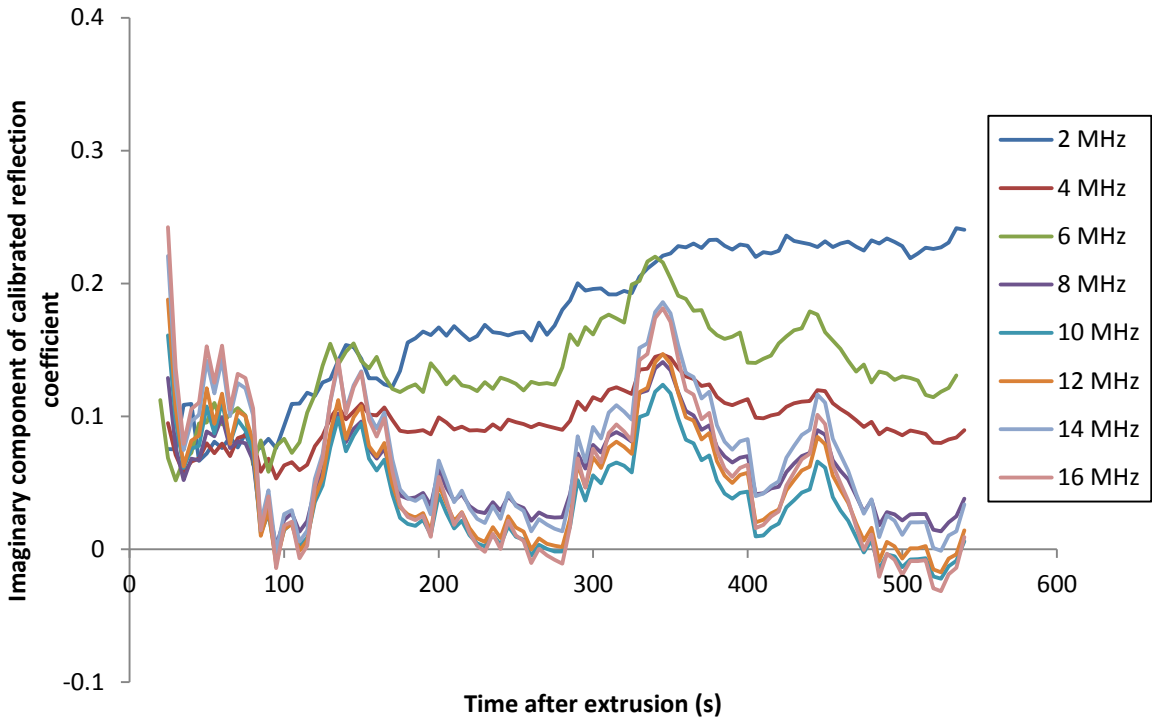

Figure 7.20 Calibrated reflection coefficient (imaginary) of extruded crumb pastes versus time post extrusion

7.5.3 Future work

This work has shown that the shear wave reflection arrangement described by Kulmyrzaev & McClements has successfully detected variations in the reflection coefficient of multiphase extruded crumb pastes exhibiting varying rheological behaviours. Given the attractive geometry of this transducer arrangement at the interface which appears to be non-destructively characterising aspects of the pastes rheology, this method is an attractive option for further development into an in-line characterisation. Further work in this area would consider the physical interpretation of the data received with respect to multiphase pastes in order to derive fundamental rheological parameters such as those considered by Kulmyrzaev & McClements for honey. Once a physical understanding of the variations seen is achieved, the technique represents a viable option for development into an in-line characterisation.

7.6 Thermogravimetric analysis (TGA) of extruded crumb paste

As a characterisation of distributive mixing performance within extruded crumb pastes, thermogravimetric analysis (as presented in Chapter 5) was performed on the extrudates of pastes S1 - S3 and S5 with varying water contents, as well as along the screw profile for paste S1 (sampling locations shown in Figure 7.6). The L1 scale of observation was selected as the most appropriate sample size following the analysis of Chapter 5. Ten samples were heated from 50 °C to 600 °C at a rate of 15 °C/min to calculate the mixing index value at each sample location.

Figure 7.21 shows the integral mixing index obtained for the extrudate of pastes mixed with varying water contents. Recalling that a lower value of integral mixing index represents a more homogenous distribution of components throughout the volume, an approximately consistent degree of distributive mixing is shown for the drier 2% (S3) and 5% (S1) pastes. However when considering the wetter 8% (S2) paste, a considerable improvement in distributive mixing at this scale of observation is seen.

Figure 7.21 shows the degree of distributive mixing within 5% paste is similar regardless of whether a mixing element is included in the screw profile or not and indicates that the influence of the mixing element on distributive mixing is not large. This is supported by Figure 7.22 which shows that the improvement in distributive mixing across the mixing element (A-B) is small compared to that seen as the paste is compacted and stretched through the die land (C-D). As expected, little change in the distributive mixing is seen in the conveying region between B and C.

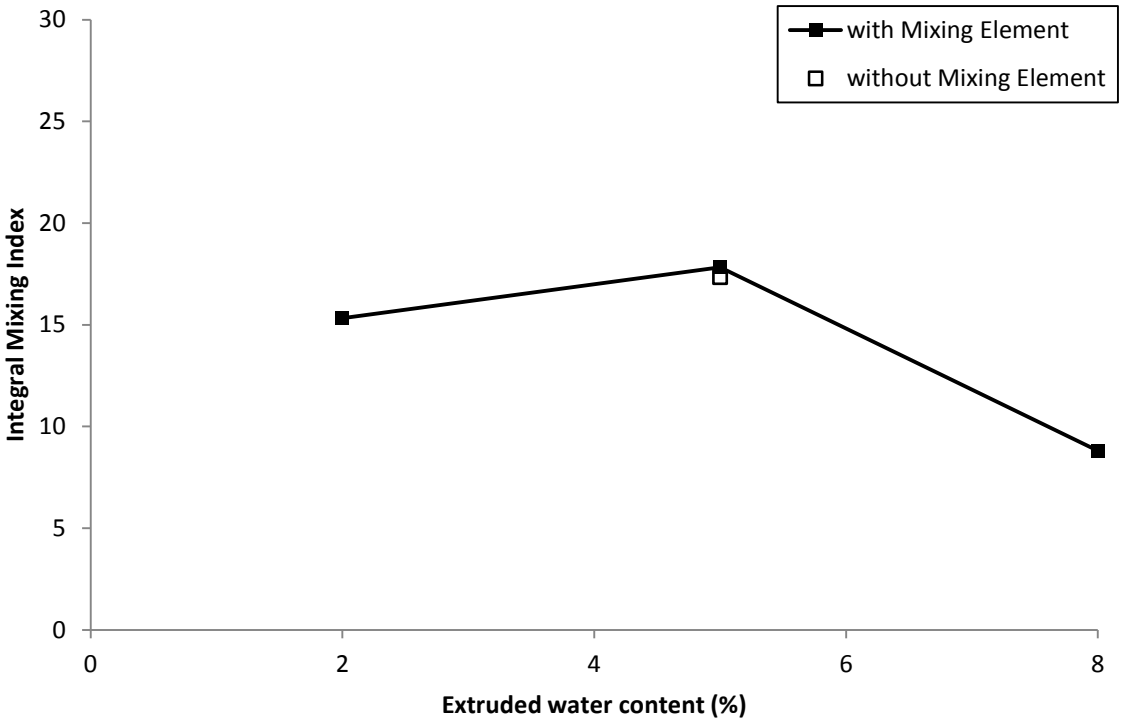

Figure 7.21 TGA Integral mixing index of extruded pastes versus water content using L1 length scale

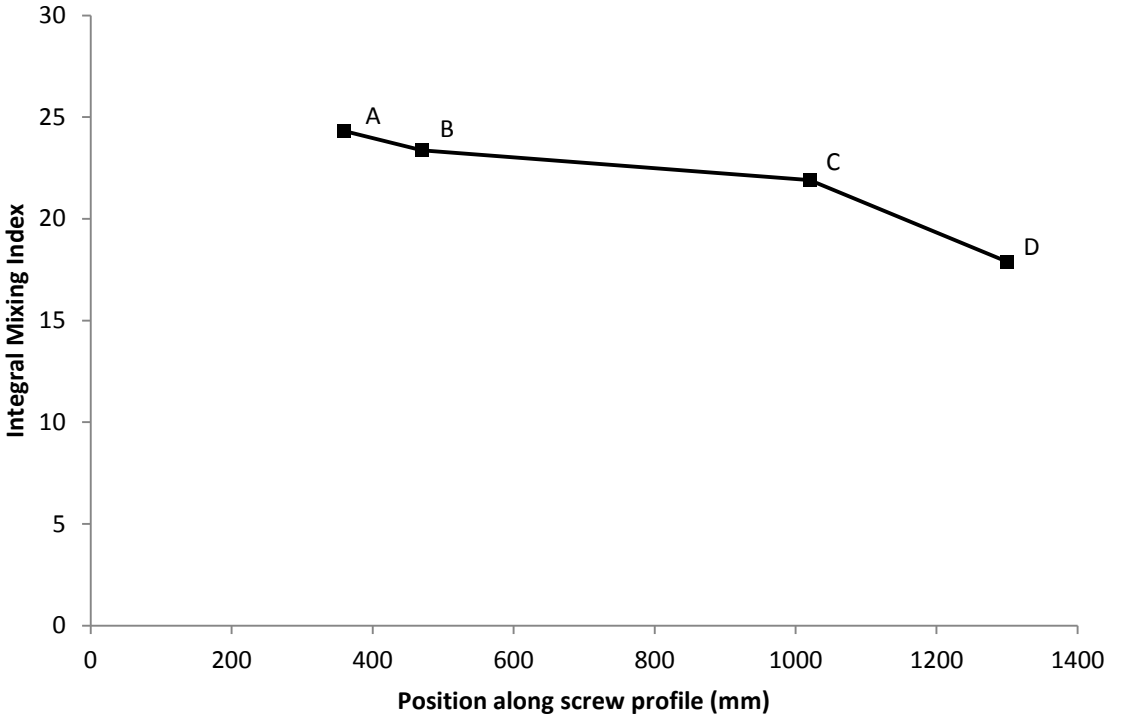

Figure 7.22 TGA Integral mixing index of extruded paste versus screw position using L1 length scale

7.6.1 Comparison with LM paste

Direct comparison between the distributive mixing seen in extruded pastes and those mixed under LM conditions has not been possible since to ensure suitable resolution within a data set that is time intensive to process, extruded samples were scanned at a slower temperature rate than the LM samples analysed in Chapter 5. Under a slower scan rate, variation between samples over a given temperature range will be more pronounced and the overall value of the integral mixing index will appear higher. The validity of the analysis made in this chapter to compare the distributive mixing of extruded samples remains valid as all samples were scanned at the same scan rate.

7.7 MPM

In an attempt to visualise microstructure and provide some insight into the level of dispersive mixing taking place within the extruder, the multiphoton microscopy (MPM) imaging used in Chapter 6 has been applied to the extrudates of pastes S6 - S9, as well as along the screw profile for paste S6 (sampling locations shown in Figure 7.6). For each configuration or sample point, three samples have been imaged at approximately 40 μm below the surface.

7.7.1 White crumb

It was shown in Chapter 6 that the spatial interaction of proteins and sugars could not be observed exclusively without modification of the paste, due to the co-fluorescence of cocoa mass and proteins in the green channel. In order to observe this interaction using MPM, a model paste was created by removing the cocoa mass from the recipe and replacing it with pure cocoa butter only to produce “white crumb”. Cone penetrometry

analysis in Section 7.4 showed that although the absence of cocoa mass led to a marginally slower rate of hardening post extrusion, the consistency of white crumb paste at the point of extrusion was indistinguishable from that of regular crumb. The dead-stop extruder screw profiles of S6 - S9 (shown in Figure 7.23 - Figure 7.26) are visually similar to those obtained for the pastes which they are designed to replicate (Figure 7.7 - Figure 7.10) and the use of "white crumb" has therefore been deemed to be an appropriate choice of model material for MPM imaging.

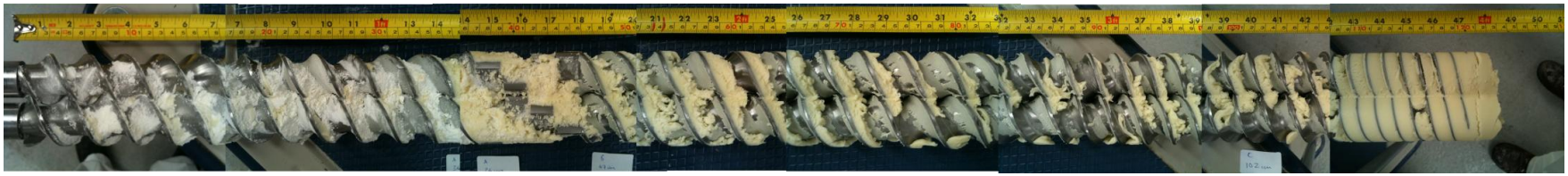

Figure 7.23 Dead-stop screw photo of paste S6 - 100 kg/hr - 300 rpm - 5% water (no CM) - with Mixing Element

Figure 7.24 Dead-stop screw photo of paste S7 - 100 kg/hr - 300 rpm - 8% water (no CM) - with Mixing Element

Figure 7.25 Dead-stop screw photo of paste S8 - 100 kg/hr - 300 rpm - 2% water (no CM) - with Mixing Element

Figure 7.26 Dead-stop screw photo of paste S9 - 100 kg/hr - 300 rpm - 5% water (no CM) - no Mixing Element

7.7.2 Extruded MPM images

In Chapter 6 it was found that fluorescence signals emitted from untreated LM crumb paste using MPM excitation were dominated in the blue channel by sugars and in the green channel by proteins (providing cocoa mass was not also present). This lead to identifiable areas of protein and sugars which were mostly discrete from one another when observed visually.

Each of the three background subtracted MPM sections for extrudates S6 - S9 are shown in Figure 7.27 - Figure 7.30. Both blue (indicating sugar) and green (indicating protein) channels are shown in these images and show largely similar spatial signals for each, leading to a more cyan like colour where the two signals coexist within a voxel (known as colocalisation) and are superimposed. If colocalisation is considered to represent the maximum form of dispersion between two components that can be resolved by an imaging technique, then the images obtained here appear to indicate that with the exception of a few small areas of discrete localisation, the elements of proteins and sugars which show up under MPM excitation are largely dispersed entirely amongst each other for each of the three water contents considered. This marks a stark contrast to what was observed for LM crumb paste, however little variation between extruded samples of differing water contents is seen by the way of visual observation.

One of the few samples to appear different visually was that of the paste extruded without a mixing element in the screw profile (S9 - Figure 7.30). Across all three images, crystal sizes appear noticeably larger than those seen in pastes extruded with the high shear mixing element. In two of the three images, larger regions of localised protein are clearly visible showing a greater resemblance to those seen for LM paste, however all three images appear to continue the trend of the other extruded pastes, showing a significant level of colocalisation of the green channel where blue sugar crystals are evident.

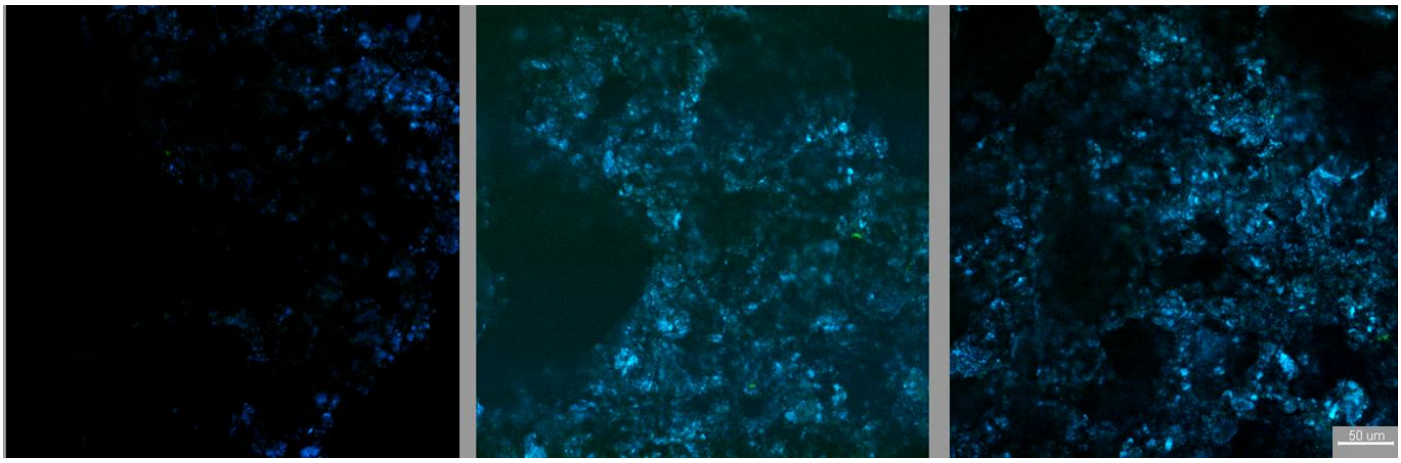

Figure 7.27 MPM images - Green & blue channel S6 - 5% water - with mixing element (scale bar = 50 μm)

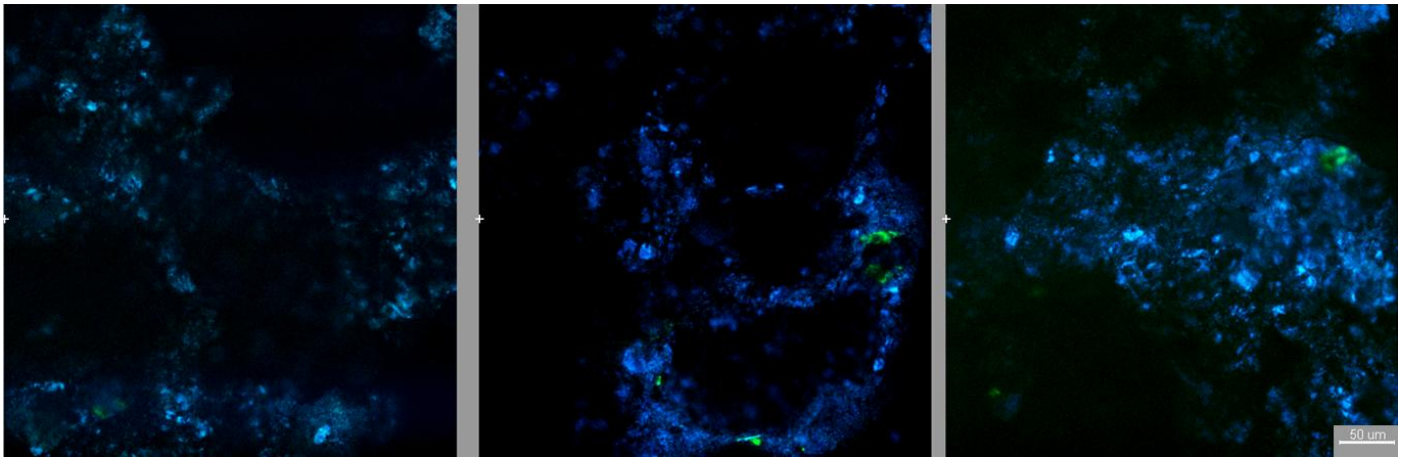

Figure 7.28 MPM images - Green & blue channel S7 - 8% water - with mixing element (scale bar = 50 μm)

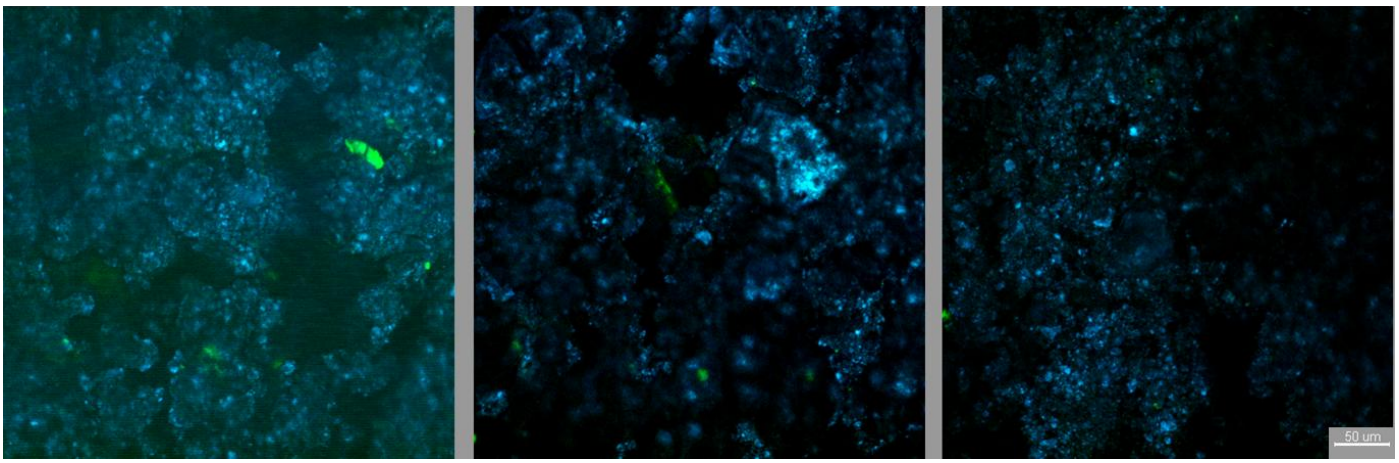

Figure 7.29 MPM images - Green & blue channel S8 - 2% water - with mixing element (scale bar = 50 μm)

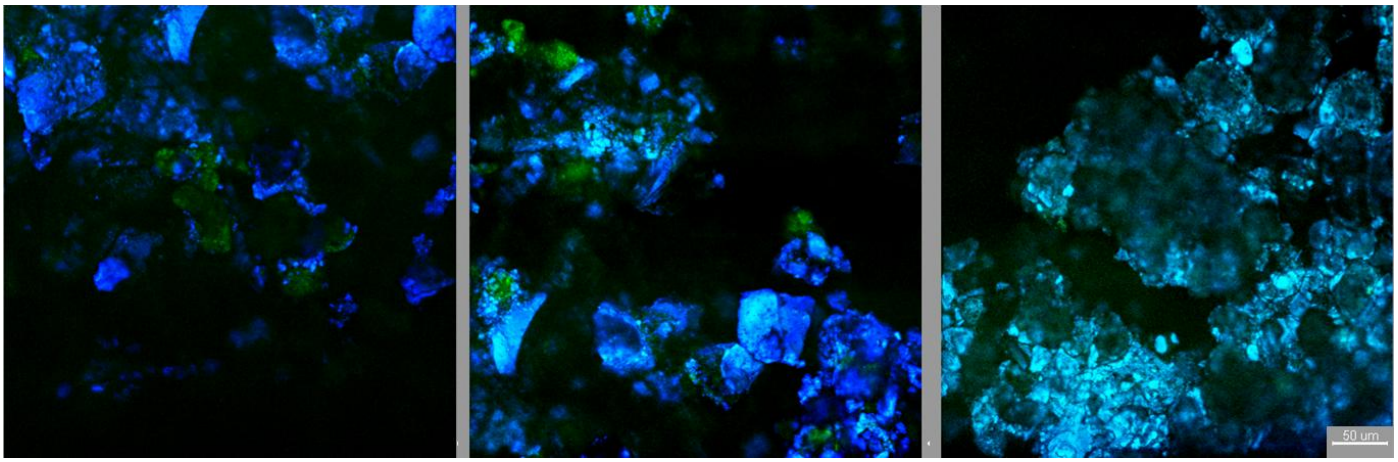

Figure 7.30 MPM images - Green & blue channel S9 - 5% water - without mixing element (scale bar = 50 μm)

7.7.3 Colocalisation image analysis

In order to evaluate the proportion of the blue sugar signal which spatially coexists with a green protein signal, image analysis of the colocalisation between the two channels has been performed using the Imaris software which accompanies the multiphoton microscope setup at the Institute of Biomedical Engineering, University of Oxford. Before performing the colocalisation analysis, the background was removed from each image by applying a Gaussian filter. To consistently determine thresholds for the colocalisation analysis of each image, the data sets for each channel were individually masked to exclude all voxels with a null signal intensity and the threshold identified which passed the strongest 30% of the remaining channel data. Each of these channel threshold values were then applied to the background subtracted image and the colocalisation algorithm performed to show what proportion of voxels that contained a channel intensity above the threshold for one signal also contained a signal intensity above the threshold for the other channel.

The results of this colocalisation analysis are shown for the blue channel (sugar) in Figure 7.31 and for the green channel (protein) in Figure 7.32. As was hypothesised by visual observation, the level of colocalisation in each channel remains relatively constant

across the range of water contents. For the colocalisation of the green channel, this is supported statistically by a one-way ANOVA F-test which confirms that for the analysis and number of duplicate images considered, the null hypothesis of equal means may not be rejected and that any differences in mean values are statistically insignificant with $p > 0.05$.

The same test does however show that the null hypothesis of equal means may be rejected for the colocalisation fraction of the blue channel. Fisher's LSD pairwise comparison of means is then shown in Table 7.4 to show which mean differences are statistically significant. This shows that the 2% data point is statistically different from that of 8%, but that the 5% point is neither significant from the 2% or the 8%. This result of statistical significance partially supports the hypothesis shown by Figure 7.31 of an increasing colocalisation of sugar with protein as water content is increased. This interaction is however small in comparison with the effect of extruding the paste rather than batch mixing using the LM method. The same colocalisation analysis applied to standard 8% water LM paste shows the degree of colocalisation to be considerably lower for both blue and green channels. Additionally this is a conservative estimate of the colocalisation factor in LM paste as the images acquired in Chapter 6 also included cocoa mass in the green channel. This serves to show that conditions within the extruder are having a significant effect on the final form of the paste microstructure when compared to pastes mixed using the LM method.

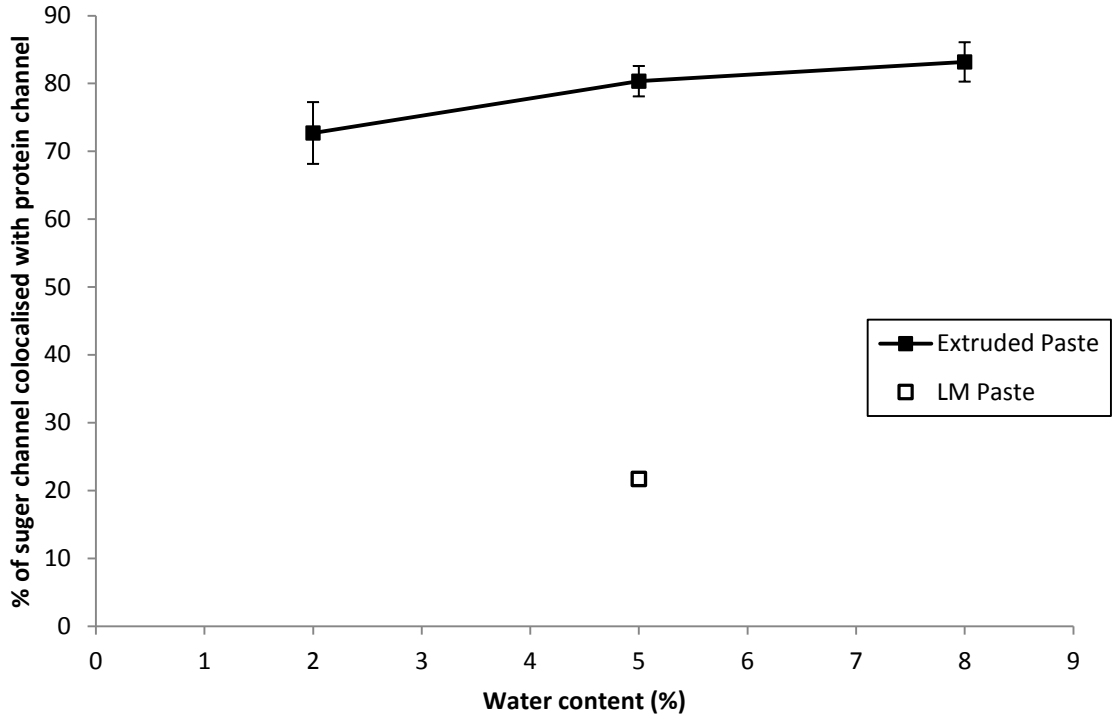

Figure 7.31 Fraction of MPM sugar signal colocalised with protein signal versus water content (error bars represent standard deviation between duplicate determinations)

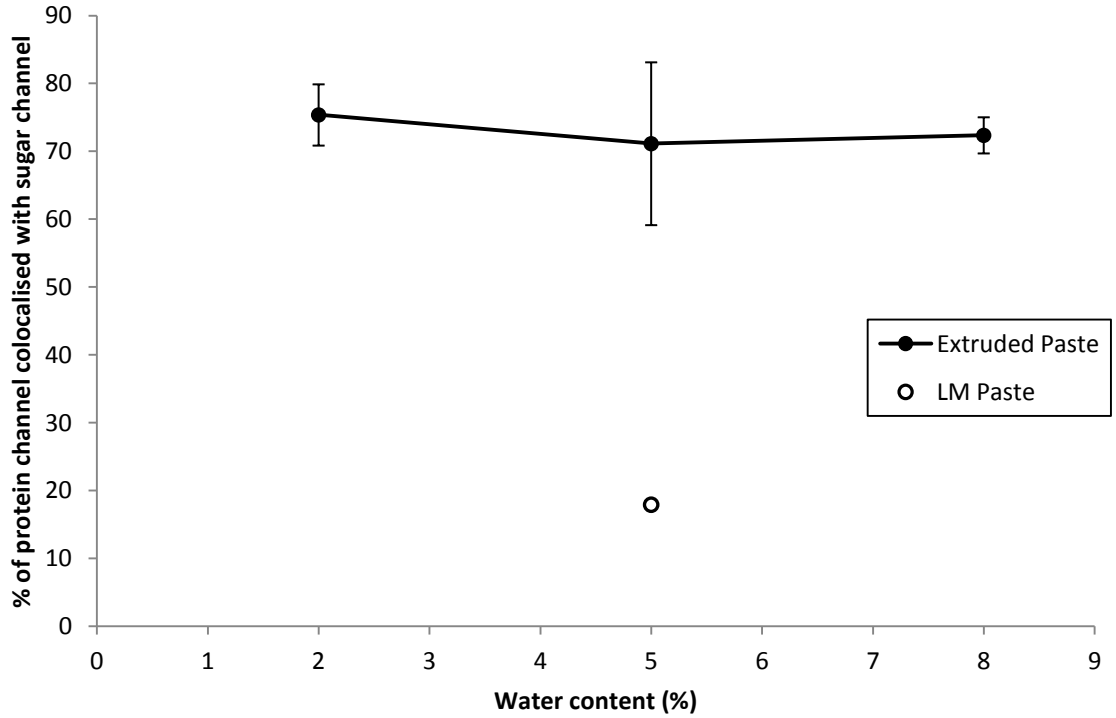

Figure 7.32 Fraction of MPM protein signal colocalised with sugar signal versus water content (error bars represent standard deviation between duplicate determinations)

Table 7.4 Sugar fraction colocalised with protein as determined by MPM colocalisation image analysis Values represent mean ± standard deviation for duplicate determinations. Means with the same letter within columns are not significantly different according to the p-value shown

Water Content (%)	Sugar fraction colocalised with protein (%)	
2	72.7 ± 4.6	a
5	80.3 ± 2.2	a,b
8	83.2 ± 2.9	b

One of the key goals of this project was to track the dispersive mixing of the crumb paste along screw profile, however results from the colocalisation analysis of samples taken from dead-stop experiments of setup S6 have not highlighted any statistically significant variations. To illustrate this, Figure 7.33 shows the colocalisation fraction of the sugar channel with the protein channel at each of the sampling points along the screw shown in Figure 7.6. The average colocalisation between images appears to suggest a moderate increase in dispersion across the mixing element (between sampling points A and B) with a significant reduction in the standard deviation seen between duplicate samples. The colocalisation then remains comparatively constant with little variation between duplicate samples as it passes through the conveying zones and is extruded through the die plate. However, the large standard deviation of samples analysed at point A means that the standard ANOVA F-test is unable to reject the null hypothesis of equal means, making the statistical significance of the hypothesis made inconclusive.

What is clear from the data however, is that at the earliest sampling location analysed here along the screw length (point A), the level of apparent colocalisation is already considerably greater than that apparent in fully mixed LM crumb. The sampling location of point A is the first screw revolution before the mixing element and it can be

seen from Figure 7.23 that this is the first screw revolution where a cohesive paste is formed. Although some small areas of unwetted powders are visible within the channel before entering the mixing element, the extraction of samples from this screw channel will predominantly select the regions of cohesive paste. Consideration of why extruded paste should exhibit such a significantly higher degree of colocalisation than LM paste at such an early stage of formation is given in Section 7.8.

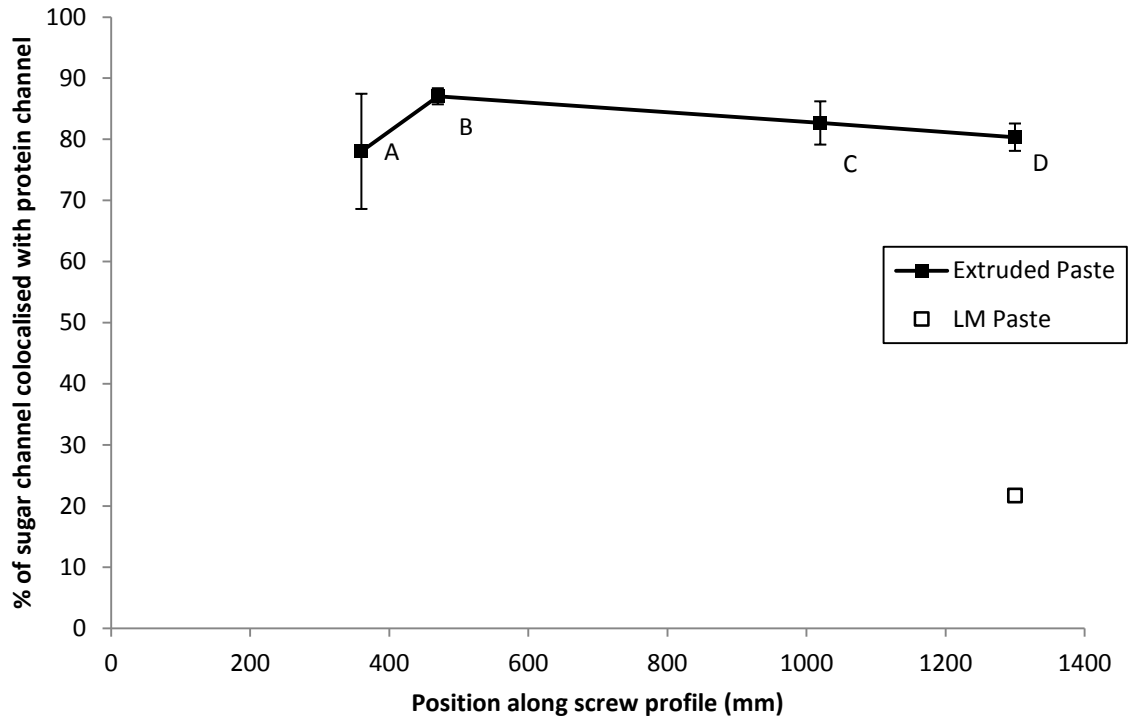

Figure 7.33 Colocalisation of MPM sugar channel as a function of position along screw profile (errors represent standard deviation between duplicate determinations)

When considering Figure 7.30, there was a visual suggestion that in two of the samples extruded without a mixing element in the screw profile, noticeable regions of undispersed protein existed. For each of these two images, a lower than average level of colocalisation in the green channel was found (65% as compared to 71%), supporting the hypothesis that the exclusion of the mixing element has had a negative impact on the

dispersion of protein amongst sugars. However, as these regions were visible only in two samples and not in the third, the statistical significance of all three samples was not sufficient to conclusively support this hypothesis when compared to paste of the same water content extruded with a mixing element. It is noted that although samples extruded without a mixing element partially contained regions of discrete protein, the level of colocalisation in the sugar channel was indistinguishable from paste extruded with a mixing element.

7.8 Evolution of paste microstructure

Off-line cone penetetrometry has shown a significant and rapid increase in crumb paste shear yield with time once mixed, which is observed visually as a post extrusion hardening. Environmental scanning electron microscopy in Section 6.1.1 has shown an apparent growth of the crystalline network throughout the paste over a ninety minute period after mixing suggesting that the continued crystallisation of sugar crystals rather than fats may be the dominant cause of paste hardening post extrusion. This hypothesis of crystalisation, which is exothermic, was additionally supported by increasing paste temperatures post extrusion seen in Section 3.4.2.

Suggested causes of this crystalisation are a combination of temperature effects and competitive adsorption of free water within the paste. As paste cools in ambient surroundings, decreased solubility of sugars would cause crystalisation out of solution to occur. If present, this mechanism of paste hardening would be most noticeable at the surface of samples exposed to harden, where the temperature gradient is largest - an effect also seen in Section 3.4.2.

In addition to the proteins in the dairy ingredients, cocoa mass is known to also include large amounts of proteins, as well as starch and dextrins (starch fragments

produced when starch is broken down by heat during roasting of cocoa beans). Proteins, starch and dextrins all absorb water and lead to hydration (Figoni, 2007). It is suggested that in the event of incomplete hydration due to the short residence times of extruders (Strahm, 2000), or the short batch mixing time used for LM paste as compared to many industrial batch mixing processes (Cauvain & Young, 2008), that competition for free water in the paste from these components additionally drives sugar out of solution. In Section 7.4, a small, but statistically significant reduction in the rate of hardening was observed following the extrusion of white crumb which omits cocoa mass from the recipe. This result, showing a reduced rate of hardening from a material where the protein, starch and dextrin content is also reduced, supports the hypothesis that the competitive adsorption of free water is a contributing factor to crystalisation. Competitive adsorption of free water is reported for a similar system of bread dough where intense competition for available water is seen between flour proteins and starch (Cauvain & Young, 2008). It is recognised there is a degree of mobility of the water held in the dough, but that the impact of the competition for the available water on the rate of dough hydration is not well understood.

The widespread crystalline network of sugar crystals is then well established when imaged using optical microscopy and multiphoton microscopy. This was true not only of extruded paste samples which harden before imaging, but also samples extracted from the screws using dead-stop experiments.

Analysis of the sugars and proteins within crumb paste, as resolved by multiphoton microscopy, has shown that the degree of colocalisation between the two components is significantly higher in all of the extruded pastes considered, than it is in batch mixed LM paste. This is true even at the earliest stages of paste formation in the screw when relatively little mixing is thought to have occurred and indicates that the twin screw

extrusion process has a significant influence on the microstructure of the paste. In order to account for this phenomenon, it is hypothesised that in the earliest stages of a cohesive paste being formed, a proportion of the sugars present in the mixture become plasticised or dissolve into solution under the heat and moisture of extrusion (Van Zuilichem *et al*., 1999) and mix with wetted dairy ingredients to form a combined sugar-dairy solution. This principle of wetting and plasticisation with heat and moisture is often utilised and encouraged to promote improved mixing in many extrusion applications via steam treated preconditioning of ingredients - the objective of this being to completely plasticise the raw material particles in order to eliminate any dry core, making raw materials more easily transformed within the extruder (Strahm, 2000).

The elements of dairy proteins which fluoresce under MPM excitation are then bound within the crystals that form, resulting in the colocalisation of sugars and protein within the voxels of MPM images. Suggested reactions that could lead to this effect are Maillard reactions, where high barrel temperatures promote the reaction of reducing sugars, including those formed during shear of starch and sucrose, react with lysine and other amino acids with free terminal amines (Camire, 2000 ; Camire 2001). The resulting binding of proteins within crystals would be similar to what is seen with α - lactose, which when crystalised below 93.5 °C, forms a monohydrate where each lactose molecule is associated with a water molecule and the water is incorporated into the crystal to form an integral part of it (Lactose in solid form, 2011).

Under this hypothesis, the significantly higher degree of colocalisation seen in extruded paste when compared to LM paste would be explained by the elevated temperatures within the extruder barrel (approximately 70 °C as opposed to approximately 30 °C) increasing sugar solubility and promoting sugar protein interactions such as the Maillard reaction. The evolution of crumb paste microstructure during formation

described here is illustrated schematically in Figure 7.34 - Figure 7.36 to reflect the findings of this study.

Figure 7.34 shows the evolution of microstructure when extruded with the full screw profile. At the beginning of the screw, sugar crystals and particles of dairy proteins enter the screw channel from the powdered feed (1) ahead of the liquid feed (2) where liquid and solid phases remain discrete. At the first point of cohesive paste formation, seen here at the start of the mixing element (3), solids are then bound in a continuous medium of liquid phases comprising cocoa butter and free water. A proportion of sugar crystals and protein particles become wetted and dissolve to form a liquid phase of sugar-dairy solution, leaving the remainder undispersed in their solid form. As paste passes through the high shear mixing element (4), droplets of sugar-dairy solution are subject to significant dispersive mixing, reducing their average size. A moderate increase in distributive mixing across the mixing element also leads to a further proportion of the undissovled sugar and protein particles combining with remaining free water. Under normal processing conditions, the paste microstructure is well established by this point, but is again subjected to a small improvement in distribution and dispersion as the paste is compressed and stretched through the dieland (5). Once extruded, the sugar-protein bound solution crystalises rapidly in the short term, bound by free water and cocoa butter, which then also crystalises over a longer time scale.

Figure 7.35 then shows the evolution of paste microstructure when extruded without a mixing element in the screw profile. Distribution of the phases and the early stages of paste formation are not seen until just ahead of the dieland (9) and continue as extruded (10). Without the intensive dispersion effect of the mixing element, the proportion of protein remaining undispersed is somewhat higher and the droplets of sugar-protein solution remain large, leading to comparatively larger crystals once hardened (11).

Finally the evolution of paste microstructure when batch mixed under LM conditions is shown in Figure 7.36. In the early stages of paste formation (14), where droplets of sugar-protein solution are formed, the reduced solubility of the sugars caused by the comparatively lower temperature and pressure of mixing, leads to a considerably smaller fraction of the sugars to dissolve and bind with wetted proteins. Dispersion and distribution then occur following intensive mixing (15) before hardening (16). Since the proportion of bound sugar-protein solution is lower in LM paste, the degree of colocalisation between sugars and proteins is lower when imaged using MPM.

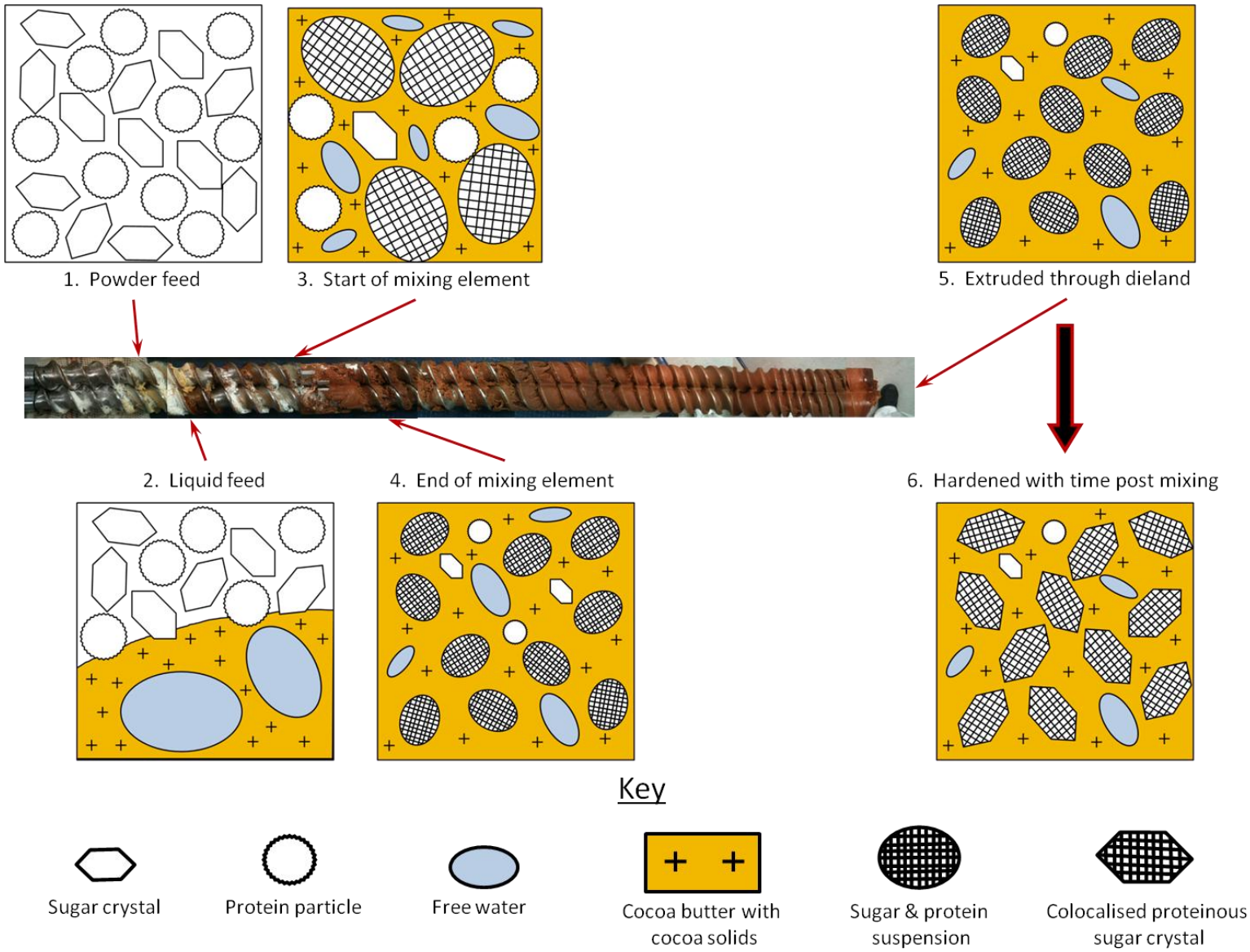

Figure 7.34 Microstructural evolution along screw profile with mixing element

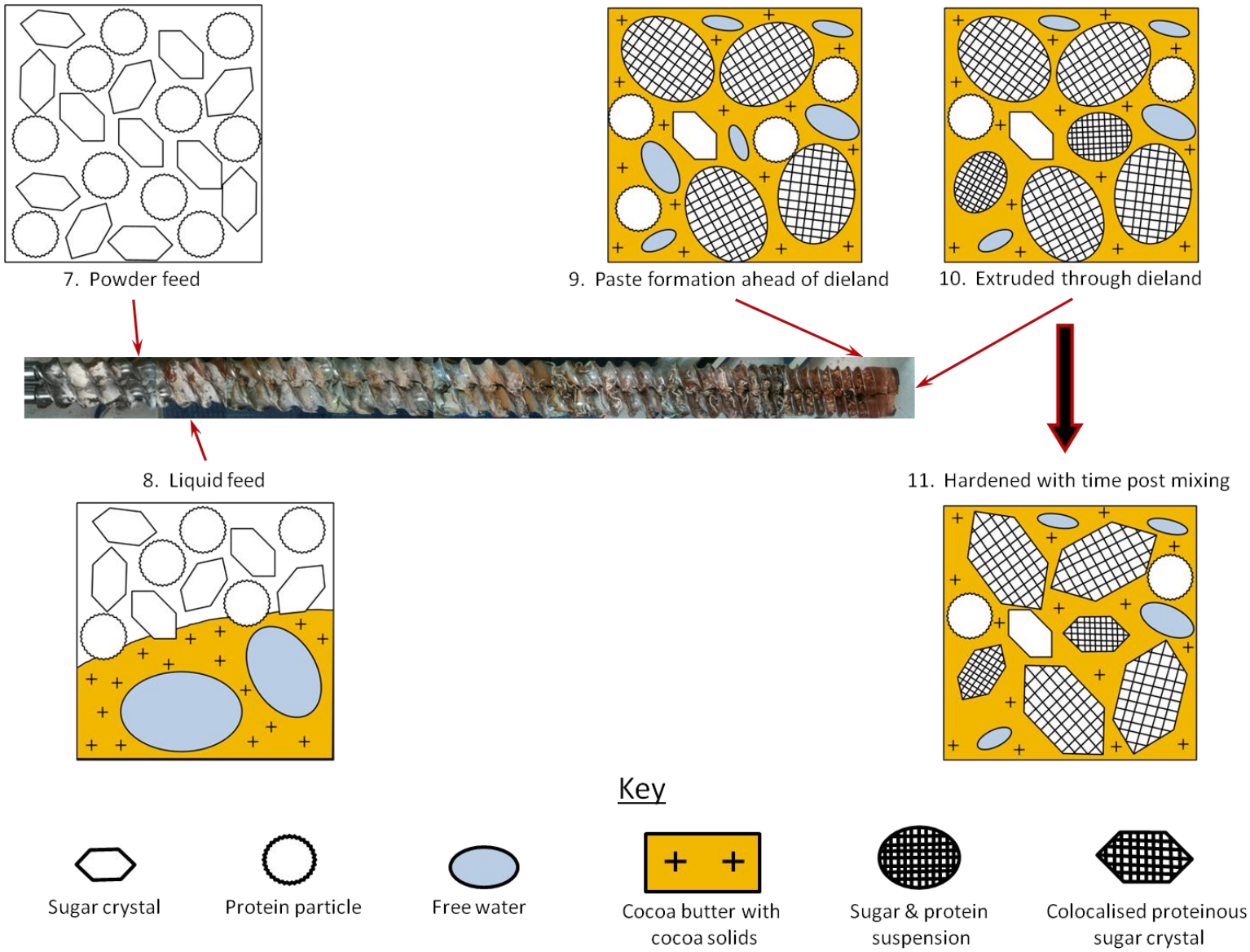

Figure 7.35 Microstructural evolution along screw profile without mixing element

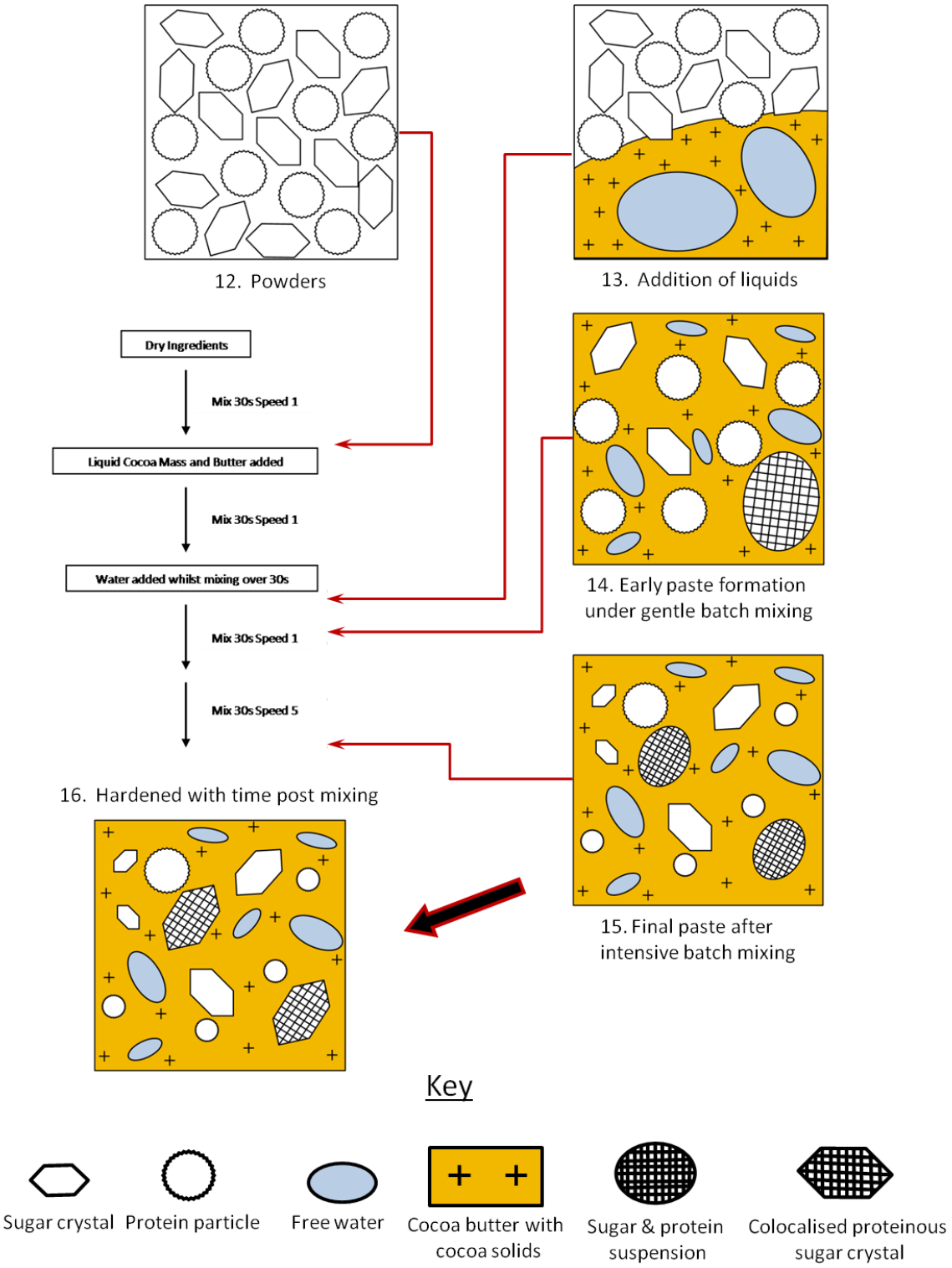

Figure 7.36 Microstructural evolution of LM crumb paste during batch mixing

7.9 Energy cost of extrusion

Figure 7.37 shows the specific mechanical energy, or SME (Wh/kg) required to extrude each of the pastes in this study and illustrates the large variation in the energy cost of extrusion that can be associated with water content and consistency, with a 2% water paste requiring more than double the energy input of an 11% paste. The trend of these results is intuitive as increased water contents have been shown in Section 7.4 to have a significant effect on consistency and lower the shear stresses (and therefore mechanical energy input) required to cause flow within the extruder.

The higher SME required to extrude the 5% water paste without a mixing element can be explained by the dead-stop extrusion image shown in Figure 7.10, which showed that without the mixing element, a cohesive paste is not formed until the die land, meaning that ingredients are transported mostly as granular materials along most of the length of the conveying screws, resulting in larger frictional forces.

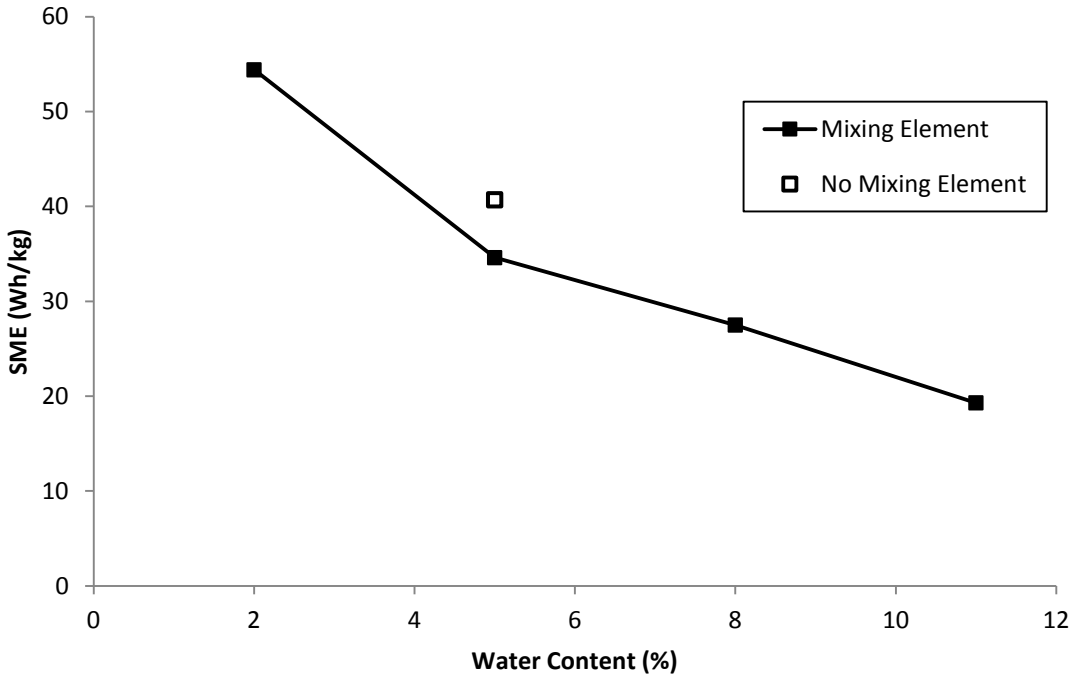

Figure 7.37 Specific Mechanical Energy (SME) input required to extrude pastes at 100 kg/hr

7.10 Conclusions

In accordance with the project aims, the extruder study of this chapter has sought to utilise the characterisation techniques developed throughout this project to gain insight into the relatively unstudied extrusion mixing of crumb paste. Characterisation tests have been performed both on a variety of paste extrudates, as well as at various sampling points along the extruder length via the use of dead-stop screw extractions. The use of dead-stop screw extractions has allowed a visualisation of paste formation along the screw length, as well as the degree of fill within the screw elements. Paste was seen to form as it passed through the single mixing block, or in the absence of a mixing block, as it compressed and passed through the die land. Whilst high in the mixing elements, the degree of fill in the conveying screw channels was generally seen to be very low, until the last few screw revolutions before the die land. This is similar to the dead-stop screw extractions seen for polypropylene/organoclay nanocomposites (Lertwimolnun & Verges, 2007) and alumina nanoparticle gels (Ozkan *et al.,* 2007).

Unlike flour based pastes such as those studied by Pansawat *et al*. (2008), extruded paste density was found to decrease as water content was increased. In agreement with similar extrusion studies, the more severe mixing environments have resulted in the densest product by expelling air and increasing the packing fraction of components. The inclusion of the mixing element in the screw profile had a densifying effect on the extrudate, as found by Van Melkebeke *et al*. (2008) and the density of comparable extruded pastes was higher than those that were batch mixed, as found by Kalyon *et al*. (2005). It was interesting to see that, unlike bread doughs which exhibit a reducing density with time after mixing (Campbell *et al.,* 2001), crumb paste density was shown to increase with time after mixing, indicating a filling of any voids within the paste. This filling of voids and increase in density may be attributable to the growth of crystals within the paste

as it hardens, as seen in SEM images of LM paste showing increased crystallinity with time after mixing.

A key finding of this study has been the identification of a substantially different sugar-protein interaction for pastes subjected to extrusion processing than is seen with LM planetary batch mixing. This microstructural variation, observed using multiphoton microscopy, has been potentially attributed to elevated temperature and pressure conditions within the extruder barrel.

Investigation of the influence of screw profile on distributive mixing using thermogravimetric analysis has shown that this mixing mechanism is most apparent as the paste undergoes compaction and elongational stretching through the die land. Whilst an improvement in distributive mixing was seen across the mixing element, it was small in comparison with the improvement seen at the point of extrusion and explains why it was possible to extrude a paste which resembles regular crumb paste when using a screw profile with only conveying elements. This observation may be explained by a related result recorded by Kalyon *et al*. (2005), who observed that when extruding graphite filled polymer suspensions, reducing the slit gap resulted in increased values of mixing indices. As the total pressure drop at the slit die was increased, the pressure in the pressurization elements of the extruder preceding the die (seen to be fully filled in this study of crumb paste) was also increased resulting in an increased intensity of back mixing and elongational stretching. Although the die diameter has not been altered in this study, the total pressure drop across the die land has evidently been sufficient to cause the large improvements in mixing index seen in this study.

Whilst not statistically conclusive from a limited number of samples and an automated image analysis, the images obtained using multiphoton microscopy give a strong suggestion that the mixing element does however play a more substantial role in the

dispersive mixing mechanism of crumb paste, with larger crystals and discrete areas of undispersed protein visible in the samples extruded without a mixing element.

A key consideration for the company was the influence of water content during extrusion mixing due to the high energy cost associated with then removing water in the drying stage which immediately follows extrusion. Analysis has shown a moderate increase in the dispersive mixing of extruded crumb paste with increased water content and a significant improvement in the distributive mixing only above 5%. Cone penetrometry analysis has shown a substantial inverse relationship between water content and shear yield strength, indicative of the consistency and rheological behaviour of the pastes formed. Shear yield strengths measured are approximately two orders of magnitude larger than typical cement pastes (Saak *et al.*, 2001) and an order of magnitude larger than typical play doughs (Tardos *et al*., 2004), indicating that crumb pastes are highly concentrated. As anticipated, significant and rapid paste hardening was found to occur within minutes of extrusion, confirming the hypothesis that off-line dynamic mode rheology, as used for the characterisation of curing cement pastes and polymers which harden over hours (Nachbaur *et al*., 2000 ; Serra *et al*., 2005 ; Rose *et al.*, 1998) is not suitable for crumb paste. As found for extruded pastes of rice flour, fish powder oil and water (Pansawat *et al*., 2008), the mechanical energy required to extrude each unit of paste was lower for increased water contents.

These results generally support the hypothesis that increased water contents promote greater mixing efficiency in crumb paste extrusion over the range of water contents considered. However it remains to be seen from further studies whether the variations characterised here have any influence on the downstream properties of chocolate and to evaluate the relative magnitude of energy cost savings that can be made by increasing the water content when compared to the associated cost in the drying stage.

Chapter 8 Conclusions and future work

8.1 Restatement of aims

The co-rotating twin screw extrusion of powdered proteins, sugars, water and fats to form chocolate crumb paste is an integral first stage in the production of chocolate by the company. As with many food industry products, the process has been developed on a trial and error basis with little quantitative understanding of how variations in processing conditions influence the formation of the extrudate. Indeed, at the commencement of the project there were no fundamental criteria for what constituted a paste of sufficient quality. The efficient evolution of process or equipment design becomes an impossible task if the most important factors affecting product quality are not recognised, let alone understood. The questions which drove this project as stated in Chapter 1 were:

1. What contribution does extrusion mixing of the ingredients make to the process and how?
2. How might the process be optimised given a greater understanding of how crumb properties evolve during extrusion?
3. How do proteins interact with sugar crystals?
4. Is batch mixed lab made (LM) paste representative of extruded crumb paste?

It was therefore the objective of this study to design and implement a variety of characterisation techniques to identify the mechanisms of mixing for crumb paste

ingredients and quantitatively relate relevant material properties to processing conditions. It was also the goal of this study to track changes in paste microstructure along the length of the screw profile, thereby facilitating the quantitative comparison of differing screw profile designs. In this concluding chapter, Section 8.2 provides an overview of the project, outlining the major and minor contributions of this work and Section 8.3 discusses the conclusions drawn from this thesis.

8.2 Project overview & contributions

The literature related to the twin screw extrusion of pastes was reviewed in Chapter 2. It was found generally, that rigorous attempts to model fluid flows in twin screw extruders were limited to simple flows of fluids with well defined constitutive equations; this was in part due to the lack of a universal approach towards characterising pastes. The heavy bias towards the modelling of purely viscous fluids was also attributed to the fact that the majority of modeling to date has been driven by the polymer plastics industry and it was reported that the incorporation of mixing knowledge from polymers into the production of food products and other bio polymers was rarely successful for a number of cited reasons.

A large number of extruder studies exist for industrially relevant pastes, however most report only the effect of processing variables on bulk properties for specific products and offer little insight into the mixing mechanisms and structural changes that occur within the extruder itself as is the subject of this study. The academic significance of this project was confirmed by a lack of studies which considered the effect of screw profile on material properties and sought to quantitatively document the statistics of microstructural variations and relate them to rheological behaviour.

The methodology for this study has therefore been to investigate and develop a range of characterisation techniques suitable for quantifying *dispersive mixing* (changes in the physical characteristics of the ingredients), *distributive mixing* (the homogeneity of components) and rheological flow properties of the resulting paste. Early work in the project showed that standard techniques and analysis used to characterise pastes of this consistency (both in terms of rheology and mixing) were not suitable for use on this complex, multiphase, viscoelastic, unstable material. Consequently, the major contribution to research from this thesis has been the development and progression of various alternative characterisation techniques. These techniques and analyses sought to deliver information on appropriate and insightful material properties suitable for an internal study on the mechanics of twin screw extruder mixing using a pilot plant twin screw extruder. The breadth of techniques and approaches considered in order to overcome the complexity of characterising this material is considered to be a strong attribute of this work.

8.2.1 Off-line characterisation of material deformation

In Chapter 3, it was shown that Haighton's formula for obtaining shear yield strengths from cone penetrometry data was unviable for crumb paste and that its use in stiff paste applications is not therefore universal. An alternative, semi-empirical model for the shear yield-penetration correlation in crumb pastes was derived using dimensional analysis, such that yield values are now reliably obtained using the simple and repeatable method of cone penetrometry.

Cone penetrometry has confirmed the existence of significant hardening in crumb paste post mixing, which poses a significant obstacle to its rheological characterisation. Samples are not sufficiently time stable over the period of measurement required by most

off-line rotational or capillary based rheometers. Despite limited available data at short times after mixing, the data suggested that the rate of hardening is most significant immediately after mixing. The finite time required to transfer and load extracted samples to an off-line rheometer, which is often some distance from a factory extruder, means that off-line rheometer based techniques are unsuitable for process design. This highlighted the need for an in-line rheological measurement technique for continuous extrusion analysis where the extruded material is time dependent and not extractable.

Although the determination of shear stresses required to initiate apparent flow using cone penetrometry represents a limited aspect of rheological behaviour, the cone penetrometry method was cheap, simple, mobile and reliable to use. As such it was employed by the company as a comparative characterisation of crumb paste in six factories around the world.

8.2.2 In-line characterisation of rheology

Chapter 4 considered the potential application of shear wave propagation and reflection techniques for future use as in-line characterisation methods for extruded pastes. A novel concept of using bender element shear wave propagation in a side mounted virtual gap arrangement was proposed. This would extend the scope of using bender elements beyond materials modelled purely as elastic at small amplitude strains and would additionally consider viscous effects for viscoelastic materials.

The preliminary implementation of the proposed concept on a model dough material was presented and encouragingly showed that using bender elements manually inserted by hand, it was possible to transmit and receive the anticipated signals required for the proposed analysis. However due to high levels of signal attenuation, vibrational noise propagated from transmitter to receiver through a test rig was seen to corrupt signals when

trying to implement accurate positioning of the transducers. Further development of this technique would require the isolation of the transmitting element from the receiver elements, such that no direct path is available and vibrational interference through any test rig is eliminated.

In Chapter 7, it was additionally shown that the shear wave reflection arrangement described by Kulmyrzaev & McClements (2000), used on single phase honey, has successfully detected variations in the reflection coefficient of multiphase extruded crumb pastes exhibiting varying rheological behaviours. Given the attractive geometry of this transducer arrangement at the interface, which appears to be non-destructively characterising aspects of the pastes rheology, this method is an attractive option for further development into an in-line characterisation.

Having been funded by an ESPRC Industrial CASE award, it was pleasing to see the establishment of contact between Mars and Industrial Tomography Systems (providers of equipment used with shear wave reflection) as a result of this project. Encouraging results provide scope for further collaborative development in this area.

8.2.3 Distributive mixing

Of the few authors that have attempted to quantify distributive mixing in industrial materials, rather than simple model fluids, the most common approach has required the addition of a foreign tracer within the material in question. In Chapter 5, a novel analysis of thermogravimetric (TGA) data for batch mixed LM crumb paste, without a tracer, has been developed to quantitatively observe the relative distributive mixing of both the bulk and individual components with mixing time.

A novel analysis of the data was required because distributive mixing analyses of TGA data reported in the literature require the accurate determination of individual

component concentrations. In contrast to simple mixtures with two or three pure components, crumb paste is a complex paste comprising seven organic ingredients with similar and relatively non discrete decomposition temperatures, making accurate determination of component concentrations unviable. The novel analysis presented therefore extends the scope of thermogravimetric analysis of distributive mixing to complex, multi-component materials such as crumb paste. The downside to the TGA analysis presented here is that it is highly time and labour intensive. It is recommended that auto-samplers, which are commonly available for thermogravimetric analysers, be employed in any future analysis to reduce this cost.

8.2.4 Dispersive mixing

In Chapter 6, the suitability of three techniques for determining dispersive mixing within crumb paste and visualising the resulting microstructure have been assessed using LM paste. These have included environmental scanning electron microscopy (ESEM) of surface topography, the staining of protein networks within microtome sections observed through an optical microscope and the application of multiphoton microscopy (MPM) to non-destructively image paste volumes below the surface.

An increasing degree of angularity in the fractured surface of SEM images with time after mixing led to the suggestion that crumb paste hardening may in part be attributed to an immediate, but prolonged formation of sugar crystals out of solution post mixing. The orientated and stretched cocoa mass imaged on the unfractured crumb paste surfaces also provided evidence that elongational, as well as shear forces, play a significant role in the final morphology of the paste.

A visual protein staining method using optical microscopy was successfully applied to 16 μm thick microtome sections, alongside a novel image analysis which

simultaneously considered the images under brightfield light and polarised light to negate the effect of artefacts. When applied to a small number of consistently prepared samples, analysis showed that both the dispersion of protein and the protein coverage of crystals increased both with mixing time and water content. However when applied to a much larger set of duplicate samples, the sensitivity of image contrast to sample preparation meant that despite efforts to apply a consistent procedure, systemic inconsistencies in protein staining caused the image analysis algorithm to fall down as it was no longer able to confidently distinguish between dispersed and undispersed protein. It was therefore concluded that optical protein staining techniques are a useful tool for detailed observation, however are difficult to implement robustly for a large scale quantitative analysis.

Finally, multiphoton microscopy has proved successful at imaging a number of microstructural features within crumb paste up to 80 μm below the surface without any form of sample preparation. This makes this form of visualisation highly attractive for future use. The successful imaging of food is a novel application of the technique, which is most widely used for biological samples. Using this technique, it has been possible to visualise the interaction between cocoa mass, sugars and proteins via the channels of fluorescence that they each emit when subjected to focused multiphoton excitation. The major advantage of this technique is the lack of sample preparation required and that samples may be imaged non-destructively without the need to section or fracture. The disadvantages of this technique are that distortion has limited images to 2D optical sections when it was hoped that 3D images would be achieved and that the co-fluorescence of cocoa mass and proteins in the green channel mean that it is not possible to distinguish between the two when both are present in the mixture.

8.2.5 Pilot plant extruder trial

In Chapter 2, a review of the literature revealed only a few studies concerning the influence of screw profile and configuration on material properties, as compared to the many studying the effects of processing conditions. The internal study of microstructural tracking within a pilot plant extruder in Chapter 7, which gave quantitative consideration to how screw profile affects paste properties and the mechanics of paste formation, is therefore a welcome contribution to the field of research into the twin screw extrusion of multiphase industrial materials. It complements the work of Lerwimolnum & Vergnes (2007) who applied a similar methodology to the study of microstructure on a polymer nanocomposite and extends on the work of Van Melkebeke *et al.* (2008) who sought to document the influence of screw profile on a pharmaceutical wet granulation process, however did so only by considering the final properties of the extrudate without considering the path taken to reach them.

In accordance with the project aims, the extruder study in this chapter has successfully utilised the characterisation techniques developed throughout the project to gain previously unstudied insight into the extrusion processing of chocolate crumb paste.

8.3 Discussion

A greater understanding of how extrusion processing influences the formation of crumb paste and the interaction of sugar crystals with protein were considered to be the key points of interest for the project. Investigation of the influence of screw profile on distributive mixing using thermogravimetric analysis has shown that this mixing mechanism is most apparent as the paste undergoes compaction and elongational stretching through the die land. Whilst an improvement in distributive mixing was seen across the mixing element, it was small in comparison with the improvement seen at the

point of extrusion and explains why it was possible to extrude a paste which resembles regular crumb paste, despite using a screw profile with only conveying elements.

Whilst not statistically conclusive from a limited number of samples and an automated image analysis, the images obtained using multiphoton microscopy gave a strong suggestion that the mixing element does however play a more substantial role in the dispersive mixing mechanism of crumb paste, with larger crystals and discrete areas of undispersed protein visible in the samples extruded without a mixing element.

Perhaps the most significant finding of this study has been the identification of a substantially greater protein binding within sugar crystals for pastes subjected to extrusion processing, than is seen with LM planetary batch mixing. It was postulated that this microstructural variation, observed using multiphoton microscopy, is caused primarily by elevated temperatures within the extruder.

8.3.1 Practical implications

Data from the trials suggests that the use of higher water contents lead to improved distributive and dispersive mixing. This also leads to lower shear yield strengths resulting in lower torques and an overall reduction in the unit energy cost of extrusion. It was interesting to see that without a mixing element, compaction and stretching in the die land alone was sufficient to form a cohesive paste. Distributive mixing in these samples was similar to that of paste mixed with the mixing element, however dispersive mixing was lower. The overall unit cost of extruding without a mixing element was also higher as the paste ingredients remained in a frictional granular state along virtually the entire extruder length. The combination of these results implies that paste should be extruded at high water contents and contain a mixing element as early in the screw profile as possible, to simultaneously achieve improved mixing and reduced energy costs. It remains to be seen

from further studies of the entire chocolate making process whether the gains in mixing performance that can be achieved at the extrusion stage have any influence on downstream properties and whether the energy savings that can be achieved are more or less than the associated cost of water removal in the drying stage.

8.3.2 LM paste

The final area of interest posed in Section 8.1 was whether batch mixed LM paste was a representative model material for extruded crumb paste. It has been shown how the processing conditions involved with LM batch mixing result in a significantly different spatial interaction between proteins and sugars within the microstructure. Owing to the range of characterisation techniques adopted in this project, a number of other comparisons are possible on more of a macro scale.

Density data was not available for LM pastes below 8% water content, but largely showed that in the range 8% - 11%, the densities of crumb pastes made using the LM method were not significantly different from those subjected to extrusion mixing. This is not an unexpected result, as SEM images of crumb paste revealed relatively few air voids within samples, leaving a continuous medium of incompressible solids and liquids. The relatively weak dependence of extruded paste density on water content in the range 2% - 8% means that both standard LM crumb paste (8% water) and standard extruded crumb paste (5% water) demonstrate similar density values of around 1.3 g/cm^3.

Cone penetrometry showed that shortly after mixing, standard 5% water extruded paste exhibited a shear yield stress of more than double that of the standard 8% water LM paste, with a faster rate of hardening from this point on. Cone penetrometry does however provide a very limited view of any rheological differences between the two. Future

developments of the in-line techniques proposed in this project, to provide comparison of the complex modulus, would be a more rigorous comparison of rheological behaviour.

Direct comparison between the distributive mixing seen in extruded pastes and those mixed under LM conditions has not been possible since to ensure sufficient resolution on such a large data set, extruded samples were scanned at a slower temperature rate than the LM samples analysed in Chapter 5. It is the opinion of this author that this study has shown that the current recipe and mixing process for LM paste produces a paste which is a poor representation of extruded crumb paste.

8.3.3 Final remarks

Twin screw extrusion of chocolate crumb paste is a not very well understood process and is indicative of the level of understanding for twin screw extrusion processes generally where multiphase pastes are concerned. The methodology and characterisation techniques developed in this thesis have provided industry specific insight into the processing of chocolate crumb paste and a platform for the continued study of chocolate crumb extrusion within the industry, as well as a wider framework for the future study of multiphase paste extrusions generally. The full potential of in-line and real-time rheological paste characterisations using wave based techniques trialled in this project have yet to be assessed.

References

Alsteens, B., Legat, V., & Avalosse, T. (2004). Parametric study of the mixing efficiency in kneading block section of a twin-screw extruder. *International Polymer Processing , 3*, 207-217.

Amarasinghe, A. D., & Wilson, D. I. (1999). On-line monitoring of ceramic extrusion. *journal of American Ceramic Society , 82*, 2305-2312.

Babatope, B., Williams, D. J., & Williams, P. R. (1999). Viscoelastic Wave Dispersion and Rheometry of Cohesive Sediments. *Journal of Hydraulic Engineering , 125* (3), 295-298.

Babatope, B., Williams, P. R., & Williams, D. J. (2006). In situ rheometry of cohesive sediments under water wave pressure. *Continental Shelf Research , 26* (4), 488-498 .

Barnes, A. H., & Nguyen, Q. D. (2001). Rotating vane rheometry - a review. *Journal of Non-Newtonian Fluid Mechanics , 98* (1), 1-14.

Barnes, H. A., & Walters, K. (1985). The yield stress myth? *Rheologica Acta , 24*, 323-326.

Bauer, E., de Sousa, J. G., Guimaraes, E. A., & Silva, F. G. (2007). Study of the laboratory Vane test on mortars. *Building and Environment , 42*, 86-92.

Belvin, A., Burrell, R., Gokhale, A., Thadhani, N., & Garmestani, H. (2009). Application of two-point probability distribution functions to predict properties of heterogenous two-phase materials. *Materials Characterization , 60*, 1055-1062.

Benbow, J., & Bridgwater, J. (1993). Paste Flow and Extrusion. Oxford, UK: Clarendon Press.

Bigio, D., & Wang, K. (1996). Scale-Up Rules for Mixing in a Non-Intermeshing Twin-Screw Extruder. *Polymer Engineering and Science , 36* (23).

Bourne, M. C. (2002). *Food Texture and Viscosity: Concept and Measurement* (Second ed.). London: Academic Press.

Brigham, O. E. (1988). *The fast fourier transform and its applications.* Prentice Hall International Edition.

Brignoli, E. G., Gotti, M., & Stokoe, K. H. (1996). Measurement of shear waves in laboratory specimens by means of piezoelectric transducers. *Geotechnical Testing Journal , 19* (4), 384-397.

Brod, H., & Liesenfelder, U. (2004). The mixing efficiency of an eccentric-disc kneading zone in intermeshing co- and counter- rotating twin screw extruders. *Chemical Engineering Technology , 27(3)*, 297-303.

Camire, M. E. (2000). Chemical and Nutritional Changes in Food during Extrusion. In M. N. Riaz, *Extruders in Food Applications* (pp. 127-147). CRC Press.

Camire, M. E. (2001). Extrusion and Nutritional Quality. In R. Guy, *Extrusion Cooking: Technology and Applications* (pp. 108-128). CRC Press.

Campbell, G. M., Herrero-Sanchez, R., Payo-Rodriguez, R., & Merchan, M. L. (2001). Measurement of Dynamic Dough Density and Effect of Surfactants and Flour. *Cereal Chemistry , 78(3)*, 272–277.

Cauvain, S., & Young, L. (2008). *Bakery Food Manufacture and Quality: Water Control and Effects* (2nd ed.). Wiley-Blackwell.

Cebollero, F. S. (2009). *Segmentation and registration of 2D multiphoton microscopy images.* Universitat Polit`ecnica de Catalunya.

Centonze, V. E., & White, J. G. (1998). Multiphoton excitation provides optical sections from deeper within scattering specimens than confocal imaging. *Biophysical Journal , 75* (4), 2015-2024.

Cheyne, A., Barnes, J., & Wilson, D. I. (2005). Extrusion behaviour of cohesive potato starch pastes: I Rheological characterisation. *Journal of Food Engineering , 66*, 1-12.

Clayton, C. R., Theron, M., & Best, A. I. (2004). The measurement of vertical shear-wave velocity using side-mounted bender elements in the triaxial apparatus. *Géotechnique , 54* (7), 495-498.

Coussot, P. (2007). Rheophysics of pastes: a review of microscopic modelling approaches. *Soft Matter , 3*, 528-540.

Covas, J. A., Maia, J. M., Machado, A. V., & Costa, P. (2008). On-line rotational rheometry for extrusion and compounding operations. *Journal of Non-Newtonian Fluid Mechanics , 148*, 88-96.

De Man, J. M. (1983). Consistency of fats: A review. *American Oil Chemists' Society , 60*, 82-87.

De Man, J. M., Dobbs, J. E., & Sherman, P. (1979). Spreadability of buter and margarine. *Food Texture and Rheology* , 43-54.

De Pilli, T., Jouppila, K., Ikonen, J., Kansikas, J., Derossa, A., & Severini, C. (2008). Study on formation of starch-lipid complexes during extrusion-cooking of almond flour. *Food Engineering , 87*, 495-504.

Densities of miscallaneous solids. (2011). Retrieved June 30, 2011, from www.engineeringtoolbox.com: http://www.engineeringtoolbox.com/density-solids-d_1265.html

Dhanasekharan, M., & Kokini, J. L. (2000). Viscoelastic flow modeling in the extrusion of a dough-like fluid. *Food Process Engineering , 23*, 237-247.

Dixon, B. D., & Parekh, J. V. (1979). Use of the cone penetrometer for testing the firmness of butter. *Texture Studies , 10*, 421-434.

Doukoglou, T. D., & Hunter, I. W. (1995). Volumetric image distortion due to refractive index mismatch in 3D confocal scanning laser microscopy. *Engineering in Medicine and Biology Society, 1995., IEEE 17th Annual Conference, 1*, pp. 505-506. Montreal, Canada.

Dyvik, R., & Madshus, C. (1985). Lab measurement of Gmax using bender elements. *Proceedings of the American Society of Civil Engineers Conference on Advances in the Art of Testing Soils under Cyclic Conditions*, (pp. 186-196). Detroit.

Fearon, A. M., & Johnston, D. E. (1989). A comparison of three instrumental techniques to evaluate butter spreadability. *Food Quality , 12*, 23-38.

Ferry, J. D. (1980). *Viscoelastic properties of polymers.* New York: Wiley.

Figoni, P. (2007). *How Baking Works: Exploring the Fundamentals of Baking Science* (2nd ed.). Wiley.

Gokhale, A. M., Tewari, A., & Garmestani, H. (2005). Constraints on microstructural two-point correlation functions. *Scripta Materialia , 53*, 989-993.

Greening, P. D., & Nash, D. F. (2004). Frequency domain determination of G(0) using bender elements. *Geotech Test J , 27* (3), 288-294.

Gujral, H. S., & Sodhi, N. S. (2002). Back extrusion properties of wheat porridge (Dalia). *Food Engineering , 52*, 53-56.

Haba, Y., & Narkis, M. (2004). Development and Characterization of Reactively Extruded PVC/Polysterene Blends. *Polymer Engineering and Science , 44(8)*, 1473-1483.

Haighton, A. J. (1959). The measurement of the Hardness of Margarine and Fats with Cone Penetrometers. *American Oil Chemists' Society , 36*, 345-348.

Harrison, G., & Barlow, A. J. (1981). Dynamic viscosity measurements. *Methods of Experimental Physics , 19*, 137-178.

Hava, Y., & Narkis, A. (2004). Development and characterization of reactively extruded PVC/polystyrene blends. *Polymer Engineering and Science , 44* (8), 1473-1483.

Hayakawa, M., & de Man, J. (1982). Interpretation of cone penetrometer consistency measurements of fats. *Journal of Texture Studies , 13*, 201-210.

Herschel, W. H., & Bulkley, R. (1926). Measurement of consistency as applied to rubber-benzene solutions. *Proc. Am. Soc. Testing Materials , 26(2)*, 621-633.

Holly, E. E., Venkataraman, S. K., & Chambon, F. (1988). Fourier transform mechanical spectroscopy of viscoelastic materials with transient structure. *Journal of Non-Newtonian Fluid Mechanics , 27* (1), 17-26.

Huber, G. R. (2000). *Extruders in Food Applications.* (R. MN, Ed.) CRC Press.

Hughes, D. J., Cui, Z., Field, R. W., & Tirlapur, U. K. (2006). In Situ Three-Dimensional Characterization of Membrane Fouling by Protein Suspensions Using Multiphoton Microscopy. *Langmuir , 22*, 6266-6272.

Hughes, D., Tirlapur, U. K., Field, R., & Cui, Z. (2006a). In situ 3D characterisation of membrane fouling by protein suspensions using multiphoton microscopy. *Langmuir , 22*, 6266-6272.

Hughes, D., Tirlapur, U. K., Field, R., & Cui, Z. (2006b). In situ 3D characterisation of membrane fouling by yeast suspensions using two-photon femtosecond near infrared non-linear optical imaging. *Membrane Science , 280*, 124-133.

Ishikawa, T., Kihara, S., & Funatsu, K. (2001). 3D non-Isothermal Flow Field Analysis and mixing Performance Evaluation of Kneading Blocks in a Co-rotating Twin Screw SExtruder. *Polymer Engineering and Science , 41* (5).

Jefferson, G., Garmestani, H., Tannenbaum, R., Gokhale, A., & Tadd, E. (2005). Two-point probability distribution function analysis of Co-polymer nano-composites. *International Journal of Plasticity , 21*, 185-198.

Kalyon, D. M., & Sangani, H. (1989). An experimental study of the degree of distributive mixing in fully intermeshing co-rotating twin screw extruders. *Polym Eng Sci , 29(15)*, 1018-1026.

Kalyon, D. M., Dalwadi, D., Erol, M., Birinci, E., & Tsenoglu, C. (2006). Rheological behaviour of concentrated suspensions as affected by the dynamics of the mixing process. *Rheologica Acta , 45*, 641- 658.

Krigstin, S. G., & Sain, M. (2008, June). Determination of the mineral constituents of recycked paper mill sludge. *Tappi* .

Kulmyrzaev, A., & McClements, J. (2000). HIgh frequency dynamic shear rheology of honey. *Journal of Food Engineering , 45*, 219-224.

Lactose in solid form. (2011). Retrieved October 3, 2011, from www.lactose.com: http://www.lactose.com/basic/lactose_in_solid_form.html

Lawal, A., & Kalyon, D. M. (1999). Analysis of nonisothermal screw extrusion processing of viscoplastic fluids with significant backflow. *Chemical Engineering Science , 54*, 999-1013.

Lertwimolnum, W., & Vergnes, B. (2007). Influence of screw profile and extrusion conditions on the microstructure of polypropylene/organoclay nanocomposites. *Polymer Engineering and Science , 2101*.

Levresse, P., Manas-Zloczower, I., & Feke, D. L. (2002). Dispersion studies of agglomerates in steady and dynamic flows of polymeric materials. *Rubber Chem Technol , 75(1)*, 119-133.

Lionetto, F., Coluccia, G., D'Antona, P., & Maffezzoli, A. (2007). Gelation of waxy crude oils by ultrasonic and dynamic mechanical analysis. *Rheologica Acta , 46* (5), 601-609.

McClements, D. J. (1997). Ultrasonic characterization of foods: principles, methods and applications. *Critical Review of Food Science and Technology , 37*, 1-46.

McKelvey, J. M. (1962). *Polymer Processing.* New York: Wiley.

McNally, J. G., Karpova, T., & Cooper, J. (1999). Three-dimensional imaging by deconvolution microscopy. *Methods* , 373-385.

Mottram, F. J. (1961). Evaluation of pseudo-plastic materials by cone penetrometers. *Lab. Pract. , 10*, 767-770.

Muller, H. G. (1969). Mechanical properties, rheology and haptaesthesis of food. *Texture Studies , 1*, 38-42.

Nachbaur, L., Nonat, A., Mutin, J. C., & Choplin, L. (2000). Dynamic Mode Rheology of Cement Pastes. *Second International Rilem Workshop on Hydration and Setting*, *13*, pp. 281-293.

Nakagawa, K., Soga, K., & Mitchell, J. K. (1996). Pulse transmission system for measuring wave propagation in soils. *Journal of Geotechnical Engineering , 122* (4), 302-308.

Narkis, M., Schach-Caplan, M., Haba, Y., & Silverstein, M. (2004). PVC Modification Through Polymerization of a Monomer Absorbed in Porous Suspension-Type PVC Particles. *Journal of Vinyl & Additive Technology , 10* (3), 109-120.

Newitt, D. M., & Conway-Jones, J. M. (1958). A contribution to the theory and practice of granulation. *Transactions of the Institution of Chemical Engineers , 36*, 422-442.

Ozkan, S., Gevgilili, H., Kalyon, D. M., Kowalczyk, J., & Mezger, M. (2007). Twin-Screw Extrusion of Nano-Alumina based Simulants of Energetic Formulations Involving Gel-Based binders. *Journal of Energetic Materials , 25*, 173-201.

Pane, I., & Hansen, W. (2005). Investigation of blended cement hydration by isothermal calorimetry and thermal analysis. *Cement and Concrete Research , 35*, 1155-1164.

Pansawat, N., Jangchud, K., Jangchud, A., Wuttijumnong, P., Saalia, F. K., Eitenmiller, R. R., et al. (2008). Effects of extrusion conditions on secondary extrusion variables and physical properties of fish, rice-based snacks. *LWT , 41*, 632-641.

Pennington, D. S., Nash, D. F., & Lings, M. L. (2001). Horizontally Mounted Bender Elements for Measuring Anisotropic Shear Moduli in Triaxial Clay Specimens. *Geotechnical Testing Journal , 24* (2).

Potluri, R., Todd, D., & Gogos, C. (2006). Mixing Immiscible Blends in an Intermeshing Counter-Rotating Twin Screw Extruder. *Advances in Polymer Technology , 25* (2), 81-89.

Povey, M. J. (1998). Ultrasonics of foods. *Contemporary Physics , 39*, 467-478.

Rebinder, P. A., & Semenenko, N. A. (1949). Use of the penetrating cone method for the characterization of structural-mechanical properties of visco-plastic material. *Proc. Acad. Sci. (U.S.S.R.) , 64*, 835-838.

Reiner, M. (1964, January). The Deborah number. *Physics Today* , 62.

Rio, J. F. (2006). *Advances in laboratory geophysics using bender elements.* Doctoral Thesis: University College London.

Rose, J., Osbaldiston, R., Smith, W., Farquharson, S., & Shaw, M. T. (1998). In-Situ Monitoring ofa Polymer Cure using Dynamic Rheometry and Raman Spectroscopy. *Technical papers of the annual technical conference - Society of plastics engineers, 56*, pp. 939-944.

Ross-Murphy, S. B. (1994). Rheological characterization of polymer gels and networks. *Polymer Gels and Networks , 2* (3-4), 229-237.

Saak, A. W., Jennings, H. M., & Shah, S. P. (2001). The influence of wall slip on yield stress and viscoelastic measurements of cement paste. *Cement and Concrete Research , 31*, 2-5-212.

Schofield, C. (1976). The definition and assessment of mixture quality in mixtures of particulate solids. *Powder Technology , 15* (2), 169-180.

Serra, C., Bouquey, M., Schlatter, G., & Muller, R. (2005). Rheological Behavior of Reactive Miscible Polymer Blends: Influence of Mixing and Annealing Before Crosslinking. *Journal of Polymer Science , 98*, 1978 - 1995.

Steffe, J. F. (1996). *Rheological Methods in Food Process Engineering* (Second ed.). East Lansing, USA: Freeman Press.

Strahm, B. S. (2000). Preconditioning. In M. N. Riaz, *Extruders in Food Applications* (pp. 115-126). CRC Press.

Tadmor, Z., & Gogos, C. G. (1979). *Principles of polymer processing.* New York: Wiley.

Tardos, G. I., Hapgood, K. P., Ipadeola, O. O., & Michaels, J. N. (2004). Stress measurements in high shear granulators using calibrated "test" particles: application to scale-up. *Powder Technology , 140* (3), 217-227.

Van Melkebeke, B., Vervaet, C., & Remon, J. P. (2008). Validation of a continuous granulation process using a twin-screw extruder. *International Journal of Pharmaceuticals* .

Van Zuilichem, D. J., Kuiper, E., Stolp, W., & Jager, T. (1999). Mixing effects of constituting elements of mixing screws in single and twin screw extruders. *Powder Technology , 106*, 147-159.

Vasic, I., & De Man, J. M. (1968). Effect of mechanical treatment on some rheological properties of butter. *Rheology and Texture of Foodstuffs , SCi Monograph no 27, 251-264*.

Viggiani, G., & Atkinson, J. H. (1995a). Interpretation of bender element tests. *Geotechnique , 45* (1), 149-154.

Viggiani, G., & Atkinson, J. H. (1995b). Stiffness of fine-grained soil at very small strains. *Geotechnique , 45* (2), 249-265.

Wallace, W., Schaefer, L. H., & Swedlow, J. R. (2001). A Workingperson's Guide to Deconvolution in Light Microscopy. *BioTechniques , 31*, 1076-1097.

Walstra, P. (1979). Physical properties of butter. *I.D.F. F-Doc. 77 Montreux* .

White, G. W. (1970). Rheology in food research. *Food Technology , 5*, 1-32.

Whorlow, R. W. (1980). *Rheological Techniques.* London: Halstead Press.

Williams, P. R., & Williams, D. J. (1992). The determination of dynamic moduli at high frequencies. *Journal of Non-Newtonian Fluid Mechanics , 42* (3), 267-282.

Williams, P. R., & Williams, D. J. (1994). The influence of wave dispersion characteristics on the determination of mechanical relaxation spectra. *Journal of Rheology , 38* (4).

Williams, P. R., Ravki, S., & Roberts, I. D. (2000). The pulse-resonance rheometers: an instrument for studying the viscoelastic properties of gels. *Measurement Science and Technology , 11* (4).

Williams, P., & Williams, R. (1996). Studies of shearwave dispersion in critical-gel systems. *Journal de chimie physique et de physico-chimie biologique , 93* (5), 870-879.

Williams, R. M., Zipfel, W. R., & Webb, W. W. (2001). Multiphoton microscopy in biological research. *Chemical Biology , 5*, 603-608.

Wilson, D. I., & Rough, S. L. (2006). Exploiting the curious characteristics of dense solid-liquid pastes. *Chemical Engineering Science , 61* (13), 4147-4154 .

Yazici, R., & Kalyon, D. M. (1993). Degree of mixing analyses of concentrated suspensions by electron probe and X-ray diffraction. *Rubber Chem Techn , 66 (4)*, 527-537.